The pressure-loaded right ventricle

Mieke MP Driessen

The pressure-loaded right ventricle

PhD-thesis University of Utrecht, Utrecht, The Netherlands

ISBN:	978-94-6233-716-9
Author:	Mieke Driessen
Cover design and lay-out:	Design by Aaf! (Aafke Driessen)
Printing:	Gildeprint drukkerijen, Enschede (www.gildeprint.nl)

The pressure-loaded right ventricle

De drukbelaste rechter ventrikel
(met een samenvatting in het Nederlands)

Proefschrift

ter verkrijging van de graad van doctor aan de Universiteit Utrecht op gezag van de rector magnificus, prof. dr. G.J. van der Zwaan, ingevolge het besluit van het college voor promoties in het openbaar te verdedigen op donderdag 28 september 2017 des middags te 12.45 uur

door

Maria Margaretha Petronella Driessen
geboren op 19 november 1984 te Venlo

Promotoren:
Prof. dr. P.A. Doevendans
Prof. dr. T. Leiner

Copromotor:
Dr. G.T. Sieswerda

The research in this thesis was financially supported by a research fellowship from the ICIN-Netherlands Heart Institute (ICIN-NHI).

Financial support by the Dutch Heart Foundation for the publication of this thesis is gratefully acknowledged.

Printing of this thesis was financially supported by Actelion Pharmaceuticals Nederland B.V., Philips Healthcare, Toshiba Medical Systems Nederland, Medis medical imaging systems B.V., Servier Nederland Farma B.V. and Chipsoft.

Table of Contents

CHAPTER 1

General introduction

Heart failure

Heart failure is a clinical syndrome characterized by typical symptoms, such as ankle swelling, breathlessness and fatigue. Currently, the prevalence is estimated at 1-2% of the adult population.[1] The majority of heart failure research and recent guidelines are focused on diastolic or systolic failure of the left ventricle, as the vast majority of patients suffer left ventricular (LV) failure.[1] However, primary right-sided heart failure is the biggest driver of morbidity and mortality in patients with congenital heart disease (CHD) and pulmonary hypertension (PH).[2-4] While systolic LV failure is often caused by coronary artery disease, right ventricular (RV) failure is generally caused by increased volume- or pressure load imposed on the ventricle.[5] Furthermore, geometry, ventricular morphology and embryological origin are different in the right ventricle.[6] Therefore, the vast majority of research in primary LV failure cannot be translated to the RV.
The RV generally tolerates right ventricular volume load much better than pressure load.[5] Consequently, the largest group of patients suffering RV failure are those with RV pressure overload.[4,7] Nevertheless, owing to improvements in CHD surgery and pulmonary vasodilator therapy (for PH), survival of CHD and PAH patients has improved much over the past decades.[4,8] With this improved survival, the group of patients suffering RV dysfunction is increasing, necessitating sensitive markers for follow-up of RV dysfunction and valve pathology.

Imaging the right ventricle

Follow up of patients at risk for RV failure is primarily done using non-invasive imaging techniques. Aims are evaluation of RV dilation, function, RV pressures and valve regurgitation and stenosis – as all of these parameters have prognostic or therapeutic consequences.[9,10] Nevertheless, while echocardiographic measurements perform reasonable well for assessment of valvular stenosis, RV systolic pressure and morphological assessment, reliable and reproducible assessment of RV dilation, systolic function and tricuspid valve regurgitation remain difficult.[10-13] There are several explanations for this: 1) The complex geometry of both the right ventricle and tricuspid valve, 2) the position of the RV behind the sternum and, 3) the complex contractile pattern of the RV, involving not only longitudinal shortening, but also bellows movement of the free wall, septal contraction and important contribution of simultaneous LV contraction.[14,15]
The echocardiographic measurements commonly used for assessment of RV function are tricuspid annular planar systolic excursion (TAPSE), tissue Doppler imaging systolic velocity (TDI S') and fractional area change. While especially TAPSE was shown to have good prognostic value for mortality in PAH patients, the value of this parameter remains unclear in CHD.[12,13,16,17] Consequently, cardiac magnetic resonance imaging (CMR) is recommended for follow up of RV dilation and RV function in patients with CHD.[10] The field of CMR has quickly developed over the past decade and new imaging sequences and post-processing software have become broadly available. However, most of these CMR techniques have been validated in healthy individuals or patients with left sided disease and validation in the RV of patients with CHD and PH is lacking. In addition, reproducibility of new techniques needs to be re-established in these patient groups, as extrapolation of data obtained in healthy controls is not necessarily applicable to the diseased RV.

The road towards better understanding the right ventricle
As is already mentioned above, increase of afterload is believed to be poorly tolerated by the RV. This is most clearly seen in the setting of massive pulmonary embolism, where a sudden increase of RV pressures leads to an instantaneous drop in stroke volume and cardiac output.[18] However, conditions associated with chronic elevations in RV pressure, such as PAH and several CHDs,

show great variance in time to RV failure and clinical outcome.[4,7,19] In pulmonary hypertension (PH), pulmonary vascular resistance and pulmonary arterial pressure increase more gradually, resulting in higher right ventricular systolic pressures (RVSP), triggering RV remodelling and RV hypertrophy - adaptive mechanisms aimed at decreasing afterload for the RV and maintaining cardiac output. However, unless PH patients are treated successfully with pulmonary vasodilator therapy, RV failure is common within a few years after diagnosis.[4] Conversely, many congenital heart defects also lead to chronically increased RV pressure, due to either high (for RV) vascular resistance or valvular stenosis, present since birth. In contrast to PH, the RV in these patients is often capable of generating high pressures and maintaining cardiac output for many decades. Even so, marked differences also exist between different CHDs, i.e. many patients with pulmonary stenosis (PS) often stay asymptomatic, while a substantial portion of patients with subaortic RVs develop RV dysfunction or failure in the 4th and 5th decade of life.[20-22]
In all entities with a chronic increase of RV pressure, measures of global and regional RV function and remodelling are prognostic for survival.[22-26] Therefore, differences in clinical course and survival are likely explained by differences in RV remodelling and function, i.e. differences in RV adaptation. In adult patients, two echocardiographic studies have shown that global RV remodelling and global RV function seem favourable in patients with CHD compared to iPAH patients.[27,28] However, this has not been studied in detail in children, nor have these studies included other than longitudinal components of RV function, RV geometry or CMR measurements. Comparing RV adaptation between patient with CHD and PH can provide insight into mechanisms contributing to RV failure, which are currently incompletely understood. Furthermore, it can uncover potential imaging markers for early identification of RV dysfunction.

Outline of this thesis
In order to optimally guide clinical management, it is essential to accurately monitor disease progression and estimate prognosis. As previously stated, follow-up of PH patients is still primarily done with (conventional) echocardiographic measurements. Consequently, in current guidelines echocardiographic measurements (TAPSE, pericardial effusion and RA area) are used to stratify risk of mortality in PH.[9] As more studies reporting on echocardiographic measurements are becoming available, it is important to systematically evaluate the prognostic value of these measurements. *Chapter 2* provides an overview of the prognostic value of currently used echocardiographic measurement in patients with PH. Most frequently used echocardiographic measurements do not perform as well in patients with CHD, showing no prognostic value in patients with subaortic RVs and no correlation to measures of global function.[12,13,29] Therefore, CMR has a much more prominent role in follow-up of CHD patients, although its additive value in PH is also being recognized.[30] Due to changes in hardware and software, the possibilities to depict various elements of anatomy and function with CMR have also vastly increased. *Chapter 3* provides an overview of currently available state-of-the-art CMR imaging techniques and how these new techniques may be used in patients with CHD.
Chapters 4 and 5 focus on validation and implementation of new CMR and post-processing techniques in patients with pressure loaded RVs. CMR is most frequently used to determine RV ejection fraction and RV volumes[10,11], but there is no consensus whether or not to exclude trabeculae from RV volumes. Although theoretically more accurate (i.e. muscle is not blood volume), reproducibility of manual delineation of trabeculae has proven to be very poor.[31] *Chapter 4* uses semi-automatic segmentation software to exclude trabeculae, investigating both the impact and reliability of the exclusion of trabeculae in patients with pressure loaded RVs.
Chapter 5 focuses on tricuspid valve regurgitation, an important contributor to patient morbidity and mortality.[32-34] Currently, tricuspid valve regurgitation is assessed using echocardiography,

which has low reproducibility.[35] Reliable assessment of tricuspid valve regurgitation is important as it influences therapeutic strategy and estimation of prognosis. *Chapter 5* evaluates quantification of tricuspid flow and regurgitation using 4D-flow MR imaging in patients with complex RV geometry and varying degrees of regurgitation.

The second part of this thesis focuses on the impact of RV pressure overload on RV remodeling, function and exercise capacity. With the introduction of the arterial switch procedure for transposition of the great arteries, it was believed that near-normal anatomy could be achieved. Although late mortality is low with 95% surviving to 25 years, re-operation, mostly on RV outflow-tract obstruction, is frequent and exercise capacity is decreased in a substantial subset of patients.[36,37] In *Chapter 6* we investigate neo-pulmonary artery obstruction, branch obstruction and blood flow distribution and its effect on RV volume, function and exercise capacity in patients post-arterial switch procedure.
As outlined above – there are substantial differences in time to RV failure and in mortality between patients with different CHDs and PAH. This thesis continues with a detailed comparison of RV characteristics (using both echocardiography and CMR) in patients with PS, a subaortic RV and PH in *Chapter 7*. In children with PAH, cardiac output remains higher and right atrial pressure remains lower at similar pulmonary pressures when compared with adults. However, also in children, outcome is much better in pulmonary stenosis compared with pulmonary hypertension.[38] *Chapter 8* compares RV remodeling, geometry and global and regional RV function in children with PS compared to those with PH. Lastly, the RV and LV are interdependent through shared myocardial fibers, the interventricular septum and pericardial space.[39,40] It is well known that LV contraction and IVS contraction contribute significantly to RV systolic function, but RV dilation and loading also impact LV geometry and ultimately function.[41-44] To study this interaction in more detail, the impact of RV pressure load on interventricular interaction in pediatric PS is compared to PAH patients in *Chapter 9*.

References

1. Ponikowski P, Voors AA, Anker SD, et al. 2016 ESC guidelines for the diagnosis and treatment of acute and chronic heart failure: The task force for the diagnosis and treatment of acute and chronic heart failure of the european society of cardiology (ESC)developed with the special contribution of the heart failure association (HFA) of the ESC. Eur Heart J. 2016;37:2129-2200.
2. Verheugt CL, Uiterwaal CS, van der Velde ET, et al. Mortality in adult congenital heart disease. Eur Heart J. 2010;31:1220-1229.
3. Zomer AC, Vaartjes I, van der Velde ET, et al. Heart failure admissions in adults with congenital heart disease; risk factors and prognosis. Int J Cardiol. 2013;168:2487-2493.
4. Humbert M, Sitbon O, Chaouat A, et al. Survival in patients with idiopathic, familial, and anorexigen-associated pulmonary arterial hypertension in the modern management era. Circulation. 2010;122:156-163.
5. Haddad F, Doyle R, Murphy DJ, Hunt SA. Right ventricular function in cardiovascular disease, part II: Pathophysiology, clinical importance, and management of right ventricular failure. Circulation. 2008;117:1717-1731.
6. Ho SY, Nihoyannopoulos P. Anatomy, echocardiography, and normal right ventricular dimensions. Heart. 2006;92 Suppl 1:i2-13.
7. Zomer AC, Vaartjes I, van der Velde ET, et al. Heart failure admissions in adults with congenital heart disease; risk factors and prognosis. Int J Cardiol. 2013;168:2487-2493.
8. van der Bom T, Zomer AC, Zwinderman AH, Meijboom FJ, Bouma BJ, Mulder BJ. The changing epidemiology of congenital heart disease. Nat Rev Cardiol. 2011;8:50-60.
9. Galie N, Humbert M, Vachiery JL, et al. 2015 ESC/ERS guidelines for the diagnosis and treatment of pulmonary hypertension: The joint task force for the diagnosis and treatment of pulmonary hypertension of the european society of cardiology (ESC) and the european respiratory society (ERS): Endorsed by: Association for european paediatric and congenital cardiology (AEPC), international society for heart and lung transplantation (ISHLT). Eur Heart J. 2016;37:67-119.
10. Baumgartner H, Bonhoeffer P, De Groot NM, et al. ESC guidelines for the management of grown-up congenital heart disease (new version 2010). Eur Heart J. 2010;31:2915-2957.
11. Valente AM, Cook S, Festa P, et al. Multimodality imaging guidelines for patients with repaired tetralogy of fallot: A report from the AmericanSsociety of echocardiography: Developed in collaboration with the society for cardiovascular magnetic resonance and the society for pediatric radiology. J Am Soc Echocardiogr. 2014;27:111-141.
12. De Caro E, Bondanza S, Calevo MG, et al. Tricuspid annular plane systolic excursion for the assessment of ventricular function in adults operated on with mustard procedure for complete transposition of the great arteries. Congenit Heart Dis. 2014;9:252-258.
13. Mercer-Rosa L, Parnell A, Forfia PR, Yang W, Goldmuntz E, Kawut SM. Tricuspid annular plane systolic excursion in the assessment of right ventricular function in children and adolescents after repair of tetralogy of fallot. J Am Soc Echocardiogr. 2013;26:1322-1329.
14. Haddad F, Hunt SA, Rosenthal DN, Murphy DJ. Right ventricular function in cardiovascular disease, part I: Anatomy, physiology, aging, and functional assessment of the right ventricle. Circulation. 2008;117:1436-1448.
15. Santamore WP, Lynch PR, Heckman JL, Bove AA, Meier GD. Left ventricular effects on right ventricular developed pressure. J Appl Physiol. 1976;41:925-930.
16. Forfia PR, Fisher MR, Mathai SC, et al. Tricuspid annular displacement predicts survival in pulmonary hypertension. Am J Respir Crit Care Med. 2006;174:1034-1041.
17. Schuuring MJ, van Riel AC, Vis JC, et al. New predictors of mortality in adults with congenital heart disease and pulmonary hypertension: Midterm outcome of a prospective study. Int J Cardiol. 2015;181:270-276.
18. MacNee W. Pathophysiology of cor pulmonale in chronic obstructive pulmonary disease. part one. Am J Respir Crit Care Med. 1994;150:833-852.
19. Verheugt CL, Uiterwaal CS, van der Velde ET, et al. Mortality in adult congenital heart disease. Eur Heart J. 2010;31:1220-1229.
20. Tinker J, Howitt G, Markman P, Wade EG. The natural history of isolated pulmonary stenosis. Br Heart J. 1965;27:151-160.
21. Cuypers JA, Eindhoven JA, Slager MA, et al. The natural and unnatural history of the mustard procedure: Long-term outcome up to 40 years. Eur Heart J. 2014;35:1666-1674.
22. Roche SL, Redington AN. The failing right ventricle in congenital heart disease. Can J Cardiol. 2013;29:768-778.
23. Ryan JJ, Huston J, Kutty S, et al. Right ventricular adaptation and failure in pulmonary arterial hypertension. Can J Cardiol. 2015;31:391-406.
24. Gerges M, Gerges C, Lang IM. Advanced imaging tools rather than hemodynamics should be the primary approach for diagnosing, following, and managing pulmonary arterial hypertension. Can J Cardiol. 2015;31:521-528.
25. van der Bom T, Winter MM, Groenink M, et al. Right ventricular end-diastolic volume combined with peak systolic blood pressure during exercise identifies patients at risk for complications in adults with a systemic right ventricle. J Am Coll Cardiol. 2013;62:926-936.
26. van Wolferen SA, Marcus JT, Boonstra A, et al. Prognostic value of right ventricular mass, volume, and function in idiopathic pulmonary arterial hypertension. Eur Heart J. 2007;28:1250-1257.
27. Jurcut R, Giusca S, Ticulescu R, et al. Different patterns of adaptation of the right ventricle to pressure overload: A comparison between pulmonary hypertension and pulmonary stenosis. J Am Soc Echocardiogr. 2011;24:1109-1117.

28. Giusca S, Popa E, Amzulescu MS, et al. Is right ventricular remodeling in pulmonary hypertension dependent on etiology? an echocardiographic study. Echocardiography. 2016;33:546-554.
29. Valente AM, Gauvreau K, Assenza GE, et al. Contemporary predictors of death and sustained ventricular tachycardia in patients with repaired tetralogy of fallot enrolled in the INDICATOR cohort. Heart. 2014;100:247-253.
30. Baggen VJ, Leiner T, Post MC, et al. Cardiac magnetic resonance findings predicting mortality in patients with pulmonary arterial hypertension: A systematic review and meta-analysis. Eur Radiol. 2016;26:3771-3780.
31. Winter MM, Bernink FJ, Groenink M, et al. Evaluating the systemic right ventricle by CMR: The importance of consistent and reproducible delineation of the cavity. J Cardiovasc Magn Reson. 2008;10:40.
32. Bokma JP, Winter MM, Oosterhof T, et al. Severe tricuspid regurgitation is predictive for adverse events in tetralogy of fallot. Heart. 2015;101:794-799.
33. Dandel M, Knosalla C, Kemper D, Stein J, Hetzer R. Assessment of right ventricular adaptability to loading conditions can improve the timing of listing to transplantation in patients with pulmonary arterial hypertension. J Heart Lung Transplant. 2015;34:319-328.
34. Nath J, Foster E, Heidenreich PA. Impact of tricuspid regurgitation on long-term survival. J Am Coll Cardiol. 2004;43:405-409.
35. Grant AD, Thavendiranathan P, Rodriguez LL, Kwon D, Marwick TH. Development of a consensus algorithm to improve interobserver agreement and accuracy in the determination of tricuspid regurgitation severity. J Am Soc Echocardiogr. 2014;27:277-284.
36. Giardini A, Khambadkone S, Rizzo N, et al. Determinants of exercise capacity after arterial switch operation for transposition of the great arteries. Am J Cardiol. 2009;104:1007-1012.
37. Khairy P, Clair M, Fernandes SM, et al. Cardiovascular outcomes after the arterial switch operation for D-transposition of the great arteries. Circulation. 2013;127:331-339.
38. Barst RJ, Ertel SI, Beghetti M, Ivy DD. Pulmonary arterial hypertension: A comparison between children and adults. Eur Respir J. 2011;37:665-677.
39. Belenkie I, Horne SG, Dani R, Smith ER, Tyberg JV. Effects of aortic constriction during experimental acute right ventricular pressure loading. further insights into diastolic and systolic ventricular interaction. Circulation. 1995;92:546-554.
40. Friedberg MK, Redington AN. Right versus left ventricular failure: Differences, similarities, and interactions. Circulation. 2014;129:1033-1044.
41. Dohi K, Onishi K, Gorcsan J,3rd, et al. Role of radial strain and displacement imaging to quantify wall motion dyssynchrony in patients with left ventricular mechanical dyssynchrony and chronic right ventricular pressure overload. Am J Cardiol. 2008;101:1206-1212.
42. Hardegree EL, Sachdev A, Fenstad ER, et al. Impaired left ventricular mechanics in pulmonary arterial hypertension: Identification of a cohort at high risk. Circ Heart Fail. 2013;6:748-755.
43. Marcus JT, Gan CT, Zwanenburg JJ, et al. Interventricular mechanical asynchrony in pulmonary arterial hypertension: Left-to-right delay in peak shortening is related to right ventricular overload and left ventricular underfilling. J Am Coll Cardiol. 2008;51:750-757.
44. Santamore WP, Lynch PR, Meier G, Heckman J, Bove AA. Myocardial interaction between the ventricles. J Appl Physiol. 1976;41:362-368.

1

CHAPTER 2

Echocardiographic findings associated with mortality or transplant in patients with pulmonary arterial hypertension: A systematic review and meta-analysis

Authors:
V.J.M. Baggen, M.M.P. Driessen, M.C. Post, A.P. van Dijk, J.W. Roos-Hesselink, A.E. van den Bosch, J.J.M. Takkenberg, G.Tj. Sieswerda

Neth Heart J (2016) 24:374–389

Abstract

Background
Identification of patients at risk of deterioration is essential to guide clinical management in pulmonary arterial hypertension (PAH). This study aims to provide a comprehensive overview of well-investigated echocardiographic findings that are associated with clinical deterioration in PAH.

Methods
MEDLINE and EMBASE databases were systematically searched for longitudinal studies published by April 2015 that reported associations between echocardiographic findings and mortality, transplant or clinical worsening. Meta-analysis using random effect models was performed for echocardiographic findings investigated by four or more studies. In case of statistical heterogeneity a sensitivity analysis was conducted.

Results
Thirty-seven papers investigating 51 echocardiographic findings were included. Meta-analysis of univariable hazard ratios (HRs) and sensitivity analysis showed that presence of pericardial effusion (pooled HR 1.70; 95% CI 1.44-1.99), right atrial area (pooled HR 1.71; 95% CI 1.38-2.13) and tricuspid annular plane systolic excursion (TAPSE; pooled HR 1.72; 95% CI 1.34-2.20) were the most well-investigated and robust predictors of mortality or transplant.

Conclusions
This meta-analysis substantiates the clinical yield of specific echocardiographic findings in the prognostication of PAH patients in day-to-day practice. In particular, pericardial effusion, right atrial area and TAPSE are of prognostic value.

Introduction

The ongoing research on pulmonary arterial hypertension (PAH) has led to increased awareness of the pathophysiological, haemodynamic and clinical consequences of this devastating disease.[1] Without intervention, progressive remodelling of the distal pulmonary arteries leads to elevated pulmonary vascular resistance, eventually resulting in right heart failure and death.[1,2] Fortunately, advances in therapeutic modalities have greatly improved the survival and quality of life in patients with PAH.[3] However, the natural course of the disease varies widely between individuals, as some patients live for decades while others die within months of diagnosis.[4] In order to guide optimal clinical management, it is therefore essential to accurately monitor disease progression and estimate prognosis in PAH.

Previously reported predictors of mortality include aetiology of PAH, gender and several functional, haemodynamic and biochemical variables.[5-8] Echocardiography is the most readily available cardiac imaging modality and is universally used in the follow-up of patients with PAH. Current literature reports several echocardiographic findings that may provide important prognostic information. The goal of this study is to provide a comprehensive overview of the most thoroughly investigated baseline echocardiographic findings that are associated with adverse clinical outcome in PAH. Separately, this study evaluates the prognostic value of a change in echocardiographic findings during a follow-up period.

Methods

This systematic review was conducted in accordance with the PRISMA statement.[9] A pre-defined review protocol, as adopted by this study, can be accessed through PROSPERO (registration number: CRD42014009231).

Literature search strategy

A comprehensive systematic search was performed in MEDLINE (via PubMed interface) and EMBASE electronic databases on 29 April 2015 using combinations of all synonyms for: PAH, echocardiography and relevant clinical outcomes (components of the Dana Point Time To Clinical Worsening composite endpoint).[1] A validated prognostic search filter with the highest sensitivity (98%) was added to the search syntax.[10] No language or publication period restrictions were applied. The full original search syntax is provided in Supplementary File 1.

Selection of papers

A flow diagram of the selection process is shown in Figure 1.[2] After deduplication, one author performed screening and selection of articles based on title and abstract, using the following exclusion criteria: inappropriate study type (cross-sectional or trial design, reviews, case reports with <10 patients, editorials or congress abstracts), non-clinical data (technical, animal and in-vitro studies), study population without PAH (e.g. acute pulmonary embolism, exercise-induced pulmonary hypertension), studies that included children <12 years, and studies that did not relate echocardiographic findings to clinical outcome. Full-text screening was performed by two authors; reasons for exclusion are described in Figure 1. All references of the excluded reviews and included articles were cross-checked to identify possible relevant articles missed in the original search syntax.

Assessment of methodological quality

Study quality was critically appraised using previously developed criteria for prognostic studies.[11] We assessed study design, missing data and loss to follow-up (selection bias), adequate description and measurement of imaging features and outcome (information bias), reported effect size, treatment of continuous risk predictors and multivariable adjustment for possible confounders.

Data extraction and analysis

Study characteristics and hazard ratios (HRs) for all investigated echocardiographic findings with accompanying 95% confidence intervals were extracted using a standardized form. Meta-analysis was performed for all echocardiographic findings that were investigated as continuous parameters by four or more studies, using random effect models. In order to unify the extracted data to allow more studies to be pooled, HRs were recalculated to one uniform clinically applicable number of units change. Heterogeneity was assessed using Cochran's Q test and the I2 statistic. Imaging findings investigated as dichotomous variables were additionally presented at the bottom of the corresponding forest plots. For all echocardiographic measurements with significant heterogeneity (I2 > 50% or Cochran's Q p -value < 0.10) a sensitivity analysis was performed by excluding specific patient subgroups.

If study data were used in multiple papers and the same echocardiographic findings were evaluated, only the study with the largest sample size was used to exclude the risk of using duplicate data in our meta-analysis. The risk of publication bias was assessed using visual inspection of funnel plots and Egger's test.

Results

Search results

The systematic literature search in MEDLINE and EMBASE and extensive reference cross-checking retrieved 2733 potentially relevant records, of which 2610 were excluded based on title and abstract (Figure 1). After full-text review of the remaining 123 articles, 37 papers were finally selected.[6, 12-47] Study and patient characteristics of the included studies are shown in Table 1.

The total number of patients per study ranged from 25 to 2716, with a mean age ranging from 31-61 years (60-98% female) and 35-100% of patients in New York Heart Association (NYHA) class III-IV. Twelve studies included patients with congenital heart disease (CHD) (6-100% of patients)[6,22,25,30,31,33,36,41-43,46,47] and seven studies included a subset of patients with pulmonary hypertension group III or IV (<30% of total study population).[18,20,29,33,35-37] The majority of studies used death or transplant as primary outcome; only five studies (14%) used a composite outcome, additionally including hospitalisation for heart failure,[20,35,41,47] need for a second vasodilator drug or worsening of functional class.[36] Mean follow-up duration varied between 11 and 53 months, with the primary outcome event occurring in 6-340 patients (10-62% of study population).

PRISMA 2009 Flow Diagram

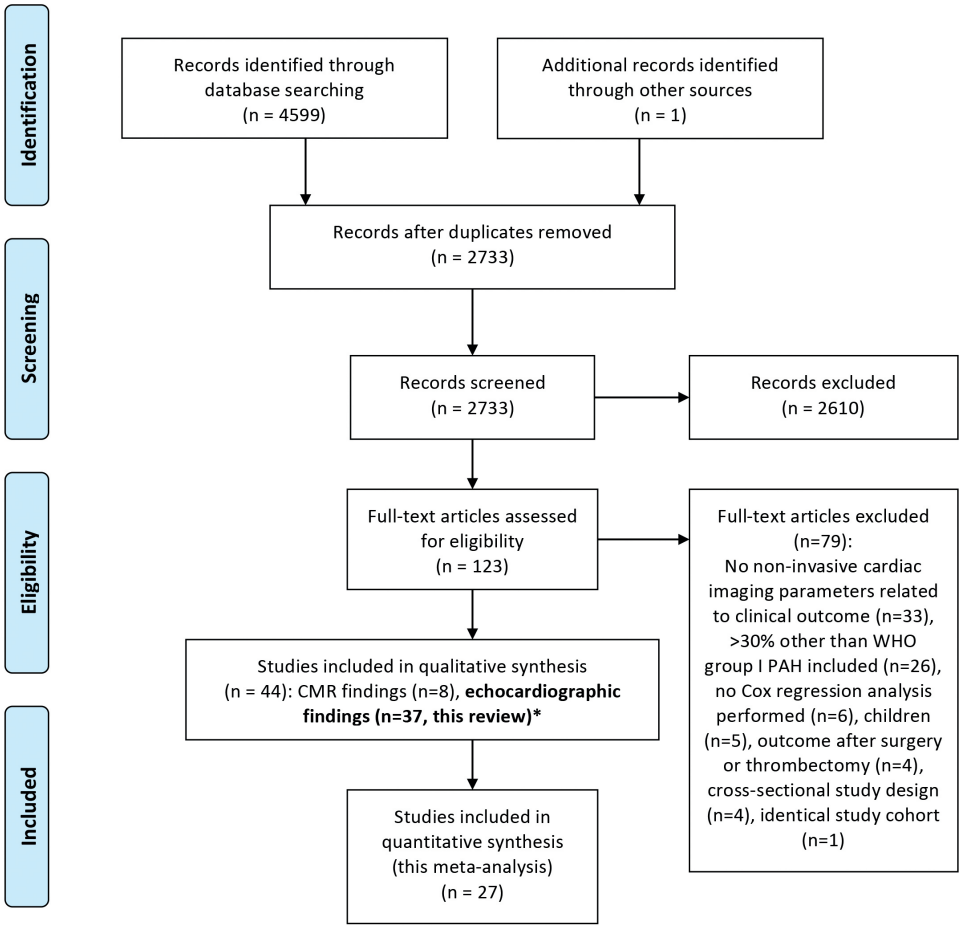

*one study investigated both echocardiographic and CMR findings.

From: Moher D, Liberati A, Tetzlaff J, Altman DG, The PRISMA Group (2009). *P*referred *R*eporting *I*tems for *S*ystematic Reviews and *M*eta-*A*nalyses: The PRISMA Statement. PLoS Med 6(6): e1000097. doi:10.1371/journal.pmed1000097

For more information, visit www.prisma-statement.org.

Figure 1. PRISMA 2009 flow diagram

Study, ref no.	Size, n	Age, years	Gender, % female	NYHA class III-IV, %	IPAH / hereditary	Drug/toxin	PAH-CTD	Po-PAH	PAH-CHD	WHO I PAH (other)	WHO III (lung disease)	WHO IV (CTEPH)	Follow-up duration, months	Events, n (%)
[11]	26	41 [16-70]	69	NR	100	_	_	_	_	_	_	_	24 ± 14	16 (62)
[12]	26	43 ± 17	73	58	100	_	_	_	_	_	_	_	NR	6 (23)
[13]	53	45 ± 14	72	70	100	_	_	_	_	_	_	_	35 [NR]	32 (60)
[14]	43	37 [14-67]	70	86	100	_	_	_	_	_	_	_	21 ± 16	12 (28)
[15]	25	38 ± 13	76	100	100	_	_	_	_	_	_	_	12 [0-84]	13 (52)
[16]	81	40 ± 15	73	100	100	_	_	_	_	_	_	_	36 ± 15	41 (51)
[17]	63	55 ± 15	83	70	37	_	38	_	_	_	21	5	19 [10-22]*	23 (37)
[18]	54	52 ± 11	76	76	100	_	_	_	_	_	_	_	50 [NR]	12 (22)
[19]	50	46 ± 13	78	42	46	_	22	_	_	4	_	28	14 [12-18]	19 (38)
[6]	2716	50 ± 17	79	54	49	5	24	5	12	5	_	_	17 [0-24]	340 (13)
[20]	76	61 ± 11	84	53	_	_	100	_	_	_	_	_	36 [NR-113]	42 (55)
[21]	32	53 ± 16	66	91	69	16	6	_	9	_	_	_	21 [NR]	17 (53)
[22]	59	46 ± 16	63	66	100	_	_	_	_	_	_	_	52 [28-79]*	23 (39)
[23]	72	52 ± 16	72	76	100	_	_	_	_	_	_	_	38 [14-71]*	22 (31)
[24]	484	52 ± 15	75	71	56	_	24	11	9	_	_	_	38 [16-60]	264 (55)
[25]	50	61 ± 11	98	70	_	_	100	_	_	_	_	_	16 [9-39]	25 (50)
[26]	80	56 ± 14	76	72	43	_	41	10	_	6	_	_	24 [NR]	33 (41)
[27]	95	31 ± 10	64	56	100	_	_	_	_	_	_	_	21 ± 15	27 (28)
[28]	57	52 ± 14	28	100	63	_	18	11	_	5	_	3	25 ± 29	29 (51)
[29]	181	39 ± 13	67	67	_	_	_	_	100	_	_	_	16 [7-46]	19 (10)
[30]	154	54 ± 9	84	NR	46	1	40	5	6	3	_	_	36 [17-71]*	71 (46)
[31]	61	48 ± 18	84	69	100	_	_	_	_	_	_	_	NR	NR
[32]	142	59 ± 15	65	44	31	9	19	4	9	1	_	27	11 [6-39]	28 (20)
[33]	577	53 ± 15	75	70	_	_	_	_	_	100	_	_	57 ± 50	NR
[34]	406	59 ± 16	65	46	_	_	_	_	_	74	14	12	16 [8-20]*	73 (18)
[35]	32	39 ± 15	69	59	22	_	16	_	53	_	_	9	14 [8-21]	15 (47)
[36]	124	54 ± 16	70	92	_	_	_	_	_	84	_	16	36 ± 22	31 (25)
[37]	71	57 ± 14	76	75	46	_	41	6	_	7	_	_	24 [NR]	20 (28)
[38]	50	56 ± 12	84	72	42	_	38	14	_	6	_	_	48 [NR]	NR
[39]	102	54 ± 16	84	NR	47	_	24	_	_	29	_	_	44 [22-79]*	43 (42)
[40]	37	46 ± 14	76	35	65	_	5	_	24	5	_	_	16 [13-18]*	7 (19)
[41]	48	44 ± 14	83	100	67	_	21	6	6	_	_	_	53 [21-80]*	18 (38)
[42]	91	42 ± 14	60	73	_	_	_	_	100	_	_	_	46 [4-64]	24 (26)
[43]	79	48 [24-65]	66	92	92	_	8	_	_	_	_	_	NR [12-92]	27 (34)
[44]	121	60 ± 14	66	63	39	_	36	18	_	6	_	_	37 ± 36	49 (40)
[45]	200	54 ± 15	71	50	47	1	33	7	12	_	_	_	43 ± 31	106 (53)
[46]	51	60 ± 15	73	71	33	_	55	6	6	_	_	_	36 ± 24	8 (16)

Table 1. Study characteristics. *CHD* congenital heart disease; *CTD* connective tissue disease; *CTEPH*, chronic thromboembolic pulmonary hypertension; *HF* heart failure; *IPAH* idiopathic pulmonary arterial hypertension; *NYHA* New York Heart Association; *PAH* pulmonary arterial hypertension; *PH* pulmonary hypertension; *SD* standard deviation; *NR* not reported; *WHO* World Health Organization. *interquartile range, otherwise reported as median [range] or mean ± SD.

Methodological aspects

In Figure 2, an overview of the methodological quality of all included studies is presented. Individual bias assessment per study is provided in Supplementary File 2. Studies prospectively included consecutive patients diagnosed with the disease (43% of studies) or retrospectively reviewed echocardiographic images. Information on missing values and loss to follow-up was not reported in 16 (43%) and 21 (57%) of the 37 studies, respectively. It is therefore important to recognize the possible impact of selection bias on individual study outcomes.

All studies used right heart catheterisation for the diagnosis of PAH in 100% of the included patients, except for one study that used right heart catheterisation in 87% and echocardiography in 13% of patients.[35] Definition and measurement of echocardiographic findings and study outcome was appropriate and consistent in the majority of studies, therefore the impact of information bias is assumed to be small.

Cox regression analysis was performed in all studies; however large differences for predictors included in the multivariable analysis were found. Twenty-nine studies performed some form of multivariable adjustment, of which only 15 adjusted for age and gender. Only nine studies (24%) used more than ten events per predictor. Because of this large variety between studies and overall poor methodological quality of multivariable adjustment, it was chosen to present only the univariable HRs in forest plots.

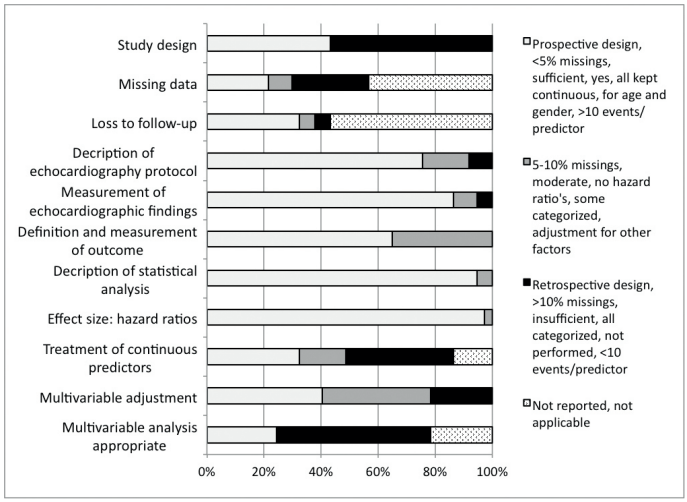

Figure 2. Methodological quality of the included studies
Methodological quality of the included studies was assessed on the following domains of potential bias: completeness of data (selection bias), standardisation of prognostic factors and study outcome (information bias) and statistical calculation of effect size (study outcome).

Prognostic value of baseline echocardiographic findings

In 37 studies, in total 51 echocardiographic findings were evaluated (Supplementary File 3). Meta-analysis was performed for ten echocardiographic findings that were suitable for pooling of results among four or more studies: presence of pericardial effusion, right atrial area, right ventricular (RV) pressure estimates, severity of tricuspid regurgitation, estimated right atrial pressure, left ventricular (LV) eccentricity index (Figure 3a), tricuspid annular plane systolic excursion (TAPSE), RV fractional area change, Tei index (an index RV myocardial performance index) and RV free wall longitudinal peak systolic strain (LPSS; Figure 3b).

Although not included in the meta-analysis, RV end-diastolic basal dimension[24,30,33,36] or area[17,25,36,37] and tissue Doppler velocity (S') of the tricuspid valve annulus[30,33,35,36,41] were investigated by several studies and could be of prognostic importance. Less investigated echocardiographic

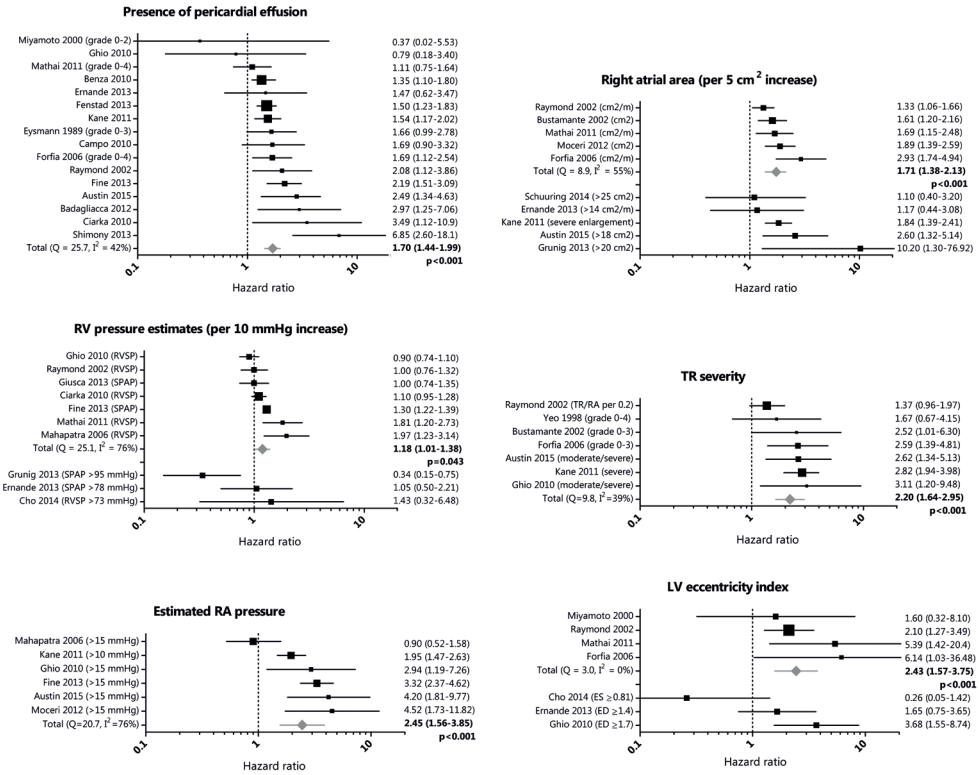

Figure 3a. Prognostic value of echocardiographic findings investigated in four or more studies

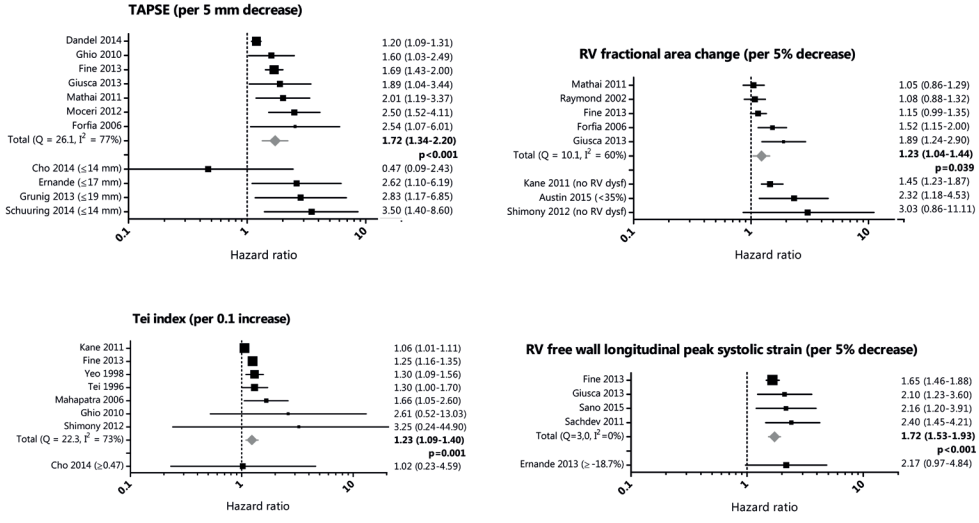

Figure 3b. Prognostic value of echocardiographic findings investigated in four or more studies

measurements such as pulmonary artery capacitance[19,35], several strain values[27,38,44], RV diastolic dysfunction[12,20,30], LV end-diastolic volume[23], systolic pulmonary artery pressure increase during exercise[37] and RV load adaptation index[44] seem promising but require further evaluation.

Serial echocardiographic evaluation

Five studies included in this review investigated the prognostic value of a change in echocardiographic findings during a follow-up period, rather than their absolute baseline values, as indicated in Supplementary File 3.[39,42,44,46,47] Patients with ≥ 5% improvement in RV free wall LPSS on PAH treatment at 6 ± 2 months follow-up had a significantly reduced mortality risk at four years (HR 0.13; 95% CI 0.03–0.50).[39] Tonelli et al. showed that overall mortality was associated with a 10% increase in RV end-diastolic area (HR 1.37; 95% CI 1.08–1.75), tricuspid regurgitation velocity (HR 1.72; 95% CI 1.12–2.70) and difference in qualitative RV function (HR per unit of improvement 0.55; 95% CI 0.31–0.96) at one-year follow-up.[42] Sano et al. recently reported that a mid-term change in RV end-systolic area (HR 0.92; 95% CI 0.86–0.98) and in right atrial area (HR 0.95; 95% CI 0.92–0.99) were significantly related to long-term outcome.[47] In addition, changes in RV load-adaptation index and pericardial effusion have been associated with clinical outcomes in PAH.[44,46]

Risk of bias assessment

Heterogeneity statistics (Cochran's Q and I^2) are presented in the corresponding forest plots in Figure 3a and Figure 3b. For all echocardiographic measurements with significant statistical heterogeneity, we performed a sensitivity analysis to evaluate possible sources for heterogeneity (Table 2). We excluded specific studies (<70% in NYHA class III-IV, <100% PAH, inclusion of CHD, <50% on PAH medication at baseline, other endpoints than mortality or transplant used) to investigate whether this impacted the pooled HR. For presence of pericardial effusion, right atrial area and TAPSE, sensitivity analysis did not change the overall conclusions. These results can therefore be regarded with a higher degree of certainty (Figure 4).

No sensitivity analysis was performed for severity of tricuspid regurgitation, LV eccentricity index and RV free wall LPSS; however the forest plots show that especially tricuspid regurgitation severity and LV eccentricity index have relatively large standard errors, and thus provide imprecise risk estimations.

A combination of visual assessment of funnel plots and Egger's test provided statistical evidence of publication bias for TAPSE (p=0.026), right atrial area (p=0.027) and the Tei index (p=0.076 and based on the funnel plot). This may indicate that studies with a positive result are overrepresented, subsequently leading to a relative overestimation of the pooled HR in the meta-analysis.

Discussion

To our knowledge, this is the first systematic review and meta-analysis on the prognostic value of specific echocardiographic findings in patients with PAH. Among 51 echocardiographic findings investigated in 37 studies, meta-analysis and additional sensitivity analysis showed that presence of pericardial effusion, right atrial area and TAPSE were the most robust predictors of mortality or transplant in patients with PAH.

Right ventricular decompensation

Most deaths in patients with PAH are due to right heart failure.[7] Once the right ventricle starts to fail, it is no longer able to overcome the high pulmonary arterial pressures. This will cause a progressive rise in RV diastolic pressure and right atrial pressure, generally accompanied by right atrial enlargement. It is thought that elevated right atrial pressure causes impaired lymphatic and venous drainage, subsequently leading to pericardial fluid accumulation.[17] These insights into the mechanistic course tilting a stable PAH state towards death clearly explain why pericardial

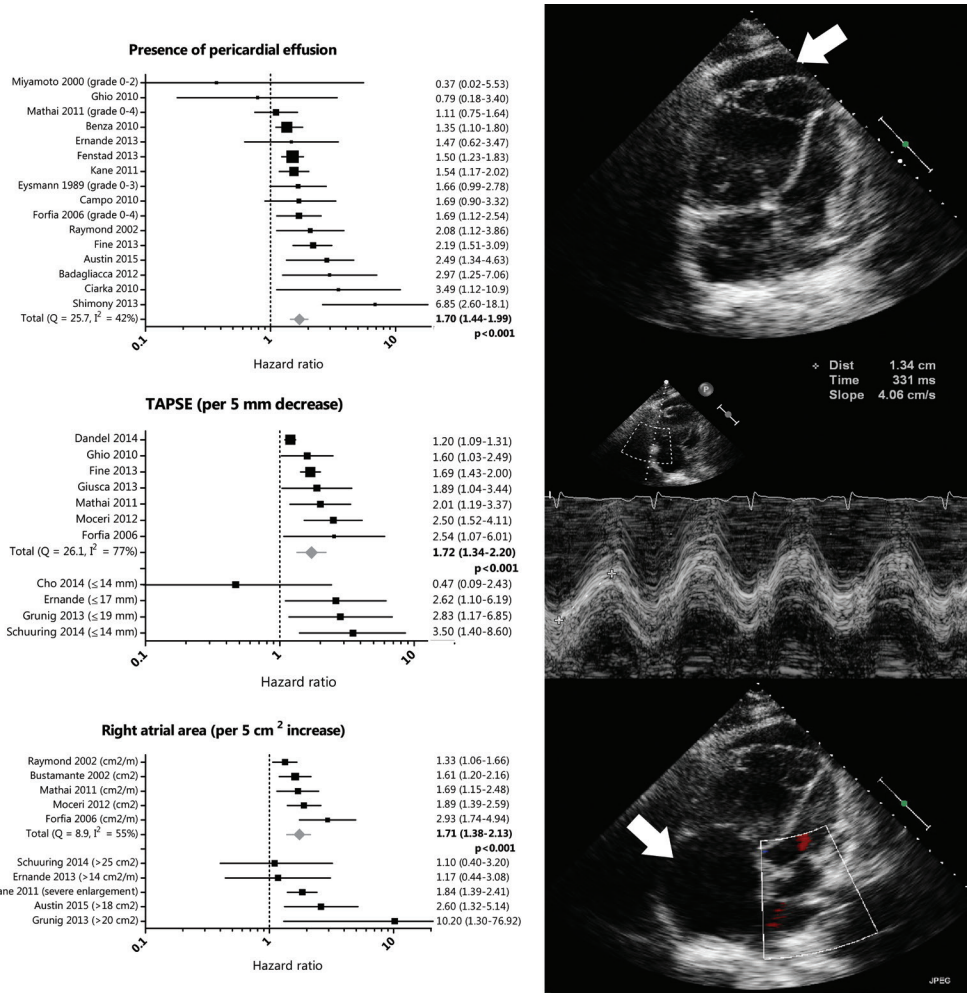

Figure 4. Key Message
Echocardiography is useful in prognostication in pulmonary arterial hypertension.
Presence of pericardial effusion, lower TAPSE and enlarged right atrial area are the most robust predictors for mortality and transplant. This is important, since accurate prognostication can aid in adequate expansion of PAH-specific therapy and timely listing for transplant.

effusion, right atrial area, estimated right atrial pressure and RV dysfunction measured on echocardiography are associated with mortality in PAH.
Studies investigating RV function and right atrial pressure as assessed with other diagnostic modalities, such as cardiac magnetic resonance imaging and right heart catheterisation, report comparable findings.[6,7,48,49] However, as echocardiography is more widely applied, non-invasive and less expensive, it is more suitable for the evaluation of PAH patients in day-to-day practice.

Serial measurements
The majority of the included studies investigated the prognostic value of baseline imaging findings, evaluated at the time of diagnosis. Complementary information on changes in haemodynamic, functional and biochemical variables may better reflect an individual's response to PAH-targeted therapy – or progression of disease.[50] Interestingly, although the first study included in this review originates from 1989, serial echocardiographic evaluation in PAH has only recently gained scientific attention, as Hardegree and colleagues were the first ones to publish on this topic in 2013.[12,39] Thus far, changes in pericardial fluid accumulation, right atrial area, tricuspid regurgitation velocity,
RV free wall LPSS and qualitative RV function, RV dimensions and RV load-adaptation index have been associated with clinical outcomes in PAH.[39,42,44,46,47] This is in line with the conclusions reached by the international working group of Vonk-Noordegraaf et al., who stated that changes in RV imaging parameters after treatment reflect altered exercise capacity and predict subsequent survival.[51] Advantages of echocardiography over more expensive or invasive imaging modalities become especially important in the serial evaluation of individual patients.

Heterogeneity
PAH prognosis depends largely on the underlying aetiology, as the right ventricle can show rapid deterioration after initial diagnosis in patients with idiopathic or connective tissue disease-PAH, while it may cope successfully with pressure overload for decades in patients with congenital heart disease.[4,6] Still, most studies in this review investigated the World Health Organisation (WHO) group I PAH as a whole. Moreover, some studies in this review additionally included small subsets (<30%) of patients with WHO group III (pulmonary hypertension due to lung disease) or IV (chronic thromboembolic pulmonary hypertension), which further increases the heterogeneity of the study population. The heterogeneity of pulmonary hypertension aetiologies among studies in this review likely plays a major role in the observed variation between the reported study results. Along the same line, disease severity and changing available treatment options over time likely contribute to this observed heterogeneity across studies. We therefore conducted a sensitivity analysis in which we excluded studies with other than WHO group I PAH, patients with CHD, <70% patients in NYHA class III-IV (thus investigating a sicker patient population) or <50% on PAH medication (representing other available treatment options). Importantly, this clearly reduced the statistical heterogeneity in specific study subgroups; however the overall conclusions for presence of pericardial effusion, right atrial area and TAPSE remained unchanged.

Study limitations
We presented only univariable HRs in this study, because of the large variety between studies in which multivariable adjustment was performed (regarding the type and number of predictors per event used). Second, formal tests for publication bias retrieved significant results for the variables

right atrial area, TAPSE and Tei index. Theoretically, publication bias may cause underreporting of non-significant HRs, leading to a relative overestimation of the pooled HRs. Exact results of the random effect models as presented in this review should be therefore interpreted with caution.

Clinical implications

In order to adequately expand PAH-specific therapy and timely list patients for transplantation, accurate prognostication is highly important. The data in this review imply that especially pericardial effusion, enlarged right atrial area and decreased TAPSE are useful echocardiographic markers to predict mortality or transplantation. This is largely concordant with the 2015 European Society of Cardiology/European Respiratory Society Guidelines for the diagnosis and treatment of pulmonary hypertension, in which right atrial area and pericardial effusion are recommended as determinants of prognosis.[2] Controversy continues to exist about the use of TAPSE; it has been suggested that progressive RV dysfunction is associated with a decline in TAPSE until a certain floor effect is reached.[52] Of note, considering the multi-faceted nature of this disease, accurate prognostication should always be based on a combination of haemodynamic, functional, biochemical and echocardiographic findings, and should not rely on just one single parameter according to the current guidelines.[2]

Conclusions

This meta-analysis substantiates the clinical yield of specific echocardiographic findings in the prognostication of PAH patients in day-to-day practice. Although accurate prognostication should not rely on just one single parameter, presence of pericardial effusion, enlarged right atrial area and decreased TAPSE are the most firmly established echocardiographic tools that can be of important additional value.

Systematic review registration number: CRD42014009231.

Table 2. Sensitivity analysis for all echocardiographic measurements with significant statistical heterogeneity (I2 >50% or p-value <0.10) in specific study subgroups.
CHD congenital heart disease; *CI* confidence interval; *FAC* fractional area change; *HR* hazard ratio; *NR* not reported; *NS* non-significant; *NYHA* New York Heart Association; *PAH* pulmonary arterial hypertension; *RV* right ventricular; *TAPSE* tricuspid annular plane systolic excursion. »

	No. of studies	HR	95% CI	p-value	I2, %	Cochran's Q (p-value)
Presence of pericardial effusion	16	1.70	1.44-1.99	<0.001	42	25.7 (0.041)
>70% NYHA class III-IV	8	1.56	1.31-1.86	<0.001	23	9.0 (0.249)
100% PAH	12	1.62	1.34-1.96	<0.001	45	20.1 (0.045)
Exclusion of CHD	12	1.81	1.45-2.25	<0.001	49	21.5 (0.028)
>50% on PAH medication / NR	10	1.86	1.40-2.47	<0.001	60	22.3 (0.008)
Mortality / transplant as outcome	15	1.64	1.39-1.94	<0.001	38	22.5 (0.069)
Right atrial area, per 5 cm2 increase	5	1.71	1.38-2.13	<0.001	55	8.9 (0.063)
>70% NYHA class III-IV	4	1.69	1.29-2.21	<0.001	61	7.8 (0.051)
100% PAH	4	1.56	1.33-1.84	<0.001	17	3.6 (0.306)
Exclusion of CHD	4	1.69	1.29-2.21	<0.001	61	7.8 (0.051)
>50% on PAH medication / NR	3	1.77	1.17-2.68	0.007	74	7.7 (0.021)
Mortality / transplant as outcome	5	1.71	1.38-2.13	<0.001	55	8.9 (0.063)
RV pressure, per 10 mmHg increase	7	1.18	1.01-1.38	0.043	76	25.1 (<0.001)
>70% NYHA class III-IV	4	1.33	1.00-1.77	NS	72	10.9 (0.012)
100% PAH	5	1.20	0.95-1.52	NS	75	15.8 (0.003)
Exclusion of CHD	5	1.26	1.00-1.59	NS	81	20.6 (<0.001)
>50% on PAH medication / NR	5	1.19	1.02-1.38	0.024	66	11.8 (0.019)
Mortality / transplant as outcome	5	1.20	0.95-1.52	NS	75	15.8 (0.003)
Right atrial pressure, >15 mmHg	6	2.45	1.56-3.85	<0.001	76	20.7 (<0.001)
>70% NYHA class III-IV	2	1.38	0.65-2.92	NS	82	5.7 (0.017)
100% PAH	6	2.45	1.56-3.85	<0.001	76	20.7 (<0.001)
Exclusion of CHD	4	2.41	1.16-4.98	0.018	82	17.0 (<0.001)
>50% on PAH medication / NR	0	-	-	-	-	-
Mortality / transplant as outcome	5	2.28	1.33-3.92	0.003	72	14.2 (0.007)
TAPSE, per 5 mm decrease	7	1.72	1.34-2.20	<0.001	77	26.1 (<0.001)
>70% NYHA class III-IV	3	1.63	1.01-2.63	0.047	69	6.5 (0.039)
100% PAH	4	1.67	1.15-2.44	0.007	77	12.8 (0.005)
Exclusion of CHD	5	1.58	1.22-2.06	<0.001	79	18.7 (<0.001)
>50% on PAH medication / NR	4	3.24	1.92-5.45	<0.001	0	1.2 (0.756)
Mortality / transplant as outcome	5	1.76	1.22-2.52	0.002	74	15.4 (0.004)
RV FAC, per 5 % decrease	5	1.23	1.04-1.44	0.039	60	10.1 (0.039)
>70% NYHA class III-IV	3	1.18	0.96-1.44	NS	60	5.0 (0.080)
100% PAH	2	1.06	1.04-1.09	<0.001	0	0.0 (0.863)
Exclusion of CHD	4	1.16	1.02-1.32	0.026	41	5.0 (0.168)
>50% on PAH medication / NR	5	1.23	1.04-1.44	0.039	60	10.1 (0.039)
Mortality / transplant as outcome	3	1.18	0.96-1.44	NS	60	5.0 (0.080)
Tei index, per 0.1 unit increase	7	1.23	1.09-1.40	0.001	73	22.3 (0.001)
>70% NYHA class III-IV	3	1.22	0.99-1.51	NS	76	8.3 (0.016)
100% PAH	6	1.25	1.05-1.48	0.012	58	12.0 (0.035)
Exclusion of CHD	5	1.46	1.24-1.72	<0.001	0	2.3 (0.677)
>50% on PAH medication / NR	2	1.25	1.16-1.35	<0.001	0	0.5 (0.775)
Mortality / transplant as outcome	6	1.25	1.05-1.48	0.012	58	12.0 (0.035)

References

1. Simonneau G, Gatzoulis MA, Adatia I, et al. Updated clinical classification of pulmonary hypertension. J Am Coll Cardiol. 2013;62:D34-41.
2. Galie N, Humbert M, Vachiery JL, et al. 2015 ESC/ERS Guidelines for the diagnosis and treatment of pulmonary hypertension: The Joint Task Force for the Diagnosis and Treatment of Pulmonary Hypertension of the European Society of Cardiology (ESC) and the European Respiratory Society (ERS): Endorsed by: Association for European Paediatric and Congenital Cardiology (AEPC), International Society for Heart and Lung Transplantation (ISHLT). Eur Respir J. 2015;46:903-75.
3. Humbert M, Lau EM, Montani D, Jais X, Sitbon O, Simonneau G. Advances in therapeutic interventions for patients with pulmonary arterial hypertension. Circulation. 2014;130:2189-208
4. McLaughlin VV, Presberg KW, Doyle RL, et al. Prognosis of pulmonary arterial hypertension. Chest. 2004;126:78S-92S.
5. Humbert M, Sitbon O, Chaouat A, et al. Survival in patients with idiopathic, familial, and anorexigen-associated pulmonary arterial hypertension in the modern management era. Circulation. 2010;122:156-63.
6. Benza RL, Miller DP, Gomberg-Maitland M, et al. Predicting survival in pulmonary arterial hypertension: insights from the Registry to Evaluate Early and Long-Term Pulmonary Arterial Hypertension Disease Management (REVEAL). Circulation. 2010;122:164-72.
7. D'Alonzo GE, Barst RJ, Ayres SM, et al. Survival in patients with primary pulmonary hypertension. Results from a national prospective registry. Ann Intern Med. 1991;115:343-9.
8. Blok IM, van Riel AC, Schuuring MJ, et al. Decrease in quality of life predicts mortality in adult patients with pulmonary arterial hypertension due to congenital heart disease. Neth Heart J. 2015;23:278-84.
9. Moher D, Liberati A, Tetzlaff J, Altman DG, Group P. Preferred reporting items for systematic reviews and meta-analyses: the PRISMA statement. Ann Intern Med. 2009;151:264-9.
10. Geersing GJ, Bouwmeester W, Zuithoff P, Spijker R, Leeflang M, Moons K. Search filters for finding prognostic and diagnostic prediction studies in Medline to enhance systematic reviews. PLoS ONE. 2012;7:e32844.
11. Hayden JA, Cote P, Bombardier C. Evaluation of the quality of prognosis studies in systematic reviews. Ann Intern Med. 2006;144:427-37.
12. Eysmann SB, Palevsky HI, Reichek N, Hackney K, Douglas PS. Two-dimensional and Doppler-echocardiographic and cardiac catheterization correlates of survival in primary pulmonary hypertension. Circulation. 1989;80:353-60.
13. Tei C, Dujardin KS, Hodge DO, et al. Doppler echocardiographic index for assessment of global right ventricular function. J Am Soc Echocardiogr. 1996;9:838-47.
14. Yeo TC, Dujardin KS, Tei C, Mahoney DW, McGoon MD, Seward JB. Value of a Doppler-derived index combining systolic and diastolic time intervals in predicting outcome in primary pulmonary hypertension. Am J Cardiol. 1998;81:1157-61.
15. Miyamoto S, Nagaya N, Satoh T, et al. Clinical correlates and prognostic significance of six-minute walk test in patients with primary pulmonary hypertension: Comparison with cardiopulmonary exercise testing. Am J Respir Crit Care Med. 2000;161:487-92.
16. Bustamante-Labarta MH, Perrone S, Leon de la Fuente R, et al. Right atrial size and tricuspid regurgitation severity predict mortality or transplantation in primary pulmonary hypertension. J Am Soc Echocardiogr. 2002;15:1160-4.
17. Raymond RJ, Hinderliter AL, Willis PW, et al. Echocardiographic predictors of adverse outcomes in primary pulmonary hypertension. J Am Coll Cardiol. 2002;39:1214-9.
18. Forfia PR, Fisher MR, Mathai SC, et al. Tricuspid annular displacement predicts survival in pulmonary hypertension. Am J Respir Crit Care Med. 2006;174:1034-41.
19. Mahapatra S, Nishimura RA, Oh JK, McGoon MD. The prognostic value of pulmonary vascular capacitance determined by doppler echocardiography in patients with pulmonary arterial hypertension. J Am Soc Echocardiogr. 2006;19:1045-50.
20. Utsunomiya H, Nakatani S, Nishihira M, et al. Value of estimated right ventricular filling pressure in predicting cardiac events in chronic pulmonary arterial hypertension. J Am Soc Echocardiogr. 2009;22:1368-74.
21. Campo A, Mathai SC, Le Pavec J, et al. Hemodynamic predictors of survival in scleroderma-related pulmonary arterial hypertension. Am J Respir Crit Care Med. 2010;182:252-60.
22. Ciarka A, Doan V, Velez-Roa S, Naeije R, Van De Borne P. Prognostic significance of sympathetic nervous system activation in pulmonary arterial hypertension. Am J Respir Crit Care Med. 2010;181:1269-75.
23. Ghio S, Klersy C, Magrini G, et al. Prognostic relevance of the echocardiographic assessment of right ventricular function in patients with idiopathic pulmonary arterial hypertension. Int J Cardiol. 2010;140:272-8.
24. Ghio S, Pazzano AS, Klersy C, et al. Clinical and prognostic relevance of echocardiographic evaluation of right ventricular geometry in patients with idiopathic pulmonary arterial hypertension. Am J Cardiol. 2011;107:628-32.
25. Kane GC, Maradit-Kremers H, Slusser JP, Scott CG, Frantz RP, McGoon MD. Integration of clinical and hemodynamic parameters in the prediction of long-term survival in patients with pulmonary arterial hypertension. Chest. 2011;139:1285-93.
26. Mathai SC, Sibley CT, Forfia PR, et al. Tricuspid annular plane systolic excursion is a robust outcome measure in systemic sclerosis-associated pulmonary arterial hypertension. J Rheumatol. 2011;38:2410-8.
27. Sachdev A, Villarraga HR, Frantz RP, et al. Right ventricular strain for prediction of survival in

patients with pulmonary arterial hypertension. Chest. 2011;139:1299-309.
28. Zeng WJ, Sun YJ, Xiong CM, Gu Q, He JG. Prognostic value of echocardiographic right/left ventricular end-diastolic diameter ratio in idiopathic pulmonary arterial hypertension. Chin Med J. 2011;124:1672-7.
29. Badagliacca R, Pezzuto B, Poscia R, et al. Prognostic factors in severe pulmonary hypertension patients who need parenteral prostanoid therapy: The impact of late referral. J Heart Lung Transplant. 2012;31:364-72.
30. Moceri P, Dimopoulos K, Liodakis E, et al. Echocardiographic predictors of outcome in eisenmenger syndrome. Circulation. 2012;126:1461-8.
31. Shimony A, Fox BD, Afilalo J, Rudski LG, Hirsch A, Langleben D. Pulmonary arterial hypertension in the elderly-clinical characteristics and long-term survival. Lung. 2012;190:645-9.
32. Tonelli AR, Plana JC, Heresi GA, Dweik RA. Prevalence and prognostic value of left ventricular diastolic dysfunction in idiopathic and heritable pulmonary arterial hypertension. Chest. 2012;141:1457-65.
33. Ernande L, Cottin V, Leroux PY, et al. Right isovolumic contraction velocity predicts survival in pulmonary hypertension. J Am Soc Echocardiogr. 2013;26:297-306.
34. Fenstad ER, Le RJ, Sinak LJ, et al. Pericardial effusions in pulmonary arterial hypertension: characteristics, prognosis, and role of drainage. Chest. 2013;144:1530-8.
35. Fine NM, Chen L, Bastiansen PM, et al. Outcome prediction by quantitative right ventricular function assessment in 575 subjects evaluated for pulmonary hypertension. Circ Cardiovasc Imaging. 2013;6:711-21.
36. Giusca S, Jurcut R, Coman IM, et al. Right ventricular function predicts clinical response to specific vasodilator therapy in patients with pulmonary hypertension. Echocardiography. 2013;30:17-26.
37. Grunig E, Tiede H, Enyimayew EO, et al. Assessment and prognostic relevance of right ventricular contractile reserve in patients with severe pulmonary hypertension. Circulation. 2013;128:2005-15.
38. Hardegree EL, Sachdev A, Fenstad ER, et al. Impaired left ventricular mechanics in pulmonary arterial hypertension identification of a cohort at high risk. Circ Heart Fail. 2013;6:748-55.
39. Hardegree EL, Sachdev A, Villarraga HR, et al. Role of serial quantitative assessment of right ventricular function by strain in pulmonary arterial hypertension. Am J Cardiol. 2013;111:143-8.
40. Shimony A, Fox BD, Langleben D, Rudski LG. Incidence and significance of pericardial effusion in patients with pulmonary arterial hypertension. Can J Cardiol. 2013;29:678-82.
41. Cho IJ, Oh J, Chang HJ, et al. Tricuspid regurgitation duration correlates with cardiovascular magnetic resonance-derived right ventricular ejection fraction and predict prognosis in patients with pulmonary arterial hypertension. Eur Heart J Cardiovasc Imaging. 2014;15:18-23.
42. Tonelli AR, Conci D, Tamarappoo BK, Newman J, Dweik RA. Prognostic value of echocardiographic changes in patients with pulmonary arterial hypertension receiving parenteral prostacyclin therapy. J Am Soc Echocardiogr. 2014;27:733-41. e2.
43. Schuuring MJ, van Riel ACMJ, Vis JC, et al. New predictors of mortality in adults with congenital heart disease and pulmonary hypertension: Midterm outcome of a prospective study. Int J Cardiol. 2015;181:270-6.
44. Dandel M, Knosalla C, Kemper D, Stein J, Hetzer R. Assessment of right ventricular adaptability to loading conditions can improve the timing of listing to transplantation in patients with pulmonary arterial hypertension. J Heart Lung Transplant. 2015;34:319-28.
45. Austin C, Alassas K, Burger C, et al. Echocardiographic assessment of estimated right atrial pressure and size predicts mortality in pulmonary arterial hypertension. Chest. 2015;147:198-208.
46. Batal O, Dardari Z, Costabile C, Gorcsan J, Arena VC, Mathier MA. Prognostic value of pericardial effusion on serial echocardiograms in pulmonary arterial hypertension. Echocardiography. 2015;32:1471-6.
47. Sano H, Tanaka H, Motoji Y, et al. Right ventricular function and right-heart echocardiographic response to therapy predict long-term outcome in patients with pulmonary hypertension. Can J Cardiol. 2015;31:529-36.
48. van Wolferen SA, Marcus JT, Boonstra A, et al. Prognostic value of right ventricular mass, volume, and function in idiopathic pulmonary arterial hypertension. Eur Heart J. 2007;28:1250-7.
49. van de Veerdonk MC, Kind T, Marcus JT, et al. Progressive right ventricular dysfunction in patients with pulmonary arterial hypertension responding to therapy. J Am Coll Cardiol. 2011;58:2511-9.
50. Nickel N, Golpon H, Greer M, et al. The prognostic impact of follow-up assessments in patients with idiopathic pulmonary arterial hypertension. Eur Respir J. 2012;39:589-96.
51. Vonk Noordegraaf A, Haddad F, Bogaard HJ, Hassoun PM. Noninvasive imaging in the assessment of the cardiopulmonary vascular unit. Circulation. 2015;131:899-913.
52. Mauritz GJ, Kind T, Marcus JT, et al. Progressive changes in right ventricular geometric shortening and long-term survival in pulmonary arterial hypertension. Chest. 2012;141:935-43.

CHAPTER 3

Advances in Cardiac Magnetic Resonance Imaging of Congenital Heart Disease

Authors:
Mieke M.P. Driessen, Johannes M.P.J. Breur, Ricardo P.J. Budde, Joep.W.M. van Oorschot, Roland R.J. van Kimmenade, Gertjan Tj. Sieswerda, Folkert J. Meijboom, Tim Leiner

Pediatr Radiol 2015;45:5-19.

Abstract

Due to advances in cardiac surgery, survival of patients with congenital heart disease has increased considerably during the past decades. Many of these patients require repeated cardiovascular magnetic resonance imaging to assess cardiac anatomy and function. In the past decade, technological advances have enabled faster and more robust cardiovascular magnetic resonance with improved image quality and spatial as well as temporal resolution. This review aims to provide an overview of advances in cardiovascular magnetic resonance hardware and acquisition techniques relevant to both pediatric and adult patients with congenital heart disease and discusses the techniques used to assess function, anatomy, flow and tissue characterization.

Introduction

Congenital heart defects (CHD) are the most frequently encountered congenital disorders.[1] The incidence of congenital heart defects reported in literature varies between 4 and 50 cases per 1,000 live births depending on the definition used.[2] Natural survival to adulthood for moderate to severe congenital heart defects – i.e. conduits, transposition of the great arteries, Tetralogy of Fallot or univentricular hearts – is less than 50%. Due to advances in cardiac surgery, survival has increased considerably during the past decades and > 96% of the patients with congenital heart defects – surviving their first year – will be alive at 16 years of age.[2, 3] Despite these advances, residual lesions requiring re-operation and complications like ventricular dysfunction and arrhythmia are prevalent in this population and require follow-up over time. Another important group in pediatric cardiology are patients with ventricular dysfunction due to a cardiomyopathy – classified as dilated, restrictive, hypertrophic, arrythomogenic or unclassified cardiomyopathy – with a cumulative incidence of about 1.24 per 100.000 children younger than 10 years of age.[4,5] The increasing number of childhood cancer survivors, expected to be one in every 540 adults in the United States, adds to this group due to anthracyclin-induced cardiotoxicity leading to left ventricular dysfunction and – in a subgroup – to dilated or restrictive cardiomyopathy.[6]
In patients with congenital heart defects and cardiomyopathies, cardiac imaging is important to diagnose the presence and extent of cardiac and extracardiac pathology, to determine the optimal treatment strategy and to provide the referring physician with a detailed overview of pre-procedural intra- and extracardiac anatomy. Although echocardiography remains the first-line imaging modality in pediatric patients, cardiac magnetic resonance imaging (MR) has become the most important subsequent imaging modality for follow-up of pediatric patients with cardiac disease. Major advantages of cardiac MR imaging over other imaging modalities such as cardiac catherization and computed tomography (CT) are that cardiac MR imaging is noninvasive, it avoids application of ionizing radiation and can provide physiological, functional and anatomical information, all within a single examination.

Challenges of cardiac magnetic resonance imaging in patients with congenital heart disease
Obtaining high-quality cardiac MR imaging examinations in pediatric patients has inherent challenges. The anatomic structures that have to be visualized are smaller, heart rates are higher and the ability to perform long and repeated breath-holds is limited. This requires the cardiac MR acquisitions to be of both higher spatial and temporal resolution than in adult patients, with short imaging times and preferably without sequential breath-holds. As spatial resolution, acquisition time and signal to noise ratio are inherently dependent on each other, higher spatial resolutions and shorter imaging times will lead to decreased signal-to-noise ratio (figure 1). Fortunately, advances in CMR hardware, acquisition techniques and image reconstruction have mitigated this tradeoff enabling high quality imaging at short acquisition times. This review aims to provide an overview of the advances in cardiac MR imaging hardware and acquisition techniques that are important for imaging pediatric and adult patients with congenital heart disease and discusses relevant advances in cardiac MR techniques used to assess function, anatomy, flow and tissue characterization (table 1).

CMR indication	New sequences
General techniques	Respiratory navigator-gating Real-time imaging
Function	3D- balanced SSFP Myocardial perfusion imaging
Anatomy	Single shot BB Non contrast enhanced MRA 4D (time-resolved) MRA
Flow	4D phase-contrast imaging
Tissue characterization	3D late gadolinium enhancement (SPIR) BB-STIR (edema) T1-mapping

Table 1: Summary of new sequences in CMR. Abbreviations: 3D= 3-dimensional; SSFP= steady-state free precession; BB= black blood; 4D= 4-dimensional; MRA= magnetic resonance angiography; PSIR= phase-sensitive inversion recovery; STIR= short-T1 inversion recovery;

Technical advances

Hardware

The most obvious change in MR hardware has been the steady introduction of higher field strengths greater than 1.5T. Many facilities worldwide have installed 3 T field strength magnets for use in cardiovascular imaging as all major vendors now offer large field-of-view capabilities with advanced transmit and receive coil arrays. Imaging at 3 T has the advantage of an intrinsically higher signal-to-noise ratio, which ameliorates the trade-off between higher spatial resolution, faster acquisitions and high signal-to-noise ratio.[7] However, imaging at higher field strengths is also associated with increased image artefacts due to inhomogeneties in the main magnetic field (B_0) and nonuniform radiofrequency excitation (B_1). Advanced radiofrequency shimming algorithms as well as adiabatic excitations have been developed to address these problems.[8]
Parallel to the introduction of high field imaging, several other developments in MR hardware have greatly impacted cardiac magnetic resonance imaging in the past decades. Improved gradient performance has enabled much shorter repetition times (TR) and image acquisition duration.[9, 10] Further improvements in gradient performance, however, are limited by physiological and safety constraints such as radiofrequency-induced heating and peripheral nerve stimulation.[11, 12]
The introduction of multi-array, highly sensitive receiver coils is another strategy that enables accelerated acquisition, while maintaining adequate signal-to-noise ratio, by using parallel imaging techniques. With parallel imaging, a reduced dataset in the phase encoding directions of k-space is acquired by using multiple coils elements simultaneously for signal reception.[13, 14] Sensitivity encoding (SENSE) and generalized autocalibrating partially parallel acquisition are the parallel imaging techniques most frequently used. These techniques are, however, fundamentally different. Generalized autocalibrating partially parallel acquisition acquires reduced data in the frequency domain – before Fourier transformation – and sensitivity encoding in the imaging domain – i.e. after Fourier transformation. The factor by which acquisition duration is reduced is roughly equal to the parallel imaging factor, depending on which parallel imaging algorithm is used. Because undersampling is inherent in parallel imaging strategies it is important to obtain a sensitivity profile of each coil element in reference to a sensitivity map of the body coil, to

avoid reconstruction artifacts. In the generalized autocalibrating partially parallel acquisition algorithm, this calibration step is integrated into the acquisition by acquiring several additional kspace lines, whereas in the sensitivity encoding algorithm the calibration is performed in a separate reference acquisition.
A final advance in MR hardware has been the introduction of small microchips that enable conversion of the analog signal picked up by the receiver coil to a digital signal in the receiver coil itself. The major advantage of this technology is the preservation of signal-to-noise, which is otherwise reduced by having to travel through receiver cables. [15]

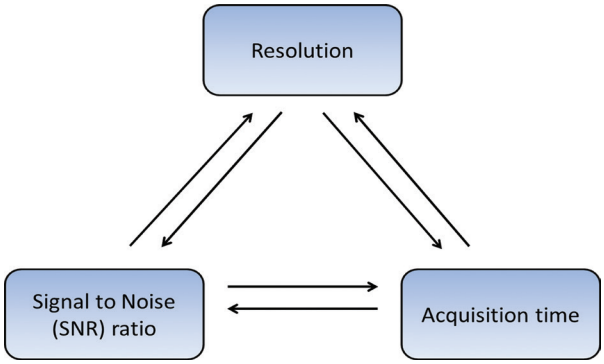

Figure 1. MR imaging constraints. With MR imaging there is an inherent trade-off in each imaging protocol between spatial and temporal resolution, acquisition time and signal-to-noise ratio. For example, increasing spatial and temporal resolution will always lead to decreased signal-to-noise ratio or longer acquisition times when all other sequence parameters are kept equal. Improving one factor will therefore always negatively influence the other unless additional adaptations are made.

Undersampled acquisition

At present, image acceleration due to advances in hardware is limited to approximately a factor of about 10, but advances in pulse sequence design have enabled further gains in imaging speed. [16] Undersampling is the most frequently applied strategy; the basic principle is that k-space is undersampled using different sampling strategies or data sharing – also called view-sharing – exploiting spatial redundancy, temporal redundancy or both. By acquiring only part of the k-space the acquisition is accelerated. Variable-density techniques are commonly used for undersampling k space. The most often used strategy is sampling the center more frequently than the peripheral k-space. As only part of k-space is filled, missing data have to be reconstructed using specific, optimized algorithms to obtain accurate and artifact-free images. Some of the most frequently used strategies include keyhole-4-D TRAK, BRISK, CURE, TRICKS, TWIST and others (Table 2). For a detailed description of these techniques, we refer to the excellent overview by Tsao and Kozerke.[16]
A recently introduced method for k-space undersampling known as compressed sensing deserves specific mention. In compressed sensing, k-space is sampled in a near-random fashion, which results in aliasing artifacts presenting as noise rather than discrete “image-like” foldover artifacts. In compressed sensing, iterative reconstruction techniques and various a priori constraints are used to suppress the noise due to aliasing, thus enabling faster and/or higher-resolution MR imaging. [17] In various studies investigators have demonstrated the synergistic benefits of parallel imaging in combination with compressed sensing in the children.[18, 19]

Motion compensation

Of particular interest in pediatric patients are techniques to compensate for patient motion. With regard to cardiac imaging, three types of motion can be distinguished: 1) cardiac motion, 2) respiratory motion and 3) bulk motion (e.g., due to the inability of the subject to lie still in one position).

For cardiac imaging, motion-free periods suitable for anatomical imaging are end systole (rest period of approximately 50 ms) or mid-diastole (variable rest period, mainly dependent on heart rate). Advanced MR imaging platforms have the ability to target both of these rest periods selectively for imaging. Note that acquisition duration can be calibrated carefully to the exact rest period duration by varying the number of k-space lines acquired (in increments of 1 TR or several ms). Thus, in contrast to CT imaging where the heart rate often needs to be adapted to the rotation time of the CT scanner by using beta-blockers, MR imaging specifically allows for tailoring the acquisition to the patients' heart rate.

The easiest way to compensate for respiratory motion is breath-holding performed by the patient. In cases where this is not possible, monitoring diaphragmatic motion with dedicated sequences offers a reliable alternative strategy, albeit at the expense of scanning efficiency.[20] Recently, several groups have proposed the idea of self-navigation, an approach whereby information about respiratory motion-induced displacement of the heart is obtained by oversampling the center of k-space relative to the peripheral part.[21-23] The main advantage of self-navigation schemes is the much better scan efficiency (up to 100% vs. approximately half this value for conventional respiratory navigator gating). The same principles employed for cardiac and respiratory motion compensation can be applied to correct for bulk motion as well. For detailed information about these techniques, the reader is referred to the excellent review on motion compensation strategies in cardiac MR imaging by Heeswijk et al.[24]

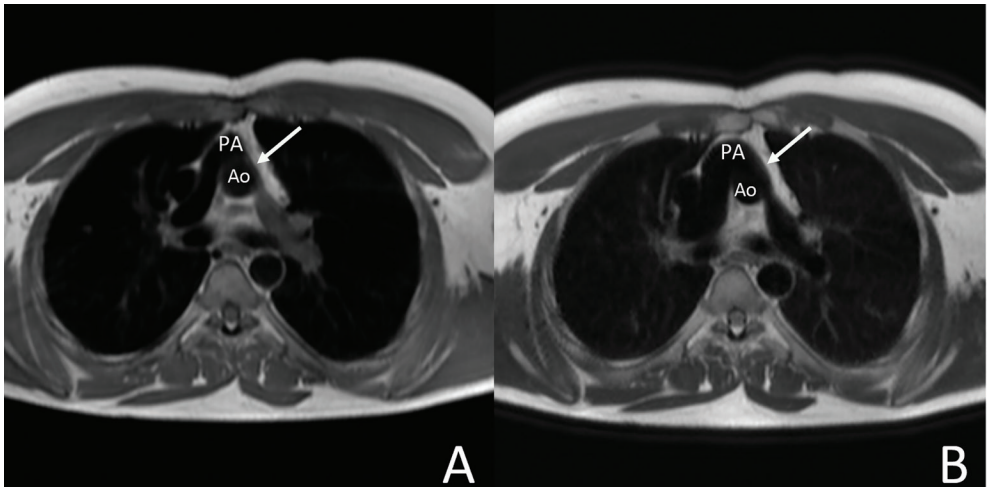

Figure 2. Black-blood imaging. Black-blood images at the level of the pulmonary bifurcation of a 22-year-old man after arterial switch operation for transposition of the great arteries. Multiple breath-hold (a) and singleshot (b) black-blood images obtained at the level of the ascending aorta both depict a stenosis of the left branch of the pulmonary artery. Multiple breath-hold (a) used a multishot turbo spin-echo sequence with scan parameters: TR/TE: 857/10 ms, flip angle 90°, matrix 212x132, acquired voxel size 1.51x2.52 mm, slice thickness 8mm, 18 slices and an acquisition duration of 120 s. For the single-shot black-blood image, a single-shot turbo spin-echo sequence was used with the following parameters: TE/TR: 857/50 ms, flip angle 90°, matrix 228x176, acquired voxel size 1.4x1.81 mm,slice thickness 8 mm, 12 slices and an acquisition duration of 11.4.

Anatomy

Black blood imaging

High-contrast black-blood images are very well suited for morphological assessment of cardiac structures. In many institutions, black-blood imaging with a standard (double inversion recovery) spin-echo pulse sequence is part of the routine imaging protocols. However, conventional black-blood imaging uses single-slice breath-holds, which is time-consuming and less favorable in children. To overcome this, various single-shot techniques, either turbo or fast spin-echo using halfscan (undersampling) with sensitivity encoding or stimulated echo acquisition mode, have been developed and validated against conventional single breath-hold black-blood techniques.[25,26] The single-shot black-blood techniques have imaging times as short as 180 msec, enabling respiratory navigator gating or single breath-hold multislice black-blood acquisitions, while maintaining high spatial resolutions (figure 2).[25]

Contrast-enhanced MR angiography

Three-dimensional contrast-enhanced MR angiography (MRA) can be considered the state-of-the-art technique for noninvasive assessment of the vasculature. The first report on feasibility of contrast-enhanced MRA in infant-like conditions was by Hernandez et al. in 2001, who simulated infant imaging conditions in small baboons. Multiphase 3-D dynamic MRA was performed using a spoiled gradient recalled-echo sequence during quiet breathing, achieving excellent image quality for the great vessels.[27] However, the imaging times were still long (average of 23s per phase) and the respiratory movement caused blurring of the images. Shorter acquisition times were achieved using the above discussed view-sharing techniques in combination with various interpolation techniques (i.e. keyhole-4-D TRAK, TWIST and TRICKS), which are very well suited for contrast-enhanced imaging. This permitted higher resolutions and time resolved – but high spatial resolution – 4-D MRA (Table 1), with almost equal signal-to-noise ratio, contrast-to-noise ratio and vessel sharpness for the great vessels as conventional single-phase 3-D MRA (Figures 3 and 4).[28] The main advantages over conventional 3-D MRA are that time-resolved MRA resolves the problem of contrast timing and adds diagnostic information such as visualization of intra- and extracardiac shunts in approximately 60% of the patients patients.[28-30] However, some smaller vascular structures might be depicted more clearly with conventional 3D single-phase MRA.[30] Therefore, both techniques are often used in clinical practice to supplement each other. As breath-hold times limit the spatial resolutions that can be obtained for MRA and motion – either cardiac or respiratory – causes blurring of the MRA images, cardiac and respiratory-gated MRA was developed as described above. In patients with congenital heart disease, ECG- and respiratory-gated high-resolution MRA resulted in significantly improved delineation of (intra) cardiac anatomical structures and image quality, and vessel sharpness was equal to first-pass MRA.[18, 30, 31] However, to achieve high contrast-to-noise ratio during these relatively long acquisitions, two out of three studies used a blood pool contrast agent and the third study – of Dabir et al. – used a higher field strength.[18,31,32]

Non-Contrast Enhanced MRA

Volume-targeted or 3-D whole heart non-contrast enhanced (NCE) MRA techniques are well suited to evaluate coronary anatomy and obstruction[33,34] or to evaluate the thoracic vasculature in infants and pediatric patients (figures 4 and 5). Free-breathing 3D radial steady-state free

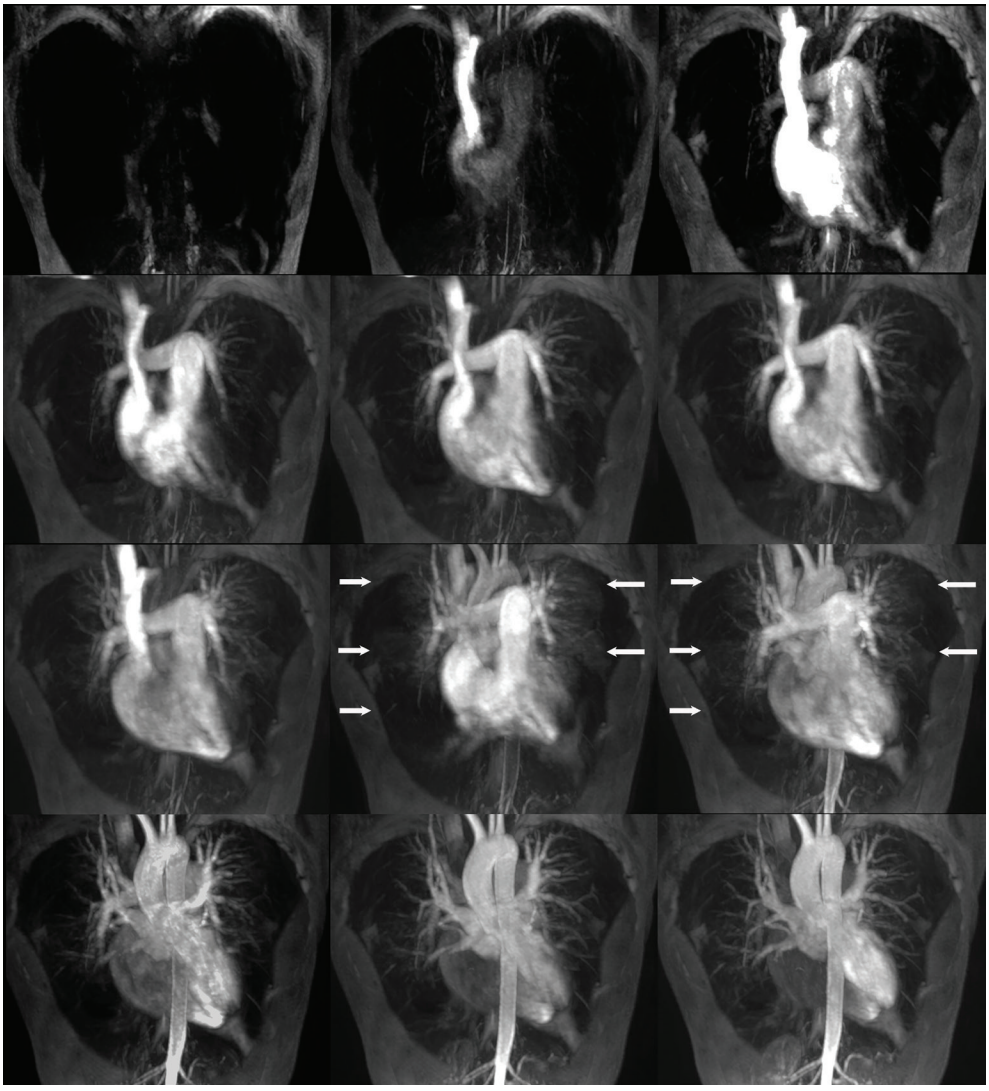

Figure 3. Four-dimensional MRA of a 21-year-old woman with chronic thrombo-embolic pulmonary hypertension shows successive full volume maximum intensity projections of a time-resolved gadolinium-enhanced MRA acquisition using a non-ECG-triggered spoiled gradient-echo sequence with SENSE (TR/TE 3.1/1.14 ms, flip angle 30°, matrix 268x267, acquired voxel size 1.49x1.49x4.6 slices, 60 slices, 12 dynamics, 3.4 s/per dynamic). There is clearly less pulmonary vascular enhancement in the right lung compared to the left lung (arrows).

precession (SSFP) using respiratory movement correction is currently the method of choice to perform NCE-MRA.[22,33,35] To achieve maximum image contrast, a T2-preperation pulse and frequency-selective fat-suppression pulse are used. Recently, Bornert et al[36] evaluated dual-echo Dixon fat suppression, which further improved image quality by delivering higher image contrast and diminishing ghosting and motion blurring. For optimal image quality, precise cardiac and respiratory gating (±2 mm) tailored to the individual patient is important. This can be hindered

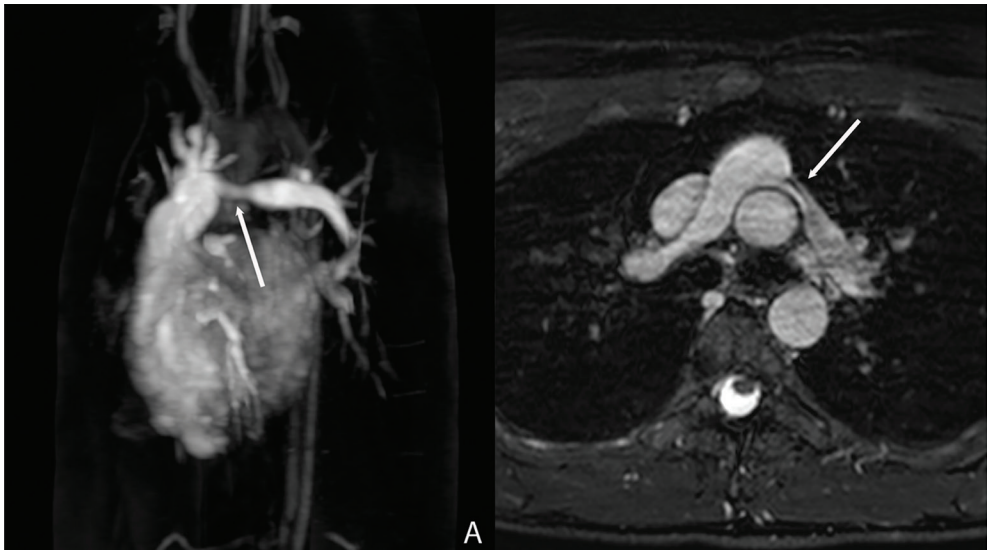

Figure 4. Gadolinium-enhanced vs. non-contrast-enhanced MRA of a 16-year-old boy after arterial switch operation with a moderately severe left pulmonary artery stenosis. a Left anterior oblique maximum intensity projection of a dynamic gadolinium-enhanced MRA using a non-ECG triggered spoiled gradient-echo sequence (TR/TE 5.2/1.49 ms, flip angle 12°, matrix 192x171, acquired voxel size 0.94x0.94x2 mm, 60 slices, 2.8 s/per dynamic). B Corresponding non-contrast-enhanced respiratory navigator-gated balanced steady-state free precession MRA (TR/TE 4.9/2.4 ms, flip angle 90°, matrix 280x176, acquired voxel size 1.25x1.25x1.50 mm and 75 slices). Trigger delay was set to the enddiastolic resting period in this patient and acquisition duration at 80 ms per cardiac cycle.

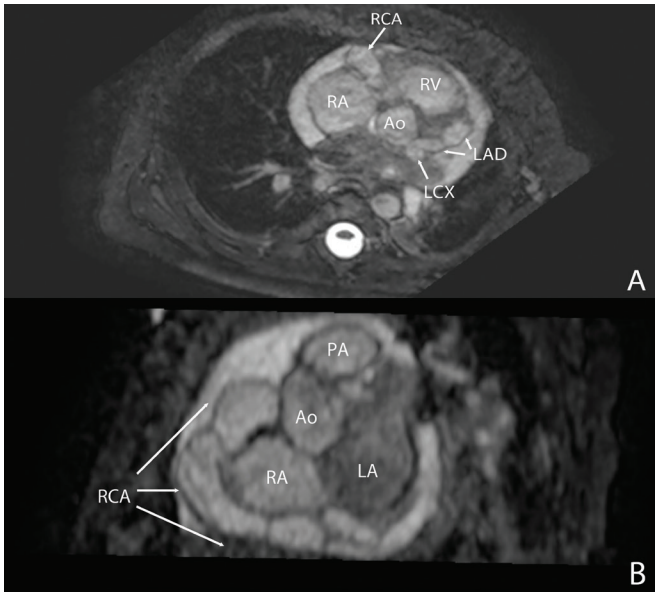

Figure5. Three-dimensional whole-heart non-contrast-enhanced (NCE) MRA in a 6-month-old boy with Kawasaki disease and grossly aneurysmatic coronary arteries. a Transverse source image at the level of the aortic root and left main coronary artery shows dilated right, left main, proximal left anterior descending and left circumflex coronary arteries (arrows). b Double oblique multiplanar reformation in left oblique sagittal orientation shows grossly dilated RCA. Note that the proximal right coronary artery has a diameter nearly equal to the aortic root (arrows; TR/TE 4.9/2.4 ms, flip angle 90°, TFE factor 16, matrix 280x176, acquired voxel size 1.25x1.25x1.50 mm and 75 slices). Because of the high heart rate the trigger delay was set to the end-systolic resting period. The acquisition duration was set to 50ms per cardiac cycle.

by heart rate variability, which decreases image quality and is especially a problem in children.[37] Generally, the imaging window is set to mid-diastolic resting period of the heart, in children – with high heart rates – this period is very short, resulting inmotion blurring of the images. To avoid this, individual adaptations of the image window should be considered, in children and infants the end systolic resting period might provide better image quality than the mid-diastolic resting period (Figure 5).

Function

B-SSFP cine imaging

Assessment of cardiac function using balanced SSFP (b-SSFP) cine imaging is one of the cornerstones of cardiovascular MR. Conventionally, single breath-hold multislice b-SSFP cine images are acquired in short-axis or axial orientation to cover the entire heart (online supplementary video), which is time-consuming and cumbersome. Starting the arrival of different acceleration techniques, single or dual breath-hold 4-D b-SSFP cine sequences have been developed using either highly parallel imaging, sensitivity encoding undersampling or compressed sensing (Figure 6).[38-40] Unfortunately, 3-D b-SSFP suffers from decreased blood-myocardial contrast and endocardial blurring, leading to underestimation of left and right ventricular volumes compared to conventional multislice techniques. To solve this, the use of intravascular contrast agents for 4-D b-SSFP was introduced, increasing image quality, blood to myocardial contrast and accuracy of volumetric measurements.[39,41] In small children, the temporal and spatial resolution that can be achieved using 4D b-SSFP might not be sufficient. To prevent multiple breath-holds in these patients, free-breathing respiratory gated multi-slice cine b-SSFP – using short echo and repetition time with multiple signal averages – can be used, which proved equally accurate as multi-slice acquisition for volumetric measurements.[42]

Myocardial perfusion CMR

In adult cardiology, ischemia detection for coronary artery disease is one of the most important diagnostic questions. Myocardial perfusion MR imaging, using first-pass contrast enhancement of the myocardium during stress (with adenosine) and rest, has an excellent sensitivity and specificity to detect coronary artery stenosis (Figure 7).[43-45] Directly following contrast, infusion images are acquired dynamically using either gradient echo, SSFP with preparation (inversion or saturation) or hybrid echo-planar imaging (EPI)-gradient echo with preparation pulse. Undersampling and parallel imaging have improved ventricular coverage and imaging times; however, specificity at 1.5 T is still hampered by low signal-to-noise ratio, contrast-to-noise ratio and darkrim artifacts.[43,46] To improve myocardial perfusion cardiovascular MR, higher field strengths (3 T) might be beneficial, as they improve signal-to-nose ratio, contrast-to-noise ratio and decrease dark-rim artifacts, improving diagnostic accuracy.[44,46] Indications to perform myocardial perfusion investigations are less widespread in the pediatric population; however, it is of supplementary value in selected patient groups (i.e. aberrant coronary arteries or after reimplantation of the coronary arteries). The few studies performed in children demonstrate that myocardial perfusion imaging is feasible in this patient group and reported no serious adverse events related to adenosine infusion.[47,48]

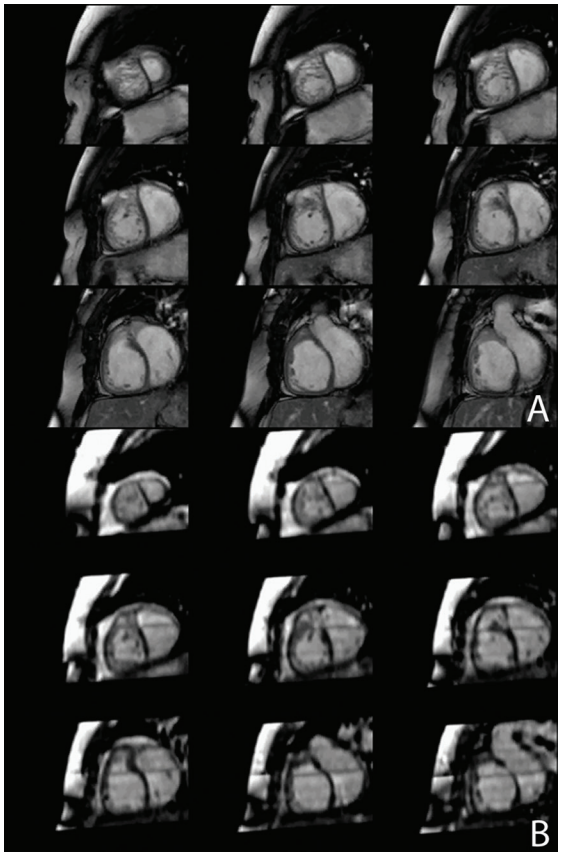

Figure 6. Dual breath-hold whole-heart cine. Conventional single breath-hold per slice 2-D cine images (a) and reconstructed dual breath-hold 3-D whole-heart cine images (b) in the short-axis orientation, obtained in a 24-yearold man with repaired Tetralogy of Fallot. Three-dimensional whole-heart cine images (b) can be retrospectively reconstructed in every desired imaging plane. However, due to the isotropic acquisition with much thinner slices compared to conventional cine imaging, there is lower in-plane spatial resolution and lower blood-to-myocardium contrast. Conventional cine images were acquired with a balanced steadystate free precession sequence (a), scan parameters: TE/TR 1.7/3.4 ms, flip angle 60°, matrix 192x183, voxel size 1.25x1.25 mm, slice thickness 8 mm, 30 cardiac phases. For the dual breath-hold whole-heart cine images (b), a balanced steady-state free precession sequence was employed with the following scan parameters: TE/TR 1.4/2.8 ms, flip angle 50°, matrix 144x144x25, voxel size 2.43x2.43x2.5 mm, 30 cardiac phases.

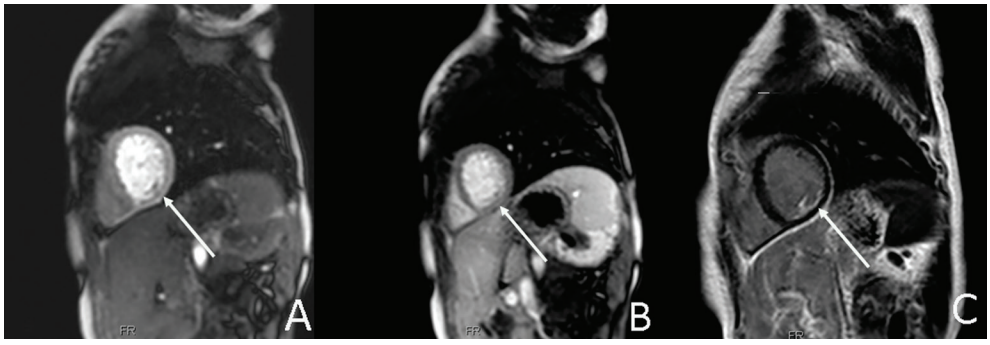

Figure 7. Myocardial perfusion in a 19-year-old woman with an anomalous left circumflex coronary artery from the pulmonary artery, which was reimplanted in the aortic root at 13 years of age. A routine follow-up nuclear myocardial perfusion scan was inconclusive and an adenosine stress myocardial perfusion cardiac magnetic resonance imaging was performed. Stress perfusion images (a) show a subendocardial perfusion defect in the mid-inferior wall, which is not seen in the matching rest perfusion images (arrows) (b). The late gadolinium enhancement image (c) shows limited subendocardial hyperenhan-cement in the same area (arrow), suggesting a mid-inferior region with subendocardial ischemia and a limited irreversible component. For myocardial perfusion imaging, a single-shot balanced-fast field echo sequence with 100 ms saturate prepulse was performed directly after ad- ministering contrast both at rest and during adenosine stress. Images were taken in short axis (3 slices), 4-chamber and 2-chamber orientation with the following scan parameters: TR/TE 2.6/1.31 ms, flip angle 50°, matrix 128x141, voxel size 2.73x2.86 mm, slice thickness 10 mm (with a gap of 9.05 mm for short-axis slices) and 60 dynamic phases.

Flow

Flow-sensitive imaging techniques allow for quantification of flow over time and are therefore useful in quantification of valve insufficiencies or shunt fractions (Qp:Qs).[49,50] Most frequently, a velocity-encoded, phase-contrast sequence is used, which is based on the principle that the phase of flowing relative to stationary spins along a magnetic gradient is proportionate to flow velocity. Velocity encoding can determine through-plane flow using phase-encoding or in-plane velocity, using frequency encoding. In case of valvular stenosis, both techniques might be used to obtain the best assessment possible. A major disadvantage of 2-D flow measurements is the inability to take into account the valve displacement during the cardiac cycle; direct measurements will

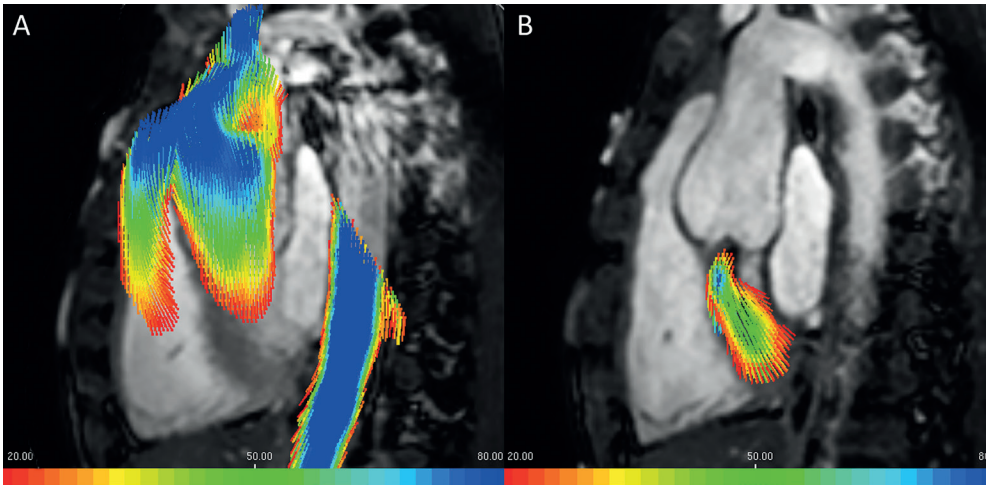

Figure 8. Four-dimensional velocity-encoded imaging. Visualization of the systolic flow patterns in the left ventricular outflow tract and ascending aorta (a), and of neo-aortic valve regurgitation (b) in a 16-year-old boy after arterial switch operation for transposition of the great arteries. A color scale is used to visualize the flow velocities recorded using 4-D velocity-encoded imaging. Images were acquired using a 3-D gradient echo with Cartesian acquisition with the following scan parameters: TR/TE 7.7/4.2 ms, flip angle 10°, matrix 108x60, acquired voxel size 3.43x3.65x3.50 mm, 18 slices using 30 phases and three directions of flow encoding.

likely underestimate the true regurgitate volumes of atrioventricular valves.[51] Furthermore, flow is measured in a single plane, underestimating eccentric regurgitations. Newer 4-D velocity-encoded phase contrast acquisitions allow for more accurate quantification of flow and regurgitant volumes and are able to visualize 3-D flow patterns (Figure 8).[52,53] Furthermore 4D velocity-encoded MR is a free-breathing technique and, using compressed sensing and parallel imaging, high spatial resolutions can be obtained (near isotropic 3 mm^3).[52,53] The high spatial resolutions even proved sufficient to accurately quantify ventricular volumes in the same 4-D dataset.[19] Furthermore, the desired slice orientation can be determined offline after acquisition. These advantages make 4-D phase contrast acquisitions very valuable in pediatric patients with congenital heart defects, in whom complex anatomy can make accurate slice orientation difficult. Disadvantages however remain the relatively long acquisition times of 5-15 minutes and the longer post-processing time.

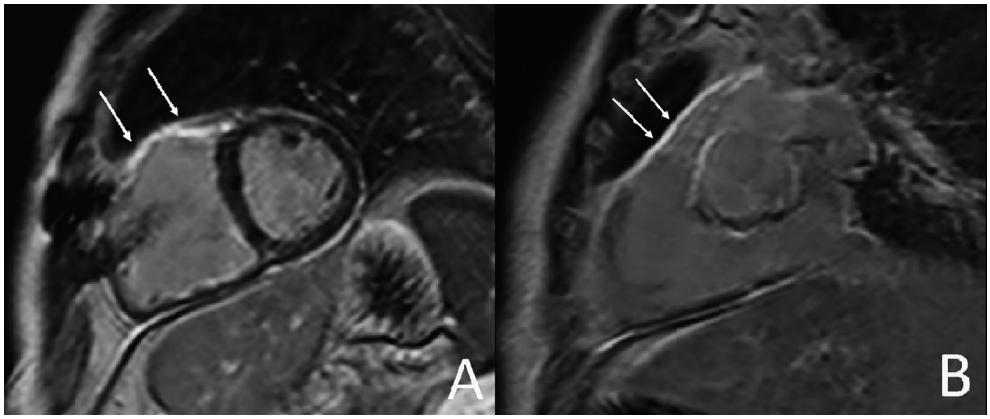

Figure 9. Conventional late gadolinium enhancement imaging in a 45-yearold patient after repair for Tetralogy of Fallot with suspected cardiac sarcoidosis. Late gadolinium enhancement imaging was performed in short axis (a) and right ventricular outflow tract view (b) 15 min after administration of 0.2 mmol/kg gadolinium contrast agent. Delayed hyperenhancement can be seen at the sight of the homograft implantation (arrows in a and b). This is a typical finding in patients after homograft implantation and is not suspect for cardiac involvement of sarcoidosis. An inversion-recovery gradient echo was performed using the following imaging parameters: TR/TE 3.5/1.15 ms, flip angle25°, matrix 160x131, acquired voxel size 2x2.44x10 mm, 10 slices.

Tissue characterization

Late gadolinium enhancement

Imaging of focal fibrosis using late gadolinium enhancement is incorporated into standard imaging protocols of both ischemic and nonischemic cardiomyopathies in many institutions. Currently, 2-D late gadolinium enhancement with (phase-sensitive) inversion-recovery (PSIR) gradient echo sequence still is the reference standard to assess viability of myocardium on cardiac MR imaging (Figure 9).[54-56] In pediatric patients, 2-D late gadolinium enhancement can be performed using respiratory gated free-breathing, achieving equal imaging quality as repeated breath-holds.[57] However, 3-D acquisition seems preferable as signal-to-noise ratio is improved for late gadolinium enhancement imaging, facilitating increased spatial resolution.[58] Without acceleration, 3-D imaging is time-consuming and artifacts may occur due to changes in inversion time and heart rate during the acquisition, both negatively influencing myocardial nulling. Compressed sensing is one of the techniques proposed to facilitate 3-D late gadolinium enhancement imaging with high isotropic spatial resolution in short acquisition time (Figure 10). The increased resolution is not only of importance for the pediatric population but was also shown to increase the success of radiofrequency ablation procedures in patients with recurrent ventricular arrhythmia. Adaptations to conventional compressed sensing have been proposed, such as low-dimensional structure self-learning and thresholding, which reduces blurring artifacts and can achieve high isotropic resolution.[59] To prevent imperfect myocardial nulling due to changes in inversion time, PSIR can be used[55] or acquisition times can be shortened by improving the efficiency of respiratory gating with for example continuously adaptive windowing strategy.[60]

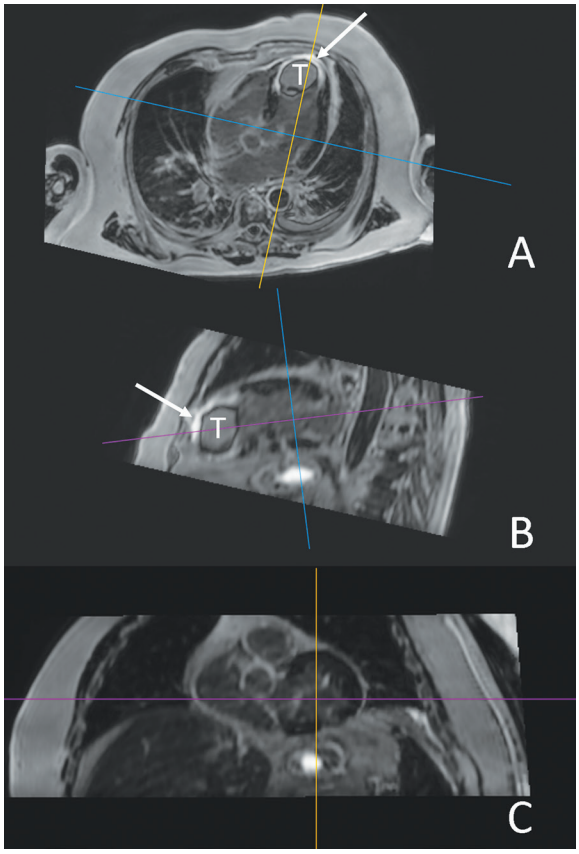

Figure 10. Near-isotropic free-breathing 3-D late gadolinium enhancement sequence. Assessment of myocardial late gadolinium enhancement and presence of thrombus in a 50-year-old uncooperative male stroke patient with severe cardiac arrhythmia. Image acquisition was done during free-breathing and 3 signals averaged to reduce motion artifacts. A 3-D inversion-recovery gradient echo sequence was employed 15 min after administration of 0.2 mmol/kg gadolinium contrast agent. Imaging parameters used were: TR/TE 3.5/1.2 ms, flip angle 25°, matrix 93x87, acquired voxel size 3.43x3.65x5.00 mm, 32 slices. In the 4-chamber orientation (a), a large thrombus is present in the left ventricular apex (marked with T), surrounded by transmurally infarcted myocardium (arrows). Because of the nearly isotropic spatial resolution reformations in the left 2-chamber (b) and short-axis orientations could be made after completion of the acquisition.

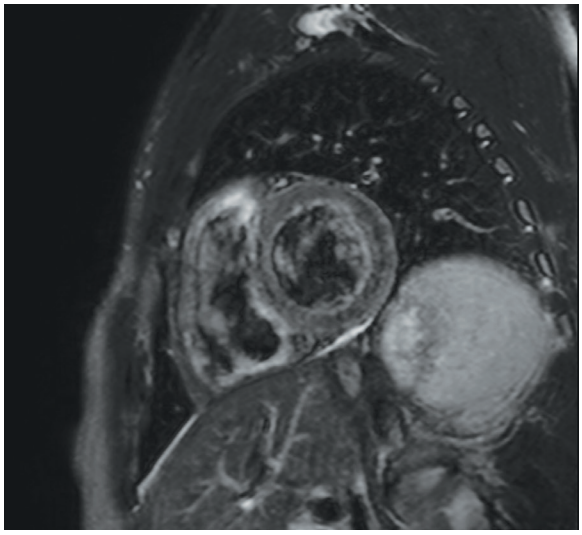

Figure 11. Myocardial edema in myocarditis in a 22-year-old man with suspected perimyocarditis. A T2-weighted short-T1 inversion (STIR) recovery sequence in short-axis orientation reveals subtle diffusely increased signal of the myocardium, which is most clearly seen when myocardial signal intensity is compared to that of skeletal muscle in the same image. The diffusely increased signal intensity indicates that there is diffuse myocardial edema, which is in line with a diagnosis of myocarditis. The following scan parameters were used: TR/TE: 2,182/100 ms, flip angle 90°, matrix 236x175, acquired voxel size 1.36x1.83 mm, slice thickness 8 mm, 15 slices

Myocardial edema

Imaging of acute myocardial edema using cardiac MR imaging was described as early as 1991 by Gagliardi et al.[9], demonstrating altered signal intensity using T2-weighted spin-echo sequences in the presence of myocarditis. Short-tau-inversion recovery (STIR) black-blood technique proved superior to T2-weighted spin-echo for musculoskeletal and abdominal MR and was introduced for cardiac imaging 1996 by Simonetta et al.[61] They demonstrated that STIR can generate myocardial images which are highly sensitive to changes in tissue relaxation times, with minimum flow and motion artifacts (Figure 11). Although introduced in the 1990s, it was not until 2004 that STIR was validated in a larger group of patients to establish its sensitivity to distinguish acute (myocardial edema) from chronic (fibrosis) myocardial infarction, with success.[10] The same research group tested the diagnostic value of a comprehensive cardiac MR imaging protocol to diagnose myocarditis, using presence of early relative enhancement (gRE), presence of late gadolinium enhancement and high signal intensity – relative to skeletal muscle – on T2-weighted black-blood STIR, as diagnostic criteria.[62] The highest diagnostic accuracy was achieved if all three were combined and ≥ 2 features were positive, which was later adapted to the Lake Louise consensus criteria for suspected myocarditis on CMR.[63,64] However, black-blood STIR has some important limitations such as signal dropout, slow-flow blood artifacts, image quality impairment in tachycardia (or normal high heart rate in children) and lower signal-to-noise ratio. To achieve optimal image contrast and quality STIR sequence, parameters should be chosen carefully with special regard for timing and design of the pulse sequence, quality of the TSE readout pulses, bandwidth and slice thickness. To improve the robustness and clinical applicability of edema imaging on cardiac MR imaging, noncontrast sequences have been developed over the past years. Aletras et al. propose Acquisition for Cardiac Unified T2 Edema (ACUT2E), a combined TSE-SFFP approach to achieve optimal CNR, signal-to-noise ratio and image quality to depict acute myocardial infarction with a reduction of artifacts, although the absolute T2 values are systematically overestimated with this method.[65] Furthermore, noncontrast T1 mapping (also see below) was compared to both conventional black-blood STIR and ACUT2E TSE-SSFP and yielded a higher diagnostic accuracy to detect acute myocardial infarction, even though more regions were affected by artifacts. The higher diagnostic accuracy is likely the result of eliminating the need to compare myocardium to a remote reference region of interest, which is mandatory for both black-blood STIR and ACUT2E.[66] Other advantages of T1 mapping include that it is robust to tachycardia and breath-holds are considerably shorter, making it advantageous for children.

T1 mapping

After the success of late gadolinium enhancement for imaging of focal fibrosis, much attention was directed to noninvasive quantification of diffuse myocardial fibrosis in the past decade. This process is presumed to be accelerated in many congenital and non-congenital cardiac diseases.[67] Multiple cardiac MR imaging methodologies have been developed to quantify diffuse myocardial fibrosis, using T1 mapping with or without contrast administration. First, a new imaging sequence was developed by Messroghli and colleagues to overcome the limitations of the conventional look-locker approach, the modified look-locker inversion recovery (MOLLI), which was later modified into shortened-MOLLI, both facilitating high-resolution T1 maps of the human myocardium within a single breath-hold.[68,69] The first clinically applicable cardiac MR imaging method was validated against myocardial biopsy in 2010 by Flett and colleagues, using equilibrium-contrast cardiac MR imaging with a standard MOLLI acquired before and after contrast equilibrium.[70]

The theory behind this method is that at contrast equilibrium, the extracellular gadolinium concentration is equal in blood and myocardium and the extracellular volume fraction of the myocardium can be determined, which correlates well to collagen volume fraction on biopsy. However, although accurate and highly repeatable, time to contrast equilibrium is relatively long and multiple breath-holds are required making this a complex and time-consuming technique, especially if used in children.[70] Several solutions were developed in the past years to shorten and simplify acquisition. First, to simplify the contrast protocol a bolus-only technique – assuming dynamic equilibrium – was designed. Both contrast protocols – bolus vs. continuous infusion – were compared to each other and to histological results by White and colleagues.[71] The bolus-only proved equally accurate in estimating ECV, provided total ECV fraction was less than 0.4.[71] Extent of diffuse myocardial fibrosis, measured by bolus or equilibrium-contrast T1 mapping, has since been linked to decreased functional status and outcome in several pathologies, including congenital heart disease and childhood cancer survivors.[72-74] To further simplify the acquisition, a third contrast protocol was investigated by Miller and colleagues, using isolated postcontrast myocardial T1 measurement. In their study, isolated post bolus-contrast T1 measurement and extracellular volume fraction estimation using pre- and post-bolus contrast T1 mapping was compared to histology, they conclude that isolated postcontrast T1 measurement is insufficient to reliably estimate extracellular volume fraction.[75] Finally, a protocol not requiring contrast administration, non-contrast T1 mapping, was used to image diffuse myocardial fibrosis. It was compared to histology in patients with aortic stenosis and, although it only moderately correlated to collagen content measured on histology, T1 mapping was able to differentiate healthy from diseased and was related to the severity of aortic stenosis.[76] Following the rapid innovations in the area of quantification of extracellular volume fraction and T1 mapping, the cardiac MR imaging working group of the European Society of Cardiology and the Society of Cardiovascular Magnetic Resonance recently released a consensus statement. In accordance with the above stated, they observe that extracellular volume fraction measurement appears to be more accurate than isolated post-contrast T1 measurement (Figure 12). Furthermore, they state that a bolus-only approach with at least 15-min delay is sufficient for most myocardial extracellular volume fraction applications.[77]

Imaging of stents and intracardiac devices

In patients with congenital heart disease, interventional devices and stents are increasingly used to decrease the need for surgery and increase convenience of the patient. Khan et al.[78] researched the disruption caused by the interventional devices and the influence of type of pulse sequence and field strength. Although signal void in the immediate vicinity of the device was common, significant disruption of surrounding tissue was only seen for the stainless steel Flipper detachable embolization coil. Field strength and pulse sequence type did not significantly influence image disruption or signal void.[78] Nordmeyer et al. investigated the diagnostic accuracy of CT angiography and different cardiac magnetic resonance imaging sequences compared to conventional angiography to assess patency and re-stenosis of nitinol, platinum-iridium and stainless steel stents. Combining high flip angle gradient recalled echo, SSFP and high flip angle MRA resulted in high diagnostic accuracy for nitinol and platinum-iridium stents. For stainless steel stents the diagnostic accuracy compared to angiography was slightly lower due to large penumbra of signal loss.[79]

Hybrid cardiac catheterizations, combining radiographic and MR imaging to accurately address

clinical questions, are being performed for both diagnostic and interventional purposes. An obvious advantage of MR guiding is decreased radiation exposure, which predisposes to development of cancer, especially when radiation is imposed on smaller infants.[80] Other advantages include improved visualization of soft tissue and cardiac structures and the ability to combine invasive pressure measurements with flow quantification performed on cardiac MR imaging, ensuring accurate assessment of the hemodynamics and pulmonary vascular resistance.[81] The development of catheters is ongoing, currently passive guidewires – not actively conveying signals to the cardiac magnetic resonance imaging scanner – are used for such guided catheterizations, as active wires carry a risk of heating. Recently, a compatible and safe guidewire for MR imaging was developed and the first studies in children are currently being conducted.[81]

Conclusions

Patients with congenital heart disease increasingly survive into adulthood and are in need of repeated high-quality cardiac MR imaging throughout life. The technical advances as outlined above enable high-fidelity assessment of anatomical as well as functional parameters and tissue characterization in short imaging times and underscore the preferential role of cardiac MR imaging as comprehensive cardiac imaging technique of first choice.

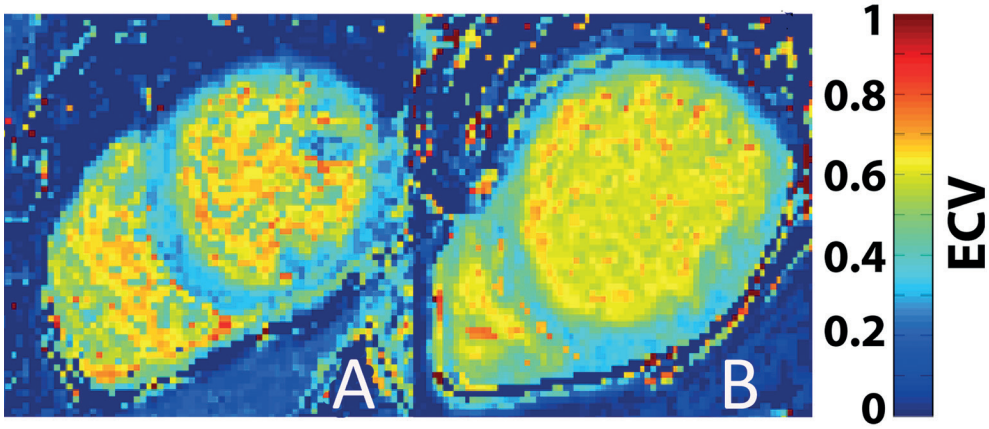

Figure 12. T1 mapping and extracellular volume measurement. Examples illustrate extracellular volume maps in a patient with no abnormalities (a) and a patient with dilated cardiomyopathy (b). Note the larger extracellular volume fraction in the patient with dilated cardiomyopathy. Extracellular volume maps were obtained by acquiring two separate T1 maps with the modified look-locker 3–5 sequence: a single-shot balanced FFE readout (TR/TE 3.2/1.17 ms, flip angle 35°, matrix 288x288, acquired voxel 2x2x8 mm, 3 slices, SENSE=1.5). One map was obtained before contrast injection, and the second was acquired 15 min after bolus injection of 0.2 ml/kg contrast agent.

Online supplementary video: Conventional single breath-hold per slice 2D cine images in a 21-year old healthy female oriented from base (top left) to apex (bottom left) in the short axis orientation. Images were acquired using a balanced steady state free precession sequence, scan parameters: TE/TR 1.7/3.4 ms, flip angle 60°, matrix 192x183, voxel size 1.25x1.25 mm, slice thickness 8 mm, 30 cardiac phases. *https://link.springer.com/article/10.1007%2Fs00247-014-3067-0*

References

1. Tennant PW, Pearce MS, Bythell M, Rankin J. 20-Year Survival of Children Born with Congenital Anomalies: a Population-Based Study. Lancet 2010;375:649-656.
2. van der Bom T, Bouma BJ, Meijboom FJ, Zwinderman AH, Mulder BJ. The prevalence of adult congenital heart disease, results from a systematic review and evidence based calculation. Am Heart J 2012;164:568-575.
3. Wren C, O'Sullivan JJ. Survival with congenital heart disease and need for follow up in adult life. Heart 2001;85:438-443.
4. Towbin JA, Lowe AM, Colan SD, et al. Incidence, causes, and outcomes of dilated cardiomyopathy in children. JAMA 2006;296:1867-1876.
5. Nugent AW, Daubeney PE, Chondros P, et al. The epidemiology of childhood cardiomyopathy in Australia. N Engl J Med 2003;348:1639-1646.
6. Lipshultz SE, Lipsitz SR, Sallan SE, et al. Chronic progressive cardiac dysfunction years after doxorubicin therapy for childhood acute lymphoblastic leukemia. J Clin Oncol 2005;23:2629-2636.
7. Hinton DP, Wald LL, Pitts J, Schmitt F. Comparison of cardiac MRI on 1.5 and 3.0 Tesla clinical whole body systems. Invest Radiol 2003;38:436-442.
8. Dietrich O, Reiser MF, Schoenberg SO. Artifacts in 3-T MRI: physical background and reduction strategies. Eur J Radiol 2008;65:29-35.
9. Gagliardi MG, Bevilacqua M, Di Renzi P, Picardo S, Passariello R, Marcelletti C. Usefulness of magnetic resonance imaging for diagnosis of acute myocarditis in infants and children, and comparison with endomyocardial biopsy. Am J Cardiol 1991;68:1089-1091.
10. Abdel-Aty H, Zagrosek A, Schulz-Menger J, et al. Delayed enhancement and T2-weighted cardiovascular magnetic resonance imaging differentiate acute from chronic myocardial infarction. Circulation 2004;109:2411-2416.
11. Cohen MS, Weisskoff RM, Rzedzian RR, Kantor HL. Sensory stimulation by time-varying magnetic fields. Magn Reson Med 1990;14:409-414.
12. Budinger TF, Fischer H, Hentschel D, Reinfelder HE, Schmitt F. Physiological effects of fast oscillating magnetic field gradients. J Comput Assist Tomogr 1991;15:909-914.
13. Pruessmann KP, Weiger M, Scheidegger MB, Boesiger P. SENSE: sensitivity encoding for fast MRI. Magn Reson Med 1999;42:952-962.
14. Sodickson DK, Manning WJ. Simultaneous acquisition of spatial harmonics (SMASH): fast imaging with radiofrequency coil arrays. Magn Reson Med 1997;38:591-603.
15. Leiner T, Habets J, Versluis B, et al. Subtractionless first-pass single contrast medium dose peripheral MR angiography using two-point Dixon fat suppression. Eur Radiol 2013;23:2228-2235.
16. Tsao J, Kozerke S. MRI temporal acceleration techniques. J Magn Reson Imaging 2012;36:543-560.
17. Lustig M, Donoho D, Pauly JM. Sparse MRI: The application of compressed sensing for rapid MR imaging. Magn Reson Med 2007;58:1182-1195.
18. Vasanawala SS, Chan FP, Newman B, Alley MT. Combined respiratory and cardiac triggering improves blood pool contrast-enhanced pediatric cardiovascular MRI. Pediatr Radiol 2011;41:1536-1544.
19. Hsiao A, Lustig M, Alley MT, et al. Rapid pediatric cardiac assessment of flow and ventricular volume with compressed sensing parallel imaging volumetric cine phase-contrast MRI. AJR Am J Roentgenol 2012;198:W250-9.
20. Stuber M, Botnar RM, Danias PG, et al. Double-oblique free-breathing high resolution three-dimensional coronary magnetic resonance angiography. J Am Coll Cardiol 1999;34:524-531.
21. Lai P, Larson AC, Park J, Carr JC, Li D. Respiratory self-gated four-dimensional coronary MR angiography: a feasibility study. Magn Reson Med 2008;59:1378-1385.
22. Stehning C, Bornert P, Nehrke K, Eggers H, Stuber M. Free-breathing whole-heart coronary MRA with 3D radial SSFP and self-navigated image reconstruction. Magn Reson Med 2005;54:476-480.
23. Spincemaille P, Nguyen TD, Prince MR, Wang Y. Kalman filtering for real-time navigator processing. Magn Reson Med 2008;60:158-168.
24. van Heeswijk RB, Bonanno G, Coppo S, Coristine A, Kober T, Stuber M. Motion compensation strategies in magnetic resonance imaging. Crit Rev Biomed Eng 2012;40:99-119.
25. Vignaux OB, Augui J, Coste J, et al. Comparison of single-shot fast spin-echo and conventional spin-echo sequences for MR imaging of the heart: initial experience. Radiology 2001;219:545-550.
26. Karaus A, Merboldt KD, Graessner J, Frahm J. Black-blood imaging of the human heart using rapid stimulated echo acquisition mode (STEAM) MRI. J Magn Reson Imaging 2007;26:1666-1671.
27. Hernandez RJ, Strouse PJ, Londy FJ, Wakefield TW. Gadolinium-enhanced MR angiography (Gd-MRA) of thoracic vasculature in an animal model using double-dose gadolinium and quiet breathing. Pediatr Radiol 2001;31:589-593.
28. Vogt FM, Theysohn JM, Michna D, et al. Contrast-enhanced time-resolved 4D MRA of congenital heart and vessel anomalies: image quality and diagnostic value compared with 3D MRA. Eur Radiol 2013;23:2392-2404.
29. Young PM, McGee KP, Pieper MS, et al. Tips and tricks for MR angiography of pediatric and adult congenital cardiovascular diseases. AJR Am J Roentgenol 2013;200:980-988.
30. Fenchel M, Saleh R, Dinh H, et al. Juvenile and adult congenital heart disease: time-resolved 3D contrast-enhanced MR angiography. Radiology 2007;244:399-410.
31. Dabir D, Naehle CP, Clauberg R, Gieseke J, Schild HH, Thomas D. High-resolution motion compensated MRA in patients with congenital heart disease using extracellular contrast agent at 3 Tesla. J Cardiovasc Magn Reson 2012;14:75-429X-14-75.
32. Naehle CP, Kaestner M, Muller A, et al. First-pass and steady-state MR angiography of thoracic vasculature in children and adolescents. JACC

Cardiovasc Imaging 2010;3:504-513.
33. Yoon YE, Kitagawa K, Kato S, et al. Prognostic value of coronary magnetic resonance angiography for prediction of cardiac events in patients with suspected coronary artery disease. J Am Coll Cardiol 2012;60:2316-2322.
34. Kato S, Kitagawa K, Ishida N, et al. Assessment of coronary artery disease using magnetic resonance coronary angiography: a national multicenter trial. J Am Coll Cardiol 2010;56:983-991.
35. Greenwood JP, Maredia N, Radjenovic A, et al. Clinical evaluation of magnetic resonance imaging in coronary heart disease: the CE-MARC study. Trials 2009;10:62-6215-10-62.
36. Bornert P, Koken P, Nehrke K, Eggers H, Ostendorf P. Water/fat-resolved whole-heart Dixon coronary MRA: An initial comparison. Magn Reson Med 2014;71:156-163.
37. Leiner T, Katsimaglis G, Yeh EN, et al. Correction for heart rate variability improves coronary magnetic resonance angiography. J Magn Reson Imaging 2005;22:577-582.
38. Jaroni J, Meier R, Beer A, et al. Three-dimensional Magnetic Resonance Imaging Using Single Breath-hold k-t BLAST for Assessment of Global Left Ventricular Functional Parameters. Acad Radiol 2013;20:987-994.
39. Parish V, Hussain T, Beerbaum P, et al. Single breath-hold assessment of ventricular volumes using 32-channel coil technology and an extracellular contrast agent. J Magn Reson Imaging 2010;31:838-844.
40. Stralen van M, Habets J, Driessen M, El Aidi H, Pluim J, Leiner T. Dual Breath-Hold 3D Whole Heart Cine Cardiac MRI: Feasibility and Initial Experience [Abstract 3843]. ISMRM 2012.
41. Makowski MR, Wiethoff AJ, Jansen CH, et al. Single breath-hold assessment of cardiac function using an accelerated 3D single breath-hold acquisition technique--comparison of an intravascular and extravascular contrast agent. J Cardiovasc Magn Reson 2012;14:53-429.
42. Bellenger NG, Gatehouse PD, Rajappan K, Keegan J, Firmin DN, Pennell DJ. Left ventricular quantification in heart failure by cardiovascular MR using prospective respiratory navigator gating: comparison with breath-hold acquisition. J Magn Reson Imaging 2000;11:411-417.
43. Coelho-Filho OR, Rickers C, Kwong RY, Jerosch-Herold M. MR myocardial perfusion imaging. Radiology 2013;266:701-715.
44. Ebersberger U, Makowski MR, Schoepf UJ, et al. Magnetic resonance myocardial perfusion imaging at 3.0 Tesla for the identification of myocardial ischaemia: comparison with coronary catheter angiography and fractional flow reserve measurements. Eur Heart J Cardiov Imaging 2013;14:1174-80.
45. Watkins S, McGeoch R, Lyne J, et al. Validation of magnetic resonance myocardial perfusion imaging with fractional flow reserve for the detection of significant coronary heart disease. Circulation 2009;120:2207-2213.
46. Cheng AS, Pegg TJ, Karamitsos TD, et al. Cardiovascular magnetic resonance perfusion imaging at 3-tesla for the detection of coronary artery disease: a comparison with 1.5-tesla. J Am Coll Cardiol 2007;49:2440-2449.
47. Manso B, Castellote A, Dos L, Casaldaliga J. Myocardial perfusion magnetic resonance imaging for detecting coronary function anomalies in asymptomatic paediatric patients with a previous arterial switch operation for the transposition of great arteries. Cardiol Young 2010;20:410-417.
48. Prakash A, Powell AJ, Krishnamurthy R, Geva T. Magnetic resonance imaging evaluation of myocardial perfusion and viability in congenital and acquired pediatric heart disease. Am J Cardiol 2004;93:657-661.
49. 49. Dulce MC, Mostbeck GH, O'Sullivan M, Cheitlin M, Caputo GR, Higgins CB. Severity of aortic regurgitation: interstudy reproducibility of measurements with velocity-encoded cine MR imaging. Radiology 1992;185:235-240.
50. Brenner LD, Caputo GR, Mostbeck G, et al. Quantification of left to right atrial shunts with velocity-encoded cine nuclear magnetic resonance imaging. J Am Coll Cardiol 1992;20:1246-1250.
51. Fujita N, Chazouilleres AF, Hartiala JJ, et al. Quantification of mitral regurgitation by velocity-encoded cine nuclear magnetic resonance imaging. J Am Coll Cardiol 1994;23:951-958.
52. Westenberg JJ, Roes SD, Ajmone Marsan N, et al. Mitral valve and tricuspid valve blood flow: accurate quantification with 3D velocity-encoded MR imaging with retrospective valve tracking. Radiology 2008;249:792-800.
53. Hsiao A, Lustig M, Alley MT, Murphy MJ, Vasanawala SS. Evaluation of valvular insufficiency and shunts with parallel-imaging compressed-sensing 4D phase-contrast MR imaging with stereoscopic 3D velocity-fusion volume-rendered visualization. Radiology 2012;265:87-95.
54. Kim RJ, Fieno DS, Parrish TB, et al. Relationship of MRI delayed contrast enhancement to irreversible injury, infarct age, and contractile function. Circulation 1999;100:1992-2002.
55. Kellman P, Arai AE, McVeigh ER, Aletras AH. Phase-sensitive inversion recovery for detecting myocardial infarction using gadolinium-delayed hyperenhancement. Magn Reson Med 2002;47:372-383.
56. Kim RJ, Wu E, Rafael A, et al. The use of contrast-enhanced magnetic resonance imaging to identify reversible myocardial dysfunction. N Engl J Med 2000;343:1445-1453.
57. Goldfarb JW, Shinnar M. Free-breathing delayed hyperenhanced imaging of the myocardium: a clinical application of real-time navigator echo imaging. J Magn Reson Imaging 2006;24:66-71.
58. Peters DC, Appelbaum EA, Nezafat R, et al. Left ventricular infarct size, peri-infarct zone, and papillary scar measurements: A comparison of high-resolution 3D and conventional 2D late gadolinium enhancement cardiac MR. J Magn Reson Imaging 2009;30:794-800.
59. Akcakaya M, Rayatzadeh H, Basha TA, et al. Accelerated late gadolinium enhancement cardiac MR imaging with isotropic spatial resolution using compressed sensing: initial experience. Radiology 2012;264:691-699.
60. Keegan J, Jhooti P, Babu-Narayan SV, Drivas P, Ernst

S, Firmin DN. Improved respiratory efficiency of 3D late gadolinium enhancement imaging using the continuously adaptive windowing strategy (CLAWS). Magn Reson Med 2014;71:1064-1074.
61. Simonetti OP, Finn JP, White RD, Laub G, Henry DA. "Black blood" T2-weighted inversion-recovery MR imaging of the heart. Radiology 1996;199:49-57.
62. Abdel-Aty H, Boye P, Zagrosek A, et al. Diagnostic performance of cardiovascular magnetic resonance in patients with suspected acute myocarditis: comparison of different approaches. J Am Coll Cardiol 2005;45:1815-1822.
63. Friedrich MG, Sechtem U, Schulz-Menger J, et al. Cardiovascular magnetic resonance in myocarditis: A JACC White Paper. J Am Coll Cardiol 2009;53:1475-1487.
64. Chu GC, Flewitt JA, Mikami Y, Vermes E, Friedrich MG. Assessment of acute myocarditis by cardiovascular MR: diagnostic performance of shortened protocols. Int J Cardiovasc Imaging 2013;29:1077-1083.
65. Aletras AH, Kellman P, Derbyshire JA, Arai AE. ACUT2E TSE-SSFP: a hybrid method for T2-weighted imaging of edema in the heart. Magn Reson Med 2008;59:229-235.
66. Ferreira VM, Piechnik SK, Dall'Armellina E, et al. Non-contrast T1-mapping detects acute myocardial edema with high diagnostic accuracy: a comparison to T2-weighted cardiovascular magnetic resonance. J Cardiovasc Magn Reson 2012;14:42-429.
67. Dweck MR, Joshi S, Murigu T, et al. Midwall fibrosis is an independent predictor of mortality in patients with aortic stenosis. J Am Coll Cardiol 2011;58:1271-1279.
68. Messroghli DR, Radjenovic A, Kozerke S, Higgins DM, Sivananthan MU, Ridgway JP. Modified Look-Locker inversion recovery (MOLLI) for high-resolution T1 mapping of the heart. Magn Reson Med 2004;52:141-146.
69. Fontana M, White SK, Banypersad SM, et al. Comparison of T1 mapping techniques for ECV quantification. Histological validation and reproducibility of ShMOLLI versus multibreath-hold T1 quantification equilibrium contrast CMR. J Cardiovasc Magn Reson 2012;14:88-429X-14-88.
70. Flett AS, Hayward MP, Ashworth MT, et al. Equilibrium contrast cardiovascular magnetic resonance for the measurement of diffuse myocardial fibrosis: preliminary validation in humans. Circulation 2010;122:138-144.
71. White SK, Sado DM, Fontana M, et al. T1 Mapping for Myocardial Extracellular Volume Measurement by CMR: Bolus Only Versus Primed Infusion Technique. JACC Cardiovasc Imaging 2013;6:955-962.
72. Plymen CM, Sado DM, Taylor AM, et al. Diffuse myocardial fibrosis in the systemic right ventricle of patients late after Mustard or Senning surgery: an equilibrium contrast cardiovascular magnetic resonance study. Eur Heart J Cardiovasc Imaging 2013;14:963-968.
73. Tham EB, Haykowsky MJ, Chow K, et al. Diffuse myocardial fibrosis by T1-mapping in children with subclinical anthracycline cardiotoxicity: relationship to exercise capacity, cumulative dose and remodeling. J Cardiovasc Magn Reson 2013;15:48-429.
74. Wong TC, Piehler K, Meier CG, et al. Association between extracellular matrix expansion quantified by cardiovascular magnetic resonance and short-term mortality. Circulation 2012;126:1206-1216.
75. Miller CA, Naish JH, Bishop P, et al. Comprehensive validation of cardiovascular magnetic resonance techniques for the assessment of myocardial extracellular volume. Circ Cardiovasc Imaging 2013;6:373-383.
76. Bull S, White SK, Piechnik SK, et al. Human non-contrast T1 values and correlation with histology in diffuse fibrosis. Heart 2013;99:932-937.
77. Moon JC, Messroghli DR, Kellman P, et al. Myocardial T1 mapping and extracellular volume quantification: a Society for Cardiovascular Magnetic Resonance (SCMR) and CMR Working Group of the European Society of Cardiology consensus statement. J Cardiovasc Magn Reson 2013;15:92-429X-15-92.
78. Khan SN, Rapacchi S, Levi DS, Finn JP. Pediatric cardiovascular interventional devices: effect on CMR images at 1.5 and 3 Tesla. J Cardiovasc Magn Reson 2013;15:54-429.
79. Nordmeyer J, Gaudin R, Tann OR, et al. MRI may be sufficient for noninvasive assessment of great vessel stents: an in vitro comparison of MRI, CT, and conventional angiography. AJR Am J Roentgenol 2010;195:865-871.
80. Andreassi MG. Radiation risk from pediatric cardiac catheterization: friendly fire on children with congenital heart disease. Circulation 2009;120:1847-1849.
81. Tzifa A, Schaeffter T, Razavi R. MR imaging-guided cardiovascular interventions in young children. Magn Reson Imaging Clin N Am 2012;20:117-128.

CHAPTER 4

Pressure overloaded right ventricles: a multicenter study on the importance of trabeculae in RV function measured by CMR

Authors:
Mieke M.P. Driessen*, Vivan J.M. Baggen*, Hendrik G. Freling, Petronella G. Pieper, Arie P.J. van Dijk, Pieter A. Doevendans, Repke J. Snijder, Marco C. Post, Folkert J. Meijboom, Gertjan Tj. Sieswerda, Tim Leiner#, Tineke P. Willems#
*Shared first authorship; #Shared last authorship

Int J Cardiovasc Imaging. 2014;30:599-608.

Abstract

Cardiac magnetic resonance (CMR) imaging is the preferred method to measure right ventricular (RV) volumes and ejection fraction (RVEF). This study aimed to determine the impact of excluding trabeculae and papillary muscles on RV volumes and function in patients with RV pressure and/or volume overload and healthy controls and its reproducibility using semi-automatic software. Eighty patients (pulmonary hypertension, transposition of the great arteries after arterial switch operation and after atrial switch procedure and repaired Tetralogy of Fallot) and 20 controls underwent short-axis multislice cine CMR. End diastolic volume (EDV), end systolic volume (ESV), RV mass and RVEF were measured using 2 methods. First, manual contour tracing of RV endo- and epi-cardial borders was performed. Thereafter, trabeculae were excluded from the RV blood volume using semi-automatic pixel-intensity based software. Both methods were compared using a Student T test and 25 datasets were reanalyzed for reproducibility. Exclusion of trabeculae resulted in significantly decreased EDV; ranging from -5.7 ± 1.7 ml/m^2 in controls to -29.2 ± 6.6 ml/m^2 in patients after atrial switch procedure. RVEF significantly increased in all groups, ranging from an absolute increase of 3.4 ± 0.8 % in healthy controls to 10.1 ± 2.3 % in patients after atrial switch procedure. Interobserver agreement of method 2 was equal to method 1 for RVEDV, RVESV and RVEF and superior for RV mass. In patients with overloaded RVs exclusion of trabeculae from the blood volume results in a significant change in RV volumes, RVEF and RV mass. Exclusion of trabeculae is highly reproducible when semi-automatic pixel-intensity based software is used.

Introduction

Both in patients with pulmonary hypertension (PH) and in patients with different types of congenital heart disease (CHD), the right ventricle (RV) performs under increased pressure loading. The RV adapts by hypertrophying, however at a certain point the RV is unable to cope with the increased pressures and RV failure will ensue. Consequently, RV function is an important determinant of prognosis and of therapeutic strategy in these patients. For instance, in patients with pulmonary valvular (PV) stenosis, timing of intervention is partly dependent on RV function.[1] In patients with PH, deterioration of right ventricular ejection fraction (RVEF), increased RV end-diastolic volume (RVEDV) and stroke index are associated with poor outcome.[2,3] Furthermore, for patients with transposition of the great arteries (TGA) after an atrial switch operation, in which the RV supplies the systemic circulation (i.e. systemic RV), decline in RV function is one of the most important clinical problems. Therefore RV volumes and function are frequently used in follow-up of these patients, making accurate and reproducible measurements highly important. As both 2D and also 3D echocardiography of the RV remain less reproducible than cardiac magnetic resonance imaging (CMR), the latter is still considered to be the reference standard for the quantification of RV volumes and EF.[4-7] Whether trabeculae and papillary muscles should be included or excluded from the blood volume is subject of debate. Throughout literature both methods are used.[2,8-10] However, many studies have not clearly described whether trabeculae and papillary muscles were included or excluded from the RV blood volume.[11-14] The impact of trabeculae is assumed to be small in healthy individuals, but Winter et al. showed that exclusion of trabeculae from the RV blood volume resulted in a substantial difference of RVEDV, RVESV and RVEF in patients with a systemic right ventricle.[15] Although theoretically more accurate, Winter et al. also showed that manual tracing of trabeculae has low reproducibility and therefore can be considered less favorable for longitudinal follow-up.[5,15]

Freling et al. recently reported that semi-automatic pixel-intensity based segmentation software is able to exclude trabeculae and papillary muscles from the RV blood volume with high reproducibility in Tetralogy of Fallot (TOF) patients with predominantly volume overloaded RVs. Moreover, this resulted in a substantial difference in RV volumes and RVEF compared to the method that includes these structures in the RV blood volume.[16] In patients with increased RV pressure the trabeculae are likely to be coarser. The impact and reproducibility of excluding trabeculae and papillary muscles with this semi-automatic software in patient groups with RV pressure overload has not been investigated up to now. The purpose of this multicenter study was to determine the impact of excluding trabeculae and papillary muscles, on RV volumes and function as assessed by CMR in patients with pressure or combined pressure and volume overload of the RV and healthy controls. Secondly, we determine the reproducibility of this methodology when semi-automatic pixel-intensity based software is used.

Methods

Study design and population

One hundred CMR studies were included in the analysis (median age 36.2 years, 51% male). Four groups of 20 adult patients with pressure overloaded RV's were analyzed: patients with pre-capillary PH, patients with right ventricular outflow tract obstruction (RVOTO) after arterial

switch operation (ASO) for TGA, patients with repaired TOF and patients with TGA and atrial switch procedure (Mustard or Senning operation). A reference group of 20 healthy controls was also included.
PH was defined in accordance with the ESC/ESR guidelines as a mean pulmonary artery pressure of ≥25 mmHg and a pulmonary capillary wedge pressure of ≤15 mmHg.[17] Only patients with pre-capillary (i.e. with arterial vascular changes) PH were included, all were diagnosed with either chronic trombo-embolic or idiopathic PH. In all patients RV systolic pressure (RVSP) was measured using Doppler echocardiography on the day of CMR investigation. RVSP was measured using the peak velocity of tricuspid regurgitation (TR) plus estimated right atrial pressure. Patients with repaired TOF were included if a RVSP of ≥ 36 mmHg was measured by Doppler echocardiography.[18] Patients after ASO were included if RVSP measured by Doppler echocardiography was ≥ 36 mmHg or if, using Doppler echocardiography, a mild or moderate RVOTO was measured, defined as a maximum gradient of ≥ 25 mmHg. For patients with TGA and atrial switch procedure systolic blood pressure was used to determine RVSP. Basic patient characteristics for each patient group are illustrated in table 1. Degree of pulmonary (PR) and TR were assessed semi-quantitatively with echocardiography, based on color-Doppler and continuous wave Doppler pattern and graded as: none or trace, mild, moderate or severe.
In this retrospective study, MR images from two tertiary referral hospitals were analyzed. One centre contributed 59 patient CMR datasets and 20 control subjects. The second centre provided the remaining 21 patient CMR datasets. The datasets in this study were obtained between May 2008 and July 2012. Prior to analysis, all patient and control data were encoded to preserve anonymity. All CMR datasets were acquired in a routine clinical setting and anonymized for analysis. The medical ethics committees waived the need for informed consent.

CMR imaging protocol
Datasets were obtained using commercially available 1.5 T MR scanners (Ingenia R4.1.2; Philips Healthcare, Best, The Netherlands [n = 79]; Magnetom Sonata, Siemens Healthcare; [n =7] and Magnetom Avanto; Siemens Healthcare, Erlangen, Germany [n=14]). For all studies dedicated chest or torso phased array parallel-imaging capable surface coils were used with 12-28 elements. CMR images were acquired during repeated end-expiratory breath holds. Cine images were acquired using a retrospectively gated balanced steady state free precession sequence with 25-30 cardiac phases per cardiac cycle. Slice thickness used were 6 mm with 4 mm gap [n=21] and 8 mm with 0 mm gap [n=79]. Sequences included multi-slice, multi-phase cine short-axis, longitudinal four-chamber, vertical two-chamber and RV outflow views. The multi-slice cine short-axis acquisitions were planned from above the mitral valve up to and including the cardiac apex. The following ranges of other scan parameters was used: TR 2.7-3.4 ms; TE 1.1-1.7 ms; flip angle 80º-90º; matrix 171-192; voxel size: 1.25x1.25x8.0 mm and 1.7x1.7x6.0 mm. Parallel imaging factors varied between 0-3.

CMR image analysis
Image analysis was performed using Qmass MR Research edition version 7.4.14.0 (Medis, Leiden, the Netherlands).[16] Segmentation was performed on end-diastolic and end-systolic phases only. The end-diastolic and end-systolic phases were selected by visual assessment as the phase with the largest and smallest RV cavity sizes respectively, taking into account the longitudinal four-chamber, vertical two-chamber and RV outflow tract as reference views. If visual assessment was

	PH *n* = 20	ASO *n* = 20	TOF *n* = 20	Atrial Switch *n* = 20	Controls *n* = 20
Male gender *n* (%)	7 (35)	11 (55)	11 (55)	12 (60)	10 (50)
Age year *	55.0 ± 14.1	24.9 ± 4.0	29.1 ± 7.8	33.0 ± 6.3	36.7 ± 10.1
BSA m^2 *	1.93 ± 0.18	1.88 ± 0.18	1.87 ± 0.19	1.96 ± 0.21	1.88 ± 0.21
RVESP mmHg #	54 (37-65) *n = 20*	40 (37-53) *n = 15*	45 (41-50) *n = 20*	120(106-125) *n = 20*	-
RVOT mmHg #	-	35 (29-42) *n = 8*	33 (30-40) *n = 15*	-	4 (3-8) *n = 20*
TR grade n (%):					
- **No/trace**	7 (35)	12 (60)	10 (50)	1 (5)	20 (100)
- **Mild**	9 (45)	7 (35)	7 (35)	14 (70)	-
- **Moderate**	4 (20)	1 (5)	3 (15)	4 (20)	-
- **Severe**	-	-	-	1 (5)	-
- **Missing**	-	-	-	-	-
PR grade:**					
- **No/trace**	14 (70)	14 (70)	9 (45)	13 (65)	20 (100)
- **Mild**	6 (30)	3 (15)	4 (20)	2 (10)	-
- **Moderate**	-	-	-	-	-
- **Severe**	-	-	6 (30)	-	-
- **Missing**	-	2 (10)	1 (5)	5 (25)	-

Table 1: Patient characteristics.
Baseline characteristics of each patient group and healthy controls. *data presented as mean ± SD; # data presented as median (IQR) ; **AR grade in patients after atrial switch

difficult, multiple frames were contoured to determine the correct end-diastolic or end-systolic phase. Using a previously described RV analysis protocol the RV epicardial and endocardial contours were manually traced from the most apical to the most basal short-axis slice.[19] Only the portion of the outflow tract below the pulmonary valve was included in the blood volume in the basal slice in which the pulmonary valve was visible. If more than 50% of the tricuspid annulus or atrium was visible in a basal slice the valve area was excluded from the blood volume. Epicardial and endocardial contours overlapped at valve borders and septum, as the septum was considered part of the left ventricle. For patients with systemic RV, the septum was considered part of the RV and included in the RV myocardial volume.
Based on the methodology described above, two methods were used for determining RV volumes, function and mass. With method 1 trabeculae and papillary muscles were included in the blood volume. With method 2, trabeculae and papillary muscles were excluded from the blood volume (Figure 1) and added to the myocardial volume. For both methods the volume between the endo- and epicardial contour was considered myocardial volume. Selection of trabeculae and papillary muscles was done using semi-automatic pixel-intensity based segmentation software. The

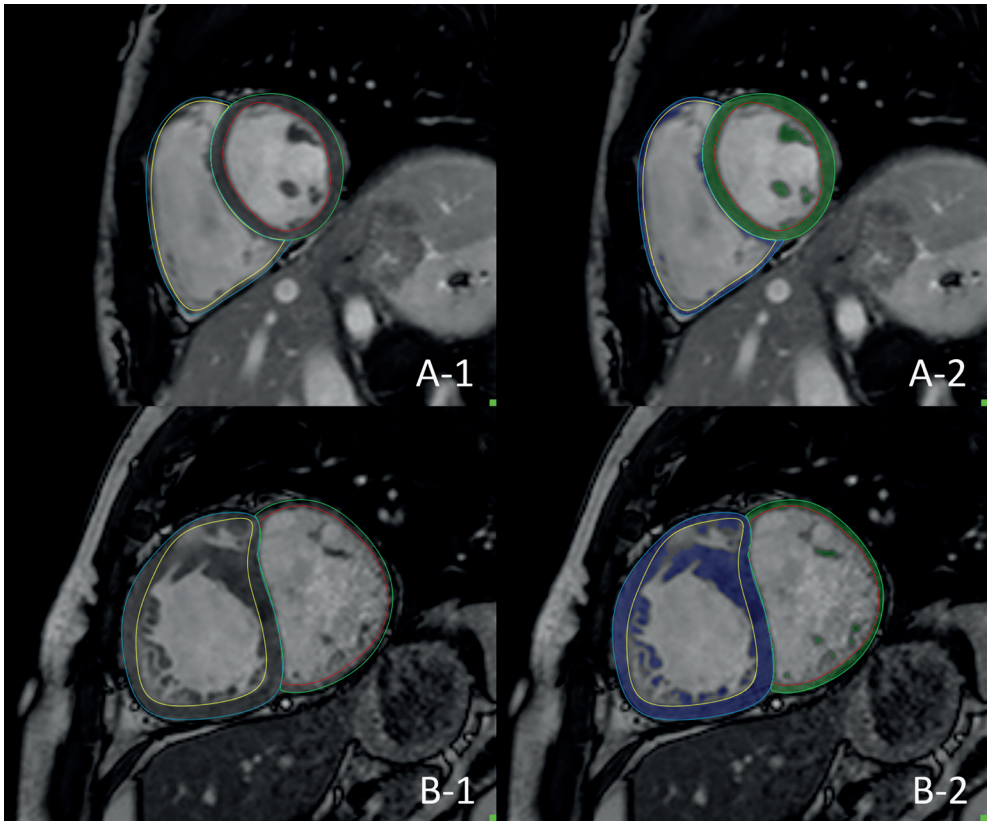

Figure 1. RV contour tracing only (A-1 and B-1) and with semiautomatic selection of trabeculae (A-2 and B-2). Two methods of measuring RV volumes in a healthy control (a) and patient after atrial switch procedure (b). Method 1: inclusion trabeculae in the blood volume (a-1 and b-1); Method 2: exclusion of trabeculae from the blood volume, using identical endocardial contours (a-2 and b-2)

segmentation software is based on the signal intensity distribution of MR images and has been described in detail by Freling et al.[16] In brief, voxels within the epicardial contour are classified as either blood volume or myocardial volume according to their signal intensity, taking into account spatial variations in signal intensity. Based on this algorithm, trabeculae and papilary muscles were excluded from the blood volume and included in the myocardial volume. The algorithm works similar for images generated by the different scanners used in this study. It was a possibility to manually change the threshold for every slice, in order to select the same trabeculae in end-diastole and end-systole. Observers selected only trabeculae with signal intensity similar to the intensity of RV myocardium. Individual voxels could also be selected or deselected in case of artifacts due to nonlaminar flow.

For both methods, RV volumetric parameters were calculated by the sums of the traced contours multiplied by slice thickness in all short-axis slices. For method 1 the volume of trabeculae and papillary muscles was included in the RV blood volume and for method 2 this was excluded from the blood volume. Stroke volume (SV) was defined as the difference between end diastolic volume (EDV) and end systolic volume (ESV). All volumetric data were indexed for body surface area (BSA), which was calculated using the Dubois-Dubois formula (0.20247 x Height(m)$^{0.725}$ x

Weight(kg)$^{0.425}$). EF was calculated by SV/ EDV * 100%. For method 1 myocardial volume was defined as epicardial minus the endocardial contour, for method 2 end-diastolic trabecular volume was added to the myocardial volume. RV mass was quantified by multiplying the specific density of myocardium (1.05 g/ml) with the end-diastolic myocardial volume.

Reproducibility

Intraobserver reproducibility of both methods was assessed by re-analyzing 5 randomly selected CMR datasets from every patient group, as well as the healthy control subjects by the primary observer. In total 25 datasets were reanalyzed. To determine interobserver variability a second observer re-analyzed the same 25 datasets. Observers were unaware of the results of the first analysis and there was an interval of at least two weeks between the first and second analysis. The observers had equal experience in RV volumetric analysis and received the same training for Qmass MR research edition.

Statistical analysis

Continuous data were expressed as median and interquartile range (IQR) or mean value ± standard deviation (SD) as appropriate. Mean differences ± SD between method 1 and 2 was calculated for RVEDV/m^2, RVESV/m^2, RVSV/m^2, RVEF and RV mass/m^2, using Paired Student's T-test. Differences in RVEDV/m^2, RVESV/m^2 and RVEF found in the patient groups were compared to the healthy control group using a one-way ANOVA with posthoc Dunnett's test. For the one-way ANOVA data underwent logarithmic transformation if necessary (i.e. if homogeneity of variances was inequal). Intra- and interobserver agreement were assessed using Bland-Altman plots and intraclass correlation coefficients (ICC). Paired Student's T-test was used to test for significant differences between observer 1 and 2 and between the first and second measurements of observer 1. Mean differences ± SD for all measurements were calculated. Lastly to compare reproducibility of both methods the inter- and intraobserver agreement coefficient of method 1 and 2 were calculated for each measurement. The calculated ACintra/inter using the following formula: ACintra/inter = 100 · (1 - 2·|Obs1-Obs2|/ Obs1+Obs2); in which Obs1 and 2 are the first and the second observation (or observer). The ACintra/inter calculated for method 1 and 2 were compared using a paired Wilcoxon signed Rank test. Using this formula the relative differences of both methods are compared. Using a Bonferonni correction for multiple measurements p-values of <0.01 were considered statistically significant. All data analysis was performed in IBM SPSS statistics version 20.0 (IBM SPSS, Chicago, IL).

Results

Exclusion of trabecular volume

RVEDV/m^2, RVESV/m^2, RVEF and RV mass/m^2 measured including (method 1) and excluding (method 2) RV trabeculae from the RV blood volume (method 2) are listed in table 2. For all patient groups and for healthy controls, exclusion of trabeculae and papillary muscles from the blood volume resulted in significantly decreased RVEDV/m^2 and RVESV/m^2 and a significantly increased RVEF and RV mass/m^2 (table 2). Of note, the differences in EDV/m^2, ESV/m^2, RVEF, and RV mass between both methods were most pronounced in the patients after atrial switch procedure and least pronounced in the PH patients, with mean absolute differences in EF of 10.1 ± 2.3% and 4.7±1.6%, respectively. In healthy controls an absolute increase in RVEF of 3.4 ± 0.8%

		PH	ASO	TOF	Atrial switch	Controls
		(mean**±SD**)	(mean**±SD**)	(mean**±SD**)	(mean**±SD**)	(mean**±SD**)
RVEDV (ml/m²)	Method 1	117.4 ± 31.8	99.4 ± 23.3	147.0 ± 42.5	139.9 ± 33.6	96.9 ± 18.9
	Method 2	105.1 ± 28.4	88.3 ± 21.2	124.8 ± 38.0	110.7 ± 28.7	91.2 ± 17.8
	Difference	*-12.3 ± 4.6**	*-11.1 ± 3.3**	*-22.2 ± 6.0**	*-29.2 ± 6.6**	*-5.7 ± 1.7**
RVESV (ml/m²)	Method 1	75.4 ± 30.0	50.1 ± 13.3	85.5 ± 27.8	85.9 ± 26.2	47.5 ± 11.5
	Method 2	62.7 ± 25.9	39.2 ± 11.3	63.7 ± 23.2	57.1 ± 21.7	41.6 ± 10.5
	Difference	*-12.7 ± 4.8**	*-10.9 ± 3.3**	*-21.8 ± 6.0**	*-28.8 ± 6.5**	*-5.9 ± 1.5**
SV	Method 1	42.0 ± 7.9	49.3 ± 11.7	61.5 ± 19.4	54.0 ± 14.9	49.4 ± 8.6
(ml/m²)	Method 2	42.4 ± 8.0	49.2 ± 11.5	61.0 ± 19.6	53.6 ± 14.7	49.6 ± 8.6
	Difference	*-0.4* **± 0.6****	*-0.2* **± 0.6**	*-0.4* **± 0.8****	*-0.4* **± 0.9**	*0.2* **± 0.5**
RV mass	Method 1	18.5 ± 5.5	20.1 ± 5.0	25.4 ± 7.1	43.3 ± 9.1	13.0 ± 3.0
(gr/m²)	Method 2	31.4 ± 9.8	31.1 ± 7.5	48.7 ± 12.3	73.9 ± 15.4	19.0 ± 4.2
	Difference	*12.9 ± 4.9**	*11.0 ± 4.8**	*23.3 ± 6.3**	*30.6 ± 6.9**	*6.0 ± 1.8**
RVEF	Method 1	37.2 ± 8.5	49.6 ± 5.0	42.1 ± 6.9	39.2 ± 7.8	51.3 ± 3.8
(%)	Method 2	41.9 ± 9.1	55.8 ± 5.1	49.4 ± 12.3	49.3 ± 9.7	54.7 ± 4.1
	Difference	*4.7 ± 1.6**	*6.1 ± 1.7**	*7.2 ± 1.7**	*10.1 ± 2.3**	*3.4 ± 0.8**

Table 2: RV volume and function
RV volume, mass and ejection fraction measured with inclusion (method 1) and exclusion of trabeculae from the RV blood volume (method 2). All volumetric data are indexed for BSA.
*p < 0.001 using paired Student's T-test; ** p < 0.05 using paired Student's T-test

was measured. Exclusion of trabeculae volume from the RV blood volume led to a significantly increased RV mass in all groups (table 2). Of note, the differences in EDV/m², EDV/m², RVEF and RV mass were significantly larger in all patients groups compared to the healthy controls (p<0.01).

Reproducibility

For both methods inter- and intraobserver agreement was high in all measurements, as illustrated by high ICCs with small limits of agreement (table 3 & figure 2). For both methods, RVEDV, RVESV and RV mass showed significant differences between repeated measurements. However, mean differences were small and considered not clinically relevant. In figure 2, Bland-Altman plots show interobserver variability for RVESV, RVEDV and RVEF for both methods. For RVEDV, RVESV and RV mass the limits of agreement were narrower when trabeculae and papillary muscles were excluded from the RV blood volume (method 2). The ACintra/inter of both methods was not statistically significantly different for RVEDV, RVESV and RVEF (p > 0.1). Method 2 had a significantly better AC inter than method 1 for RV mass measurement, with a median (IQR) AC inter of respectively 94.1% (92.1-97.1%) and 77.2% (72.1-82.6%).

ICC		Interobserver (obs 2 – obs 1^{I})			Intraobserver (obs 1^{II} – obs 1^{I})		
		Mean difference ± SD	P-value	ICC	Mean difference ± SD	P-value	
RVEDV (mL/m^2)	Method 1	0.981	-2.4 ± 6.7	0.089	0.990	2.8 ± 5.1	0.012
	Method 2	0.987	1.8 ± 4.5	0.059	0.985	3.0 ± 5.0	0.006
RVESV (mL/m^2)	Method 1	0.970	-2.3 ± 5.2	0.039	0.982	1.1 ± 4.2	0.209
	Method 2	0.974	1.7 ± 3.5	0.027	0.969	1.0 ± 3.8	0.194
RVEF (%)	Method 1	0.934	0.9 ± 2.6	0.086	0.965	0.4 ± 1.8	0.241
	Method 2	0.934	-0.5 ± 2.6	0.354	0.954	0.6 ± 2.2	0.189
RVmass (gr/m^2)	Method 1	0.965	5.8 ± 3.5	0.000	0.983	0.5 ± 2.3	0.283
	Method 2	0.993	1.4 ± 2.6	0.012	0.990	0.3 ± 3.2	0.694

Table 3: Inter- and intraobserver agreement
Intra-class correlation coefficient and the absolute mean difference± SD for all measurements. P-value obtained using paired student T-test.
Abbreviations: Obs 2 = second observer; Obs 1I = first measurement of primary observer; Obs 1II = second measurement of primary observer.

Discussion

Exclusion of trabeculae and papillary muscles resulted in substantial alterations of RV volumes, RVEF and RV mass in a wide range of patient populations with pressure and volume overloaded RVs. Furthermore, we found that these differences in RV parameters vary widely depending on the exact condition underlying RV overload. Although prior studies already established this fact in general terms, the major impediment to widespread adoption of this method in clinical practice was the lack of a fast and reproducible way to measure the exact amount of RV trabeculae and papillary muscles. We found that exclusion of RV trabeculae using semi-automatic pixel-intensity based software resulted in fast and highly reproducible RV measurements. This is opposed to manual tracing of trabeculae which has previously been shown to be unreliable.[15,20]

Accurate and reproducible measurement of RV volume and function is mandatory because of the prognostic and therapeutic implications in patients with PH and CHD.[1,3,21,22] The current study underscores that exclusion of trabeculae has a significant impact on RV volumes, RVEF and RV mass in both CHD and PAH patients with overloaded RVs. Moreover, the impact of excluding trabeculae varied widely between patient groups, from a change in RVEDV of -12.3±4.6 ml/m^2 in PH patients to -29.2±6.6 ml/m^2 in patients with a systemic RV. Healthy controls also exhibited significant differences in all RV measurements, but these were significantly smaller ($p<0.01$) compared to the differences observed in patient groups. Consequently, RV volume and function in most patients will be closer to or in the normal range after exclusion of trabeculae from the RV blood volume.

Currently, there is no clear standard for RV volumetric analysis or consensus on how trabecular structures should be handled. Major obstacles to exclude trabeculae and papillary muscles from the RV blood volume have been the time investment of performing manual tracing of these structures and the low reproducibility.[15,20] Several studies in CHD patients differ on the point of in-

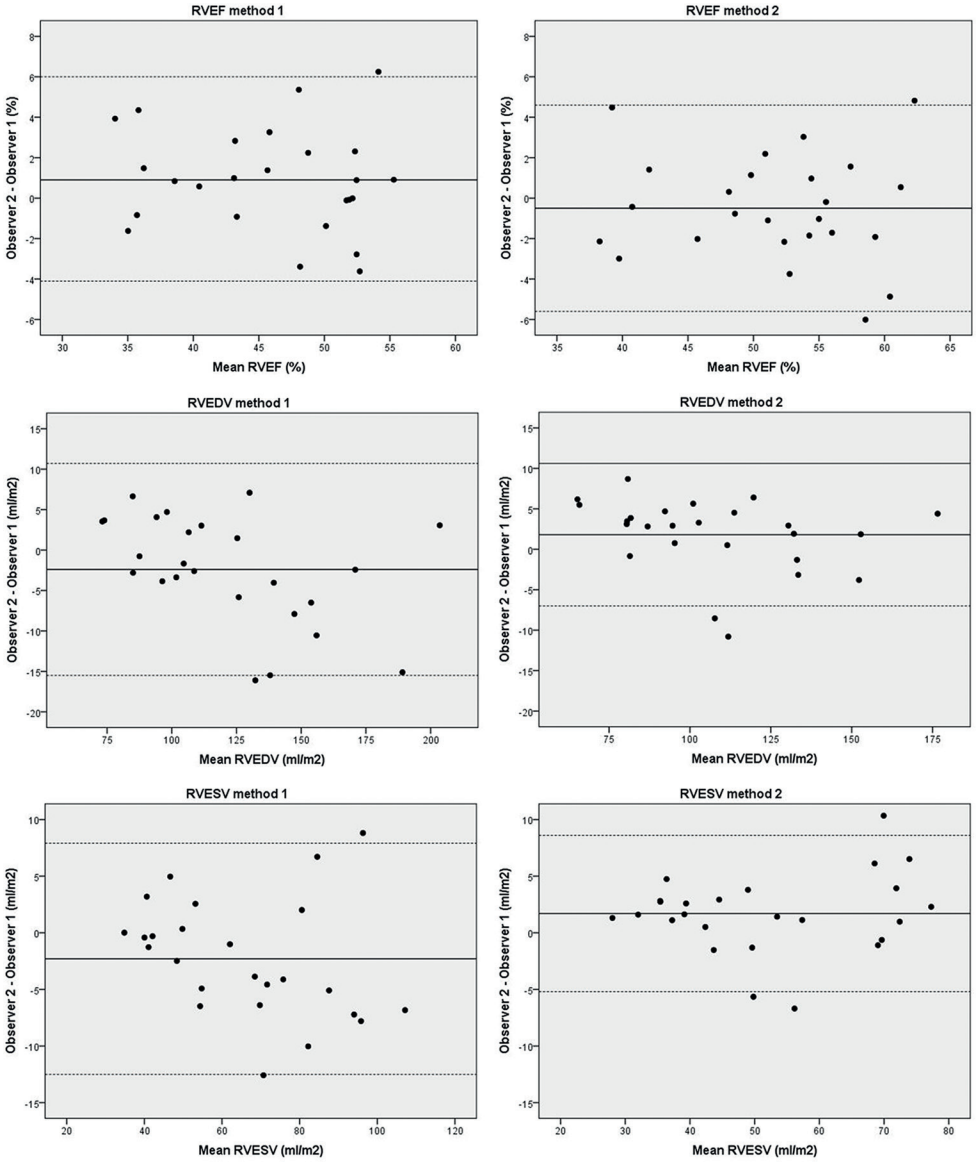

Figure 2. Bland-Altman plots showing the mean value of both observers on the x-axis and absolute differences between the observers on the y-axis for each paired observation. Limits of agreement are defined as ± 2 SD.

or excluding RV trabeculae and papillary muscles from the RV blood volume[3,4,11,12,20,22,23] or are not clear about the methodology used.[13,14] In the current study we found that using semi-automatic pixel-intensity based segmentation software results in highly reproducible RV volumetric measurements. Because in- or exclusion of trabeculae has a major impact on RV parameters as measured with CMR, studies using different methodologies are incomparable. Application of the

method described in this study may be a step forward to achieve uniformity of RV volumetric measurements, which is important to compare the effect of interventions aimed at preserving or improving RV function. However, there are only few reports using this new methodology and it is of great importance that new studies are undertaken to determine clinically relevant cut-off values using this semi-automated method.

When comparing the current study to prior studies investigating the impact of trabeculae and papillary muscles on RV volume and function, some important differences can be observed. Winter et al. studied 29 patients with systemic right ventricles and found an increase in RVEF of 7.4± 3.9 % compared to 10.1 ± 2.3 % in our report. In contrast to our results, which are based on semi-automated pixel-intensity based segmentation, manual exclusion of trabeculae was substantially less reproducible in the study of Winter et al.[15] Moreover, both our study and the study by Freling et al. even demonstrated a higher reproducibility, for respectively RV mass and RVEDV and RV mass, using this semi-automatic method to exclude trabeculae compared to only endocardial contour tracing.[16] We attribute this finding to observer variation in handling of trabeculae adjacent to the endocardial border. This can result in small differences for endocardial contour tracing, which will be rectified if all trabeculae are excluded. Sievers et al. studied the effect of trabeculae on RV volumes in healthy controls and reported a difference in RVEF of only 1.72% compared to 3.4±0.8% in our study, however baseline RVEDV values also differed considerably with ours, indicating that these study populations are not comparable.[24] Freling et al. investigated a different group of TOF patients, with volume overloaded RV's, using the same software package as described in the current study and found a similar increase in RVEF of 7 ± 4 %, versus 7 ± 2% in our study.[16]

The current study only focused on one of the possible sources of error in RV volumetric assessment with CMR. An important source of error remains basal slice selection and delineation of the tricuspid valve. In this study a short-axis orientation for RV volumetric measurement was used, as this is standard practice in our hospitals. Axial orientation, however, might result in higher reproducibility than short-axis orientation in CHD patients with severely dilated RVs, decreasing the difficulty of valve delineation in the basal slices.[25,26] To minimize errors at the tricuspid and pulmonic valve, images were cross-linked to RV 2-chamber, 4-chamber and RV outflow tract views. Furthermore, only a small portion of the patients had severely dilated RVs, therefore it is unlikely that the slice orientation would have resulted in important differences for the current study. The impact and reproducibility of the semi-automatic software used in the current study will likely be similar in axial slice orientation, as the software is not restricted by geometric assumptions and uses signal intensity to select trabeculae. Finally, another source of error might be inadequate selection of the RV end-systolic frame. In daily practice both RV ESV and LV ESV are often assessed in the LV end-systolic frame. However in patients with CHD, who often have right bundle branch block, timing of the RV end-systolic frame can be delayed compared to the LV end-systolic frame.[27] Therefore RV end-diastolic and end-systolic phase was based solely on RV cavity size.

Study limitations

This study is unable to determine whether in- or excluding trabeculae best represents true RV volumes, as a gold standard in vivo is lacking. Because the SV remains equal with both methodologies other CMR measurements are unable to serve as a reference standard. However, theoretically exclusion of trabeculae is more accurate as these do not contribute to RV blood

volumes in end-diastole or end-systole.
Furthermore no invasive measurements were available to determine the true RV pressure in these patients. Therefore estimations of RVESP and RVOT gradient based on Doppler-derived flow velocities were used, which might not always be accurate and have limitations. Nonetheless these are the best available non-invasive alternatives to assess degree of RV pressure overload or RVOT stenosis.

Conclusion
Exclusion of trabeculae and papillary muscles has a significant impact on measured RV volumes, mass and EF. The magnitude of the differences varies between patient groups and is significantly larger in all investigated patient groups with overloaded RVs than in healthy controls. Importantly, exclusion of trabeculae with semi-automatic pixel-intensity based software is highly reproducible and superior compared to manual contour tracing for RV mass.

References

1. Baumgartner H, Bonhoeffer P, De Groot NM, et al. Task Force on the Management of Grown-up Congenital Heart Disease of the European Society of Cardiology (ESC), Association for European Paediatric Cardiology (AEPC), ESC Committee for Practice Guidelines (CPG) ESC Guidelines for the management of grown-up congenital heart disease. Eur Heart J 2010; 31:2915-2957.
2. van de Veerdonk MC, Kind T, Marcus JT, et al. Progressive right ventricular dysfunction in patients with pulmonary arterial hypertension responding to therapy. J Am Coll Cardiol 2011;58:2511-2519.
3. van Wolferen SA, Marcus JT, Boonstra A, et al. Prognostic value of right ventricular mass, volume, and function in idiopathic pulmonary arterial hypertension. Eur Heart J 2007; 28:1250-1257.
4. Valsangiacomo Buechel ER, Mertens LL. Imaging the right heart: the use of integrated multimodality imaging. Eur Heart J 2012;33:949-960.
5. Kilner PJ, Geva T, Kaemmerer H, Trindade PT, Schwitter J, Webb GD. Recommendations for cardiovascular magnetic resonance in adults with congenital heart disease from the respective working groups of the European Society of Cardiology. Eur Heart J 2010;31:794-805.
6. van der Zwaan HB, Geleijnse ML, McGhie JS, et al. Right ventricular quantification in clinical practice: two-dimensional vs. three-dimensional echocardiography compared with cardiac magnetic resonance imaging. Eur J Echocardiogr 2011;12:656-664.
7. Iriart X, Montaudon M, Lafitte S, et al. Right ventricle three-dimensional echography in corrected tetralogy of fallot: accuracy and variability. Eur J Echocardiogr 2009;10:784-792.
8. Beerbaum P, Barth P, Kropf S, et al. Cardiac function by MRI in congenital heart disease: impact of consensus training on interinstitutional variance. J Magn Reson Imaging 2009;30:956-966.
9. Rominger MB, Bachmann GF, Pabst W, Rau WS. Right ventricular volumes and ejection fraction with fast cine MR imaging in breath-hold technique: applicability, normal values from 52 volunteers, and evaluation of 325 adult cardiac patients. J Magn Reson Imaging 1999;10:908-918.
10. Lorenz CH, Walker ES, Morgan VL, Klein SS, Graham TP,Jr. Normal human right and left ventricular mass, systolic function, and gender differences by cine magnetic resonance imaging. J Cardiovasc Magn Reson 1999;1:7-21.
11. Oosterhof T, van Straten A, Vliegen HW, Meijboom FJ, et al. Preoperative thresholds for pulmonary valve replacement in patients with corrected tetralogy of Fallot using cardiovascular magnetic resonance. Circulation 2007;116:545-551.
12. Therrien J, Provost Y, Merchant N, Williams W, Colman J, Webb G. Optimal timing for pulmonary valve replacement in adults after tetralogy of Fallot repair. Am J Cardiol 2005;95:779-782.
13. Lidegran M, Odhner L, Jacobsson LA, Greitz D, Lundell B. Magnetic resonance imaging and echocardiography in assessment of ventricular function in atrially corrected transposition of the great arteries. Scand Cardiovasc J 2000;34:384-389.
14. Lee C, Kim YM, Lee CH, et al. Outcomes of pulmonary valve replacement in 170 patients with chronic pulmonary regurgitation after relief of right ventricular outflow tract obstruction: implications for optimal timing of pulmonary valve replacement. J Am Coll Cardiol 2012;60:1005-1014.
15. Winter MM, Bernink FJ, Groenink M, et al. Evaluating the systemic right ventricle by CMR: the importance of consistent and reproducible delineation of the cavity. J Cardiovasc Magn Reson 2008;10:40.
16. Freling HG, van Wijk K, Jaspers K, et al. Impact of right ventricular endocardial trabeculae on volumes and function assessed by CMR in patients with tetralogy of Fallot. Int J Cardiovasc Imaging 2013;29:625-31.
17. Task Force for Diagnosis and Treatment of Pulmonary Hypertension of European Society of Cardiology (ESC), European Respiratory Society (ERS), International Society of Heart and Lung Transplantation (ISHLT), Galie N, Hoeper MM, et al. Guidelines for the diagnosis and treatment of pulmonary hypertension. Eur Respir J 2009;34:1219-1263.
18. Rudski LG, Lai WW, Afilalo J, et al. Guidelines for the echocardiographic assessment of the right heart in adults: a report from the American Society of Echocardiography endorsed by the European Association of Echocardiography, a registered branch of the European Society of Cardiology, and the Canadian Society of Echocardiography. J Am Soc Echocardiogr 2010;23:685-713.
19. Prakken NH, Velthuis BK, Vonken EJ, Mali WP, Cramer MJ. Cardiac MRI: standardized right and left ventricular quantification by briefly coaching inexperienced personnel. Open Magn Reson J 2008;1:104-111.
20. Papavassiliu T, Kuhl HP, Schroder M, et al. Effect of endocardial trabeculae on left ventricular measurements and measurement reproducibility at cardiovascular MR imaging. Radiology 2005;236:57-64.
21. Warnes CA. Adult congenital heart disease importance of the right ventricle. J Am Coll Cardiol 2009;54:1903-1910.
22. Knauth AL, Gauvreau K, Powell AJ, et al. Ventricular size and function assessed by cardiac MRI predict major adverse clinical outcomes late after tetralogy of Fallot repair. Heart 2008;94:211-216.
23. Helbing WA, Rebergen SA, Maliepaard C, et al. Quantification of right ventricular function with magnetic resonance imaging in children with normal hearts and with congenital heart disease. Am Heart J 1995;130:828-837.
24. Sievers B, Kirchberg S, Bakan A, Franken U, Trappe HJ. Impact of papillary muscles in ventricular volume and ejection fraction assessment by cardiovascular magnetic resonance. J Cardiovasc Magn Reson 2004;6:9-16.

25. Clarke CJ, Gurka MJ, Norton PT, Kramer CM, Hoyer AW. Assessment of the accuracy and reproducibility of RV volume measurements by CMR in congenital heart disease JACC Cardiovasc Imaging 2012;5:28-37.
26. Fratz S, Schuhbaeck A, Buchner C, et al. Comparison of accuracy of axial slices versus short-axis slices for measuring ventricular volumes by cardiac magnetic resonance in patients with corrected tetralogy of fallot. Am J Cardiol 2009;103:1764-1769.
27. Freling HG, Pieper PG, Vermeulen KM, et al. Improved cardiac MRI volume measurements in patients with tetralogy of Fallot by independent end-systolic and end-diastolic phase selection. PLoS One 2013;8:e554-62.

CHAPTER 5

Tricuspid flow and regurgitation in congenital heart disease and pulmonary hypertension: Comparison of 4D-flow MRI and echocardiography

Authors:
Mieke M.P. Driessen, Marjolijn A. Schings, Gertjan Tj. Sieswerda, Pieter A. Doevendans, Erik H. Hulzebos, Marco C. Post, Repke J. Snijder, Jos J.M. Westenberg, Arie P.J. van Dijk, Folkert J. Meijboom, Tim Leiner

Submitted to JCMR

Abstract

Background
Tricuspid valve (TV) regurgitation (TR) is a common complication of pulmonary hypertension and right-sided congenital heart disease, and is associated with increased morbidity and mortality. Estimation of TR grade by echocardiography and conventional cardiac magnetic resonance is not well validated and has high variability. 4D velocity-encoded Magnetic Resonance Imaging (4D-flow MRI) was used to measure tricuspid flow in patients with complex RV geometry and varying degrees of TR. The aims of the present study were: 1) to assess accuracy of 4D-flow MRI across the TV by comparing TV effective flow to effective flow across the pulmonary valve assessed by 2D-flow MRI; 2) to assess reproducibility of 4D-flow MRI across the TV, and 3) to compare TR grade by 4D-flow MRI to TR grade by echocardiography.

Methods
TR was assessed by both 4D-flow MRI and echocardiography in 21 healthy controls (age 41.2±10.5 yrs, female 7/21 (33%)) and 67 RV loaded patients (age 42.7±17.0 yrs, female 32/67 (48%)). The MRI protocol included tricuspid flow derived by 4D-flow MRI, pulmonary flow derived by 2D-flow MRI and conventional planimetric measurements. TV regurgitation grade on echocardiography was performed based on the international recommendations. Bland-Altman analysis and intra-class correlation coefficients (ICC) were used to assess accuracy and reproducibility of 4D-flow MRI.

Results
Effective flow measured by 4D-flow MRI across TV showed good correlation and agreement with PV effective flow measured by 2D-flow MRI, ICC=0.899 ($p<0.001$) and mean difference of -1.79 ml [limits of agreement -20.39 to 16.81] ($p=0.084$). Intra-observer agreement for effective flow (ICC=0.981; mean difference -1.51ml [-12.88 to 9.86]) and regurgitant fraction (ICC=0.910; mean difference 1.08% [-7.90; 10.06]) was good. Inter-observer agreement for effective flow (ICC=0.935; mean difference 2.12ml [-15.24 to 19.48]) and regurgitant fraction (ICC=0.968; mean difference 1.10% [-7.96 to 5.76]) was comparable. In 25/65 (38.5%) TR grade differed by at least 1 grade using 4D-flow MRI compared to echocardiography.

Conclusion
Four-dimensional flow MRI is an accurate and reproducible method to measure TV flow and regurgitation. Twenty-five out of 65 patients (38.5%) were classified differently by at least one grade using quantitative 4D-flow MRI compared to echocardiographic TR grade.

Background

Tricuspid valve (TV) regurgitation (TR) frequently complicates pulmonary hypertension (PH) and congenital heart defects (CHD) associated with right ventricular (RV) pressure or volume overload. The presence and severity of TR in these patient groups is independently associated with both increased morbidity and increased mortality.[1-3]

The complex structure of the valve and the degree of motion throughout the cardiac cycle, make assessment of TR difficult. When the right ventricle (RV) dilates, RV geometry is altered, making valve structure and flow patterns even more difficult to evaluate.[4] Severity of TR is primarily assessed using qualitative and semi-quantitative (color) Doppler echocardiography.[5,6] However, these measurements are less well validated for TR than for other valvular regurgitations and have high inter-observer variability.[5,7,8] Consequently, if only echocardiography is used, there is substantial risk of misjudging severity of TR8, influencing clinical decision-making.

Cardiac magnetic resonance imaging (MRI), using 2D velocity-encoded (2D-flow) MRI, is the reference standard for assessment and follow-up of aortic and pulmonary regurgitation in patients with CHD.[9] However, for both atrio-ventricular valves, direct flow measurement with 2D-flow MRI is regarded as less reliable[9,10], mostly due to the large degree of valvular through-plane motion.[11,12] Alternatively, indirect quantification – combining planimetric RV stroke volume and direct flow measurement across the pulmonary valve (PV) – is used, but this approach also introduces multiple sources of error.[12,13]

Four-dimensional velocity-encoded (4D-flow) MRI encodes velocity simultaneously in three orthogonal directions, thereby enabling direct flow measurement, perpendicular to the annular plane, throughout the entire cardiac cycle.[10,14] Tricuspid flow measurement by 4D-flow MRI has been validated in patients with normal RVs, as well as in patients with Tetralogy of Fallot without TR.[14,15] However, to the best of our knowledge, a validation study in patients with complex RV geometry and varying degrees of TR has not been done. Furthermore, it is unknown to what extent TR grade by 4D-flow MRI differs from the current clinical standard for assessing TR; echocardiography.

The aims of the present study were: 1) to assess accuracy of 4D-flow MRI derived tricuspid flow in patients with complex RV geometry, by comparing TV effective flow derived from 4D-flow MRI to pulmonary valve (PV) effective flow derived from 2D-flow MRI; 2) to assess 4D-flow MRI reproducibility for TV flow measurements, and 3) to compare TR grade by 4D-flow MRI to TR grade by echocardiography.

Methods

A prospective, cross-sectional cohort study was performed in three tertiary referral hospitals including healthy controls (n=21), patients with pulmonary hypertension (PH; n=30), patients with isolated valvular pulmonary stenosis or tetralogy of Fallot (n=21) and systemic RV patients (n=16). CMR and echocardiography were performed at a single center by dedicated and experienced staff.

In- and exclusion criteria

The PH group comprised only patients with pre-capillary pulmonary hypertension – either idiopathic pulmonary arterial hypertension or chronic thromboembolic pulmonary hypertension. In all PH patients, the diagnosis of pre-capillary PH had been previously confirmed by right heart

catheterization. Pre-capillary PH was defined as mean pulmonary artery pressure (RVSP) of ≥ 25 mmHg and a pulmonary capillary wedge pressure of ≤ 15 mmHg.[16] All PH patients were on PH-specific therapy when entering the study. The CHD cohort consisted of two major groups: 1) patients with a systemic RV either after atrial switch procedure for transposition of the great arteries or congenitally corrected transposition of the great arteries, and 2) patients with isolated valvular pulmonary stenosis or tetralogy of Fallot with pulmonary valvular or homograft stenosis. Patients with contra-indications for MRI were excluded. A group of healthy subjects between 18-60 years old served as control population. Subjects were screened using physical examination, medical history and electrocardiogram and excluded if these investigations or subsequent MRI and echocardiogram showed any abnormalities.
The study protocol conformed to the ethical guidelines of the 1975 Declaration of Helsinki. The medical ethics committees of all participating centers approved the study and written informed consent was obtained from all participants prior to inclusion.

General patient data
Demographic data, electrocardiogram, basic echocardiographic measurements and functional capacity were obtained for each patient. Exercise testing was performed using an electronically braked cycle ergometer (Lode Corrival, Lode BV, Groningen, the Netherlands), following a ramp protocol at a cadence of 70 revolutions per minute until exhaustion. Peak oxygen uptake per kilograms bodyweight (pVO_2/kg) was expressed as the percentage of the predicted value (%pVO_2/kg).

Cardiac Magnetic Resonance imaging
Cine imaging, 2D flow imaging & functional analysis
All participants were imaged using a pre-defined imaging protocol without sedation. A commercially available 1.5-T MRI system (Ingenia R4.1.2; Philips Healthcare, Best, the Netherlands) was used, with a dedicated chest phased-array parallel-imaging capable surface coil. Steady-state free precession cine images were acquired in various orientations during repeated end-expiratory breath holds. Multi-slice cine short-axis acquisitions were acquired from the apex up to and including the atrioventricular valves and the entire left and right ventricle. The following sequence parameters were used: TR/TE 3.4/1.69 ms, voxel size 1.3x1.3x8.0mm, flip angle: 55° and a temporal resolution of 30 phases per cardiac cycle. Two-dimensional quantitative through-plane flow (Q-flow) was measured at the level of the pulmonary valve - or aortic valve in case of systemic RV - with a retrospectively ECG-gated, velocity-encoded phase-contrast sequence (TR/TE 5.2/3.1 ms, voxel size 2.5x2.5x8mm, flip angle 12o, field of view 320, matrix 128x100, 20 phases per cardiac cycle). The VENC was set to 150 cm/sec, in case of a pulmonary artery stenosis it was individually adapted to yield images without aliasing artifacts.
RV and LV volumetric analysis was performed by manual tracing of endocardial and epicardial contours in end-diastolic and end-systolic phase in all slices, using Qmass MR Research edition (version 7.4, Medis, Leiden, The Netherlands), with a previously described RV analysis protocol, excluding the trabeculae and papillary muscles from the ventricular blood pool volume.[17]
The following parameters were determined for the right ventricle: end-diastolic volume (EDV), end-systolic volume (ESV), stroke volume (SV), ejection fraction (EF) and RV mass. Quantification of 2D flow across the pulmonary valve (or aortic valve in systemic RVs) was performed using Medis Qflow (version 5.5, Medis, Leiden, the Netherlands) and used to calculate the effective

flow across the pulmonary valve (2D-flow PV). All volumetric data were indexed for body surface area. At end-diastole the maximum tricuspid annular diameters were measured in cine RV 2-chamber and 4-chamber views.

4-dimensional velocity encoded CMR

For planning purposes four-chamber, two-chamber (of both ventricles) and perpendicular views of each of the four cardiac valves were used – to ensure that the 4D-flow volume would enclose all valves during diastole and systole. Velocity data were acquired in three orthogonal directions. The 4D-flow MRI acquisition was based on the protocol previously described by Westenberg et al.14 The following acquisition parameters were used: repetition time msec/ echo time msec 7.3/3.9; field of view 370 x 219 x 63 mm; 3D volume imaging with 63-mm slab thickness reconstructed into 28 3.5 mm slices; 10° flip angle; acquisition voxel 3.43 x 3.65 x 3.5 mm; reconstructed voxel size 2.9 x 2.9 x 3.5 mm; 1 signal acquired; retrospective gating with 20-30% acceptance window, with 30 phases reconstructed during 1 average cardiac cycle; maximal velocity encoding of 150 cm/s in all 3 directions. To reduce acquisition time, echo planar imaging was used with a factor of 5.

Analysis of through-plane flow across the tricuspid valve was performed with Mass (version 5.1, Medis B.V., Leiden, Netherlands) In short, the TV plane was reconstructed in each cardiac phase using two orthogonal planes, perpendicular to the flow across the tricuspid valve (Figure 1 a-d). After the valve plane was reconstructed for each phase of the cardiac cycle, the through-plane flow was reformatted in 5 parallel planes with a slice gap of 5 mm (Figure 1-e&f). Subsequently, contours were drawn outlining the flow of the valve of interest (image 1D) for each phase. Through-plane motion correction using the velocity of myocardium was taken into account by a indicating a region of interest in the myocardium. Finally, forward and backward flow, regurgitant fraction and effective flow were derived from 4D-flow MRI.

To assess the accuracy of the 4D flow measurement across the TV, 4D-flow MRI derived tricuspid effective flow was compared to the current reference: 2D-flow MRI pulmonary effective flow. Severity of TR was classified according to regurgitation fraction: 0-10% (absent/trace); 10-20% (mild); 20-40% (moderate); > 40% (severe).[18]

Echocardiography

Echocardiography was performed using a Toshiba Artida system (Toshiba, Tokyo, Japan) with a 5-MHz transducer. Analysis was performed offline in XCelera (version 4.1.1.1133 - 2013; Philips, Best, Netherlands). RVSP was calculated using the Bernoulli equation with maximum velocity of TR or by maximal pulmonary valve gradient (only in PS patients with valvular stenosis), plus estimated right atrial pressure. In systemic RV patients the systemic systolic blood pressure at rest was used as RVSP. Tricuspid annular plane systolic excursion (TAPSE) and systolic velocity using tissue (TDI S') Doppler imaging were measured in 4-chamber view.

TR was visualized in a parasternal 2-CH RV, parasternal short axis aorta orientation and in the modified apical 4-CH view – if possible an apical 2CH-RV view was also used. To quantify TR the following parameters were taken into account: vena contracta width, early tricuspid inflow velocity, hepatic vein systolic flow reversal and density of regurgitant Doppler signal.[19] Lastly, the severity of TR was graded none/trace, mild, moderate or severe based on semi-quantitative and qualitative assessment - by an experienced imaging-cardiologist (F.M.) blinded to 4D-flow MRI results.

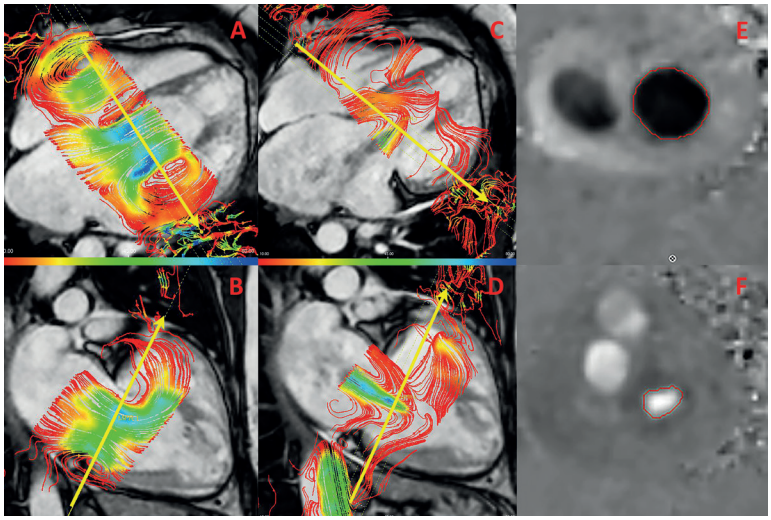

Figure 1: example of 4D flow in CHD patient
Example of 4D-flow analysis. In a-d the annular plane is reconstructed – perpendicular to the flow direction, in figure e+f the flow contours are drawn in the reconstructed through-plane flow slice.

Reproducibility
To assess intra-observer reproducibility 15 patients were re-analyzed by the first observer (M.S.). Inter-observer reproducibility was assessed in the same 15 patients by a second observer (M.D.). Both observers were blinded for the previous results and the first and second analysis were at least 1 month apart.

Statistical analysis
For all continuous variables, the distribution was tested using the Shapiro-Wilk test and by plotting histograms. Continuous data were expressed as mean value ± standard deviation (SD) or median [range] as appropriate. Continuous data were compared between groups using ANOVA with posthoc Dunnet's test or the Kruskal Wallis analysis of variance, depending on distribution of data and residuals. Categorical data was presented as absolute number followed by percentage; the agreement of TR grade by echocardiography and 4D-flow was assessed using linear weighted Kappa (<0.2 slight, 0.2-0.4 fair, 0.4-0.6 moderate, 0.6-0.8 considerable and >0.80 almost perfect agreement).
Agreement between 2D-flow derived PV effective stroke volume and 4D-flow derived TV effective stroke volume as well as between repeated measures was assessed using intraclass correlation coefficients (ICC) and paired-samples T-test. Furthermore, Bland Altman plots were constructed. All data analyses were performed in IBM SPSS statistics (version 20.0, IBM, Chicago, IL). P-values of <0.05 were considered statistically significant.

Results

Demographic data
All demographic and baseline data are listed in table 1. In short, PH patients were older than the control group and CHD patients. Patients with systemic RVs had the highest RVSP. Average VO_2max/kg predicted for age and weight (%PredVO_2/kg) was slightly decreased in the PS/TOF and

	Controls (n=21)	CHD (n=37)		PH (n=30)	p-value
		PS (n=21)	SystRV (n=16)		
Age, yrs	41.2±10.5	30.6±12.6#	36.6±8.4	54.4±15.6**	<0.001
BSA, m^2	1.93±0.21	1.90±0.15	1.94±0.15	1.92±0.26	0.974
RVSP, mmHg	-	50 [40-111]	108 [89-127]	54 [23-100]	0.025
VO_2/kg, ml/min	-	29.7±6.6	27.1±6.6	17.0±4.1	<0.001
%PredVO_2/kg	-	83.8±17.2	83.0±18.5	62.9±12.9	<0.001
QRS, msec	93.1±13.7	133.1±34.4**	107.2±16.2	97.5±24.2	<0.001
Heart rate	61±9	69±9	59±8	69±12	0.013
RVEDV, ml/m^2	97 [60-134]	95 [71-170]	109 [73-222]	110 [52-343]	0.476
RVESV, ml/m^2	46 [20-59]	49 [26-122]	58 [26-170] *	60 [16-271]*	0.009
RVEF, %	54.8±4.6	49.0±9.2	45.5±10.7#	41.1±11.4**	0.017

Table 1: Demographic data

General demographic data for all groups. To test for differences between the different groups (last column) ANOVA with posthoc Dunnets (controls as reference) was used for normally distributed data and Kruskal Wallis analysis of variance with Mann Whitney U tests for non-normally distributed data. #p<0.05, *p<0.01, **p<0.001

5

	Controls (n=21)	CHD (n=37)		PH (n=30)	
		PS (n=21)	Syst RV (n=16)		p-value
4D-TV FW, ml	111.5±27.3	91.2±15.2#	95.4±19.8	87.2±21.7**	0.232
4D-TV BW, ml	8.3 [2.0-24.1]	8.4 [5.1-25.9]	10.7 [3.7-34.0]	7.3 [2.2-57.7]	0.613
4D-SV TV, ml/m^2	52.4±9.4	42.5±5.7**	41.7±8.0**	38.7±9.6**	0.130
4D-TV reg, %	7.9 [1.9-17.6]	9.3[5.4-25.0]	12.5 [5.1-40.1]	9.2 [3.2-49.6]	0.307
2D-SV PA, ml/m^2	49.5±7.7	42.1±4.8*	42.8±7.5#	38.0±9.6**	<0.001
TVann 4CH, mm	37.4±4.1	38.8±5.8	42.3±5.0*	39.6±4.4	0.032
TVann 2CH, mm	37.5±4.3	37.7±5.3	38.5±4.5	38.5±3.6	0.835

Table 2: results of CMR measurements

Results of volumetric and 4D flow measurements on cardiac magnetic resonance imaging.

To test for differences between the different groups (last column) ANOVA with posthoc Dunnets (controls as reference) was used for normally distributed data and Kruskal Wallis analysis of variance with Mann Whitney U tests (controls as reference) for non-normally distributed data. #p<0.05, *p<0.01 and **p<0.001.

Syst RV groups and severely decreased in the PH group. Basic volumetric CMR measurements are also listed in table 1; RV volumes were increased in systemic RV and PH patients compared to controls.

Accuracy of 4D-SV TV compared to reference 2D-SV PV

TV 4D-flow analysis was possible in 67/67 patients (100%). Effective flow measured across the TV by 4D-flow MRI could be compared to 2D-flow effective flow across the PV in 85/88 subjects, due to poor quality of 2D-flow MRI in three subjects (Figure 2a-c). The intra-class correlation coefficient between both measurements was 0.90 (95% confidence interval 0.85-0.94; p<0.001) and the R2 was 0.83. Mean difference in 4D-flow MRI derived TV stroke volume vs 2D-flow MRI derived PV stroke volume was -1.6 ml (p=0.083) with limits of agreement: -20.0 to 16.8 ml.

Reproducibility of 4D flow measurements

Reproducibility measurements are listed in table 3 and are shown in figure 3. Both intra- and interobserver measurements yielded good intra-class correlation coefficients (all > 0.91 and p<0.001). Mean intra- and interobserver differences in forward flow and effective flow were

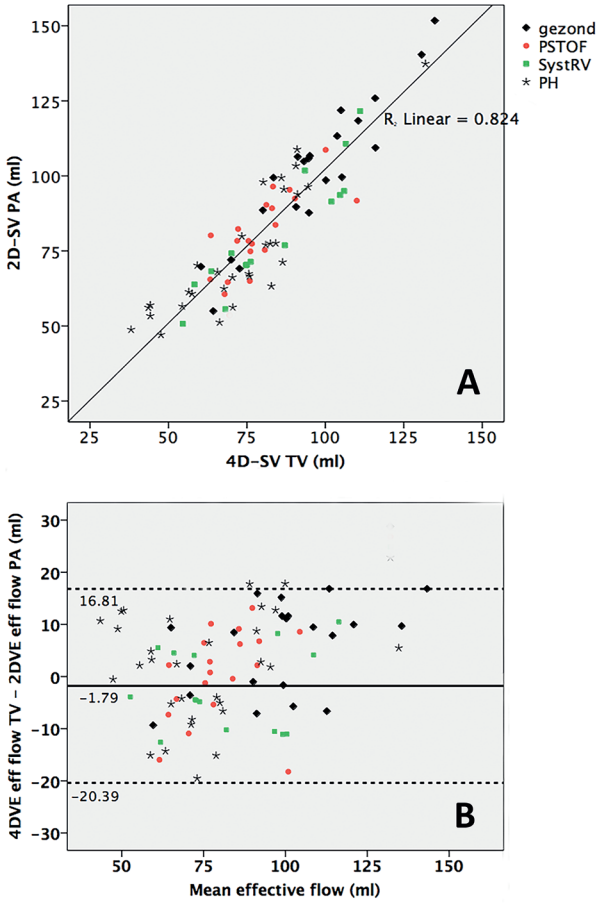

Figure 2: accuracy of 4D-VE TV flow and 2D-VE PA flow

2a depicts the correlation between effective flow across the tricuspid valve using 4D-VE CMR (4D-VE TV flow) and effective flow across the pulmonary valve using 2D-VE CMR (2D-VE PA). 2b depicts a Bland-Altman analysis with the difference between both effective flow measurements on the x-axis and the average of both measurements on the y-axis.

Intraobserver	Mean Δ	p-value[1]	ICC	p-value[2]
Forward flow, ml	1.08 ± 4.58	0.911	0.963	<0.001
Stroke volume, ml	-1.51 ± 5.80	0.329	0.981	<0.001
Regurgitance, %	-1.07 ± 4.58	0.378	0.910	<0.001
Interobserver				
Forward flow, ml	1.44 ±9.26	0.370	0.911	<0.001
Stroke volume, ml	2.12 ±8.86	0.556	0.935	<0.001
Regurgitance, %	-1.1 ± 3.5	0.242	0.968	<0.001

Table 3: Intra- and interobserver agreement
Mean difference (Δ) between repeated measures and significance were tested with a paired Student T-test and agreement using intra-class correlation coefficient (ICC).
1p-value using paired Student T test; 2p-value for intra-class correlation coefficient (ICC).

small with good limits of agreement (table 3). The mean difference and limits of agreement for measurement of TR (%) were acceptable for both intra- and inter-observer measurements (1.08% [-7.90; 10.06] and -1.10% [-7.96; 5.76], respectively).

Tricuspid regurgitation classified by CMR vs. echocardiography
Severity of TR could be graded by 4D-flow MRI in all 67 patients, and in 65/67 (97%) patients by echocardiography. Of these patients, 40/65 patients (61.5%) showed consistent results for echo and MRI, but 25/65 (38.5%) were reclassified by at least 1 grade using 4D-flow MRI compared to echocardiographic grading (table 4). TR grade assessed by echocardiography only showed moderate agreement to TR grade assessed by 4D-flow MRI, the linear weighted kappa was 0.52 (95%-confidence interval 0.37-0.67).
A trace to mild TR grade by echocardiography excludes moderate or severe TR by 4D-flow MRI in 95% of patients (i.e. negative predictive value). However, moderate or severe TR grade by echocardiography corresponded to a similar TR grade by MRI in only 60% of patients (i.e. positive predictive value).

Discussion

In this study, we assessed the feasibility, accuracy and reproducibility of 4D-flow MRI derived TV flow in patients with RV heart disease and varying degrees of TR. Four-dimensional-flow across the TV proved to be feasible in all patients and is accurate when compared to the reference standard 2D-flow derived PV effective flow. Furthermore, reproducibility of 4D-flow derived TV flow and regurgitation were good, even in this complex patient population. In 25/65 (38.5%) of the patients, 4D-flow MRI led to a different grading of TR compared to echocardiography.

4D-flow MRI of tricuspid valve
In our patient cohort, effective flow across the TV measured with 4D-flow MRI is accurate when

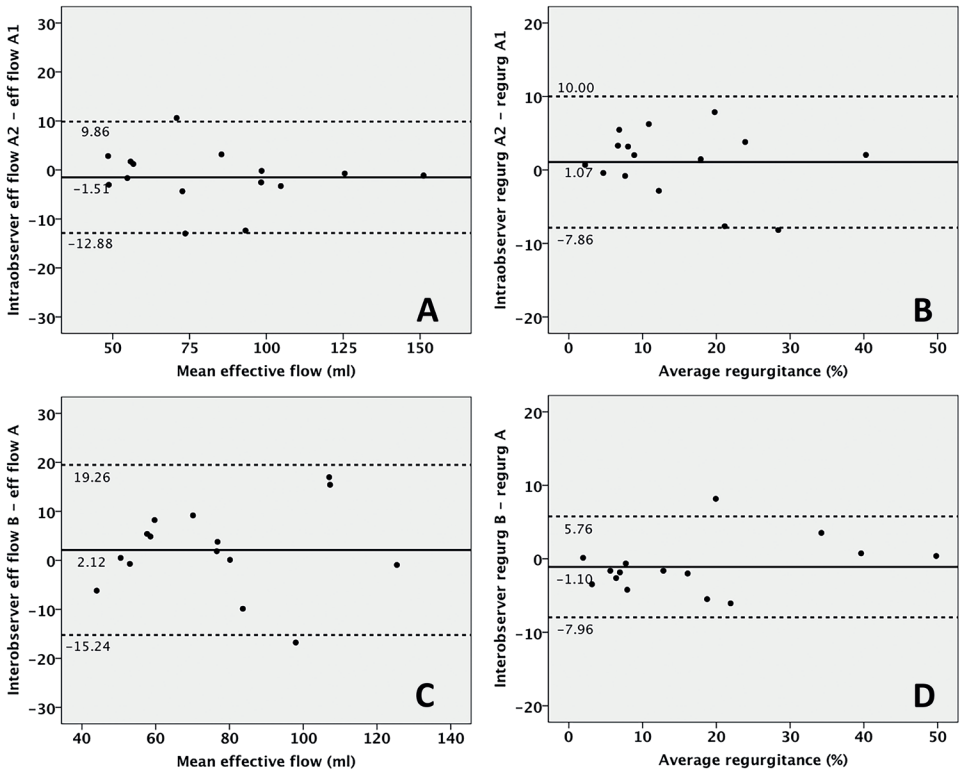

Figure 3: reproducibility of 4D flow measurements
3a&3b Bland-Altman analysis of intra-observer repeated measurements of effective flow (a) and regurgitation (b). 3c&3d Bland-Altman analysis of inter-observer repeated measurements of effective flow (c) and regurgitation (d).

compared to effective flow across the PV with 2D-flow MRI. This is true for both patient groups (ICC 0.870) as well as healthy controls (ICC 0.895). Our results are in line with previous reports on 4D-flow MRI derived TV flow in patients without RV heart disease, by Westenberg et al., and those with tetralogy of Fallot without TR, by van der Hulst et al.[14,15] The limits of agreement for effective flow (i.e. stroke volume) difference between 4D-flow across the TV and 2D-flow across the PV varied between -20.0 to +16.8 ml. These values are acceptable, as even for repeated 2D-flow measurements of semi-lunar valves there is considerable inter-observer and interscan variation.20,21 For example, Kondo et al. reported a relative difference of 7.0±5.6% for repeated 2D-flow derived PV flow measurements.[21] The difference between 4D-flow derived TV flow and 2D-flow derived PV flow can further be explained by several other factors: 1) 2D-flow suffers from through plane movement; 2) 2D-flow across the PV was obtained during end-expiratory breath-hold while 4D-flow was obtained during free-breathing and 3) interscan variability (even though time between acquisitions was <10 minutes).

Thus far, reproducibility measurements have been mostly obtained in patients with structurally normal hearts or focused on other applications of 4D-flow MRI (i.e. peak flow velocity and wall stress).[14,22] In patients with RV dilation and hypertrophy TV geometry is distorted.[4] Hence,

reproducibility of TV flow measured by 4D-flow MRI in this population, cannot be extrapolated from healthy controls or patients with structurally normal hearts. The present study provides this data and demonstrates good intra-observer and inter-observer agreement with acceptable limits of agreement and excellent ICC coefficients (all >0.90). The reproducibility in our cohort is comparable to limits of agreement reported in TV flow of healthy controls by Westenberg et al. and 2D-flow MRI of pulmonary or aortic valves.[20,21]

Echocardiography vs 4D-flow MRI

We demonstrate a discrepancy between 4D-flow MRI and echocardiographic TR grading in our patient cohort. Twenty-five out of 65 patients (38.5%) were classified differently by at least one grade using quantitative 4D-flow MRI measurements compared to echocardiographic assessment. With the lack of a gold standard it is difficult to be sure which of these techniques provides the most accurate results. However, since 4D-flow derived TV flow assessment has been validated both in vitro and in vivo[10, 14,23] and TR grading by echocardiography has shown less consistent results [5,7,8], we assume that the 4D-flow MRI results are more reliable. Importantly, a trace to mild TR grade by echocardiography still excludes moderate or severe TR by 4D-flow MRI in 95% of patients.

Clinical implications

As is the case for many other measurements of right ventricular size and function, echocardiography is an excellent screening tool. However, for assessment of degree of TR, 4D-flow MRI likely is more reliable and reproducible. If moderate or severe TR is seen on echocardiography, additional assessment of TR by means of 4D-flow MRI may help or guide clinical decision-making. In patients in whom surgery is considered, TR grading using 4D-flow MRI may improve selection of patients that potentially benefit from TV annuloplasty.[24-27] Moreover, the detailed anatomical information obtained with 4D-flow MRI (figure 1) may be helpful in identifying the mechanism of regurgitation and planning of intervention.

In both pulmonary hypertension patients as well as CHD the degree of TR is related to symptoms and mortality.[1-3,28] Accurate determination of the degree of TR can help physicians better understand a patients' physiology and ensure timely referral of patients for surgery or transplant.

Echo grade	CMR grade				
	None/trace	Mild	Moderate	Severe	Total
None/trace	**23**	3	0	0	26
Mild	12	**14**	3	0	29
Moderate	1	3	**2**	2	8
Severe	0	0	1	**1**	2
Not gradable	0	0	2	0	2
Total	36	20	8	3	67

Table 4: Contingency table of TV regurgitation grade by echocardiography vs 4D-VE CMR

Crosstab depicting the results for TR grading by echocardiography versus 4D-flow CMR. The linear weighted kappa for agreement between both methods was 0.52 (95%-confidence interval 0.37-0.67).

Limitations

This study has limitations. First, 4D-flow MRI post-processing and analysis remains time-consuming and labor-intensive. This limits its current use in clinical practice for many institutions. Improvements in software may accelerate post processing and make it less user-dependent.

We chose to use 2D-flow derived PV flow as reference measurement for stroke volume, introducing interscan variability and through plane motion. Invasively measured stroke volumes across the pulmonary valve were not available. We did not use 4D-flow for PV flow as many of our patients had severe pulmonary stenosis with a large degree of aliasing or a homograft – for which 4D-flow MRI is not yet validated.

Conclusion

Four-dimensional flow MRI is an accurate and reproducible method to measure TV flow and regurgitation. Twenty-five out of 65 patients (38.5%) were classified differently by at least one grade using quantitative 4D-flow MRI TR measurements compared to echocardiographic assessment. However, a trace to mild TR by echocardiography excludes moderate or severe TR by 4D-flow MRI in 95% of patients. As software developments accelerate 4D-flow MRI post-processing, it can provide a more reliable and reproducible method of grading TR in clinical practice and future studies.

References

1. Bokma JP, Winter MM, Oosterhof T, et al. Severe tricuspid regurgitation is predictive for adverse events in tetralogy of Fallot. Heart 2015;101:794-799.
2. Nath J, Foster E, Heidenreich PA. Impact of tricuspid regurgitation on long-term survival. J Am Coll Cardiol 2004;43:405-409.
3. Dandel M, Knosalla C, Kemper D, Stein J, Hetzer R. Assessment of right ventricular adaptability to loading conditions can improve the timing of listing to transplantation in patients with pulmonary arterial hypertension. J Heart Lung Transplant 2015;34:319-328.
4. Di Mauro M, Bezante GP, Di Baldassarre A, et al. Functional tricuspid regurgitation: an underestimated issue. Int J Cardiol 2013;168:707-715.
5. Valente AM, Cook S, Festa P, et al. Multimodality imaging guidelines for patients with repaired tetralogy of fallot: a report from the AmericanSsociety of Echocardiography: developed in collaboration with the Society for Cardiovascular Magnetic Resonance and the Society for Pediatric Radiology. J Am Soc Echocardiogr 2014;27:111-141.
6. Lancellotti P, Moura L, Pierard LA, et al. European Association of Echocardiography recommendations for the assessment of valvular regurgitation. Part 2: mitral and tricuspid regurgitation (native valve disease). Eur J Echocardiogr 2010;11:307-332.
7. Grant AD, Thavendiranathan P, Rodriguez LL, Kwon D, Marwick TH. Development of a consensus algorithm to improve interobserver agreement and accuracy in the determination of tricuspid regurgitation severity. J Am Soc Echocardiogr 2014;27:277-284.
8. Grossmann G, Stein M, Kochs M, et al. Comparison of the proximal flow convergence method and the jet area method for the assessment of the severity of tricuspid regurgitation. Eur Heart J 1998;19:652-659.
9. Fratz S, Chung T, Greil GF, et al. Guidelines and protocols for cardiovascular magnetic resonance in children and adults with congenital heart disease: SCMR expert consensus group on congenital heart disease. J Cardiovasc Magn Reson 2013;15:51-429X-15-51.
10. Westenberg JJ, Danilouchkine MG, Doornbos J, et al. Accurate and reproducible mitral valvular blood flow measurement with three-directional velocity-encoded magnetic resonance imaging. J Cardiovasc Magn Reson 2004;6:767-776.
11. Morcos P, Vick GW,3rd, Sahn DJ, Jerosch-Herold M, Shurman A, Sheehan FH. Correlation of right ventricular ejection fraction and tricuspid annular plane systolic excursion in tetralogy of Fallot by magnetic resonance imaging. Int J Cardiovasc Imaging 2009;25:263-270.
12. Myerson SG. Heart valve disease: investigation by cardiovascular magnetic resonance. J Cardiovasc Magn Reson 2012;14:7-429X-14-7.
13. Kon MW, Myerson SG, Moat NE, Pennell DJ. Quantification of regurgitant fraction in mitral regurgitation by cardiovascular magnetic resonance: comparison of techniques. J Heart Valve Dis 2004;13:600-607.
14. Westenberg JJ, Roes SD, Ajmone Marsan N, et al. Mitral valve and tricuspid valve blood flow: accurate quantification with 3D velocity-encoded MR imaging with retrospective valve tracking. Radiology 2008;249:792-800.
15. van der Hulst AE, Westenberg JJ, Kroft LJ, et al. Tetralogy of fallot: 3D velocity-encoded MR imaging for evaluation of right ventricular valve flow and diastolic function in patients after correction. Radiology 2010;256:724-734.
16. Galie N, Humbert M, Vachiery JL, et al. 2015 ESC/ERS Guidelines for the diagnosis and treatment of pulmonary hypertension: The Joint Task Force for the Diagnosis and Treatment of Pulmonary Hypertension of the European Society of Cardiology (ESC) and the European Respiratory Society (ERS): Endorsed by: Association for European Paediatric and Congenital Cardiology (AEPC), International Society for Heart and Lung Transplantation (ISHLT). Eur Heart J 2016;37:67-119.
17. Driessen MM, Baggen VJ, Freling HG, et al. Pressure overloaded right ventricles: a multicenter study on the importance of trabeculae in RV function measured by CMR. Int J Cardiovasc Imaging 2014;30:599-608.
18. Renella P, Aboulhosn J, Lohan DG, et al. Two-dimensional and Doppler echocardiography reliably predict severe pulmonary regurgitation as quantified by cardiac magnetic resonance. J Am Soc Echocardiogr 2010;23:880-886.
19. Lancellotti P, Tribouilloy C, Hagendorff A, et al. Recommendations for the echocardiographic assessment of native valvular regurgitation: an executive summary from the European Association of Cardiovascular Imaging. Eur Heart J Cardiovasc Imaging 2013;14:611-644.
20. Dulce MC, Mostbeck GH, O'Sullivan M, Cheitlin M, Caputo GR, Higgins CB. Severity of aortic regurgitation: interstudy reproducibility of measurements with velocity-encoded cine MR imaging. Radiology 1992;185:235-240.
21. Kondo C, Caputo GR, Semelka R, Foster E, Shimakawa A, Higgins CB. Right and left ventricular stroke volume measurements with velocity-encoded cine MR imaging: in vitro and in vivo validation. AJR Am J Roentgenol 1991;157:9-16.
22. van Ooij P, Powell AL, Potters WV, Carr JC, Markl M, Barker AJ. Reproducibility and interobserver variability of systolic blood flow velocity and 3D wall shear stress derived from 4D flow MRI in the healthy aorta. J Magn Reson Imaging 2016;43:236-248.
23. Bollache E, van Ooij P, Powell A, Carr J, Markl M, Barker AJ. Comparison of 4D flow and 2D velocity-encoded phase contrast MRI sequences for the evaluation of aortic hemodynamics. Int J Cardiovasc Imaging 2016;32:1529-1541.
24. Baumgartner H, Bonhoeffer P, De Groot NM, et al. ESC Guidelines for the management of grown-up congenital heart disease (new version 2010). Eur

Heart J 2010;31:2915-2957.
25. Dreyfus GD, Corbi PJ, Chan KM, Bahrami T. Secondary tricuspid regurgitation or dilatation: which should be the criteria for surgical repair? Ann Thorac Surg 2005;79:127-132.
26. Cramer JW, Ginde S, Hill GD, et al. Tricuspid repair at pulmonary valve replacement does not alter outcomes in tetralogy of Fallot. Ann Thorac Surg 2015;99:899-904.
27. Kogon B, Patel M, Leong T, McConnell M, Book W. Management of moderate functional tricuspid valve regurgitation at the time of pulmonary valve replacement: is concomitant tricuspid valve repair necessary? Pediatr Cardiol 2010;31:843-848.
28. Bokma JP, Winter MM, Mulder BJ, Bouma BJ. Tricuspid Regurgitation Secondary to Severe Pulmonary Regurgitation: When to Operate on Which Valves? Ann Thorac Surg 2015;100:2417-2418.

CHAPTER 6

Main pulmonary artery area limits exercise capacity in patients long-term after arterial switch operation

Authors:
Mieke M.P. Driessen*, Vivan J.M. Baggen*, Folkert J. Meijboom, Gertjan Tj. Sieswerda, Nicolaas J.G. Jansen, Sebastiaan W.H. van Wijk, Pieter A. Doevendans, Tim Leiner, Paul H. Schoof, Tim Takken, Johannes M.P.J. Breur
*Shared first authorship

J Thorac Cardiovasc Surg 2015;150:918-25.

Abstract

Background
Despite excellent survival in patients after the arterial switch operation, reintervention is frequently required and exercise capacity is decreased in a substantial number of patients. This study relates right-sided imaging features in patients long-term after the arterial switch operation to exercise capacity and ventilatory efficiency to investigate which lesions are functionally important.

Methods
Patients operated in the UMC Utrecht, the Netherlands (1976-2001) and healthy controls underwent cardiac magnetic resonance imaging and cardiopulmonary exercise testing within 1 week. We measured main, left, and right pulmonary artery cross-sectional areas, pulmonary blood flow distribution, peak oxygen uptake, and minute ventilation relative to carbon dioxide elimination.

Results
A total of 71 patients (median age, 20 [12-35] years, 73% were male) and 21 healthy controls (median age, 26 [21-35] years, 48% were male) were included. Main, left, and right pulmonary artery areas were decreased compared with controls (190 vs 269 mm^2/m^2, 59 vs 157 mm^2/m^2, 98 vs 139 mm^2/m^2, respectively, all P <0.001); however, pulmonary blood flow distribution was comparable (P=0.722). Peak oxygen uptake and minute ventilation relative to carbon dioxide elimination were 88%±20% and 23.7±3.8, respectively, with 42% and 1% of patients demonstrating abnormal results (≤84% and ≥34, respectively). The main pulmonary artery area significantly correlated with peak oxygen uptake (r=0.401, P<0.001) and pulmonary blood flow distribution with minute ventilation relative to carbon dioxide elimination (r=0.329, P=0.008). Subanalysis (<18, 18-25,>25 years) showed that the main pulmonary artery area was smaller in older age groups. In multivariable analysis, the main pulmonary artery area was independently associated with peak oxygen uptake (P=0.032).

Conclusion
In adult patients after the arterial switch operation, narrowing of the main pulmonary artery is a common finding and is the main determinant of limitation in functional capacity, rather than pulmonary branch stenosis.

Introduction

Transposition of the great arteries is the most common cyanotic congenital heart defect, occurring in 4.7 out of 10.000 newborns.[1] The current treatment of choice is neonatal arterial switch operation, as described in 1975 by Jatene and collegues.[2]
Follow-up studies show excellent results with low perioperative mortality and high 25-year survival (> 95%). However, the cumulative risk of reintervention increases up to 25% in adult patients.[3,4] Most of these patients have supravalvular neopulmonary artery or pulmonary branch stenosis and undergo balloon dilatation or stenting by catheter intervention or surgical pulmonary artery reconstruction.[4] Apart from reintervention, longterm follow-up studies show that exercise capacity is decreased in a significant subset of patients.[5-7] Reduced exercise capacity has been associated with right-sided obstructive lesions.[6,7] Still, long-term follow-up data are limited, and defined management strategies for subclinical anatomic or physiologic abnormalities are lacking.[8]
This study compared patients long-term after arterial switch operation with healthy controls, focusing on right ventricular (RV) function, pulmonary artery and branch cross-sectional areas, pulmonary branch relative area change, and pulmonary blood flow (PBF) distribution. Second, these imaging features were related to exercise capacity and ventilatory efficiency, in order to determine which lesions are functionally important and therefore potentially amenable to re-intervention.

Methods

Study population
We performed a cross-sectional cohort study between August 2011 and February 2014. All patients who underwent an arterial switch operation in our center who were aged more than 12 years (1976-2001) were approached. Patients prospectively underwent cardiac magnetic resonance (CMR) imaging, echocardiography, and cardiopulmonary exercise testing within 1 week, without any change in clinical condition. Healthy control subjects (aged 18-35 years) underwent CMR and echocardiography with the same study protocol. Exercise testing was not performed in healthy controls because reference values are well established.[9] The institutional review committee of the University Medical Center Utrecht approved this study. Informed consent was obtained from all patients, parents if aged less than 18 years of age, and healthy controls. Patient characteristics were obtained from the patient chart. Patients with a homograft, signs of myocardial ischemia during the exercise test, or claustrophobia were excluded.

CMR acquisition
Patients and controls were scanned according to a predefined imaging protocol without anesthesia or sedation. A 1.5-T system (Ingenia R4.1.2, Philips Healthcare, Best, The Netherlands) was used with a dedicated chest phased-array parallel imaging–capable surface coil with a maximum of 36 active elements.
Steady-state free precession cine images were acquired in various orientations (short axis, 4-chamber and 2-chamber long axis, right and left ventricular outflow tract views in 2 planes) during repeated end-expiratory breath holds. Multi-slice cine short-axis acquisition was planned

from the apex to well above the tricuspid and mitral valve: TR/TE 3.4/1.69 ms, voxel size 1.25 × 1.25 × 8 mm, flip angle 90°, matrix 192 × 171 mm, 30 frames/cycle.
Gadolinium-enhanced magnetic resonance angiography (MRA) images of the pulmonary vasculature were performed with non–electrocardiographygated time-resolved 3-dimensional (3D) spoiled gradient echo sequence: TR/TE 5.2/1.49, voxel size 0.94×0.94×2 mm, 60 slices, field of view 300, matrix 308 × 125, keyhole percentage 25%, 3 dynamics, keyhole scan time 2.8 seconds. Gadopentetate dimeglumine (0.2 mL/kg, injection rate 1.5 mL/s) was injected intravenously followed by saline flush (25 mL).
Quantitative through-plane flow through the left pulmonary artery (LPA) and right pulmonary artery (RPA) was measured with a retrospectively electrocardiography gated, velocity encoded phase-contrast sequence: TR/TE 5.2/3.1 ms, voxel size 2.5×2.5×8 mm, flip angle 12°, field of view 320, matrix 128×100, temporal resolution 20 frames/cycle.[10] In case of aliasing, the sequence was rescanned at a higher velocity encoding range. LPA and RPA flow measurements were performed on the narrowest points identified on scout, black-blood, and MRA images.

CMR analysis
RV volumetric analysis was performed by manual tracing of endocardial and epicardial contours, using Qmass MR Research edition (version 7.4, Medis, Leiden, The Netherlands), with a previously described RV analysis protocol.[11] Trabeculae and papillary muscles were selected and excluded from the blood volume using semiautomatic threshold-based segmentation software, which is based on the signal intensity distribution of the voxels.[12]
Diameters and areas of the main pulmonary artery (MPA), LPA, and RPA were measured on 3DMRAimages in OsiriX Imaging Software for MacOS 10.7 (version 5.5.2, 32-bit, Pixmeo, Geneva, Switzerland). Narrowest vessel lumina were selected in 2 perpendicular views to obtain the smallest cross-sectional area in the third view. The full width at half maximum method was used to distinguish vessel from surrounding tissue.[13]
Velocity-encoded CMR data were analyzed using QFlow (version 5.6, Medis, Leiden, The Netherlands). Contours were manually traced for the LPA and RPA lumina in all phases. In this way, maximal and minimal areas of the pulmonary branches were obtained. Flow data were determined with a velocity analysis of each voxel in all phases. One researcher performed all CMR analyses and was blinded for the results of the cardiopulmonary exercise test.

Calculation of right-sided imaging features
All volumetric data were indexed for body surface area, calculated by the Dubois formula. Pulmonary branch relative area change was calculated by (maximal area – minimal area) / minimal area x 100%. To express the degree of unilateral pulmonary branch stenosis, relative branch area was calculated by smallest pulmonary branch area / (LPA + RPA area) x 100%. Significant unilateral pulmonary branch stenosis was defined as a relative branch area of <30%. PBF distribution was calculated by relative effective stroke volume (forward flow – backward flow per heart beat) to the left and right lung: LPA (or RPA) effective stroke volume / (LPA + RPA effective stroke volume) x 100%. Abnormal PBF distribution was defined as a greater than 15% point deviation from normal (45:55 L:R, thus <30% LPA relative flow or <40% RPA relative flow).

Echocardiography
Doppler transthoracic echocardiography was performed on a Toshiba Artida (Toshiba, Tokyo,

Japan) with a 5-MHz transducer. The greatest continuous wave velocity of the tricuspid regurgitation jet was used to express RV systolic pressure, using the Bernoulli equation ($4TR^2$). The greatest continuous wave velocity measured across the pulmonary valve was used as an index of RV outflow tract (RVOT) obstruction.[6]

Exercise testing

Patients performed a cardiopulmonary exercise test using an electronically braked cycle ergometer (Lode Corrival, Lode BV, Groningen, The Netherlands). Before exercise, forced expiratory volume in the first second was measured. After a rest period of 3 minutes and 3 minutes of unloaded cycling, the work rate was increased in a ramp-like protocol with 15, 20, or 25 Watts per minute. It was aimed to complete the test within 8 to 12 minutes.[14] Maximum effort was defined as a peak respiratory exchange ratio of greater than 1.0 for children and greater than 1.1 for adults. Indications for premature test termination are provided by the American Thoracic Society/ American College of Chest Physicians.[9]

During exercise, oxygen uptake (VO_2), carbon dioxide elimination (VCO_2), and minute ventilation (VE) were recorded using a computerized breath-by-breath analyzer (ZAN 600, ZAN Mebgeräte GmbH, Accuramed BVBA, Herk-de-Stad, Belgium). Respiratory exchange ratio was calculated by VCO_2/VO_2 and breathing reserve by (1 - peak VE/[FEV1 x 40]) x 100%. Peak oxygen uptake (VO_2peak%) was expressed as percentage of the predicted value, based on age, sex, height, and body weight.[15] Ventilatory efficiency (minute ventilation relative to carbon dioxide elimination [VE/VCO_2slope]) was calculated using linear regression, up to the respiratory compensation point. Peak heart rate 85% or less, VO_2peak 84% or less, and VE/VCO_2slope 34 or greater were considered abnormal.[9] Specific reference values for children were applied in patients aged 12 to 18 years.[16]

Reproducibility

Intra- and inter-observer reproducibility of RV function analysis was previously assessed and published.[11] In addition, we assessed reproducibility of 3D MRA analysis by blinded re-analysis of 10 random datasets by a second observer.

Statistical analysis

For all variables the distribution was tested using the Shapiro-Wilk test. Continuous data were expressed as mean value ±standard deviation (SD) or median [interquartile range (IQR)] as appropriate. Depending on the distribution of data, the independent-samples T-test or the Mann-Whitney U test was used to compare groups. For categorical data, the Chi-Square test was used. Associations were evaluated using Pearson or Spearman's rho (r) coefficient as appropriate.

For the sub analysis, we could not define clear changes in surgical strategies over time. Therefore, we chose to define three age groups (<18, 18-25, >25 years), based on approximately equal years and patients per subgroup. Sub analysis for three pre-defined age groups was performed using Chi-Square Mantel-Haenszel tests and linear regression for dichotomous and continuous outcomes, respectively. Associations were adjusted for age, sex and operative characteristics using multivariable linear regression. Reproducibility was tested with intraclass correlation coefficients and paired-samples T-test. Mean relative differences were calculated with (Obs1 – Obs2) / ((Obs1 + Obs2) / 2) x 100%. All data analysis was performed in IBM SPSS statistics (version 20.0, IBM, Chicago, IL). P-values of <0.05 were considered statistically significant.

Results

Study population

Eighty-six perioperative survivors were approached, of whom 74 participated. Three patients with a homograft were excluded, because this predisposes to obstruction and decreased exercise capacity. None of the patients had ST-T–segment dynamics typical of myocardial ischemia. The remaining 71 patients represented the cohort as analyzed in the present study (median age, 20.1 [14.5-26.1] years; range, 12-35, 52 male, 73%). Exercise testing was performed in 69 patients. Eight patients (11%) underwent pulmonary artery banding, and 48 patients (68%) underwent the Rashkind procedure. The median age at arterial switch operation was 7 (5-20) days (range, 0-755 days). The Lecompte maneuver was performed in 63 patients (89%).[17] Ventricular septal defect was surgically closed in 20 patients (28%), of whom 2 had Taussig–Bing anomaly; aortic coarctation was repaired in 5 patients (7%). Eleven patients (16%) underwent 1 or multiple RVOT reinterventions, of whom 7 (10%) underwent a surgical procedure. Twenty-one healthy controls were included (median age, 26.4 [23.2-29.9] years; range, 21-35, 10 male, 48%).

Patients after arterial switch operation compared with healthy controls

Doppler echocardiography and CMR measurements in patients after the arterial switch operation are compared with healthy controls in Table 1. All measured cross-sectional areas of the pulmonary tree (MPA, LPA, and RPA) were significantly and substantially reduced in patients (P< 0.001). Significant unilateral branch stenosis (relative branch area of< 30%) was present in 26 of 70 patients with available 3D MRA data (37%). Abnormal PBF distribution was present in only 5 of 66 patients with representative flow data (7%), of whom 4 had less than 30% relative LPA flow and 1 had less than 40% relative RPA flow. PBF distribution and smallest relative and absolute pulmonary branch flow in patients were not significantly different from those in controls (P= 0.722, P= 0.444, and P= 0.210, respectively).

LPA and RPA relative area change did not significantly differ from controls; however, the range of data distribution was larger. The maximal flow velocities across the pulmonary valve (echocardiography) and pulmonary branches (CMR phase-contrast) were increased compared with controls (P< 0.001).

Cardiopulmonary exercise testing

Exercise testing results are presented in Table 2. Patients achieved a median peak heart rate of 98% of predicted (interquartile range, 94-102), 4 out of 69 patients (6%) had an inadequate increase of heart rate during exercise (range, 71 to 83% of predicted). Mean VO_2peak% was 88±20%, 29 patients (42%) were qualified as abnormal (69±11%). Mean VE/VCO_2slope was 23.7±3.8; one patient (1%) had an abnormal VE/VCO_2slope (35).

Age, sex and imaging features related to functional outcome

Univariable correlations of age, sex and imaging features with exercise capacity and ventilatory efficiency are presented in Table 3. Age negatively correlated with VO_2peak% (r= -0.315, P= 0.008) and males generally had better exercise capacity (r= 0.318, P= 0.008). RV end-diastolic volume and stroke volume were both significantly associated with exercise capacity and ventilatory

	Patients (n=71)	Controls (n=21)	p-value
Age, years*	20.1 [14.5-26.1]	26.4 [23.2-29.9]	<0.001
Sex, male n (%)†	52 (73)	10 (48)	0.028
RV systolic pressure, mmHg	29 ±10	-	-
Maximal velocity across pulmonary valve, cm/s	207 ±68	107 ±15	<0.001
RV function			
RV end-diastolic volume, mL/m²*	95 [85-104]	104 [91-116]	0.014
RV end-systolic volume, mL/m²*	41 [35-48]	50 [45-58]	0.003
RV stroke volume, mL/m²	53 ±9	56 ±9	0.160
RV ejection fraction, %	55 ±5	53 ±4	0.048
RV mass, gr/m²*	30 [27-35]	23 [21-26]	<0.001
Pulmonary artery cross-sectional areas			
MPA area, mm²/m²*	190 [137-238]	269 [242-301]	<0.001
LPA area, mm²/m²*	59 [41-86]	157 [141-186]	<0.001
RPA area, mm²/m²*	98 [63-147]	139 [123-175]	<0.001
LPA + RPA area, mm²/m²*	175 [109-228]	300 [272-343]	<0.001
Smallest branch area, mm²/m²*	51 [37-77]	139 [123-169]	<0.001
Qflow measurements			
LPA relative area change, %*	43 [31-61]	42 [35-53]	0.754
RPA relative area change, %*	56 [40-66]	51 [45-65]	0.966
LPA:RPA flow, %	45:55 ±8	45:55 ±4	0.722
Smallest branch flow, %*	44 [39-47]	46 [41-47]	0.444
Smallest branch flow, mL/m²*	21 [19-25]	23 [21-26]	0.210
LPA peak flow velocity, cm/s*	168 [139-204]	73 [66-82]	<0.001
RPA peak flow velocity, cm/s*	166 [140-207]	88 [77-97]	<0.001
LPA regurgitation fraction, %*	2.7 [0.6-10.0]	3.0 [2.2-7.0]	0.565
RPA regurgitation fraction, %*	5.8 [1.6-8.5]	1.7 [0.6-2.7]	0.001

Table 1. Patients after arterial switch operation compared with healthy controls. Abbreviations: RV, right ventricular; MPA, main pulmonary artery; LPA, left pulmonary artery; RPA, right pulmonary artery.
**Legend: ***median [interquartile range] and Mann-Whitney U test; †n (%) and Chi-Square test; other mean ±SD and independent-samples T-test).

efficiency. MPA area significantly correlated with VO_2peak% (r=0.401, P= 0.001), however the sum of LPA and RPA area, and smallest pulmonary branch area were not related to VO_2peak%. Smallest pulmonary branch area (mm^2/m^2) and smallest relative branch flow (%) were significantly associated with VE/VCO_2slope (r=-0.301, P= 0.013 and r=-0.307, P= 0.014 respectively).
The MPA area was also significantly related to RV stroke volume (r=0.273, P= 0.022) and RV systolic pressure (r=-0.493, P= 0.001). We repeated all analyses with exclusion of patients after pulmonary artery banding, because this is usually not an accepted practice in the contemporary era. This did not yield different conclusions.

Sub analysis in three age groups
Results of the sub analysis in 3 pre-defined age groups (<18, 18-25 and >25 years) are presented in Figure 1 and Table 4. As presented in Figure 1, MPA area was not associated with exercise capacity in patients <18 years (β=-0.034, P= 0.635), who had largest MPA areas, while it was significantly related to exercise capacity both in patients 18-25 and >25 years (β=0.134, P= 0.008 and β=0.219, P= 0.045, respectively).
Table 4 shows the operative characteristics and imaging features per age group. Pulmonary artery banding was almost exclusively performed in the oldest age group (P< 0.001). Patients from the earliest surgical era underwent repair at an older age (P < 0.001), and for the reconstruction of the MPA mostly separate patches were used (vs pantaloon-type patch in younger patients) using pericardium treated with glutaraldehyde (vs untreated pericardium in younger patients). Oldest patients also had smallest MPA areas (229.6±47.7 mm^2/m^2, 196.3±77.7 mm^2/m^2, and 133.6±51.2 mm^2/m^2, P< 0.001), highest maximal velocity across the pulmonary valve (P< 0.001), highest RV mass (P= 0.035), highest RV systolic pressures (P< 0.001), and a trend toward a lower VO_2 peak% (P= 0.051). Pulmonary branch areas, flow, and VE/VCO_2 slope were not significantly different among the 3 age groups.

Lecompte Maneuver
Pulmonary branch areas were smaller in patients who underwent the Lecompte maneuver compared with patients who did not (LPA 52 [39-75] mm^2/m^2 vs 128 [91-149] mm^2/m^2, P< 0.001 and RPA 89 [58-139] mm^2/m^2 vs 145 [109-187] mm^2/m^2, P= 0.053); however, this did not translate into an abnormal PBF distribution (mean LPA:RPA relative flow 46:54 vs 47:53%, P= 0.181). MPA area, VO2 peak%, and VE/VCO_2 slope were comparable in both groups (P= 0.971, P= 0.216, and P= 0.555, respectively).

Multivariable analysis
MPA area remained significantly associated with exercise capacity (β=0.102, P= 0.032) after adjustment for age, sex and operative characteristics (age at repair, pulmonary artery banding, patch type and treatment, RVOT re-intervention). In this multivariable model, MPA area was the only significant predictor of exercise capacity.

Reproducibility
Inter- and intra-observer variability for measurement of MPA area on MRA was reflected by intraclass correlation coefficients of 0.993 and 0.997 and mean differences of 2.1±10.7 mm^2/m^2 (p=0.564) and 7.3 ±8.0 mm^2/m^2 (p=0.019), respectively. Mean relative differences for inter- and intra-observer variability were 0.7 ±5.3% and -3.7 ±3.2%.

Variable	Mean ±SD or median [IQR]
Weight, kg	64.2 ±17.7
Body surface area, m^2	1.75 ±0.29
Body mass index, kg/m^2	21.4 ±4.0
Peak minute ventilation, L/min	83.4 ±24.1
Forced expiratory volume in first second, L	3.44 ±0.91
Breathing reserve, %	37 [27-47]
Peak heart rate	
Beats/min	184 [177-192]
% predicted	98 [94-102]
Peak systolic blood pressure, mmHg	183 ±27
Peak workload	
Watt	208 ±55
% predicted	96 ±19
Peak oxygen uptake	
mL/kg/min	40.1 ±10.8
% predicted	88 ±20
Abnormal (≤84%), n (%)	29 (42)
mL/peak heart rate	13.6 ±3.9
% predicted	90 ±18
Minute ventilation/carbon dioxide elimination	
Slope	23.7 ±3.8
Abnormal slope (≥34), n (%)	1 (1)
Peak respiratory exchange ratio	1.17 ±0.10

Table 2. Exercise testing results of patients after arterial switch operation (n=69).

Discussion

In this cross-sectional cohort study of patients long-term after arterial switch operation, both MPA and pulmonary branch areas were significantly decreased compared with healthy controls and abnormal exercise capacity was common (42%). Cross-sectional MPA area was independently associated with exercise capacity in patients more than 18 years of age and correlated with stroke volume at rest and RV systolic pressure.

Significant unilateral pulmonary branch stenosis was present in 37% of patients; however this resulted in abnormal blood flow distribution in only 7% of patients. Other factors that potentially could inhibit exercise capacity in this group of patients, such as RV dysfunction or chronotropic incompetence, were uncommon in our cohort. These results indicate that narrowing of the MPA is a common finding in adult patients after arterial switch operation and that it is the main right-

	VO_2peak% (r)	VE/VCO_2slope (r)
Age, years†	−0.315**	0.073
Sex, male	0.318**	−0.279*
RV systolic pressure, mmHg	−0.112	−0.076
Maximal velocity across PV, cm/s	−0.304*	0.012
RV function		
RV end-diastolic volume, mL/m²†	0.305*	−0.306*
RV end-systolic volume, mL/m²†	0.159	−0.200
RV stroke volume, mL/m²	0.400**	−0.347**
RV ejection fraction, %	0.142	0.025
RV mass, gr/m²†	0.208	−0.235
Pulmonary artery cross-sectional areas		
MPA area, mm²/m²	0.401**	−0.043
LPA area, mm²/m²†	0.044	−0.249*
RPA area, mm²/m²†	0.115	−0.182
LPA + RPA area, mm²/m²†	0.093	−0.233
Smallest branch area, mm²/m²†	0.109	−0.301*
Qflow measurements		
LPA relative area change, %†	−0.032	−0.178
RPA relative area change, %†	−0.051	0.152
LPA : RPA flow, %	0.141: −0.141	−0.329**: 0.329**
Smallest branch flow, %†	0.105	−0.307*
Smallest branch flow, mL/m²†	0.260*	−0.264*
LPA peak flow velocity, cm/s	−0.070	0.154
RPA peak flow velocity, cm/s†	−0.249*	0.288*
LPA regurgitation fraction, %†	−0.076	−0.156
RPA regurgitation fraction, %†	0.002	0.245

Table3. Univariable correlations of age, sex and imaging features with exercise capacity and ventilatory efficiency in patients after arterial switch operation.
Abbreviations: VO2peak%, exercise capacity reflected by percentage of predicted peak oxygen uptake; VE/VCO_2 slope, ventilatory efficiency reflected as minute ventilation relative to carbon dioxide elimination; RV, right ventricular; PV, pulmonary valve; MPA, main pulmonary artery; LPA, left pulmonary artery; RPA, right pulmonary artery.
Legend: *p<0.05; **p<0.01; †Spearman's correlation; other Pearson's correlation.

sided lesion limiting functional capacity, rather than RV dysfunction or unilateral pulmonary branch stenosis.
Although abnormal PBF distribution was uncommon in our cohort, smallest relative pulmonary branch flow was associated with ventilatory efficiency. This was also reported by Giardini and collegues, who identified abnormal PBF distribution as an independent predictor of both decreased exercise capacity and ventilatory efficiency.[7] In contrast to our results, abnormal PBF distribution was more common in their study (18%) and MPA area was not an independent predictor of exercise capacity. This is probably explained by the younger age of the patient group in their study (13.3 ±3.4 years), because MPA area was not related to exercise capacity in the youngest patients of our cohort.

Limitation of stroke volume increase during exercise

In normal subjects, the RV stroke volume increases during exercise with only mild elevation of RV pressures. This is a consequence of low pulmonary vascular resistance, mediated by recruitment of closed vessels and distension of already opened vessels.[18,19] We found that MPA area significantly correlated with RV stroke volume at rest and RV systolic pressure. This may imply that in patients with pulmonary artery narrowing, RV systolic pressure increases disproportionately during exercise, limiting the increase in RV stroke volume during exercise, subsequently limiting exercise capacity.

Relative area change

Decreased distensibility of the MPA or branches has been proposed as a possible mechanism for reduced exercise capacity in patients after the arterial switch operation. Grotenhuis and colleagues[20] and Voges and colleagues[21] demonstrated a reduced distensibility of the proximal aorta in these patients. This was potentially mediated by increased aortic wall stress of the

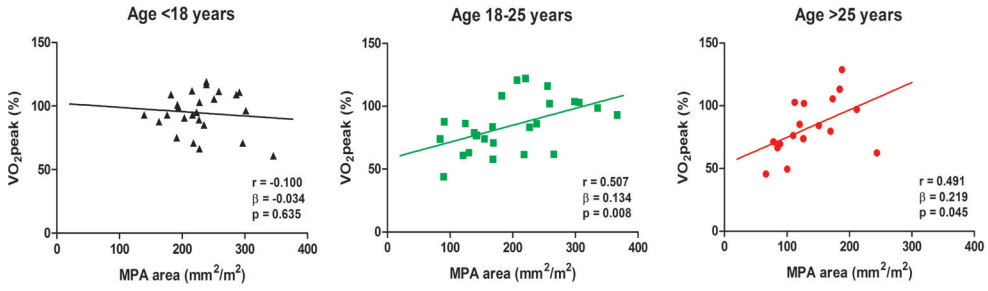

Figure 1. MPA area is not associated with exercise capacity in patients <18 years, who have largest MPA areas (β=-0.034, P= 0.635), while it is significantly related to exercise capacity in patients 18-25 and >25 years (β=0.134, P= 0.008 and β=0.219, P= 0.045, respectively).
Abbreviations: MPA, main pulmonary artery; VO_2peak%, exercise capacity reflected by percentage of predicted peak oxygen uptake.

Variable	<18 years (n=25)	18-25 years (n=26)	>25 years (n=20)	p-value
Sex, male n (%)†	18 (72)	20 (77)	14 (70)	0.910
Operative characteristics				
Rashkind procedure, n (%)†	22 (88)	14 (54)	12 (60)	0.089
Pulmonary artery banding, n (%)†	0 (0)	1 (4)	7 (35)	<0.001**
Age at surgical repair, days	9.2 ±8.8	15.5 ±26.9	125.8 ±201.2	0.001**
Pantaloon type patch, n (%)	23 (92)	10 (40[a])	1 (8[b])	<0.001**
Untreated pericardium, n (%)	25 (100)	14 (56[a])	0 (0[b])	<0.001**
Lecompte maneuver, n (%)†	23 (92)	23 (89)	17 (85)	0.463
Ventricular septal defect repair, n (%)†	5 (20)	8 (31)	7 (35)	0.260
Cardiopulmonary bypass time, min	153 ±59	207 ±53	187 ±45	0.104
Cross clamp time, min	92 ±18	125 ±34	106 ±27	0.171
RVOT reintervention, n (%)†	0 (0)	2 (8)	9 (45)	<0.001**
Imaging features				
RV systolic pressure, mmHg	22.7 ±9.6	29.2 ±6.8	36.5 ±9.9	<0.001**
Maximal velocity across PV, cm/s	183.7 ±58.0	194.5 ±72.4	254.6 ±52.7	0.001**
RV end-diastolic volume, mL/m^2	94.1 ±12.0	96.9 ±12.4	94.5 ±23.7	0.909
RV stroke volume, mL/m^2	51.7 ±8.3	53.3 ±7.0	52.6 ±10.5	0.690
RV mass, gr/m^2	29.6 ±4.7	30.6 ±6.0	34.1 ±9.5	0.035*
MPA area, mm^2/m^2	229.6 ±47.7	196.3 ±77.7	133.6 ±51.2	<0.001**
LPA + RPA area, mm^2/m^2	171.0 ±55.5	176.2 ±81.4	184.5 ±102.1	0.581
Smallest branch area, mm^2/m^2	57.7 ±28.9	58.3 ±35.0	67.6 ±44.7	0.388
Smallest branch flow, mL/m^2	22.0 ±4.5	21.0 ±4.0	21.2 ±4.3	0.494
Smallest branch flow, %	43.7 ±6.0	41.7 ±5.9	42.5 ±5.0	0.435
Functional outcome				
VO_2peak, %	94.7 ±16.1	84.4 ±20.6	83.4 ±21.9	0.051
VE/VCO_2 slope	23.0 ±2.9	24.3 ±3.6	24.0 ±5.1	0.379

Table 4. Sub analysis for operative characteristics, imaging features and functional outcome among three age groups. Abbreviations: RVOT, right ventricular outflow tract; PV, pulmonary valve; other as defined in Table 3. Legend: *p<0.05; **p<0.01; †n (%) and Chi-Square Mantel-Haenszel test, other mean ±SD and univariable linear regression; adata available in 25 of 26 patients; bdata available in 12 of 20 patients.

dilated root, fibrous tissue, and intrinsic wall abnormalities near the suture line and pulmonary artery branches embracing the aorta after the Lecompte maneuver.[17] Most of these features could theoretically also affect distensibility of the MPA and branches, contributing to a functional stenosis on exercise.[7,22] This study approximated distensibility of the pulmonary branches by relative area change, which is uncorrected for pulse pressure, because our study protocol did not include invasive measurements. To our knowledge, these measurements have not been performed in patients after the arterial switch operation. Our data do not provide evidence for a decreased relative area change of the LPA and RPA. However, relative area change of the MPA was not assessed in this study and could be altered because of different elastic properties of the pericardial patch.

Smaller MPA areas in older age groups

Patients aged more than 18 years had smaller MPA areas compared with younger patients. Because this is a cross-sectional study, it is uncertain whether this diminution of size is a reflection of learning curve and changing surgical techniques over time or the result of rapid somatic growth with inadequate growth at the anastomotic site, as suggested by Prifti and colleagues.[23] The operative characteristics of patients aged more than 25 years showed clear differences with both other age categories. Pulmonary artery banding was almost exclusively performed in this age group;patients were markedly older at time of surgical repair, and for the reconstruction of the MPA, mostly separate patches of pericardium treated with glutaraldehyde were used (vs untreated pantaloon type patch). Single pantaloon-type patch has been reported to result in less residual RVOT obstruction, and, in contrast to treated pericardium, untreated pericardial tissue potentially retains the ability to grow and adapt.[23] Therefore, pulmonary artery banding and type of MPA reconstruction (separate patches, treated pericardium with inadequate growth) are probably important causes of MPA narrowing.

Prolonged cyanosis and low PBF in patients who underwent the arterial switch operation at an older age also may adversely affect the microscopic pulmonary vasculature, myocardium, and systemic circulation, leading to a reduced VO2 peak%.

By using multivariable linear regression, we adjusted for the effects of age, sex, and operative characteristics (age at repair, pulmonary artery banding, patch type and treatment, RVOT reintervention). In multivariable analysis, MPA area was the only significant predictor of exercise capacity.

Clinical implications

In this study the importance of MPA narrowing as a determinant for exercise capacity is highlighted. This could imply that during the arterial switch operation, optimization of MPA size is important for functional outcomes. Moreover, this suggests that the long-term follow-up of patients after arterial switch operation should focus on presence or progression of MPA stenosis. Pulmonary branch re-interventions in patients with unilateral pulmonary branch stenosis might only improve functional capacity in the small subgroup of patients with an abnormal PBF distribution. This hypothesis requires further investigation in longitudinal studies.

Study limitations

Limitations of this study are inherent to its design, because this is a single-center, cross-sectional study. Therefore, variance in operation procedures and surgical experience among surgical centers could result in different outcomes in other patient cohorts. Second, we need longitudinal follow-

up studies to assess the actual impact of RVOT reinterventions on functional outcome in adult patients after the arterial switch operation. Individual follow-up data should elucidate whether the observation of decreased MPA areas in older age groups can be partially explained by rapid somatic growth. Finally, patients and controls were not perfectly matched, because patients were younger than healthy controls and included more male patients. To account for this, all measurements were indexed for body surface area. Moreover, because patients aged less than 18 years exhibited the smallest differences compared with healthy controls and male patients generally had better exercise capacity, age and sex matching would have only strengthened the differences found in this study.

Conclusion

In this cross-sectional study of patients long-term after arterial switch operation, MPA area was increasingly smaller in older age groups. MPA area was significantly related to exercise capacity, independently of age, sex and operative characteristics. Although branch pulmonary artery areas were smaller than in healthy controls, PBF at rest and ventilatory efficiency were generally not compromised. Our data therefore suggest that MPA narrowing is an important and thus far under-appreciated determinant in the limitation of functional capacity in adults after arterial switch operation.

References

1. Centers for Disease Control and Prevention. Improved national prevalence estimates for 18 selected major birth defects - United States, 1999-2001. MMWR Morb Mortal Wkly Rep. 2006;54:1301–5.
2. Jatene AD, Fontes VF, Paulista PP, et al. Anatomic correction of transposition of the great vessels. J Thorac Cardiovasc Surg. 1976;72:364–70.
3. Angeli E, Raisky O, Bonnet D, Sidi D, Vouhe PR. Late reoperations after neonatal arterial switch operation for transposition of the great arteries. Eur J Cardiothorac Surg. 2008;34:32–6.
4. Khairy P, Clair M, Fernandes SM, et al. Cardiovascular outcomes after the arterial switch operation for D-transposition of the great arteries. Circulation. 2013;127:331–9.
5. Fredriksen PM, Pettersen E, Thaulow E. Declining aerobic capacity of patients with arterial and atrial switch procedures. Pediatr Cardiol. 2009;30:166–71.
6. Giardini A, Khambadkone S, Rizzo N, et al. Determinants of exercise capacity after arterial switch operation for transposition of the great arteries. Am J Cardiol. 2009;104:1007–12.
7. Giardini A, Khambadkone S, Taylor A, Derrick G. Effect of abnormal pulmonary flow distribution on ventilatory efficiency and exercise capacity after arterial switch operation for transposition of great arteries. Am J Cardiol. 2010;106:1023–8.
8. Villafañe J, Lantin-Hermoso MR, Bhatt AB, et al. D-transposition of the great arteries: the current era of the arterial switch operation. J Am Coll Cardiol. 2014;64:498–511.
9. American Thoracic Society/American College of Chest Physicians. ATS/ACCP Statement on cardiopulmonary exercise testing. Am J Respir Crit Care Med. 2003;167:211–77.
10. Lotz J, Meier C, Leppert A, Galanski M. Cardiovascular flow measurement with phase-contrast MR Imaging: basic facts and implementation. Radiographics. 2002;22:651–71.
11. Driessen MMP, Baggen VJM, Freling HG, et al. Pressure overloaded right ventricles: a multicenter study on the importance of trabeculae in RV function measured by CMR. Int J Cardiovasc Imaging. 2014;30:599–608.
12. Freling HG, van Wijk K, Jaspers K, et al. Impact of right ventricular endocardial trabeculae on volumes and function assessed by CMR in patients with tetralogy of Fallot. Int J Cardiovasc Imaging. 2012;29:625–31.
13. Merkx MAG, Bescós JO, Geerts L, et al. Accuracy and precision of vessel area assessment: manual versus automatic lumen delineation based on full-width at half-maximum. J Magn Reson Imaging. 2012;36:1186–93.
14. Godfrey S. Exercise testing in children. London: W.B. Saunders Company, 1974.
15. Wasserman K, Sue D. Principles of exercise testing and interpretation. 2nd edition. Philadelphia: Lea & Febiger, 1994.
16. Ten Harkel AD, Takken T, Van Osch-Gevers M, Helbing WA. Normal values for cardiopulmonary exercise testing in children. Eur J Cardiovasc Prev Rehabil. 2011;18:48-54.
17. Lecompte Y, Zannini L, Hazan E, et al. Anatomic correction of transposition of the great arteries. J Thorac Cardiovasc Surg. 1981;82:629–31.
18. Kovacs G, Berghold A, Scheidl S, Olschewski H. Pulmonary arterial pressure during rest and exercise in healthy subjects: a systematic review. Eur Respir J. 2009;34:888-94.
19. Naeije R, Chesler N. Pulmonary circulation at exercise. Compr Physiol. 2012;2:711-41.
20. Grotenhuis HB, Ottenkamp J, Fontein D, et al. Aortic elasticity and left ventricular function after arterial switch operation: MR imaging-initial experience. Radiology. 2008;249:801–9.
21. Voges I, Jerosch-Herold M, Hedderich J, et al. Implications of early aortic stiffening in patients with transposition of the great arteries after arterial switch operation. Circ Cardiovasc Imaging. 2013;6:245–53.
22. Gutberlet M, Boeckel T, Hosten N, et al. Arterial switch procedure for D-transposition of the great arteries: quantitative midterm evaluation of hemodynamic changes with cine MR imaging and phase-shift velocity mapping-initial experience. Radiology. 2000;214:467–75.
23. Prifti E, Crucean A, Bonacchi M, et al. Early and long term outcome of the arterial switch operation for transposition of the great arteries: predictors and functional evaluation. Eur J Cardiothorac Surg. 2002;22:864-73.

CHAPTER 7

Elevated RV pressures in Pulmonary Hypertension leads to different RV remodeling and RV function than elevated RV pressure in Adult Congenital Heart Disease

Authors:
Mieke M.P. Driessen, Tim Leiner, Gertjan T.j. Sieswerda, Arie P.J. van Dijk, Marco C. Post, Mark K. Friedberg, Luc Mertens, Pieter A. Doevendans, Repke J. Snijder, Erik H. Hulzebos, Folkert J. Meijboom

Submitted to International Journal of Cardiovascular imaging

Abstract

Background
There is great variance in time to right ventricular (RV) failure between different conditions causing chronic increase of RV pressure. To get a better understanding of the differences, we compare RV remodeling, longitudinal function and transverse function in patients with pulmonary stenosis (PS), subaortic RV and pulmonary hypertension (PH).

Methods
This prospective cross-sectional study includes: controls (n=37), patients with PS (n=15), subaortic RV (n=19) and PH (n=20). All subjects underwent CMR, functional echocardiogram and cardiopulmonary exercise testing. Statistical analysis was performed using ANOVA with posthoc Bonferonni.

Results
PS patients had smaller RV volumes with higher RV ejection fraction ($p<0.05$) compared to controls. PH and subaortic RV patients had dilated RVs with lower RV ejection fraction (34.8±9.6% and 46.3±10.1%; $p<0.01$). PH patients had lower RV stroke volume ($p=0.02$), RV ejection fraction ($p<0.01$) and VO_2 peak/kg% ($p<0.001$) compared with subaortic RV patients. PH patients exhibited decreased apical transverse RV free wall motion and prolonged RV free wall shortening ($p<0.001$) – resulting in post-systolic shortening and intra-ventricular dyssynchrony. Apical transverse shortening and global longitudinal RV deformation showed the best correlation to RV ejection fraction (respectively $r=0.853$, $p<0.001$ and $r=0.812$, $p<0.001$).

Conclusion
While PS patients exhibit hyperdynamic RVs, both subaortic RV and PH patients have dilated RVs with spherical geometry and decreased ejection fraction. PH patients have worse global RV function compared to subaortic RV patients, and exhibit decreased transverse function as well as prolonged RV free wall contraction resulting in; post-systolic shortening, intra-ventricular dyssynchrony. Apical transverse function and global RV strain showed the best correlations to RV ejection fraction across all patient groups.

Introduction

The normal right ventricle (RV) works at low pressures and increased afterload is believed to be poorly tolerated by the RV. This is certainly true for sudden increase of afterload in the setting of massive pulmonary embolism, which leads to an instantaneous decrease in stroke volume and cardiac output.[1] However in conditions associated with chronic elevations in RV pressure, i.e. pulmonary hypertension (PH) and several congenital heart defects, there is great variance in time to RV failure and clinical outcome. In pulmonary hypertension (PH), the pulmonary vascular resistance and pulmonary arterial pressure increase more gradually than in massive pulmonary embolism. The chronic elevation of RV pressures results RV remodeling and RV hypertrophy, adaptive mechanisms aimed at decreasing afterload for the RV and maintaining cardiac output. In PH patients these adaptive mechanisms often fall short and, unless treated successfully with pulmonary vasodilator therapy, RV failure is common within a few years after diagnosis.[2] Many congenital heart defects also lead to chronically increased RV pressure, due to either high vascular resistance or RV outflow tract obstruction, present since birth. In contrast to PH, the RV in these patients is often capable of generating high pressures and maintaining cardiac output for many decades.[3-5] However, survival and time to RV failure also differ substantially between patients with pulmonary valvular stenosis (PS), in whom RV failure is rare, and patients with an RV facing systemic vascular resistance. [3, 4]

In all entities with chronic increase of RV pressure, prognosis is dependent on the adequacy of RV adaptation[5-7]: the clear differences in clinical course are likely explained by differences in adaptation.[8] RV adaptation to different conditions suffering from elevated pressure is currently incompletely understood.

The current study compares three distinct patient populations: PH (increase of vascular resistance later in life), subaortic RV (lifelong systemic vascular resistance), PS (lifelong valvular stenosis) and healthy controls. We use cardiac magnetic resonance imaging (CMR) and echocardiography to characterize RV remodeling, longitudinal function and transverse function in these groups. The aim of the study is to improve the understanding of RV adaptation to chronically increased pressure, by detailed assessment of the components contributing to RV function.

Methods

This is a prospective cross-sectional study. Study participants were prospectively recruited between August 2012 and November 2013 in three tertiary referral hospitals, all investigations were performed in one centre (UMCU) on the same day.

Inclusion and exclusion criteria

Included were adult patients (≥18 years) with diagnosis of: PH (idiopathic or inoperable thrombo-embolic pulmonary hypertension), PS and RV in subaortic position (either congenitally corrected transposition of the great arteries or after atrial switch procedure). Patients had no associated congenital heart defects. The diagnosis of pre-capillary PH was previously confirmed by right heart catheterization. [9] At time of study entry, PH patients were still required to fit the criteria for “high echocardiographic probability of PH”.[9]

The treating physician determined therapeutic regimen in each patient. PH patients were on

PH-specific therapy and approached when clinically stable during last out-patient clinic visit. Patients with overt clinical RV heart failure, i.e. signs of fluid retention on physical examination, were excluded.

A group of healthy volunteers, free of known disease, aged 18-60 years were recruited to serve as a reference. Volunteers were screened by physical examination, medical history and electrocardiogram and excluded if these investigations or subsequent CMR and echocardiogram showed abnormalities.
The study protocol conforms to the ethical guidelines of the 1975 Declaration of Helsinki and was approved by the human research committees of all recruiting centers. Written informed consent was obtained in all participants prior to enrolment.

RV systolic pressures
RVSP was calculated using the Bernoulli equation with maximum velocity of tricuspid regurgitation or by maximal pulmonary valve gradient (in PS patients), plus estimated right atrial pressure.[10] In subaortic RV patients the systemic systolic blood pressure at rest was used as RVSP. We estimated end-systolic RV wall stress using an adaptation of Laplace's law. To take into account different RV geometries and eccentric RV remodeling,[11,12] end-systolic volume (RVESV) and RV mass were used instead of diameters, in the following formula: Estimated global RV wall stress = RV systolic pressure x RVESV x 0.5 / RVmass.

CMR sequence
A commercially available 1.5-T system (Ingenia R4.1.2; Philips Healthcare, Best, the Netherlands) was used. Steady-state free precession cine images were acquired during end-expiratory breath holds. Multi-slice cine short-axis acquisition was planned from the apex up to and including the atrio-ventricular valves or basal bulge of the RV (TR/TE 3.4/1.69 ms, voxel size 1.3x1.3x8.0mm, flip angle 55o; 30 phases per cycle). Quantitative through-plane flow (Q-flow) was measured at the level of the pulmonary valve with a retrospectively ECG gated, velocity-encoded phase-contrast sequence (TR/TE 5.2/3.1 ms, voxel size 2.5x2.5x8mm, flip angle 12o, field of view 320, matrix 128x100, 20 phases per cycle).

CMR: RV volumetrics & geometry
RV volumetric analysis was performed by manual tracing of endocardial and epicardial contours in end-diastolic and end-systolic phase in all slices, using Qmass MR Research edition (version 7.4, Medis, Leiden, the Netherlands), excluding trabeculae and papillary muscles from the blood volume. [13] The following parameters were measured: RV end-diastolic volume (EDV), RVESV, RV stroke volume (SV), RV ejection fraction, RV mass and RV mass-volume ratio. Q-flow measurements (Medis Qflow, version 5.5, Medis, Leiden, the Netherlands) were used to generate effective RVSV and cardiac output (RVSV*heart rate). All volumetric data were indexed for Body Surface Area.
RV geometry, transverse motion and longitudinal free wall motion was assessed on steady-state free precession cine in 4-chamber orientation, as indicated in figure 1. Systolic dimensions were measured at maximum RV free wall thickening and before potential rapid septal displacement

towards the left. The mid to basal and apex to basal ratios, transverse and longitudinal motion (diastolic-systolic dimension) and shortening ([diastolic-systolic dimension]/diastolic dimension) were calculated.

Echocardiography: longitudinal deformation

Echocardiography was performed on a Toshiba Artida system (Tokyo, Japan) with a 5-MHz transducer. Echocardiographic RV measurements were taken in a RV–centric 4-chamber view (example in figure 1), including off-line longitudinal speckle tracking analysis (Advance Cardiac package version 3.0, Toshiba). Tracking quality was visually assessed and optimized by the observer. Peak systolic strain and post systolic-shortening ([peak strain – peak systolic strain]/peak strain) were measured for RV free wall, the interventricular septum (IVS) and global RV strain. Pulmonic valve closure and ejection time were measured from pulsed wave Doppler in the RV outflow tract. Intra-ventricular dyssynchrony was the time difference between peak septal and peak free wall strain.

All timing measurements were matched and normalized to RR interval.

Exercise testing

Exercise testing was performed using an electronically braked cycle ergometer (Lode Corrival, Lode BV, Groningen, the Netherlands), following a ramp protocol adjusted to the patients' estimated exercise tolerance, at a cadence of 70 revolutions per minute until exhaustion. Peak oxygen uptake was calculated per kilograms bodyweight (pVO2/kg), per heart rate (pVO2/HR) and expressed as the percentage of the predicted value using Koch et al. (patients >25 yrs) or Jones et al. (patients <25 yrs).[14,15] Respiratory efficiency was assessed using VE/VCO_2 slope.

Statistical analysis

All continuous variables are presented as mean ± standard deviation or median [range] as appropriate. Categorical variables are presented as frequency (%) and were compared with Chi-square. All patient groups were compared to controls using ANOVA with posthoc Dunnet's – for normally distributed parameters – or Kruskal-Wallis with Mann-Whitney U test – for non-normally distributed parameters. Patient groups were compared to each other using ANOVA with posthoc Bonferonni.

Simple linear regression was used to correlate conventional echocardiographic measurements, deformation imaging and transverse measures and RV ejection fraction. Multiple linear regression, including underlying disease as additional variable, was used to correlate the same measurements to VO_2max/kg. Simple regression is depicted as correlation coefficient r and "goodness-of-fit"measure R^2, multiple regression in R^2 and beta.

Intra- and interobserver reproducibility were assessed by re-analysing 15 datasets >1 month apart. Agreement was assessed using intra-class correlation coefficients, mean difference with limits of agreement and a paired Student T-test. Reproducibility of the CMR measurements were previously reported by our own group and Kind et al.[13,16] An alpha level of 0.05 was considered significant.

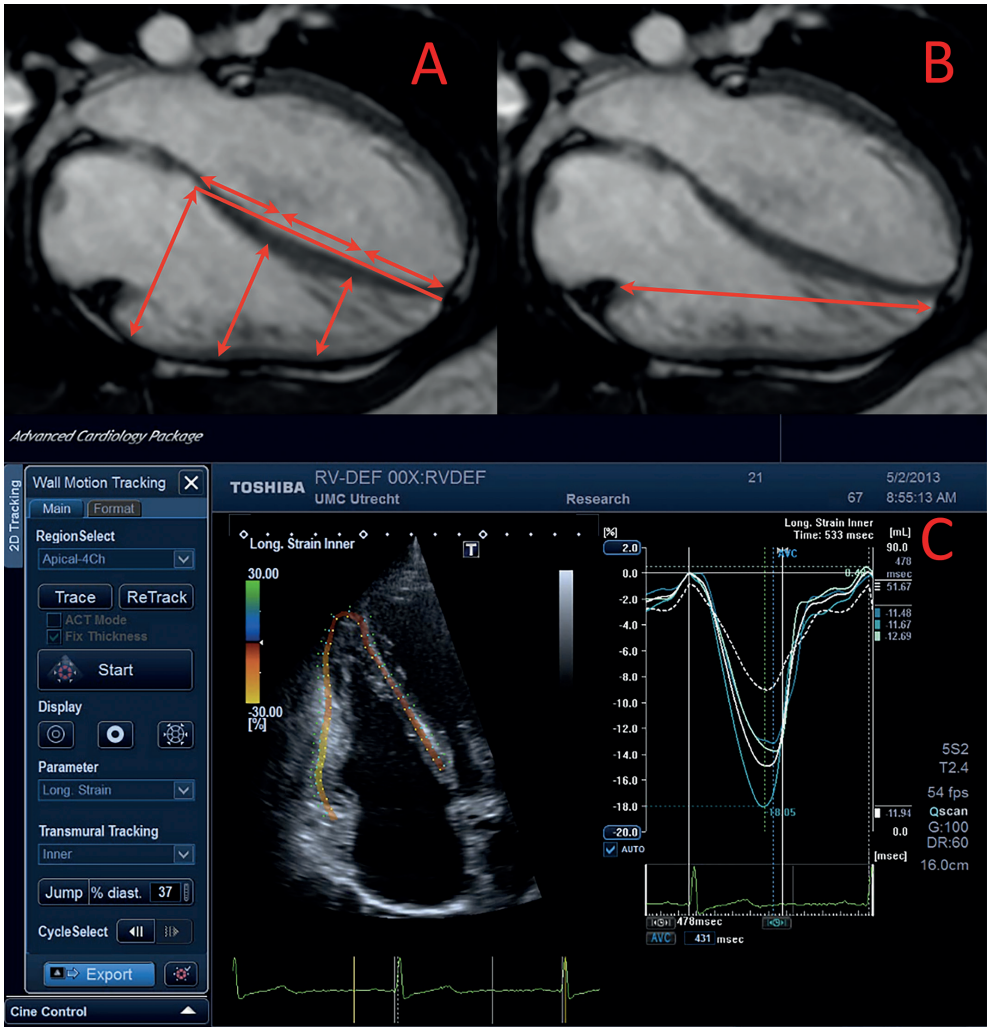

Figure 1. example of analysis. A&B:
Image of CMR analysis for transverse motion (a) perpendicular to apex-base axis and of longitudinal motion (b). C: Image of longitudinal deformation analysis of the RV.

Results

Ninety-one subjects included in the study, 37 controls, 15 PS, 19 subaortic RV (15 post-atrial switch and 4 congenitally corrected transposition of the great arteries) and 21 PH patients (9 idiopathic & 12 chronic thrombo-embolic; median 4.8 [0.6-35.0] yrs since diagnosis). Demographic data are listed in table 1. All patients were in sinus rhythm. PH patients were on the following PH-specific medication: prostacyclin 4/21 (19%), PDE5-inhibitor 14/21 (67%) and endothelin-receptor antagonist in 19/21 (90%).

RVSP was significantly higher in subaortic RV patients than PH and PS patients ($p<0.001$), but did

not differ significantly between PS and PH patients (p=0.111; supplementary table). Percentage of predicted pVO_2/kg and pVO_2/heart rate were significantly lower in PH patients than PS and subaortic RV patients (both p<0.01). VE/VCO_2 slope was significantly higher in PH patients (both p<0.001).

RV size and mass

CMR measurements of size and mass are detailed in table 2 and figure 2. PS patients had decreased RV volumes compared to controls, conversely subaortic RV and PH patients had increased RV volumes. Indexed RV mass, RV mass/volume ratio and estimated global RV wall stress were significantly increased in all patient groups (table 2; all p<0.001). PH patients had higher RVESV/m^2 compared to PS and subaortic RV patients. They also had higher estimated wall stress (p<0.001) and lower mass-volume ratio (p=0.05) compared to PS (figure 2). Subaortic RV and PH patients had more spherical RV geometry compared with controls (figure 3) and PS patients (p<0.002 apical-base ratio).

	Controls (n=37)	PS (n=15)	SubAo RV (n=19)	PH (n=21)
Age (yrs)	33.2 [21.0-60.2]	25.5 [18.2-43.3]	32.7 [28.4-52.9]	54.3 [19.5-74.0]‡
Male (%)	22 (59.5%)	4 (26.7%)*	13 (68.4%)	6 (28.6%)*
BSA (m^2)	1.89±0.20	1.86±0.14	1.94±0.14	1.89±0.20
Medication:				
- Beta-blocker	-	-	7 (36.8%)	1 (4.8%)
- ACE-inhibitor	-	-	5 (26.3%)	3 (14.3%)
- Diuretics (any kind)	-	-	2 (10.5%)	15 (71.4%)
QRS_dur (msec)	96 [66-114]	96 [78-148]	100 [70-130]	80 [70-140]
RVSP (mmHg)	20.0±3.3	56.0±15.7	110.8±11.8	66.7±16.7
None/trace TR	37 (100%)	9 (60%)	3 (16%)	5 (24%)
Mild TR	-	5 (33%)	12 (63%)	9 (43%)
Moderate TR	-	1 (7%)	3 (16%)	6 (29%)
Severe TR	-	-	1 (5%)	1 (5%)
Performance measurements				
NYHA I	37 (100%)	15 (100%)	17 (89.5%)	1 (4.8%)
NYHA II	-	-	2 (10.5%)	16 (76.2%)
NYHA III	-	-	-	4 (19.0%)
pVO_2/kg	-	30.1±7.8	26.3±6.4	16.5±4.9
%pVO_2/kg	-	92.2±16.9	80.8±16.9	62.4±15.5
VE/VCO_2 slope	-	26.2±5.8	27.7±3.9	41.5±10.3
% pred VO_2/HR	-	97.6±17.7	96.7±27.3	72.3±16.9

Table 1: Patient characteristics.
Data presented as mean±standard deviation, compared using ANOVA and posthoc Dunnet's, or median [range], with Kruskall wallis and mann Whitney U test. *P<0.05, †p<0.01 and ‡p<0.001.
SubAo= subaortic; BSA = Body surface area; BMI = body mass index; pVO2/kg = peak oxygen uptake per kilogram body weight (ml/kg/min); %pVO2/kg= percentage of predicted; VE/VCO2 = minute ventilation relative to carbon dioxide elimination; %pred VO2/HR = oxygen uptake/peak heart rate

Global RV function and cardiac output

CMR measures of global RV function are detailed in table 2 and figure 2. PS patients had significantly higher RV ejection fraction compared to controls, while subaortic RV and PH patients had a significantly lower RV ejection fraction. The indexed RV stroke volume was significantly lower in all patient groups compared with controls, RV cardiac output only in Subaortic RV and PH patients (figure 2). The RV ejection fraction and indexed RV stroke volume of PH patients were lower than those of subaortic RV patients.

Longitudinal and transverse motion

Measurements of longitudinal RV free wall motion were significantly higher in PS compared with subaortic RV and PH patients (all p<0.001; table 2&3).

Transverse motion is detailed in figure 3. PS patients had increased apical transverse motion compared to controls (p=0.03). Conversely, apical transverse motion and shortening in PH patients was significantly lower compared with controls (p<0.001), PS (p<0.001) and subaortic RV patients (p=0.02). Midlevel transverse motion was significantly lower in subaortic RV and PH patients compared with controls and PS patients (p<0.001).

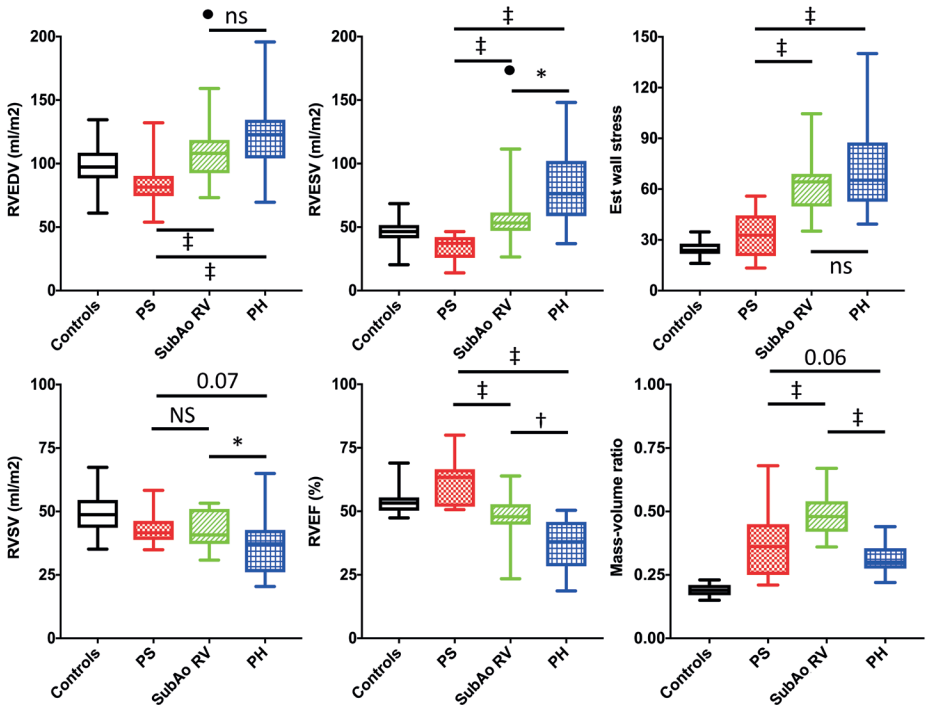

Figure 2. CMR measurements

2a: RV end-diastolic (EDV), end-systolic volume (ESV) and estimated wall stress; outlier in subaortic RV group (•).
2b: RV stroke volume (RVSV), RV ejection fraction (RVEF) and mass-volume ratio.
Patient groups were compared using ANOVA with posthoc Bonferonni. *p<0.05; †p<0.01; ‡p<0.001. PH= pulmonary hypertension; PS= pulmonary stenosis; SubAo RV= subaortic right ventricle

Timing of contraction

Data are shown in table 3 and figure 2. Normalized time to peak RV free wall contraction is significantly longer in PH compared with controls and subaortic RV patients (PS p=0.09), continuing after pulmonic valve closure. Post-systolic shortening of the RV free wall was much more frequent in PH patients (n=5; 45%) compared to controls (n=1; 7%), PS n=1 (10%) and subaortic RV n=2 (13%). Post-systolic shortening was <1% in all but 1 congenital heart disease patient, but ranged from 1.1-14.9% in PH patients.

Association of specific imaging markers to RVEF and exercise capacity

Of the conventional echocardiographic parameters; only fractional area change and RA area correlated significantly to RV ejection fraction (respectively r=0.735, r^2 0.540, p<0.001 and r= -0.428, r^2 0.183, p=0.002; TAPSE r=0.260, p=0.07; TDI S' r=0.117, p=0.368). Global systolic RV longitudinal deformation (r=0.812, r^2=0.683; p<0.001) and apical transverse shortening (r=0.853, r^2 0.728; p<0.001) showed the highest correlation to RVEF of deformation and transverse motion parameters. Using multiple linear regression, combination of global systolic RV longitudinal deformation (β=-1.324) and apical transverse shortening (β=0.588) yielded the highest predictive value for RVEF with an R^2=0.838 (p<0.001).

Global systolic RV longitudinal deformation was the only parameter associated to VO_2max (p=0.025) independent of underlying pathology in multiple linear regression (R^2 increase from 0.377 to 0.449).

Reproducibility of deformation imaging

Both intra-observer and inter-observer agreement yielded good intra-class correlation coefficients and acceptable limits of agreement (table 4).

Volumetric data	Controls (n=37)	PS (n=15)	SubAo RV (n=19)	PH (n=19)
RVEDV (ml/m²)	97.2 [61.0-134.5]	81.5† [53.9-132.1]	110.0* [73.2-222.1]	122.9‡ [69.6-195.8]
RVESV (ml/m²)	46.4 [20.4-68.5]	37.1‡ [13.9-46.4]	56.2† [26.4-170.1]	76.3‡ [36.9-148.2]
RVEF (%)	53.2±4.5	61.1±9.6*	46.3±10.1†	36.9±9.6‡
RV mass (g/m²)	18.4±3.7	29.3±11.0‡	54.9±13.5‡	37.9±10.9‡
SV (ml/m²)	49.3±7.7	42.3±5.8*	42.7±7.5*	36.1±10.6‡
RV cardiac output (l/min)	5.78±1.24	5.38±0.84	4.70±0.84*	4.72±1.55†
Geometric data				
Longitudinal motion (mm)	23.5±3.2	20.0±3.0†	14.6±3.2‡	15.4±3.6‡
Trans shortening apex(%)	31.5±7.5	39.2±13.3*	17.4±6.9‡	9.3±7.7‡
Trans shortening mid (%)	23.4±5.7	28.7±13.3	13.4±6.2‡	12.4±6.4‡

Table 2:CMR measurements.
Data presented as mean±standard deviation, compared using ANOVA and posthoc Dunnet's, or median [range], with Kruskall wallis and mann Whitney U test. *P<0.05, †p<0.01 and ‡p<0.001.
SubAo=subaortic; EDV= end-diastolic volume; ESV= end-systolic volume; EF = ejection fraction; RV= Right ventricular; SV = stroke volume;

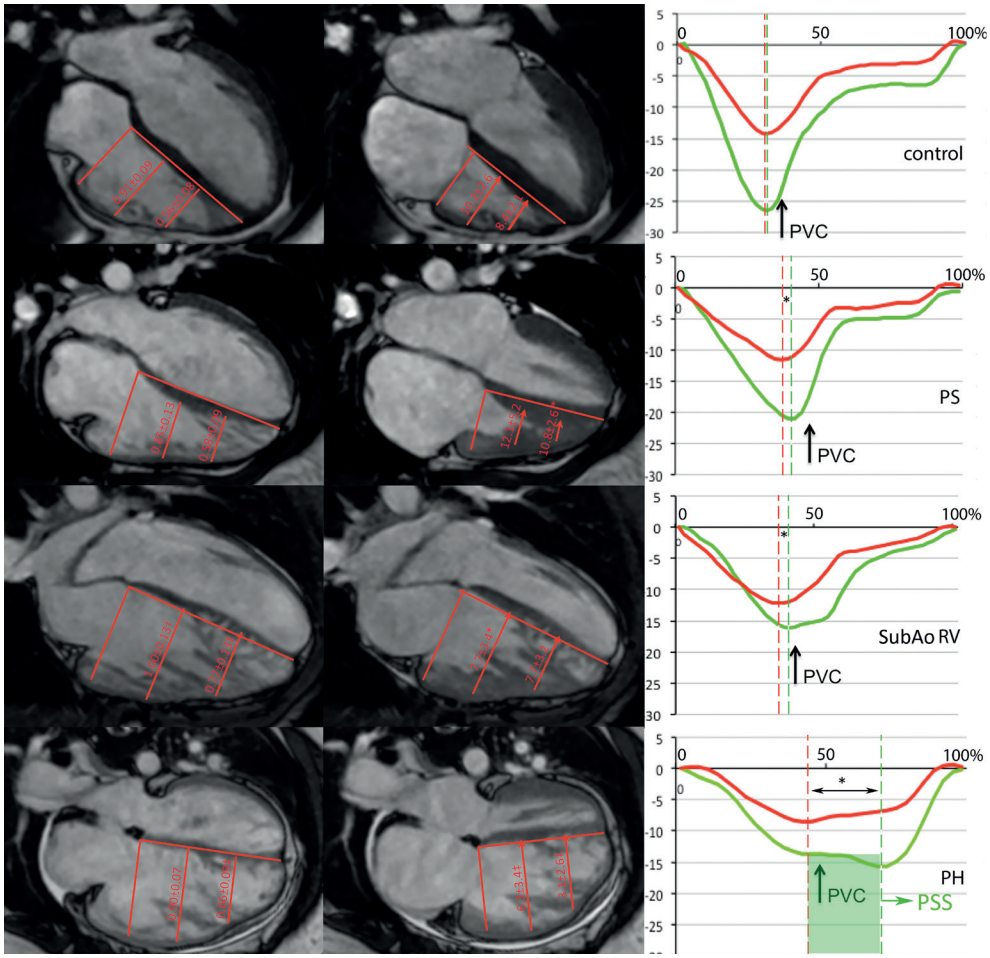

Figure2.RV geometry, transverse motion and timing of contraction.
Left column: RV mid-basal and apical-basal ratio. Mid column: RV transverse motion at mid and apical level. The right column: timing of RV free wall (green) and septal (red) longitudinal strain from a representative patient, pulmonary valve closure (PVC) and difference between septal and free wall peak (*) are marked. Patients were compared to controls using ANOVA with posthoc Dunnet's; *p<0.05; †p<0.01; ‡p<0.001.
PS= pulmonary stenosis; SubAo RV= subaortic righ ventricle; PH= pulmonary hypertension

	Controls (n=30)	PS (n=15)	Syst RV (n=19)	PH (n=21)
Functional measurements				
FAC (%)	40.5±6.65	41.6±8.8	27.7±6.8‡	23.6±10.5‡
RA area (cm²)	17.8±3.8	19.2±3.6	19.2±7.5	23.4±6.4‡
TAPSE (mm)	23.5±2.9	20.7±5.1*	14.3±3.3‡	19.4±3.7‡
TDI S' (cm/sec)	13.8±1.8	10.7±2.4‡	8.1±3.0‡	11.4±2.4‡
RVFW long strain (%)[1]	-25.0±2.6	-21.8±5.9	-14.0±4.5‡	-14.7±3.2‡
IVS long strain (%)[1]	-15.0±1.6	-13.5±2.5	-10.6±2.6‡	-10.4±3.4‡
RV global long strain (%)[1]	-20±1.8	-17.8±3.9	-12.5±3.7‡	-12.8±2.8‡
Timing of contraction				
Heart rate (bpm)	64±9	67±12	60±11	74±11‡
Ejection time RVOT (ms)	359±128	430±66	310±42	410±69
PVC (ms)	414±55	464±75†	411±58	473±7‡
TTP RVFW (ms)[1]	403±55	452±87	406±78	537±118‡
ΔIVS_RVFW (ms)[1]	-18 [-60; 72]	-46[-103; 67]†	-27[-170; 30]*	-73[-273; -13]†

Table 3: Echocardiographic measurements.
All patient groups compared with controls using ANOVA with posthoc Dunnet's test or Kruskall Wallis, as appropriate. *p<0.05; †p<0.01; ‡p<0.001. 1Speckle tracking analysis was available in 76/91 (73.6%) participants (median frame rate 57, ranging 42-116 fps).
FAC = fractional area change; RA= right atrial; TDI S'= Tissue Doppler Imaging systolic velocity of the tricuspid annulus; PVC= pulmonic valve closure; RV=right ventricle; TTP= time to peak; ΔIVS_RVFW= difference between septal and free wall time to peak.

	ICC	p-value	Absolute mean Δ‡ [limits of agreement]	p-value[II]
Intra-observer				
RV free wall	0.98	<0.001	-0.18% [-1.96; 1.60]	0.471
Septal	0.85	<0.001	-0.18% [-2.64; 2.29]	0.600
RV total	0.95	<0.001	-0.06% [-2.08; 1.94]	0.850
Inter-observer				
RV free wall	0.87	<0.001	2.04% [-1.29; 5.37]	0.004
Septal	0.77	<0.001	1.02% [-1.43; 3.47]	0.016
RV total	0.91	<0.001	1.14 % [-0.96; 3.24]	0.008

Table 4: Reproducibility of longitudinal deformation.
Reproducibility measurements. ‡mean difference and limits of agreement; II significance of paired T-test. ICC= intra-class correlation coefficient; RV = right ventricular

Discussion

Although the differences in clinical outcome between PS, subaortic RV and PH patients are well known, mechanisms and determinants of RV adaptation that are (largely) responsible for these differences are not fully understood. This cross-sectional, prospective, study focussed on these differences in RV remodeling and function. The most striking results of the study are: 1) Patients with valvular stenosis exhibit hyper dynamic ventricles; with low volumes, supra-normal RV ejection fraction and increased transverse function. Both subaortic RV and PH patients show RV dilation, spherical RV geometry and decreased ejection fraction. 2) PH patients had lower RV ejection fractions and lower RV stroke volumes compared to subaortic RV patients – mediated by more post-systolic shortening, more intra-ventricular dyssynchrony and decreased transverse RV free wall function. 3) Transverse function and global strain, instead of TAPSE or TDI S', showed the best correlations to global RV ejection fraction across the entire patient group.

Valvular stenosis vs. increased vascular resistance

Higher systolic ventricular pressures need to be met by proportional RV hypertrophy in order to reduce afterload and/or increase contractile strength. If this process is adequate, acceptable stroke volumes can be maintained. However, if the change in afterload is incompletely compensated by hypertrophy, RV dilation will ensue to maintain stroke volume through the Frank-Starling mechanism, a phenomenon known as pre-load recruitable stroke work. In patients with valvular stenosis, the RV seems to have effectively reduced its afterload, by hypertrophying. In contrast, the RV of subaortic RV and PH patients, facing high vascular resistance, dilates to maintain its stroke volume (figure 2). The RV hypertrophy that develops in these settings is apparently insufficient to compensate for the increased afterload (figure 2). Additionally, patients with subaortic RVs or PH exhibit greater degrees of tricuspid regurgitation (table 1); adding volume load to the already strained RV, likely aggravating dilation and RV dysfunction.

Indeed, global RV systolic function is markedly different – with a hyperdynamic RV ejection fraction in PS patients, compared to mild and moderate decrease of RV ejection fraction in respectively subaortic RV and PH patients. RV free wall longitudinal shortening were decreased in all patient groups compared to controls (table 3). As RV ejection fraction is increased in PS, other components of RV contraction – radial or circumferential strain and the transverse component of bellows effect – likely become more important for overall RV performance in PS.[17,18] To reflect these components, we measured transverse motion of the RV free wall as a surrogate marker. PS patients showed increased transverse motion compared to controls and both vascular resistance groups, which contributes to the higher RV ejection fraction.

Pulmonary hypertension vs. subaortic RV

As discussed above, the RV will adapt to its increased afterload by hypertrophing and using prework recruitable stroke work. If the combination of both mechanisms is insufficient to compensate the afterload, the ventricle myocytes will remain stretched throughout systole, which decreases velocity of fiber shortening and prolongs duration of contraction.[19] However, global function and stroke volume are much better preserved in subaortic RV patients than in PH patients. Its seems RV hypertrophy and utilization of pre-work recruitable stroke work are sufficient for the subaortic RV to maintain acceptable stroke volumes. Conversely, stroke volume drops in PH, needing an increased resting heart rate (table 3) to maintain acceptable cardiac output. The

difference in ejection fraction likely relates to two important mechanisms: 1) prolonged RV free wall contraction and 2) decreased transverse motion in PH patients.[20]
The prolonged time to peak RV free wall longitudinal deformation in PH patients (figure 3) leads to post-systolic shortening, intra-ventricular dyssynchrony and rapid leftward septal motion leading to inefficient RV contraction.[8,12,20] Following the rationale above, the prolonged contraction is likely a sign insufficiently compensated afterload in PH patients, causing a mechanical RV free wall delay, associated to RV dysfunction in PH patients.[13, 20]
Although often overlooked in daily RV assessment, apical transverse motion and shortening – measured before rapid leftward septal displacement – is decreased in PH patients compared to subaortic RV patients. In PH patients, transverse motion has been related to survival in mixed populations with pulmonary hypertension – underlining its importance in RV assessment.[21,22]

Theoretical considerations

The ultimate goal of RV adaptation is for the ventricle to stay coupled to its afterload.[23] This coupling can be estimated using the ratio between end-systolic ventricular elastance (load-independent measure of ventricular contractility) and arterial elastance (ventricular-independent measure of arterial function).[23] In the individual patient this will be determined by ventricular load, adequacy of RV remodeling and ability to increase myocardial contractile force (by intrinsic myocardial properties). Differences in function and remodeling can originate from differences in these characteristics.
First, the load cardiomyocytes encounter can not be measured directly and is often estimated taking into account only the static load on the ventricle (determined by increased resistance). However, total hydraulic load is also determined by the oscillatory load (i.e. vascular stiffness, compliance and reflected waves).[24] The RV facing valvular stenosis exhibits entirely different characteristics than that facing high vascular resistance, despite comparable RVSP, which indicates that these are likely entirely different loading entities, akin to data in the pressure loaded left ventricle.[25, 26] Furthermore, oscillatory load is almost certainly different between patient groups (although invasive data are lacking). The pulmonary vascular bed beyond the narrowed valve is normal in PS. In PH, capacitance is decreased and arterial stiffness as well as reflected pressure waves are increased.[24,27] The subaortic RV has access to a much larger vascular bed than PH patients, with likely normal systemic vascular properties. Along these lines of reasoning, oscillatory load is much higher in PH patients than both other groups, conversely the static load caused by the resistance is likely highest in patients with subaortic RVs. What this implicates for total hydraulic load is as yet unclear.
Secondly, myocardial response in terms of RV hypertrophy differs substantially between groups. Both congenital heart disease groups show superior mass-volume ratios compared to PH, indicating a higher degree of hypertrophy, also reported in previous studies.[8,28] This may be explained by different time of onset of disease, as the RV exposed to high pressures from fetal life onwards (in CHD but not PH) may maintain its "fetal" fenotype – with a thick RV myocardium.[29,30]
Lastly, the better preservation of global function and stroke volume in subaortic RVs compared with PH patients, may be explained by differences in myocardial properties between both groups. Myocardial damage might progress faster in PH, as studies have demonstrated relative RV ischemia, causing fibrosis – which aggravates RV dilation and reduces contractility, although also shown to lesser extent in subaortic RVs.[6,31] The fact that patients with Eisenmenger's syndrome have much better survival and RV remodeling than other PH patients, suggests there

might be differences in myocardial response depending on onset time of disease.[28]

Practical considerations: How to evaluate the pressure-loaded ventricle

Although CMR-derived RVEF is considered one of the reference standards for assessment of RV function, follow-up is preferably done by repeated echocardiographic examinations. Echocardiographic markers that correlate to RVEF and detect deterioration of RVEF or clinical worsening are therefore of great importance. In our patient population with pressure-load, fractional area change was the only "conventional" echocardiographic measurement that showed a fairly good correlation (R^2=0.54) to RVEF. In accordance with recent studies, correlation of TAPSE to RVEF was poor in our study.[33,34] Both global RV systolic longitudinal deformation and transverse shortening (which can also be done on echo) showed a good correlation to RV ejection fraction. Combining both measurements improved the predictive value of the regression model to R^2=0.84. Although their value in follow-up will need to be further studied, systolic longitudinal deformation and transverse function seem to be of added value to current echocardiographic assessment.

Limitations

No invasive pressure measurements are available – as they are not routinely performed in most congenital heart disease patients. The subaortic RV patients had significantly higher RVSP than PS and PH patients, due to adherence to treatment guidelines in both latter groups. As all imaging measurements of RV function are load dependent; it is important to note that differences in ejection/deformation do not always reflect contractility, but may be a result of different afterload (also see supplementary table).

Although it was attempted to reduce heterogeneity of the patient groups to a minimum, sex and age distribution were different between the groups, concordant to different epidemiology. As the normal effect of age on RV function and volumes is opposite to the differences demonstrated between patient groups, it is unlikely these factors importantly influence our results.[37]

There is no agreed-upon way to calculate wall stress for the RV. We estimated end-systolic wall stress with a modified Laplace's law; using wall mass and end-systolic volumes to obtain a more global estimate of wall stress as RV geometry varies greatly between patient entities.

Conclusion

While the RV of patients with valvular stenosis seems to effectively adapt to chronic increase of RV pressure – maintaining cardiac output without dilating – the RV of subaortic RV and PH patients has to dilate in order to maintain acceptable output. Despite shared dilation, global RV function and stroke volume are much better preserved in subaortic RV patients than PH patients. The decreased global function in PH patients is related to prolonged RV free wall shortening, resulting in post-systolic shortening and intra-ventricular dyssynchrony, and decreased transverse motion. In our patient cohort, global RV systolic longitudinal deformation and apical transverse motion showed the best correlation to RV ejection fraction. The prognostic values of these parameters in different patient categories need to be further evaluated.

Supplementary table – ANCOVA analysis PS vs PH

	RVSP (r)	ANOVA	ANCOVA result
RVEDV/m^2	0.173 NS	-	-
RVESV/m^2	0.188 NS	-	-
RV mass/m^2	0.631 ‡	<0.001	P=0.100
RV mass-volume ratio	0.651 ‡	<0.001	P=0.045
RV ejection fraction	-0.146^{NS}	<0.001	-
RVSV/m^2	-0.017^{NS}	<0.001	-
RV cardiac output	-0.217^{NS}	<0.001	-
Apex basal ratio	0.554 ‡	<0.001	Not significant
Mid basal ratio	0.448 ‡	<0.001	Not significant
Longitudinal motion	-0.385†	<0.001	p<0.001
Apical shortening	-0.250^{NS}	<0.001	-
Mid shortening	-0.266^{NS}	<0.001	-
RV free wall strain	0.297^{NS}	<0.001	-
RV total strain	0.214^{NS}	<0.001	-

Although RV systolic pressures did not significantly differ between PH and PS, we performed additional analysis to strengthen the notion that differences between patient groups are not explained by RVSP. The first column shows correlation of RVSP to imaging parameter. If a correlation with significance of p<0.1 was found ANCOVA (third column), with RVSP as covariate, was performed in addition to ANOVA (second column). NS= non significant; ‡ p<0.001; †p<0.01.

References

1. MacNee W. Pathophysiology of cor pulmonale in chronic obstructive pulmonary disease. Part One. Am J Respir Crit Care Med 1994;150:833-852.
2. Humbert M, Sitbon O, Chaouat A, et al. Survival in patients with idiopathic, familial, and anorexigen-associated pulmonary arterial hypertension in the modern management era. Circulation 2010;122:156-163.
3. Tinker J, Howitt G, Markman P, Wade EG. The Natural History of Isolated Pulmonary Stenosis. Br Heart J 1965;27:151-160.
4. Cuypers JA, Eindhoven JA, Slager MA, et al. The natural and unnatural history of the Mustard procedure: long-term outcome up to 40 years. Eur Heart J 2014;35:1666-1674.
5. Roche SL, Redington AN. The failing right ventricle in congenital heart disease. Can J Cardiol 2013;29:768-778.
6. Ryan JJ, Huston J, Kutty S, et al. Right ventricular adaptation and failure in pulmonary arterial hypertension. Can J Cardiol 2015;31:391-406.
7. Gerges M, Gerges C, Lang IM. Advanced imaging tools rather than hemodynamics should be the primary approach for diagnosing, following, and managing pulmonary arterial hypertension. Can J Cardiol 2015;31:521-528.
8. Jurcut R, Giusca S, Ticulescu R, et al. Different patterns of adaptation of the right ventricle to pressure overload: a comparison between pulmonary hypertension and pulmonary stenosis. J Am Soc Echocardiogr 2011;24:1109-1117.
9. Galie N, Humbert M, Vachiery JL, et al. 2015 ESC/ERS Guidelines for the diagnosis and treatment of pulmonary hypertension: The Joint Task Force for the Diagnosis and Treatment of Pulmonary Hypertension of the European Society of Cardiology (ESC) and the European Respiratory Society (ERS): Endorsed by: Association for European Paediatric and Congenital Cardiology (AEPC), International Society for Heart and Lung Transplantation (ISHLT). Eur Heart J 2016;37:67-119.
10. Rudski LG, Lai WW, Afilalo J, et al. Guidelines for the echocardiographic assessment of the right heart in adults: a report from the American Society of Echocardiography endorsed by the European Association of Echocardiography, a registered branch of the European Society of Cardiology, and the Canadian Society of Echocardiography. J Am Soc Echocardiogr 2010;23:685-713; quiz 786-8.
11. Badagliacca R, Poscia R, Pezzuto B, et al. Right ventricular dyssynchrony in idiopathic pulmonary arterial hypertension: Determinants and impact on pump function. J Heart Lung Transplant 2014.
12. Marcus JT, Gan CT, Zwanenburg JJ, et al. Interventricular mechanical asynchrony in pulmonary arterial hypertension: left-to-right delay in peak shortening is related to right ventricular overload and left ventricular underfilling. J Am Coll Cardiol 2008;51:750-757.
13. Driessen MM, Baggen VJ, Freling HG, et al. Pressure overloaded right ventricles: a multicenter study on the importance of trabeculae in RV function measured by CMR. Int J Cardiovasc Imaging 2014;30:599-608.
14. Jones NL, Makrides L, Hitchcock C, Chypchar T, McCartney N. Normal standards for an incremental progressive cycle ergometer test. Am Rev Respir Dis 1985;131:700-708.
15. Koch B, Schaper C, Ittermann T, et al. Reference values for cardiopulmonary exercise testing in healthy volunteers: the SHIP study. Eur Respir J 2009;33:389-397.
16. Kind T, Mauritz GJ, Marcus JT, van de Veerdonk M, Westerhof N, Vonk-Noordegraaf A. Right ventricular ejection fraction is better reflected by transverse rather than longitudinal wall motion in pulmonary hypertension. J Cardiovasc Magn Reson 2010;12:35-429X-12-35.
17. Haddad F, Hunt SA, Rosenthal DN, Murphy DJ. Right ventricular function in cardiovascular disease, part I: Anatomy, physiology, aging, and functional assessment of the right ventricle. Circulation 2008;117:1436-1448.
18. Klima U, Guerrero JL, Vlahakes GJ. Contribution of the interventricular septum to maximal right ventricular function. Eur J Cardiothorac Surg 1998;14:250-255.
19. ter Keurs HE, Rijnsburger WH, van Heuningen R, Nagelsmit MJ. Tension development and sarcomere length in rat cardiac trabeculae. Evidence of length-dependent activation. Circ Res 1980;46:703-714.
20. Palau-Caballero G, Walmsley J, van Empel VP, Lumens J, Delhaas T. Why Septal Motion is a Marker of Right Ventricular Failure in Pulmonary Arterial Hypertension: Mechanistic Analysis Using a Computer Model. Am J Physiol Heart Circ Physiol 2016:ajpheart.00596.2016.
21. Mauritz GJ, Kind T, Marcus JT, et al. Progressive changes in right ventricular geometric shortening and long-term survival in pulmonary arterial hypertension. Chest 2012;141:935-943.
22. Moceri P, Bouvier P, Baudouy D, et al. Cardiac remodelling amongst adults with various aetiologies of pulmonary arterial hypertension including Eisenmenger syndrome-implications on survival and the role of right ventricular transverse strain. Eur Heart J Cardiovasc Imaging 2016.
23. Vonk Noordegraaf A, Westerhof BE, Westerhof N. The Relationship Between the Right Ventricle and its Load in Pulmonary Hypertension. J Am Coll Cardiol 2017;69:236-243.
24. Lankhaar JW, Westerhof N, Faes TJ, et al. Quantification of right ventricular afterload in patients with and without pulmonary hypertension. Am J Physiol Heart Circ Physiol 2006;291:H1731-7.
25. Bogaard HJ, Natarajan R, Henderson SC, et al. Chronic pulmonary artery pressure elevation is insufficient to explain right heart failure. Circulation 2009;120:1951-1960.
26. Borow KM, Colan SD, Neumann A. Altered left ventricular mechanics in patients with valvular aortic stenosis and coarction of the aorta: effects on systolic performance and late outcome. Circulation 1985;72:515-522.
27. Wang Z, Chesler NC. Pulmonary vascular wall stiffness: An important contributor to the increased right ventricular afterload with pulmonary hyper-

tension. Pulm Circ 2011;1:212-223.
28. Giusca S, Dambrauskaite V, Scheurwegs C, et al. Deformation imaging describes right ventricular function better than longitudinal displacement of the tricuspid ring. Heart 2010;96:281-288.
29. Zhang L, Allen J, Hu L, Caruthers SD, Wickline SA, Chen J. Cardiomyocyte architectural plasticity in fetal, neonatal, and adult pig hearts delineated with diffusion tensor MRI. Am J Physiol Heart Circ Physiol 2013;304:H246-52.
30. Hopkins WE. The remarkable right ventricle of patients with Eisenmenger syndrome. Coron Artery Dis 2005;16:19-25.
31. Plymen CM, Sado DM, Taylor AM, et al. Diffuse myocardial fibrosis in the systemic right ventricle of patients late after Mustard or Senning surgery: an equilibrium contrast cardiovascular magnetic resonance study. Eur Heart J Cardiovasc Imaging 2013.
32. Gomez-Arroyo J, Sandoval J, Simon MA, Dominguez-Cano E, Voelkel NF, Bogaard HJ. Treatment for pulmonary arterial hypertension-associated right ventricular dysfunction. Ann Am Thorac Soc 2014;11:1101-1115.
33. Spruijt OA, Di Pasqua MC, Bogaard HJ, et al. Serial assessment of right ventricular systolic function in patients with precapillary pulmonary hypertension using simple echocardiographic parameters: A comparison with cardiac magnetic resonance imaging. J Cardiol 2017;69:182-188.
34. Mercer-Rosa L, Parnell A, Forfia PR, Yang W, Goldmuntz E, Kawut SM. Tricuspid annular plane systolic excursion in the assessment of right ventricular function in children and adolescents after repair of tetralogy of Fallot. J Am Soc Echocardiogr 2013;26:1322-1329.
35. Delcroix M, Vonk Noordegraaf A, Fadel E, Lang I, Simonneau G, Naeije R. Vascular and right ventricular remodelling in chronic thromboembolic pulmonary hypertension. Eur Respir J 2013;41:224-232.
36. Giusca S, Popa E, Amzulescu MS, et al. Is Right Ventricular Remodeling in Pulmonary Hypertension Dependent on Etiology? An Echocardiographic Study. Echocardiography 2016;33:546-554.
37. Maceira AM, Prasad SK, Khan M, Pennell DJ. Reference right ventricular systolic and diastolic function normalized to age, gender and body surface area from steady-state free precession cardiovascular magnetic resonance. Eur Heart J 2006;27:2879-2888.

CHAPTER 8

Regional right ventricular remodeling and function in children with idiopathic pulmonary arterial hypertension versus those with pulmonary valve stenosis: Insights into mechanics of RV dysfunction

Authors:
Mieke M.P. Driessen, Folkert J. Meijboom, Wei Hui, Andreea Dragulescu, Luc Mertens, Mark K. Friedberg

Echocardiography 2017;34:888-897.

Abstract

Background
RV pressure overload in the context of pulmonary stenosis (PS) has a much better prognosis than in the context of idiopathic pulmonary arterial hypertension (iPAH), which may be related to differences in global and regional RV remodeling and systolic function. We compared RV mechanics in children with PS to those with iPAH, aiming to identify mechanisms and markers of RV dysfunction.

Methods
Eighteen controls, 18 iPAH and 16 PS patients were retrospectively studied. Age, BSA and sex distribution were comparable. Two-dimensional echocardiography, blood flow and tissue Doppler and longitudinal RV deformation were analyzed. ANCOVA - including RV systolic pressure (RVSP) and length as covariates – was used to compare patient groups.

Results
RVSP was higher in iPAH versus PS (96.8±25.4 vs. 75.4±18.9 mmHg, p=0.011). Compared to controls, PS patients showed mild dilation (p<0.01) and decreased longitudinal deformation (p<0.001) at the RV apex. Compared to both PS and controls, iPAH patients showed marked spherical RV dilation (p<0.001), reduced global RV free wall and septal longitudinal deformation (iPAH -22.07±4.35% vs. controls -28.18±1.69%; -9.98±4.30% vs. -17.45±2.52%; p<0.001) and RV post-systolic shortening (p<0.001). RV transverse shortening (radial performance) was increased in PS (31.75±10.35%; p<0.001) but reduced in iPAH (-1.62±11.11% vs. controls 12.00±7.74%; p<0.001).

Conclusion
Children with iPAH demonstrate adverse global and regional RV remodeling and mechanics compared to those with PS. Mechanisms of RV systolic dysfunction in iPAH include decreased longitudinal deformation, decreased or absent transverse shortening and post-systolic shortening. These markers may be useful to identify children at risk of RV failure.

Introduction

Right ventricular (RV) dysfunction is an important determinant of morbidity and mortality in various cardiovascular pathologies, especially those related to RV pressure- or volume overload.[1-3] However, early identification and characterization of a poorly adapting RV, and consequently RV failure, continues to be difficult.

Patients with pulmonary valvular stenosis (PS) and idiopathic pulmonary arterial hypertension (iPAH) both experience chronically increased RV systolic pressure, but the clinical course and natural history of these conditions differ vastly.[4,5] While a large proportion of iPAH patients present with, or rapidly develop, symptomatic heart failure,[5,6] PS patients are often asymptomatic or present with only mild exercise intolerance.[4] Moreover, mortality vastly differs between the groups - high in iPAH and very low in PS.[4,5]

Although the duration and possibly character of increased RV pressure differs between the 2 conditions, the RV response also seems very different. A study by Jurcut et al. demonstrated this difference in adult iPAH and PS patients, showing global RV dilation and decreased global RV free wall (RVFW) longitudinal deformation in iPAH versus PS patients.[7] Although contraction is predominantly longitudinal in the normal RV; septal contraction, regional RVFW deformation, RVFW radial function and septal-RVFW synchrony all contribute to RV performance.[8,9] Thus, differences in radial function, septal deformation, regional RV remodeling and regional deformation may all contribute to differences in RV function, and consequently clinical outcome, of pediatric PS vs. iPAH patients. However, these are incompletely characterized in children. Furthermore, comparing RV mechanics in these two clinically distinct patient groups may provide useful insights into the mechanisms of RV failure in pediatric patients with increased RV pressure, as well as imaging markers of RV dysfunction.[7] Accordingly, the aim of this study was to characterize regional and global RV remodeling and mechanics in children with PS compared to iPAH – to provide insights into mechanisms of RV maladaptation and potential imaging markers for identification of RV dysfunction.

Methods

Study population

We retrospectively studied children with iPAH and PS, comparing them to healthy controls with similar age and BSA. The study population has previously been described in a paper on interventricular interaction and LV diastolic function.[10] Echocardiographic studies performed between 2006 and 2013 were included. The diagnosis of iPAH was established by right-heart catheterization with a mean pulmonary artery pressure ≥ 25 mmHg, pulmonary capillary wedge pressure ≤15 mmHg and pulmonary vascular resistance of >3 Wood units.[11] All iPAH patients were on pulmonary vasodilator therapies. Valvular PS patients were included if they had a peak pulmonary valve gradient of ≥36 mmHg and did not have previous interventions or additional intra-cardiac abnormalities - with the exception of a small, hemodynamically insignificant atrial or ventricular septal defect. An electrocardiogram within 3 months from echocardiography was used to measure QRS duration and possible bundle branch block. Healthy controls served as a reference group for RV geometry and function. Controls were healthy volunteers or children evaluated for an innocent

murmur with normal medical history, physical examination and echocardiography. The study was approved by the institutional research ethics board.

Echocardiography

Two-dimensional echocardiographic measurements were made offline using commercially available software (SyngoDynamics, Siemens, Erlangen, Germany). Measurements were performed in accordance with pediatric guidelines.[12] Images were acquired at our institution with either Philips or GE ultrasound platforms. In PS patients, the echocardiogram closest to potential balloon valvuloplasty was analyzed (all but one patient subsequently underwent balloon angioplasty) to include the echocardiogram with the highest pulmonary valve gradient. As many iPAH patients were diagnosed prior to implementation of a functional echo protocol – we chose to include the first echocardiogram with full functional evaluation rather than the echocardiogram at time of right heart catheterization. Systemic blood pressure was measured manually at the time of echocardiography, placing the cuff on the right upper arm.

Two-dimensional measurements

M-mode measurements of the RV and LV end-diastolic diameters were made at the level of the mitral valve leaflet tips. Z-scores were calculated using institutional reference values. Using the same M-mode registration, RVFW inward transverse displacement was measured and transverse shortening calculated (Figure 1). RV fractional area change (FAC), tricuspid annular plane systolic excursion (TAPSE) and RV dimensions were measured from a focused apical 4-chamber view.[12] To

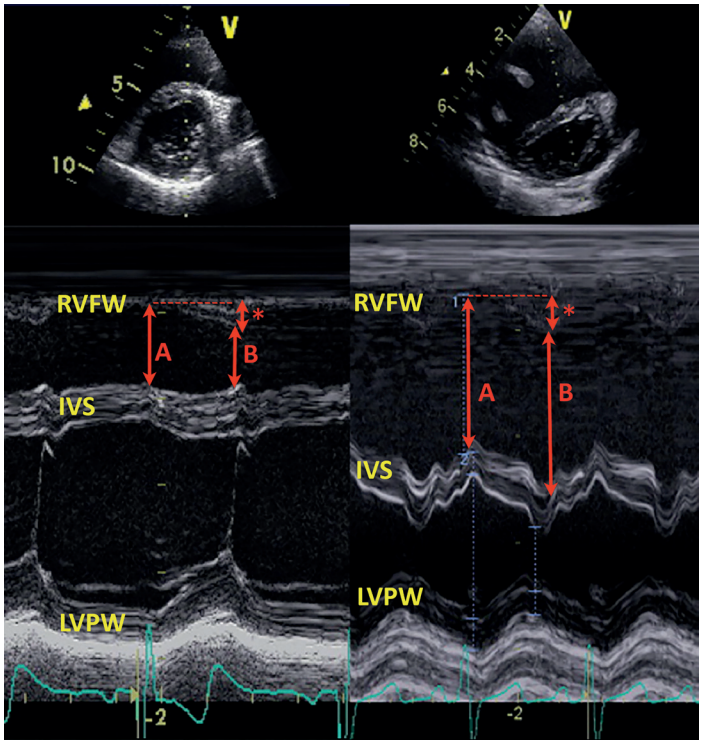

Figure 1: Short-axis M-mode echocardiography depicting transverse RV shortening.
The left hand panel depicts an example of a healthy control and on the right an example of an iPAH patient. Transverse shortening is calculated as [a – b] / a. The asterisks (*) indicate the absolute RVFW displacement. RVFW= right ventricular free wall; IVS= interventricular septum; LVPW= left ventricular posterior wall.

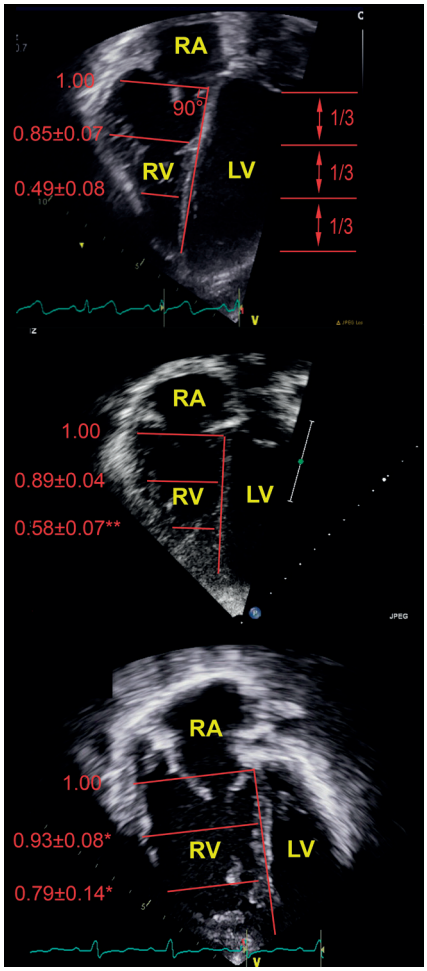

Figure 2: RV geometry.
Mid and apical to basal ratios measured in the modified-RV apical 4-chamber view. Continuous data were normally distributed and represented as mean ± standard deviation. Patient groups are compared to controls using ANOVA with posthoc Dunnet's and to each other using ANCOVA with covariate RVSP; #p≤0.05; **p≤0.01; *p≤0.001. A= controls; B= pulmonary valve stenosis; C= idiopathic pulmonary arterial hypertension. RA= right atrium; RV= right ventricle; LV= left ventricle.

assess RV geometry, RV dimensions were measured at the apical, mid and basal levels (Figure 2). Right atrial (RA) area was measured at end RV systole and end RA systole.

Blood flow and Tissue Doppler imaging

Continuous wave (CW) Doppler was used to measure maximal pulmonary valve flow velocities in systole and end-diastole. RVSP was estimated using the modified Bernoulli equation from tricuspid regurgitation CW Doppler. We did not add an assumed right atrial pressure to the RVSP. Many PS patients did not have tricuspid regurgitation. The resistance the ventricle has to overcome during systole determines RVSP, we therefore used the maximal pulmonary valve gradient in these patients to estimate RVSP.

Pulsed wave tissue Doppler imaging (TDI) at the basal RV free wall (RVFW), interventricular septum (IVS) and LV free wall (LVFW) were used to measure peak systolic (S') and early diastolic (E') tissue velocities and TDI-derived RV myocardial performance index.

Speckle tracking analysis
A focused RV apical 4-chamber view was used for speckle tracking strain analysis (Tomtec4.6, UnterSchleissheim, Germany). The RVFW and IVS endocardial borders were traced and adequate tracking visually confirmed. If more than one segment did not track adequately the patient was excluded from analysis. The following parameters were measured for both regional and global IVS and RVFW strain: peak systolic longitudinal strain (peak deformation during ejection time, i.e. before or at pulmonic valve closure), time to peak (TTP) and post-systolic shortening (PSS). Post-systolic shortening is defined as deformation continuing after pulmonic valve closure, calculated as (%)= ((peak strain – peak systolic strain))/peak strain) *100.[13] Time to pulmonic valve closure was determined using pulsed wave Doppler measurement in the RV outflow tract – using a cardiac cycle with an equivalent RR interval. All timing measurements were normalized for the RR interval, to allow comparisons between different heart rates.

Reproducibility
Ten representative datasets were randomly selected for reproducibility measurements. The second analysis by the first observer was performed at least 1-month after the first measurement. Both observers were blinded to the prior results. The same cardiac cycle was used to perform reproducibility measurements.

Statistical analysis
Distribution of the continuous variables was assessed using a combination of boxplot, normal probability plot and Shapiro-Wilk test. Normally distributed variables are represented as mean [± standard deviation] and non-normally distributed variables as median [range]. Categorical variables are presented as a frequency (%) and were compared using Chi-square test. Normally distributed continuous data of PS and PAH patients were compared to healthy controls using ANOVA with posthoc Dunnet's. Non-normally distributed data was compared using Mann-Whitney U test. To compare the imaging parameters between patient groups ANCOVA analysis was used, to adjust for covariates (RVSP and RV length) that possibly confound the association of patient group to the dependent variable. A bonferonni test was used for multiple comparisons. In other words, if the differences in outcome variables between patient groups are completely determined by differences in RVSP or RV length (for strain) – between group analysis with ANCOVA will yield a non-significant result.[13] As a rule of thumb at least 10 subjects are needed for each factor in a multivariable model. Using 3 factors: RVSP, diagnosis and RV length, 30 subjects are needed for analysis. Correlation between continuous parameters was assessed using squared correlation coefficient. Reproducibility was assessed by determining the mean difference with limits of agreement, intra-class correlation coefficient (for absolute agreement) and paired Student T-test. A two-sided alpha level of 0.05 was considered statistically significant. All data analyses were performed using IBM SPSS statistics version 22.0.

Results

Patient characteristics are listed in Table 1. There were no significant differences in age, BSA or sex distribution between groups. iPAH patients had higher RVSP and RV:LV pressure ratio compared with PS. Therefore, we corrected all analyses for RVSP as described above. Right bundle

	Controls (n=18)	PS (n=16)	PAH (n=18)	p-value PS vs. IPAH
Age, years	11.2±5.0	10.3±4.7	11.5±5.6	0.736
BSA, m^2	1.31±0.44	1.23±0.48	1.16±0.41	0.547
Male sex, %	10 (56%)	9 (56%)	9 (50%)	0.716
Medication:	None	None		-
- PDE-5 Inhibitor			7 (39%)	
- ETR-antagonist			13 (72%)	
- Prostaglandins			9 (50%)	
RVSP, mmHg[1]	-	75.4±18.9	96.8±25.4	0.011
RV : LV pressure ratio[1]	-	0.71 [0.41 – 1.57]	1.10 [0.46-1.50]	0.007
Heart rate, bpm	70±12.5	81±17.5	89.2±22.3**	0.261
TR severity n(%)				
- None/Trace	18 (100%)	15 (94%)	6 (33%)	
- Mild	-	1 (6%)	3 (17%)	
- Moderate	-	-	5 (28%)	
- Severe	-	-	4 (22%)	

Table 1: Patient characteristics.
Normally distributed continuous data is presented as mean ± standard deviation and non-normal as median [range]. Normally distributed data of PS and PAH were compared to controls using ANOVA with Dunnet's, Non-normally distributed data using Mann-Whitney U test. Categorical data were compared using Chi-square test. 1 Student T-test was used. #p≤0.05; **p≤0.01; *p≤0.001.

branch block was present in none of the PS patients and in 2/18 (11%) of the iPAH patients, mean QRS duration was respectively 84 vs. 99 msec.

General echocardiographic measurements

Children with iPAH had significantly more dilated RVs compared with healthy controls and children with PS (Table 2). Compared to controls, the RV apex in PS trended to be mildly dilated, but the normal triangular geometry was maintained (Figure 2). In contrast, iPAH patients demonstrated spherical RV geometry with significantly higher mid:basal and apical:basal diameter ratio (Figure 2). TAPSE and S' were decreased in both patient groups compared to controls (Table 2) but did not differ significantly between iPAH and PS (Table 2).

Measurements of diastolic function were worse in iPAH compared to controls and PS including larger end-diastolic and end-systolic RA area, lower TV E/A ratio and lower TDI E'. TV E and A waves were fused in 1 PS and 3 iPAH patients (Table 2). RV E/E' ratio was mildly higher in PS compared to controls and PH patients.

	Healthy (n=18)	PS (n=16)	iPAH (n=18)	P-value PS vs. iPAH
RVDd, mm	18.5 ± 4.4	20.3 ± 5.2	34.3 ± 9.9*	<0.001
z-score	*0.24 ± 1.02*	*1.2 ± 1.56*	*4.80 ± 2.00**	<0.001
LVEDD, mm	42.6±6.6	39.2±7.3	31.4±8.1*	0.106
z-score	0.16±0.92	-0.53±1.12	-3.86±3.26*	0.011
FAC, %	47.2 [39.2-53.7]	42.5 [36.7-68.1]	18.5 [8.1-34.3]*	<0.001
RVd basal, mm	33.5 ± 5.0	34.4 ± 7.4	48.3 ± 10.0*	<0.001
RVd major, mm	60.4 ± 10.9	56.4 ± 11.2	66.6 ± 12.3	0.007
TDI s', cm/sec	12.9 ± 1.9	10.7 ± 1.7**	11.7 ± 2.5	0.233
TAPSE, mm	21.4 ± 3.2	18.5 ± 2.9#	16.8 ± 4.7**	0.303
RVFS MM, %	12.00 ± 7.74	31.75 ± 10.35*	-1.62 ± 11.11**	<0.001
RVFW disp, mm	4.41 ± 0.86	8.50 ± 2.77*	6.27 ± 2.00	0.046
RV TEI index	0.29 ± 0.05	0.25 ± 0.04	0.50 ± 0.13*	<0.001
RA ED area, mm^2	12.1 ± 3.73	13.8 ± 4.7	20.12 ± 8.7*	0.013
RA ES area, mm^2	6.6 ± 2.7	8.1 ± 3.2	13.2 ± 6.8*	0.022
TV E/A ratio[1]	2.37 [1.24-5.44]	1.81 [0.92-2.60]	1.51[0.71-1.69]**	0.043
RV TDI e', cm/sec	14.2 ± 2.5	13.1 ± 3.6	10.5 ± 3.5**	0.009
RV E/e'	4.1 ± 0.8	6.2 ± 1.0*	4.8 ± 1.5	0.029

Table 2: Basic echocardiographic measurements.
Normally distributed continuous data is presented as mean ± standard deviation, and compared using ANOVA with Dunnet's or ANCOVA including RVSP, and non-normal as median [range], compared with Mann-Whitney U test. #p≤0.05; **p≤0.01; *p≤0.001. 1 E/A fusion in 1 PS and 3 iPAH patients; TV inflow was available in 15 controls, 11 PS patients and 13 iPAH patients. RVd = right ventricular dimension; TDI S'= Tissue Doppler imaging Systolic velocity; TAPSE = tricuspid annular systolic excursion; RVFS= Right ventricular fractional shortening; RVFW= right ventricular free wall; RVtr = right ventricular transverse movement slope; RA ES = right atrial end-systolic; RA ED= right atrial end-diastolic

RVFW transverse shortening

Absolute RVFW transverse displacement was increased in both PS and iPAH patients compared with healthy controls (PS p<0.001&PAH p=0.07) and highest in PS patients (p=0.046). However, the transverse shortening fraction was increased only in PS patients compared with controls (p<0.001; Table 2 & Figure 1). In contrast, despite maintained transverse RVFW displacement, transverse shortening fraction was decreased or even reversed in iPAH (-1.62±11.11%; p<0.001) compared with controls and PS patients due to paradoxical leftward septal motion in RV systole.

Longitudinal strain

Strain analysis was feasible in 44 out of 52 subjects (85%). RVFW and IVS longitudinal strain were significantly reduced in iPAH patients compared with PS and controls, independent of RV length and RVSP (Figure 3a). That RVSP alone does not adequately explain the differences in longitudinal deformation is also evident in Figure 4 where at similar RVSP, longitudinal strain in iPAH is lower than PS. Moreover, the correlation between RVSP and RVFW, IVS and RV total strain is opposite in iPAH and PS (Figure 4). Longitudinal deformation in PS *increases* with increasing RVSP

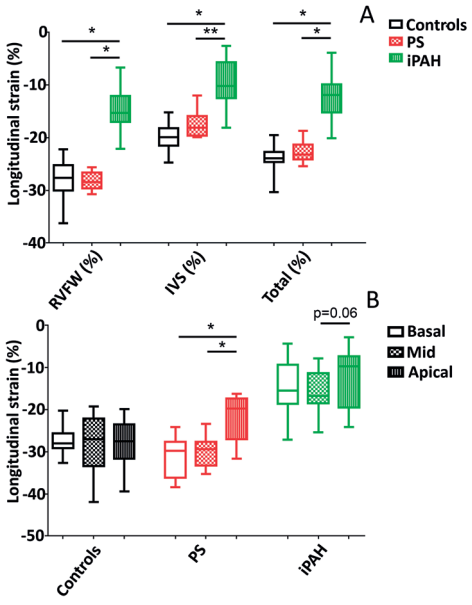

Figure 3a: Differences in global strain between patient groups.
Patient groups were compared to controls using ANCOVA and Bonferroni correction with RV length as covariate. They were compared to each other using RV length and RVSP as covariates.*p<0.001 and **p<0.01.

Figure 3b: Regional strain differences within patient groups. Differences in regional longitudinal strain within each group were assessed using a paired t-test; *p<0.001.
RVFW= right ventricular free wall; IVS=interventricular septum; PS= pulmonary valve stenosis; iPAH= idiopathic pulmonary arterial hypertension;

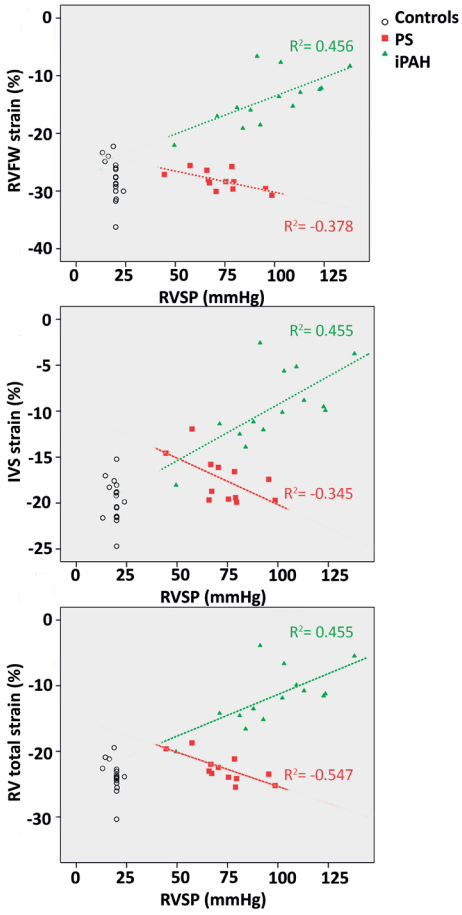

Figure 4: Longitudinal strain vs RVSP
Longitudinal strain of each individual patient plotted against RVSP, healthy controls in black, PS patients in red and iPAH in green. The squared correlation coefficient (R2) for RVFW, IVS and total RV strain versus RVSP was calculated in PS and iPAH patients. Top: RVFW strain, middle: IVS strain and bottom: RV total.

whereas in iPAH patients it *decreases* with increasing RVSP. RV total and RVFW longitudinal strain in PS patients were comparable to controls while IVS longitudinal strain trended to being mildly reduced vs. controls (p=0.062).
Regional RVFW strain is shown in Figure 3b. In healthy controls strain values were comparable in all segments. In both PS and iPAH patients apical RVFW strain was reduced compared with mid (iPAH & PS both p<0.05) and basal segments (PS p<0.01, iPAH not significant p=0.06).
Post-systolic shortening was more frequent and of greater magnitude in iPAH patients compared to PS and controls (Table 3). Furthermore, in controls and PS, post-systolic shortening occurred almost exclusively at the basal segment; whereas in iPAH both the mid and basal segments were affected. In addition, there was significantly more RV intra-ventricular delay – indicated by a

	Healthy n=17	PS N=12	iPAH n=15	
Number of pts with PSS (%)				
- basal	5 (29.4%)	3 (25.0%)	10 (66.7%)#	0.031
- mid	1 (5.8%)	-	10 (66.7%)*	<0.001
- apical	2 (11.8%)	-	2 (13.3%)	0.704
Severity of PSS (%)				
- basal	0.9 [0.1-10.0]	5.4 [0.6-5.7]	15.4 [0.5-45.9]	-
- mid	0.4	-	4.2 [0.4-18.8]	-
- apical	0.5 & 1.4	-	2.9 & 50.2	-
RVFW TTP, msec	444 ± 60	494 ± 59	553 ± 92*	0.063
IVS TTP, msec	437 ± 64	493 ± 77	542 ± 125**	0.208
RV-IVS diff, msec	12 [0-45]	16 [1-92]	51 [14-300]**	0.005

Table 3: Longitudinal strain analysis.
Post-systolic shortening and time to peak longitudinal strain (TTP) compared between all groups. Categorical data were compared using Chi-square test, only apical PSS was assessed using Fisher's exact test. Normally distributed continuous data is presented as mean ± standard deviation, and compared using ANOVA with Dunnet's or ANCOVA including RVSP, and non-normal as median [range], compared with Mann-Whitney U test. #p≤0.05; **p≤0.01; *p≤0.001. RVFW= right ventricular free wall; IVS= interventricular septum

	Intra-observer			Inter-observer		
	Mean Δ [Limits]	**p-value**	**ICC**	**Mean Δ [Limits]**	**p-value**	**ICC**
RVFW strain, %	1.01 [-4.00; 6.11]	p=0.252	0.94*	-0.66 [-6.46; 5.14]	p=0.501	0.93*
IVS strain, %	-2.10 [-7.59; 3.39]	p=0.042	0.79*	-1.21 [-7.87; 5.45]	p= 0.289	0.83*
RVtot strain, %	-1.42 [-6.03; 3.19]	p=0.089	0.91*	-1.05 [-6.46; 4.46]	p= 0.268	0.91*
RVFW disp, mm	0.12 [-1.82; 2.06]	p=0.710	0.96*	-6.7 [-12.2; -1.14]	p<0.001	0.91*
RVFS mm, %	-1.47 [-10,27; 7.33]	p=0.327	0.93*	2.81 [-12.47; 18.09]	p= 0.285	0.85*
Mid:bas ratio	-0.025 [-0.107; 0.057]	p= 0.09	0.66**	-0.11 [-0.39; 0.07]	p=0.003	NS
Ap:bas ratio	0.033 [-0.109; 0.043]	p= 0.03	0.87*	-0.12 [-0.32; 0.08]	p=0.004	NS

Table 4: Inter- and Intraobserver reproducibility.
Mean difference and limits of agreement; significance tested using paired T-test and interclass correlation coefficient (ICC), * p<0.001 and **p<0.01. RV= right ventricular; RVFW= RV free wall; IVS= interventricular septum; RVFS MM= RV fractional shortening on m-mode; mid:bas = mid to basal; ap:bas = apical to basal; NS= not significant

larger IVS to RVFW TTP delay in iPAH patients (iPAH 45 [15-300] vs. PS 16 [1-92] vs. controls 12 [0-45] ms; p<0.001).
As the mean RVSP was higher in the iPAH group, a sub-analysis was performed in 11 iPAH patients and 15 PS patients with comparable RVSP between 50-110 mmHg, to further control for RVSP. The mean RVSP of these subgroups was 83.8 ± 18.6 mmHg in iPAH vs. 77.4 ± 17.6 mmHg in PS (p=0.387). Despite similar RVSP, RVFW, IVS and RVtot longitudinal strain were decreased in iPAH compared with PS (15.1±4.8% vs 30.7±1.7% (p<0.001), 10.3±4.6% vs. 17.7±2.5% (p=0.001) and 12.6±4.8% vs. 23.0±1.9% (p<0.001), respectively) and post-systolic shortening was more frequent in iPAH vs. PS (6 (55%) vs. 0 (0%)). Similarly, RVFS and RV displacement were decreased in iPAH vs. PS (-4.64±11.28% vs. 31.75±10.35% (p<0.001) and 6.00±2.25 mm vs. 8.50±2.77 mm (p=0.034), respectively).

Reproducibility (Table 4)
Intra- and interobserver reproducibility were good for strain measurements and RVFW transverse displacement and fractional shortening. RV apical:basal and mid:basal diameter ratio had good intra-observer, but poor inter-observer agreement.

Discussion

The current study assessed the effect of RV pressure overload on global and regional right ventricular remodeling and function, comparing two distinct patient groups. Our results show that 1) global RV dilation and RV systolic dysfunction in iPAH patients is characterized by: spherical geometry, apical remodeling and dysfunction, decreased longitudinal deformation of both IVS and RVFW and highly inefficient RV kinetics – as evidenced by increased post-systolic shortening and increased IVS-RVFW discoordination – compared to PS and controls. 2) In contrast, PS patients maintain near-normal RV geometry, normal RV cavity size and global systolic function. Nevertheless, they also exhibit mild apical remodeling with a corresponding decrease in regional apical deformation. 3) Transverse shortening is augmented in pediatric PS while effective RV transverse shortening is reduced in pediatric iPAH – suggesting that the iPAH-RV inadequately compensates for the loss in longitudinal function. 4) iPAH patients demonstrate diastolic dysfunction while PS patients have comparable diastolic function to controls. These differences are not entirely explained by differences in RVSP alone and suggest either different RV adaptation or different progression rate of RV disease in iPAH vs. PS – possibly explaining the differences in clinical outcomes.

RV regional remodeling and function
In both PS and iPAH, the RV has to generate a higher RV systolic pressure to eject blood. Higher RV systolic pressure increases RV systolic wall stress – which leads to RV hypertrophy in an attempt to reduce wall stress. If the reduction of wall stress is insufficient – RV dysfunction and dilation will eventually ensue. The RV in iPAH is markedly dilated, and moreover, remodels to a spherical shape, with the most pronounced dilation at the apex. Conversely, although PS patients have mild apical remodeling, they do not exhibit global RV dilation or increased sphericity. This suggests that the RV in PS is adapted better to increased pressure-loading and possibly has reduced wall stress compared to iPAH.

The differences in RV remodeling in iPAH vs. PS are paralleled by worse ventricular performance. Longitudinal RVFW function is the most frequently used vector to assess RV function in clinical practice.[7,14,15] TAPSE and TDI S' are used most frequently and were equally decreased in both pressure overloaded groups compared to controls. In contrast, overall RV function clearly differs between PS and iPAH patients, although TAPSE and TDI S' may still be useful in follow-up of each individual patient group. This finding may relate to more severe tricuspid regurgitation and apical rotation in iPAH, as reported by Motoji et al. to overestimate TAPSE in iPAH.[16,17] In our study, global longitudinal RVFW deformation was worse in iPAH compared to PS and marked post-systolic shortening – not accounted for by TAPSE and TDI S' – was present exclusively in iPAH. Post-systolic shortening has also been reported in adult iPAH and relates to intra-ventricular dyssynchrony and inefficient RV contraction leading to decreased RV output.[7,18] We further demonstrate that the correlation of RVSP to global longitudinal deformation is divergent in iPAH versus PS: in iPAH higher RVSP corresponds with decreased deformation, while in PS it corresponds with increased deformation. Several possible explanations may account for these differences: RV remodeling and maladaptation is present in iPAH, but not in PS, with progressive dilation.[19] Secondly, more TR in iPAH may contribute to RV dilatation and decreased deformation.[20] Lastly, higher end-systolic wall stress may occur in iPAH vs. PS, akin to higher LV end-systolic wall stress reported in aortic coarctation vs. valvar aortic stenosis.[21]

Analysis of regional RVFW longitudinal deformation shows that apical RVFW longitudinal deformation is decreased in both conditions. This can be explained by apical remodeling in both groups, which – following Laplace's law - will lead to higher regional wall stress and in turn decreased regional deformation. As the volume of the RV apex is proportionally increased, apical remodeling and dysfunction may be an important determinant of RV function and reduced cardiac output. Both our group and Dambrauskaite et al. have previously shown that apical strain is related to disease severity in iPAH.[22, 23 21, 22] Furthermore, Fernandez-Friera et al. demonstrated reduced apical RV ejection fraction – by magnetic resonance imaging – in adult iPAH patients.[24] As apical remodeling and decreased longitudinal deformation were also found in PS – with normal global systolic RV function – it might be a sensitive echocardiographic marker of RV dysfunction.

Transverse RV free wall motion and septal deformation

Reduced longitudinal deformation should ideally be compensated by a commensurate increase in circumferential deformation or transverse function to maintain adequate cardiac output.[9] We assessed this by M-mode, using the RV transverse fractional shortening fraction. In PS patients this measurements was increased, but in iPAH severely decreased, and even paradoxical compared to controls. Therefore, it seems this compensatory mechanism fails in iPAH patients, possibly contributing to RV dysfunction and failure. Transverse RV function was previously related to survival in iPAH by Kind et al.[26] It is important to note that the transverse inward RVFW movement itself trended towards being *increased* in iPAH patients vs. controls and decreased transverse shortening is related to the paradoxical leftward IVS displacement, caused by an adverse septal gradient during prolonged RV free wall shortening.[14] This displacement interferes with efficiency of RV ejection and LV function.[25] Transverse RV fractional shortening could be a simple and easily quantifiable imaging marker for evaluation of RV performance, in addition to conventional measures. Its relation to parameters of global RV systolic function, such as RV ejection fraction, and inter-test variability need to be further investigated before implementing this measure in

clinical practice.
Besides RVFW longitudinal and transverse function, septal deformation and LV contraction contribute to RV ejection.[8,14 26] Longitudinal deformation of the IVS is decreased in pediatric iPAH patients compared to controls and PS, whereas it is maintained in PS patients. Furthermore, iPAH patients show a greater dispersion between IVS and RVFW time to peak systolic deformation, resulting in discoordinated RV contraction (i.e. dyssynchrony).[27] Prolonged RVFW time to peak and RVFW-IVS delay may be an effect of electromechanical delay – as demonstrated in tetralogy patients – mechanical delay or both. While QRS duration was mildly increased in iPAH patients vs. PS patients, right bundle branch block was infrequent in our iPAH patients. As the difference in time to peak RVFW deformation was >60 msec between iPAH patients vs PS and controls, delayed time to RVFW peak and intra-RV delay seem mainly related to mechanical delay in our cohort. Together with post-systolic shortening and regional dysfunction, this leads to highly inefficient RV contraction.

Pathophysiology
Adverse RV mechanics in iPAH versus PS reflects either faster progression to RV failure in pediatric iPAH patients, a different RV response to pressure load or a combination of both. Our study design cannot determine these pathophysiological mechanisms and further research is clearly needed. However, there are theoretical considerations that might explain the observed differences. Firstly, as discussed above, characteristics of the RV afterload might differ between iPAH and PS. Total RV work is a composite of multiple factors and depends on the properties of the proximal and distal pulmonary vasculature. These properties include pulmonary vascular resistance, compliance and pressure wave reflection. These are worse in iPAH leading to increased RV load.[1,28]
Secondly, the RV response to its given afterload might differ. In PS the RV faces increased pressure load from fetal or early post-natal life. In contrast, in pediatric iPAH postnatal adaptation to low pulmonary resistance has likely already occurred, as many of our results are similar to the results of Jurcut et al in adult patients. The RV encounters increased workload after the neonatal period, requiring adaptation to higher afterload over a much shorter time span.[29] Related molecular differences may determine RV adaption to increased pressure load, which is supported by the usually better RV function seen in Eisenmenger syndrome.[30] Moreover, factors such as RV myocardial ischemia and deranged RV metabolism are likely more prominent in iPAH versus PS.[31] These factors contribute to RV dilation, wall stress, and fibrosis and ultimately worsen oxygen demand/supply mismatch.[31] Fibrosis in itself may differ between the 2 conditions, as it relates to ventricular compliance and diastolic function, which in our study was largely maintained in PS but impaired in iPAH.[32]

Clinical implications
Although pulmonary vasodilators have improved survival in iPAH, in many patients the disease progresses and survival depends on RV (dys)function.[33] Thus far, drug treatment in iPAH has been mainly aimed at lowering pulmonary vascular resistance, thereby improving RV function. Moreover, independently of pulmonary vascular resistance, early identification of RV maladaptation and failure remains a challenge. Therefore, early detection and evaluation of RV (apical) dilation, systolic and diastolic dysfunction, increased post-systolic shortening and decreased transverse shortening may identify patients with poorly adapted RVs who are at higher risk of RV failure and

death. These parameters should therefore be further assessed in future studies.

Limitations

This was a retrospective study in a relatively small sample with inherent limitations, as some measurements could not be reliably performed (i.e. degree of hypertrophy). Nonetheless, all measurements of systolic RV function were available and differences were highly significant between groups. We used echocardiographic estimates of RVSP and not invasive measurements, as the latter were not routinely available within 6-months of the echocardiogram. Echocardiographic estimates might lead to both over- and underestimation of invasive measurements. TR estimates of RVSP may be overestimated when severe tricuspid regurgitation is present.[34] Likewise, estimation of RVSP using PV Doppler gradients may be inaccurate, but adequate TR to estimate RVSP was not present in most of the PS patients. Furthermore, RVSP was significantly lower in PS vs. iPAH patients, due to interventional thresholds in PS. We accounted for this important difference in 2-ways: 1) We performed linear regression to account for RVSP and 2) we performed additional subgroup analysis in PS and iPAH patients with similar RVSP – all showing consistent results. This was a mechanistic, descriptive study and while the differences in natural history and clinical presentation between PS and iPAH are well recognized [4,11] – and form the very basis for this study – we could not evaluate functional capacity.

Conclusion

In conclusion, children with iPAH demonstrate adverse RV remodeling and mechanics compared to children with PS. This may explain the markedly different natural history and clinical presentation and reflects either a faster progression of RV disease and/or a difference in RV adaptation. In this study, we highlight several mechanisms of RV maladaptation in pediatric iPAH patients that, although potentially applicable in clinical practice, are not routinely used or largely overlooked. These include – post-systolic shortening, apical remodeling, regional strain differences, decreased transverse shortening and diastolic dysfunction. Our results form the basis for further investigation of these parameters as markers of RV failure to identify children at risk of adverse outcome in congenital heart disease and iPAH.

References

1. Di Maria MV, Younoszai AK, Mertens L, et al. RV stroke work in children with pulmonary arterial hypertension: estimation based on invasive haemodynamic assessment and correlation with outcomes. Heart 2014;100:1342-1347.
2. Valente AM, Gauvreau K, Assenza GE, et al. Contemporary predictors of death and sustained ventricular tachycardia in patients with repaired tetralogy of Fallot enrolled in the INDICATOR cohort. Heart 2014;100:247-253.
3. van Wolferen SA, Marcus JT, Boonstra A, et al. Prognostic value of right ventricular mass, volume, and function in idiopathic pulmonary arterial hypertension. Eur Heart J 2007;28:1250-1257.
4. Tinker J, Howitt G, Markman P, et al. The Natural History of Isolated Pulmonary Stenosis. Br Heart J 1965;27:151-160.
5. Haworth SG, Hislop AA. Treatment and survival in children with pulmonary arterial hypertension: the UK Pulmonary Hypertension Service for Children 2001-2006. Heart 2009;95:312-317.
6. Berger RM, Beghetti M, Humpl T, et al. Clinical features of paediatric pulmonary hypertension: a registry study. Lancet 2012;379:537-546.
7. Jurcut R, Giusca S, Ticulescu R, et al. Different patterns of adaptation of the right ventricle to pressure overload: a comparison between pulmonary hypertension and pulmonary stenosis. J Am Soc Echocardiogr 2011;24:1109-1117.
8. Klima U, Guerrero JL, Vlahakes GJ. Contribution of the interventricular septum to maximal right ventricular function. Eur J Cardiothorac Surg 1998;14:250-255.
9. Pettersen E, Helle-Valle T, Edvardsen T, et al. Contraction pattern of the systemic right ventricle shift from longitudinal to circumferential shortening and absent global ventricular torsion. J Am Coll Cardiol 2007;49:2450-2456.
10. Driessen MM, Hui W, Bijnens BH, et al. Adverse ventricular-ventricular interactions in right ventricular pressure load: Insights from pediatric pulmonary hypertension versus pulmonary stenosis. Physiol Rep 2016;4:10.
11. Barst RJ, Ertel SI, Beghetti M, et al. Pulmonary arterial hypertension: a comparison between children and adults. Eur Respir J 2011;37:665-677.
12. Lopez L, Colan SD, Frommelt PC, et al. Recommendations for quantification methods during the performance of a pediatric echocardiogram: a report from the Pediatric Measurements Writing Group of the American Society of Echocardiography Pediatric and Congenital Heart Disease Council. J Am Soc Echocardiogr 2010;23:465-95.
13. D'hooge J, Heimdal A, Jamal F, et al. Regional strain and strain rate measurements by cardiac ultrasound: principles, implementation and limitations. Eur J Echocardiogr 2000;1:154-170.
14. Haddad F, Hunt SA, Rosenthal DN, et al. Right ventricular function in cardiovascular disease, part I: Anatomy, physiology, aging, and functional assessment of the right ventricle. Circulation 2008;117:1436-1448.
15. Forfia PR, Fisher MR, Mathai SC, et al. Tricuspid annular displacement predicts survival in pulmonary hypertension. Am J Respir Crit Care Med 2006;174:1034-1041.
16. Weidemann F, Eyskens B, Sutherland GR. New ultrasound methods to quantify regional myocardial function in children with heart disease. Pediatr Cardiol 2002;23:292-306.
17. Motoji Y, Tanaka H, Fukuda Y, et al. Association of Apical Longitudinal Rotation with Right Ventricular Performance in Patients with Pulmonary Hypertension: Insights into Overestimation of Tricuspid Annular Plane Systolic Excursion. Echocardiography 2016;33:207-215.
18. Marcus JT, Gan CT, Zwanenburg JJ, et al. Interventricular mechanical asynchrony in pulmonary arterial hypertension: left-to-right delay in peak shortening is related to right ventricular overload and left ventricular underfilling. J Am Coll Cardiol 2008;51:750-757.
19. Dragulescu A, Grosse-Wortmann L, Redington A, et al. Differential effect of right ventricular dilatation on myocardial deformation in patients with atrial septal defects and patients after tetralogy of Fallot repair. Int J Cardiol 2013;168:803-810.
20. Kamperidis V, Marsan NA, Delgado V, et al: Left ventricular systolic function assessment in secondary mitral regurgitation: left ventricular ejection fraction vs. speckle tracking global longitudinal strain. Eur Heart J 2016;37:811-816.
21. Borow KM, Colan SD, Neumann A. Altered left ventricular mechanics in patients with valvular aortic stenosis and coarction of the aorta: effects on systolic performance and late outcome. Circulation 1985;72:515-522.
22. Dambrauskaite V, Delcroix M, Claus P, et al. Regional right ventricular dysfunction in chronic pulmonary hypertension. J Am Soc Echocardiogr 2007;20:1172-1180.
23. Okumura K, Humpl T, Dragulescu A, et al. Longitudinal assessment of right ventricular myocardial strain in relation to transplant-free survival in children with idiopathic pulmonary hypertension. J Am Soc Echocardiogr 2014;27:1344-1351.
24. Fernandez-Friera L, Garcia-Alvarez A, Guzman G, et al. Apical right ventricular dysfunction in patients with pulmonary hypertension demonstrated with magnetic resonance. Heart 2011;97:1250-1256.
25. Dohi K, Onishi K, Gorcsan J,3rd, et al. Role of radial strain and displacement imaging to quantify wall motion dyssynchrony in patients with left ventricular mechanical dyssynchrony and chronic right ventricular pressure overload. Am J Cardiol 2008;101:1206-1212.
26. Kind T, Mauritz GJ, Marcus JT, et al. Right ventricular ejection fraction is better reflected by transverse rather than longitudinal wall motion in pulmonary hypertension. J Cardiovasc Magn Reson 2010;12:35-429X-12-35.
27. Lopez-Candales A, Dohi K, Bazaz R, et al. Relation of right ventricular free wall mechanical delay to right ventricular dysfunction as determined by tissue Doppler imaging. Am J Cardiol 2005;96:602-

606.
28. Mahapatra S, Nishimura RA, Sorajja P, et al. Relationship of pulmonary arterial capacitance and mortality in idiopathic pulmonary arterial hypertension. J Am Coll Cardiol 2006;47:799-803.
29. Zhang L, Allen J, Hu L, et al. Cardiomyocyte architectural plasticity in fetal, neonatal, and adult pig hearts delineated with diffusion tensor MRI. Am J Physiol Heart Circ Physiol 2013;304:H246-52.
30. Hopkins WE, Waggoner AD. Severe pulmonary hypertension without right ventricular failure: the unique hearts of patients with Eisenmenger syndrome. Am J Cardiol 2002;89:34-38.
31. Bogaard HJ, Natarajan R, Henderson SC, et al. Chronic pulmonary artery pressure elevation is insufficient to explain right heart failure. Circulation 2009;120:1951-1960.
32. Okumura K, Slorach C, Mroczek D, et al. Right ventricular diastolic performance in children with pulmonary arterial hypertension associated with congenital heart disease: correlation of echocardiographic parameters with invasive reference standards by high-fidelity micromanometer catheter. Circ Cardiovasc Imaging 2014;7:491-501.
33. Peacock AJ, Crawley S, McLure L, et al. Changes in right ventricular function measured by cardiac magnetic resonance imaging in patients receiving pulmonary arterial hypertension-targeted therapy: the EURO-MR study. Circ Cardiovasc Imaging 2014;7:107-114.
34. Ozpelit E, Akdeniz B, Ozpelit EM, et al. Impact of Severe Tricuspid Regurgitation on Accuracy of Echocardiographic Pulmonary Artery Systolic Pressure Estimation. Echocardiography 2015;32:1483-1490.

CHAPTER 9

Adverse ventricular-ventricular interactions in right ventricular pressure load: Insights from pediatric pulmonary hypertension versus pulmonary stenosis

Authors:
Mieke M.P. Driessen, Wei Hui, Bart H. Bijnens, Andreea Dragulescu, Luc Mertens, Folkert J. Meijboom, Mark K. Friedberg

Phys rep 2016;4:e12833

Abstract

Background
Right ventricular (RV) pressure overload has a vastly different clinical course in children with idiopathic pulmonary arterial hypertension (iPAH) than in children with pulmonary stenosis (PS). While RV function is well recognized as a key prognostic factor in iPAH, adverse ventricular–ventricular interactions and LV dysfunction are less well characterized and the pathophysiology is incompletely understood. We compared ventricular–ventricular interactions as hypothesized drivers of biventricular dysfunction in pediatric iPAH versus PS.

Methods and Results
Eighteen iPAH, 16 PS patients and 18 age- and size-matched controls were retrospectively studied. Cardiac cycle events were measured by M-mode and Doppler echocardiography. Measurements were compared between groups using ANOVA with post hoc Dunnet's or ANCOVA including RV systolic pressure (RVSP; iPAH 96.8±25.4 mmHg vs. PS 75.4±18.9 mmHg; P= 0.011) as a covariate. RV-free wall thickening was prolonged in iPAH versus PS, extending beyond pulmonary valve closure (638±76 msec vs. 562±76 msec vs. 473±59 msec controls). LV and RV isovolumetric relaxation were prolonged in iPAH (P< 0.001; LV 102.8±24.1 msec vs. 63.1±13.7 msec; RV 95 [61–165] vs. 28 [0–43]), associated with adverse septal kinetics; characterized by rightward displacement in early systole and leftward displacement in late RV systole (i.e., early LV diastole). Early LV diastolic filling was decreased in iPAH (73±15.9 vs. PS 87.4±14.4 vs. controls 95.8±12.5 cm/sec; P= 0.004).

Conclusion
Prolonged RVFW thickening, prolonged RVFW isovolumetric times, and profound septal dyskinesia are associated with interventricular mechanical discoordination and decreased early LV filling in pediatric iPAH much more than PS. These adverse mechanics affect systolic and diastolic biventricular efficiency in iPAH and may form the basis for worse clinical outcomes.

Introduction

In both idiopathic pulmonary arterial hypertension (iPAH) and pulmonary valvular stenosis (PS) the right ventricle (RV) increases its systolic pressure in order to overcome the increased impedance. However, pediatric iPAH is associated with worse exercise capacity, morbidity and mortality compared to PS.[1,2] While RV morphology and dysfunction are well-established drivers of morbidity and mortality in iPAH, and are different from PS[3,4], adverse ventricular-ventricular interactions and left ventricular (LV) dysfunction are emerging as important determinants of iPAH outcomes.[5]

The RV and left ventricle (LV) are interdependent through common myocardial fibers, the interventricular septum (IVS) and the pericardial space.[6,7] Of these, the IVS plays a crucial role in mediating ventricular-ventricular interactions as it shares fibers with both ventricles, is subject to interventricular pressure gradients and directly impacts biventricular geometry.[8,9] Septal and LV contraction contribute substantially to RV systolic function and ultimately cardiac output.[10,11] Likewise, RV loading, geometry and function impact LV function.[5,9,12,13] In RV pressure overload, these adverse ventricular-ventricular interactions negatively impact LV filling, geometry and systolic function.[5,12,13] The mechanisms and pathophysiology of these adverse interactions is incompletely characterized, but may partly explain the different clinical course of these groups.[7] Comparing ventricular-ventricular interactions in pediatric iPAH versus PS can further our understanding of RV adaptation to increased pressure-load.

Accordingly, the aim of this study was to characterize the pathophysiology and mechanisms of ventricular–ventricular interactions and their impact on biventricular function in the pressure-loaded RV in iPAH versus PS, using detailed analysis of septal kinetics and cardiac cycle-timing events. We hypothesized that adverse septal kinetics and temporal mechanics are associated with worse ventricular–ventricular interactions in children with iPAH versus PS.

Methods

Patients with echocardiography performed between 2004 and 2013 were retrospectively studied. iPAH patients were diagnosed according to the Dana Point guidelines – that is, a mean pulmonary arterial pressure of ≥25 mmHg at rest with a pulmonary vascular resistance of ≥3 Wood units and a pulmonary capillary wedge pressure of ≤15 mmHg.[14] Accordingly, the aim of this study was to characterize the pathophysiology and mechanisms of ventricular–ventricular interactions and their impact on biventricular function in the pressure-loaded RV in iPAH versus PS, using detailed analysis of septal kinetics and cardiac cycle-timing events. We hypothesized that adverse septal kinetics and temporal mechanics are associated with worse ventricular–ventricular interactions in children with iPAH versus PS.

Echocardiography

Analysis was performed on digitally stored echocardiograms (SyngoDynamics, Siemens, Erlangen, Germany) by *a single* observer. In iPAH patients the first full functional echocardiogram at our institution was analyzed. Measurements were performed as suggested in the 2010 guidelines for the pediatric echocardiogram by Lopez et al. A full functional study includes the following 2-D echocardiography views: parasternal short axis at mid-papillary level (M-mode & 2-D

echocardiography), standard apical 4-chamber, separate RV focused 4-chamber view, and apical 2-chamber. Pulsed and continuous wave Doppler interrogation was performed for all valves and Tissue Doppler Imaging (TDI) of RV free wall (RVFW), LV lateral wall and interventricular septum (IVS).

Echocardiographic dimensions

M-mode RV and LV end-diastolic (EDD) and end-systolic dimensions (ESD) and LV ejection fraction[16] were measured from parasternal short-axis views; and Z-scores calculated using institutional values. The LV eccentricity index (lateral divided by anterior-posterior LV diameter) was measured using a mid-LV short-axis view at end-systole, early-diastole and end-diastole.[17] RV end-diastolic and end-systolic areas were measured in the apical 4-chamber view to calculate the RV fractional area change.[15] Tricuspid annular planar systolic excursion (TAPSE) and TDI systolic velocity (s') were measured as measurements of RV systolic performance.

Biventricular and Septal kinetics

Detailed qualitative and quantitative analysis of IVS, RVFW and LV posterior wall (LVPW) motion throughout the cardiac cycle used parasternal midventricular M-mode tracings to define septal motion in relation to the RVFW and LVPW. Pulsed wave Doppler echocardiography was used to measure valve events (i.e., valve opening and closure – detailed below) in relation to the mechanical events. Quantitative measurements included: time to onset and peak septal, RVFW and LVPW contraction and time to peak leftward septal displacement (when present; # Fig. 1). The electrocardiogram (ECG) QRS onset was used as a reference for timing and event measurements.

Doppler echocardiography

Right ventricular systolic pressure (RVSP) was estimated from the TR jet using the modified Bernoulli equation. In PS patients the PV systolic gradient was used to estimate RVSP if the TR spectral Doppler tracing was incomplete. As inferior vena cava collapsibility is not validated or measured routinely in children, right atrial pressure was not added to the RVSP.

Pulsed Doppler tracings were sampled in the RV and LV inflow and outflow tracts. Atrio-ventricular and ventriculo-arterial valve opening and closure times and mitral and tricuspid valve early (E) and late (A) filling velocities were measured. LV isovolumetric relaxation time was derived from a pulsed wave Doppler tracing straddling the LV inflow and outflow.

Pulsed wave Tissue Doppler imaging (TDI) at the basal RV-free wall, IVS and LV-free wall was acquired and the peak systolic (TDI s') and early diastolic (TDI e') tissue velocities measured. The isovolumetric contraction and relaxation times were also measured on TDI. An average of three measurements was used for all TDI and Doppler velocity measurements.[15]

Timing measurements were taken from cardiac cycles with <10% variation in RR interval. To allow comparison between different heart rates, all timing measurements were normalized for the RR interval.

Reproducibility

In 15 randomly selected patients all M-mode and blood flow Doppler measurements including IVS, RVFW and LVPW timing and valve events were re-measured by the first observer (with a 1 month interval) and by a second observer, blinded to the first measurement.

Statistical analysis
Continuous variables are represented as mean±standard deviation or median [range] as appropriate. Categorical variables are presented as a frequency (%). PS and iPAH were compared to controls using the ANOVA with posthoc Dunnet's or Mann–Whitney U test, as appropriate. To assess the effect of patient group on the dependent variable (outcome measurements) we used ANCOVA – as it enables analysis of a covariate that possibly confounds the analysis (in our case RVSP). In other words, if the relationship between patient group and the outcome variable is completely determined by RVSP – statistical analysis would yield a nonsignificant result for between group analysis.
Intra- and interobserver reproducibility was assessed by determining: the mean difference with limits of agreement, intraclass correlation coefficient (absolute agreement) and comparing measurements with a paired Student's t-test. An alpha level of 0.05 was considered statistically significant.

Results

A total of 52 subjects, including 18 iPAH, 16 PS patients, and 18 age- and BSA-matched controls were studied. Baseline and demographic data are listed in Table 1. Age, BSA, and sex were similar between the three groups. All iPAH patients were on pulmonary vasodilator treatments at time of echocardiography: 7 (39%) on phosphodiesterase inhibitors, 13 (72%) on endothelin-receptor antagonists and 9 (50%) on prostacyclins. iPAH patients had significantly higher resting heart rates compared with controls. ECG QRS duration was significantly longer in iPAH versus PS patients and controls, although none met criteria for complete RBBB. RVSP and RV:LV pressure ratio were higher in iPAH patients compared with PS. iPAH patients had significantly more RV dilatation compared with controls and with PS patients; and measures of regional longitudinal and global RV function were worse (all $P < 0.001$; Table 1).

LV dimensions and functional parameters
Measures of LV dimensions and function are listed in Table 2. In PS patients these were comparable to controls. Using linear regression to account for differences in RVSP, iPAH patients had smaller LV EDD and LV ESD compared with PS patients and controls. LVEF was higher in iPAH. Both PS and iPAH patients had lower MV E/A ratio and similar E/E' ratio compared with controls. The early diastolic LV filling velocity was lower in iPAH compared with controls and PS patients ($P<0.001$ and $P=0.004$, respectively).

Event timing and septal movement
Figure 1 shows representative M-mode examples of each group. In Figure 2 the average timing of peak contraction and valve timing are represented schematically, including only patients with a complete dataset.

Healthy controls
Normal IVS motion is characterized by three major components (Figures 1a and 2a): 1) the IVS starts to contract on average 58±3 ms after QRS onset, maintaining a stable position throughout systole; 2) Peak IVS systolic excursion occurs ~30 ms before peak RVFW and LVPW thickening,

	Controls (n=18)	PS (n=16)	iPAH (n=18)	p-value PS vs iPAH
Age (yrs.)*	11.2 ± 5.0	10.3 ± 4.7	11.5 ± 5.6	0.736
BSA (m^2)*	1.31 ± 0.44	1.23 ± 0.48	1.16 ± 0.41	0.547
Male sex (%)	10 (56%)	9 (56%)	9 (50%)	0.716
Heart rate (bpm)	70 ± 13	81 ± 18	89 ± 22#	0.261
QRS ECG (ms)	-	84 ± 11	99 ± 18	0.005
RVSP (mmHg)	-	75.4 ± 18.9	96.8 ± 25.4	0.011
RV : LV pressure	-	0.71 [0.41-1.57]	1.10 [0.46-1.50]	0.007
RVDd (mm) *z-score*	18.5 ± 4.4 *0.24 ± 1.02*	20.3 ± 5.2 *1.2 ± 1.56*	34.4 ± 9.9* *4.82 ± 1.99**	<0.001 <0.001
RVDbas (mm)	33.5 ± 5.0	34.4 ± 7.4	48.3 ± 10.0*	<0.001
RVDmaj (mm)	60.4 ± 10.9	56.4 ± 11.2	66.6 ± 12.3	0.010
FAC (%)	47.2 [39.2-53.7]	42.5 [36.7-68.1]	18.5 [8.1-34.3]*	<0.001

Table 1: Baseline characteristics
Patients were compared to controls using ANOVA with posthoc Dunnet's test # p=0.002 and *p<0.001. PS and iPAH were compared using independent Student T-test.
PS=pulmonary stenosis; iPAH=idiopathic pulmonary arterial hypertension; Yrs.= years; BSA= body surface area; bpm= beats per minute; RVSP=right ventricular systolic pressure; LV=left ventricular; RVDd=right ventricular diastolic dimension parasternal long-axis; RVDbas = basal AP4CH-dimension; RVmajor= long AP4CH-dimension; FAC= fractional area change.

	Controls (n=18)	PS (n=16)	iPAH (n=18)	P-value iPAH to PS
LVEDd (mm) *z-score*	42.6 ± 6.6 *-0.01 ± 1.05*	39.2 ± 7.3 *-0.53 ± 1.12*	31.4 ± 8.1* *-3.86 ± 3.27**	0.101 0.011
LVEDs (mm) *z-score*	26.2 ± 4.6 *-0.24 ± 0.85*	23.6 ± 4.9 *-0.82 ± 1.14*	16.9 ± 6.9* *-3.70 ± 3.27**	0.052 0.029
LVEF-teich (%)	76.1 ± 6.0	77.2 ± 7.3	83.7 ± 8.7**	0.032
E vel (cm/sec)[1]	95.8 ± 12.5	87.4 ± 14.4	73.9 ± 15.9*	0.004
MV E/A ratio[1]	2.66 ± 0.90	1.70 ± 0.56*	1.44 ± 0.40*	0.594
MV E/E' ratio[2]	5.0 [4.3-9.1]	5.1 [4.1-7.1]	6.1 [4.3-9.9]	0.238
Sys ecc index	1.07 ± 0.03	1.23 ± 0.15#	2.49 ± 0.96*	<0.001
BDia ecc index[3]	1.17 ± 0.05	1.38 ± 0.16**	3.23 ± 1.22*	<0.001

Table 2: LV dimensions and global function
Controls compared with pulmonary stenosis (PS) and idiopathic pulmonary arterial hypertension (iPAH) patients using ANOVA with posthoc Dunnet's; *p≤0.001, **p≤0.01 and # P<0.05. Patient groups are compared using ANCOVA including right ventricular systolic pressure as a covariate.
[1]total fusion in 1 iPAH, missing in 4 iPAH and 1 PS patient; 2missing in 6 iPAH and 2 PS patients. LV= left ventricular; EDd=end-diastolic dimension; EF=ejection fraction; E=early diastolic filling velocity; A=late diastolic filling velocity; ecc=eccentricity index; Sys=systolic; Bdia= begin diastolic.

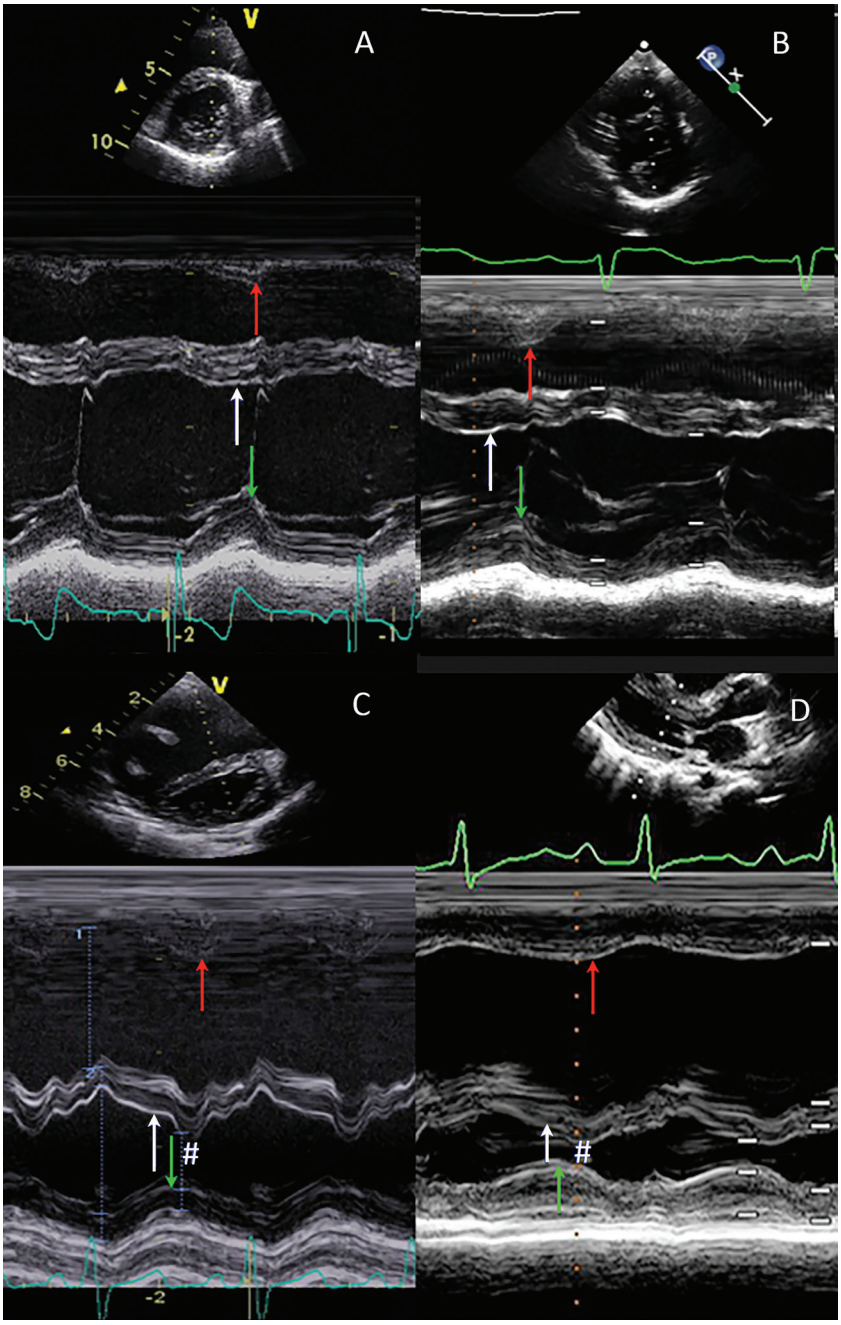

Figure 1: M-mode cross-sections
Four representative examples of m-mode cross-section parasternal short or long axis at the level of MV annulus are shown. The time to peak radial motion of right ventricular free wall, septum and left ventricular posterior wall are depicted with arrows. Figure 1A: control, figure 1B: pulmonary stenosis and figure 1C+1D: idiopathic pulmonary arterial hypertension. Abnormal septal motion in iPAH patients at the beginning of LV diastole is marked with # (1C+D).

which peak near-simultaneously (Table 3); 3) During early RVFW and LVPW relaxation there is subtle bidirectional post-systolic IVS motion (# in Figure 1a). The pulmonary valve (PV) opens slightly before, and closes simultaneously with, the aortic valve (AV). The mitral (MV) and tricuspid valves (TV) open and close near-simultaneously (Figures 1a+2a).

PS

In PS, qualitative IVS motion is similar to controls with some differences in the timing and position of the IVS: Onset of IVS contraction is delayed compared to controls (90±23 msec vs. 58±3 msec; P< 0.01), with a corresponding mild delay in AoV opening (95±15 msec vs. 83±14 msec; P< 0.05) which coincides with PV opening. Peak IVS systolic excursion and the early diastolic bidirectional IVS motion (Figures 1A and B) are similar to controls. Peak RVFW and LVPW thickening are delayed compared with controls but remain near simultaneous (peak RVFW 562±76 and LVPW 538±70 msec, Table 3, Figs. 1B and 2B). This results in prolonged mechanical discoordination between the IVS and both free walls (IVS to LVPW delay 121 msec) compared to controls. The septum is mildly leftward displaced during systole. Peak RVFW thickening is slightly later than peak LVPW thickening; correspondingly the PV closes later than the AoV with a prolonged RV ejection time (514±68 msec vs. 461±57 msec in controls). As systole lasts longer in PS compared to controls, MV and TV opening are delayed in PS despite normal isovolumetric relaxation times. The opening of the MV and TV valves is simultaneous.

iPAH

Qualitatively and quantitatively septal motion and timing of biventricular contraction and relaxation in iPAH patients differ substantially from PS patients and controls (Figures 1A–D). Onset of IVS contraction is delayed to 122±36 msec after QRS-onset (PS 90±23; controls 58±3 msec; P< 0.01). The IVS is displaced toward the RVFW during this delay and RVFW isovolumetric contraction is prolonged (iPAH 90 [58–139] vs. PS 61 [48–85] & controls 70 [61–102] msec; P < 0.01). The delayed onset of effective IVS and RVFW contraction corresponds with a delay in both PV and AoV opening compared to PS and controls (Table 3). In contrast to controls and PS, the PV opens after the AoV. In contrast to PS and controls the IVS thickens only mildly and is displaced markedly toward LVPW throughout systole (Figures 1 and 2), reflected by the high LV eccentricity index (Table 2). Similar to PS, both RVFW and LVPW peak thickening are prolonged compared to controls. Peak RVFW thickening is more prolonged in iPAH versus PS (iPAH 638±76 vs. PS 562±76 and controls 473±59 msec; P< 0.05), extending well beyond peak LVPW thickening and PV closure (564±80 & 500±73 msec, respectively) resulting in LV-RV systolic discoordination and postsystolic RVFW thickening. Despite prolonged RVFW thickening, effective RV ejection time is short (364±62 msec vs. 374±48 msec in controls). During postsystolic RVFW thickening, the IVS displaces even further leftward (# Figs. 1C, D and 2C), persisting throughout diastole. LV and RV isovolumetric relaxation times are prolonged in iPAH compared with PS and controls. Both MV and TV opening are delayed and discoordinated compared to controls and PS – the TV opening much later than the MV. The MV opens whilst the septum is still displaced toward the LVPW (MV opening 592±90 vs. peak IVS displacement 613±63 msec). This is associated with decreased early mitral diastolic filling velocity (E) compared to PS and controls (73.9±15.9 vs. 87.4±14.4 and 95.8±12.5 cm/sec; P= 0.004) and both LV and RV inflow durations are significantly shortened compared with controls (but not PS).

	Controls (n=18)	PS (n=16)	iPAH (n=18)	P-value iPAH to PS
RVFW peak (ms)[1]	473 ± 59	562 ± 76**	638 ± 76*	0.031
LVPW peak (ms)[1]	478 ± 48	538 ± 70#	564 ± 80*	0.547
Septal peak (ms)[1]	442 ± 74	435 ± 70	478 ± 51	0.212
Septal-D peak*[1]	-	-	613 ± 63	-
TOC (ms)[1]	58 ± 31	91 ± 24**	122 ± 36*	0.003
PV opening (ms)[2]	66 ± 12	81 ± 29	178 ± 76*	0.001
PV closure (ms)[2]	445 ± 52	514 ± 68*	500 ± 73	0.079
ET RVOT (ms)	374 ± 48	451 ± 60*	364 ± 62	0.001
AV opening (ms)[2]	83 ± 14	95 ± 15#	130 ± 40*	0.15
AV closure (ms)[2]	433 ± 52	461 ± 57	490 ± 63#	0.923
ET LVOT (ms)	354 ± 44	362 ± 46	375 ± 45	0.538
MV opening (ms)[3]	492 ± 52	537 ± 69#	592 ± 90*	0.520
TV opening (ms)[3]	478 ± 55	541 ± 88#	667 ± 98*	0.04
IVRT LV (ms)	63 ± 14	73 ± 16	103 ± 24*	0.015
TDI IVCT RV (ms)	70 [61-102]	61 [48-85]	90 [58-139]**	<0.001
TDI IVRT RV (ms)	28 [0-43]	33 [24-123]	95 [61-165]*	<0.001
MV inflow (ms)[3]	545 ± 49	531 ± 63	482 ± 82#	0.827
TV inflow (ms)[3]	557 ± 62	484 ± 87	399 ± 88*	0.251

Table 3: Timing of contraction and valve opening and closure
Timing measurements normalized for the RR interval, patients compared with controls using ANOVA with Dunnet's; #p<0.05, **p≤0.01 and *p≤0.001. Pulmonary stenosis (PS) are compared to idiopathic pulmonary arterial hypertension (iPAH) patients using ANCOVA using right ventricular systolic pressure as a covariate. RVFW= Right ventricular free wall; LVPW= Left ventricular posterior wall; D= diastolic peak; TOC= time to onset of contraction; PV= pulmonary valve; AV= aortic valve; MV= mitral valve; TV= tricuspid valve; IVRT= isovolumetric relaxation time. 1 RVFW peak missing in 4 controls, 2 PS and 1 iPAH patients, these were excluded for all M-mode measurements; 2 VA valve opening missing in 6 iPAH and 1 PS patient; 3AV opening was missing in 5 iPAH and 1 PS patient.

Subgroup analysis similar RVSP

A sub-analysis was performed in patients with comparable RVSP (50-110 mmHg); 11 iPAH patients and 15 PS patients could be included, with mean RVSP of 83.8±18.6 mmHg vs. 77.4±17.6 mmHg (P= 0.387). Differences in timing between iPAH and PS patients were similar to those observed in the entire cohort; time to peak RVFW thickening was delayed in iPAH (630±82 vs 562±76 msec; P= 0.042), ending well after PVC (477±82 vs. 514±70 msec in PS) and peak LVPW thickening (566±81 vs. 538±69 msec; p=0.369). The time to onset of IVS contraction was prolonged in iPAH versus PS patients (123±38 vs. 90±24 msec; p=0.015), moving rightward during this interval. All iPAH patients showed IVS displacement (#) after peak LVPW thickening (611±67 vs. peak LVPW 566±81 msec). In PS patients IVS displacement was only seen during end-systole, preceding or coinciding with peak LVPW thickening.

Discussion

Our results show that adverse ventricular-ventricular interactions and septal displacement are markedly worse in RV pressure-load associated with pediatric iPAH compared to PS. Pediatric iPAH was associated with profound RV early and end systolic (i.e. early LV diastolic) septal displacement and biventricular mechanical discoordination in both systole and diastole – reducing contractile efficiency and early LV filling. In contrast, in PS LV-RV coordination was preserved in both in systole and diastole and only mild septal displacement was seen at end-systole. These adverse v-v interactions seem primarily related to altered timing of RVFW systolic events seen in iPAH more than PS, and attest to both RV inefficiency and LV diastolic compromise.

Systolic interaction

Septal position depends on the trans-septal pressure-gradient combined with the tendency of the septum to straighten when contracting.[18] Changes of RV load therefore influence septal configuration and end-systolic septal curvature was one of the first sensitive, non-invasive markers of RV pressure overload.[9,17,18] Furthermore, adult iPAH studies have related septal kinetics to disease severity.[19,20] However, studies detailing IVS kinetics throughout the cardiac cycle remain very limited. Our results extend those of previous studies and demonstrate abnormal septal kinetics in pediatric iPAH patients throughout the entire cardiac cycle, while those in PS were limited to end-systole. In iPAH pronounced septal displacement was not only seen in late RV systole (prolonged RVFW thickening) – towards the LVPW – but also during early systole - towards the RVFW (# Figures 1C, D & Figure 2C).

Abnormal iPAH septal motion coincided with differences in timing of RVFW systolic events in iPAH versus PS patients. First, iPAH patients have prolonged RV isovolumetric contraction (median 90 msec vs. 61 msec in PS) – and hence prolonged pressure generation – coinciding with the early systolic rightward septal displacement. This delays not only effective RV, but also LV ejection in iPAH. Secondly, prolonged peak RVFW systolic excursion is delayed in iPAH much more than PS (mean of

638 msec vs. 562 msec) and results in end-systolic LVPW-RVFW-IVS mechanical discoordination and postsystolic thickening only in the iPAH group. Previous studies in adults described the negative impact of end-systolic RV-LV dyssynchrony on RV systolic function.[12,21] During endsystolic discoordination – RV work is inefficiently spent on displacing the septum leftward rather than ejecting blood – thereby decreasing RV pump efficiency (Figure 2). Moreover, despite the delayed peak RVFW thickening also observed in PS patients, their isovolumetric times remain short and RVFW and LVPW remain coordinated, without impediment of RV systolic function.

Diastolic interactions

Early LV filling was decreased in our pediatric iPAH population but was normal in PS when compared to controls (Table 2). Additionally, isovolumetric relaxation times were prolonged in iPAH resulting in pronounced delay of MV and TV opening and also diastolic discoordination. Previous studies attributed abnormal LV filling in adult iPAH, to both direct ventricular-ventricular interaction, that is, septal displacement, or in-series interaction, that is, LV underfilling due to decreased RV cardiac output.[6,9,12,22-24] Contrary to our findings, Lurz et al. demonstrated similar results in patients with RV pressure overload in the context of congenital heart disease.[25] We observed marked septal displacement – that is direct interaction – in iPAH but not PS during early LV dia-

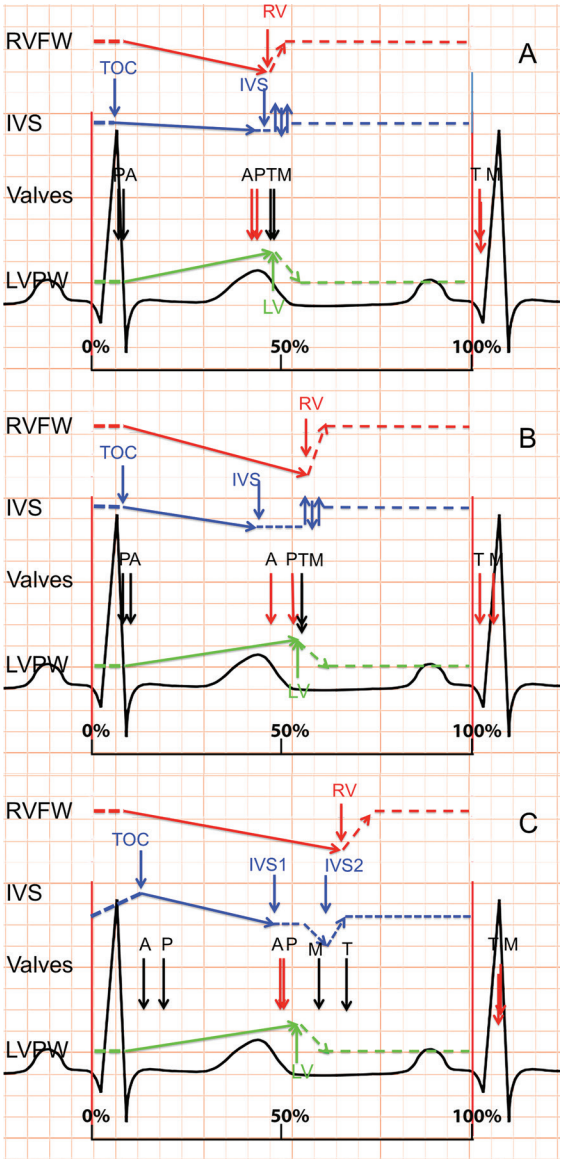

Figure 2: Schematic representation of cardiac events
Schematic representation of peak contraction and valve timing (opening in black and closure in red), relative to RR interval, for each group. A=controls; B=pulmonary stenosis; C= idiopathic pulmonary arterial hypertension. Abbreviations: TOC=time of onset contraction; IVS=interventricular septum; LV=left ventricular free wall; RV=right ventricular free wall; A=aortic valve; P=pulmonic valve; M=mitral valve; T=tricuspid valve

stole (Figure 2), occurring at time of mitral valve opens – impeding filling. Likewise, pediatric iPAH patients exhibited both post-systolic RVFW thickening and leftward septal displacement, both previously associated with RV systolic dysfunction and lower RV stroke volume.[12,21,22] In addition, our pediatric iPAH cohort had markedly remodeled RVs. Santamore et al. showed that increased RV end-diastolic volume independently alters LV diastolic pressure-volume relations, decreasing LV filling.[9] Lastly, in contrast to PS and controls – there was a marked delay between MV and TV opening (592 vs. 667 ms after QRS onset) – which is a novel finding. In light of literature and our current results, it would seem that both in-series and direct interactions are present.[26]

Differences between iPAH and PS

Septal kinetics and ventricular–ventricular interactions differed substantially between PS and iPAH. Peak systolic RV pressures were higher in pediatric iPAH versus PS. Although this contributes to the differences between the patient populations, RVSP was included as a covariate in our analysis and the results were consistent across the entire range of RVSP – rendering this an insufficient explanation in and of itself.[27] As outlined above – altered timing of RVFW systolic events seems to be the main driver of adverse ventricular–ventricular interactions and septal displacement. The prolonged RV isovolumetric contraction time might partly relate to the longer QRS duration (mean 99.4 msec vs. 83.9 msec in PS), but seems insufficient to explain the large dispersion in peak RVFW thickening (638 msec in iPAH vs. 562 msec in PS). Irrespective of peak RV systolic pressures, afterload as defined by end-systolic wall stress, may be higher in iPAH versus PS – in analogy with LV data, thereby resulting in a higher RV load in iPAH.[28] RV load in iPAH patients might be even further augmented by factors such decreased capacitance and reflected waves. The marked RV dilation in iPAH also contributes to septal displacement and decreased early LV filling – both directly and as a result of confinement within the common pericardial space.[9,29] Evidence of different RV adaptation to congenital lesions – such as PS, versus – later onset – iPAH is growing and the subject of separate studies investigating myocardial remodeling.[27] Furthermore, changes in RV afterload also alter IVS stress, possibly triggering adverse myocardial remodeling – with increased myocardial fibrosis.30 In combination, with the adverse hemodynamics detailed above, this would be expected to worsen the biventricular inefficiency observed in the current study.

Clinical implications

Pulmonary vasodilators are the cornerstone of iPAH treatment and – by lowering pulmonary vascular resistance – decrease wall stress, improve trans-septal gradient and thus ventricular-ventricular interactions. However, despite combination therapy, RV pressure often remains elevated as observed in our iPAH cohort. Our data suggest that improvement of the timing of contraction, to decrease mechanical LVPW and RVFW discoordination, may be a worthwhile therapeutic target in iPAH. This may be achieved electro-mechanically – via pacing – or medically – by reversing myocardial remodeling that causes mechanical delays. Both approaches have been explored. Lumens et al. investigated RV pacing in a computer model of iPAH-RV failure and demonstrated improved RV end-diastolic volumes, RVFW myofiber work and pump function through improved distribution of workload.[31] Likewise, RV pacing improved LV diastolic filling in experimental isolated hearts and in an observational human study of chronic thrombo-embolic PAH.[32,33] We previously showed that pharmacological intervention can also modulate adverse ventricular-ventricular interactions. In a rat model of iPAH, carvedilol improved biventricular remodeling, myocardial fibrosis and improved LV and RV Tau – shortening biventricular isovolumetric periods.[34]

Study limitations

This was a retrospective study with inherent limitations. Doppler data was missing in a small number of patients. Likewise, invasive hemodynamic data were not consistently available at time of echocardiography. iPAH is uncommon in children and the sample size is relatively small. However, the observations were consistent between patients. We were unable to provide clinical outcomes or exercise data. Although this is a drawback of the retrospective nature of our study – differences in natural history between iPAH and PS have been well described and we emphasized

the mechanics and pathophysiology underlying these known differences.

Conclusion

Prolonged RVFW thickening, prolonged isovolumetric times and profound early and late systolic septal displacement are related to RV mechanical inefficiency, interventricular mechanical discoordination, and decreased early LV filling in pediatric iPAH patients. These were absent in PS – suggesting that increased RVSP in itself is insufficient to explain the differences. Our findings show that iPAH affects systolic and diastolic mechanics in the right and left ventricles, and that the interaction between them is a prominent component of abnormal mechanics.

References

1. Haddad F, Doyle R, Murphy DJ, Hunt SA. Right ventricular function in cardiovascular disease, part II: pathophysiology, clinical importance, and management of right ventricular failure. Circulation 2008;117:1717-1731.
2. Haworth SG, Hislop AA. Treatment and survival in children with pulmonary arterial hypertension: the UK Pulmonary Hypertension Service for Children 2001-2006. Heart 2009;95:312-317.
3. Peacock AJ, Crawley S, McLure L, et al. Changes in right ventricular function measured by cardiac magnetic resonance imaging in patients receiving pulmonary arterial hypertension-targeted therapy: the EURO-MR study. Circ Cardiovasc Imaging 2014;7:107-114.
4. van Wolferen SA, Marcus JT, Boonstra A, et al. Prognostic value of right ventricular mass, volume, and function in idiopathic pulmonary arterial hypertension. Eur Heart J 2007;28:1250-1257.
5. Hardegree EL, Sachdev A, Fenstad ER, et al. Impaired left ventricular mechanics in pulmonary arterial hypertension: identification of a cohort at high risk. Circ Heart Fail 2013;6:748-755.
6. Belenkie I, Horne SG, Dani R, Smith ER, Tyberg JV. Effects of aortic constriction during experimental acute right ventricular pressure loading. Further insights into diastolic and systolic ventricular interaction. Circulation 1995;92:546-554.
7. Friedberg MK, Redington AN. Right versus left ventricular failure: differences, similarities, and interactions. Circulation 2014;129:1033-1044.
8. Buckberg GD, RESTORE Group. The ventricular septum: the lion of right ventricular function, and its impact on right ventricular restoration. Eur J Cardiothorac Surg 2006;29 Suppl 1:S272-8.
9. Santamore WP, Lynch PR, Meier G, Heckman J, Bove AA. Myocardial interaction between the ventricles. J Appl Physiol 1976;41:362-368.
10. Klima U, Guerrero JL, Vlahakes GJ. Contribution of the interventricular septum to maximal right ventricular function. Eur J Cardiothorac Surg 1998;14:250-255.
11. Santamore WP, Lynch PR, Heckman JL, Bove AA, Meier GD. Left ventricular effects on right ventricular developed pressure. J Appl Physiol 1976;41:925-930.
12. Marcus JT, Gan CT, Zwanenburg JJ, et al. Interventricular mechanical asynchrony in pulmonary arterial hypertension: left-to-right delay in peak shortening is related to right ventricular overload and left ventricular underfilling. J Am Coll Cardiol 2008;51:750-757.
13. Dohi K, Onishi K, Gorcsan J,3rd, et al. Role of radial strain and displacement imaging to quantify wall motion dyssynchrony in patients with left ventricular mechanical dyssynchrony and chronic right ventricular pressure overload. Am J Cardiol 2008;101:1206-1212.
14. Barst RJ, Ertel SI, Beghetti M, Ivy DD. Pulmonary arterial hypertension: a comparison between children and adults. Eur Respir J 2011;37:665-677.
15. Lopez L, Colan SD, Frommelt PC, et al. Recommendations for quantification methods during the performance of a pediatric echocardiogram: a report from the Pediatric Measurements Writing Group of the American Society of Echocardiography Pediatric and Congenital Heart Disease Council. J Am Soc Echocardiogr 2010;23:465-95; quiz 576-7.
16. Teichholz LE, Kreulen T, Herman MV, Gorlin R. Problems in echocardiographic volume determinations: echocardiographic-angiographic correlations in the presence of absence of asynergy. Am J Cardiol 1976;37:7-11.
17. Ryan T, Petrovic O, Dillon JC, Feigenbaum H, Conley MJ, Armstrong WF. An echocardiographic index for separation of right ventricular volume and pressure overload. J Am Coll Cardiol 1985;5:918-927.
18. Kingma I, Tyberg JV, Smith ER. Effects of diastolic transseptal pressure gradient on ventricular septal position and motion. Circulation 1983;68:1304-1314.
19. Mori S, Nakatani S, Kanzaki H, et al. Patterns of the interventricular septal motion can predict conditions of patients with pulmonary hypertension. J Am Soc Echocardiogr 2008;21:386-393.
20. Sciancalepore MA, Maffessanti F, Patel AR, et al. Three-dimensional analysis of interventricular septal curvature from cardiac magnetic resonance images for the evaluation of patients with pulmonary hypertension. Int J Cardiovasc Imaging 2012;28:1073-1085.
21. Lopez-Candales A, Dohi K, Rajagopalan N, et al. Right ventricular dyssynchrony in patients with pulmonary hypertension is associated with disease severity and functional class. Cardiovasc Ultrasound 2005;3:23.
22. Lumens J, Blanchard DG, Arts T, Mahmud E, Delhaas T. Left ventricular underfilling and not septal bulging dominates abnormal left ventricular filling hemodynamics in chronic thromboembolic pulmonary hypertension. Am J Physiol Heart Circ Physiol 2010;299:H1083-91.
23. Gan C, Lankhaar JW, Marcus JT, et al. Impaired left ventricular filling due to right-to-left ventricular interaction in patients with pulmonary arterial hypertension. Am J Physiol Heart Circ Physiol 2006;290:H1528-33.
24. Marcus JT, Vonk Noordegraaf A, Roeleveld RJ, et al. Impaired left ventricular filling due to right ventricular pressure overload in primary pulmonary hypertension: noninvasive monitoring using MRI. Chest 2001;119:1761-1765.
25. Lurz P, Puranik R, Nordmeyer J, et al. Improvement in left ventricular filling properties after relief of right ventricle to pulmonary artery conduit obstruction: contribution of septal motion and interventricular mechanical delay. Eur Heart J 2009;30:2266-2274.
26. Baker AE, Dani R, Smith ER, Tyberg JV, Belenkie I. Quantitative assessment of independent contributions of pericardium and septum to direct ventricular interaction. Am J Physiol 1998;275:H476-83.
27. Bogaard HJ, Natarajan R, Henderson SC, et al. Chronic pulmonary artery pressure elevation is insufficient to explain right heart failure. Circulation 2009;120:1951-1960.

28. Borow KM, Colan SD, Neumann A. Altered left ventricular mechanics in patients with valvular aortic stenosis and coarction of the aorta: effects on systolic performance and late outcome. Circulation 1985;72:515-522.
29. Belenkie I, Sas R, Mitchell J, Smith ER, Tyberg JV. Opening the pericardium during pulmonary artery constriction improves cardiac function. J Appl Physiol (1985) 2004;96:917-922.
30. Sanz J, Dellegrottaglie S, Kariisa M, et al. Prevalence and correlates of septal delayed contrast enhancement in patients with pulmonary hypertension. Am J Cardiol 2007;100:731-735.
31. Lumens J, Arts T, Broers B, et al. Right ventricular free wall pacing improves cardiac pump function in severe pulmonary arterial hypertension: a computer simulation analysis. Am J Physiol Heart Circ Physiol 2009;297:H2196-205.
32. Handoko ML, Lamberts RR, Redout EM, et al. Right ventricular pacing improves right heart function in experimental pulmonary arterial hypertension: a study in the isolated heart. Am J Physiol Heart Circ Physiol 2009;297:H1752-9.
33. Hardziyenka M, Surie S, de Groot JR, et al. Right ventricular pacing improves haemodynamics in right ventricular failure from pressure overload: an open observational proof-of-principle study in patients with chronic thromboembolic pulmonary hypertension. Europace 2011;13:1753-1759.
34. Okumura K, Kato H, Honjo O, et al. Carvedilol improves biventricular fibrosis and function in experimental pulmonary hypertension. J Mol Med (Berl) 2015.

CHAPTER 10

General discussion

Imaging the RV in pressure-loaded RVs

Heart failure is the main driver of mortality and morbidity in patients with pulmonary hypertension (PH) and in patients with various congenital heart defects (CHD).[1-3] Consequently, contemporary clinical follow-up of these patients is mostly focused on monitoring RV function and remodeling.

In the *second chapter* of this thesis we focused on the prognostic value of frequently used echocardiographic measurements in PH. Tricuspid annular plane systolic excursion (TAPSE), right atrial area and pericardial effusion were the most robust prognostic parameters in this review. However, we found evidence of publication bias for TAPSE and right atrial area – meaning that the value of these parameters may be overestimated in everyday clinical practice. These findings are supported by recent publications in which the concern was raised that TAPSE might pseudo-normalize under specific circumstances.[4,5] Furthermore, TAPSE correlates poorly to measures of global RV function in patient groups with CHD – which we also demonstrate in *Chapter 7* of this thesis.[6,7] Fractional area change (r=0.735) and right atrial area (r=0.42) were the only conventional echocardiographic parameters associated to RVEF in the mixed group of patients with pressure loaded RVs (*chapter* 7). Global RV longitudinal deformation by echocardiography (r=0.812) and apical transverse shortening (r=0.853; which can be assessed echocardiographically) were best correlated with RV ejection fraction in our study.

Because of the well-known limitations of echocardiography, cardiac magnetic resonance imaging (CMR) has become an important adjunct imaging modality. In *Chapter 3* we discuss the technical challenges of CMR in congenital heart disease and provide an overview of currently available CMR techniques. We conclude that contemporary CMR can provide a complete overview of functional measurements, anatomical characteristics as well as myocardial tissue characterization.

New imaging techniques

Measurements of RV volume and function are the cornerstone of CMR in patients with CHD and PH.[8-10] Unfortunately, there is still no consensus on the preferred method of measuring RV volumes – in neither guidelines nor research [11], rendering studies virtually incomparable.[12-14]

As we show in *Chapter 4,* the effect of excluding trabeculae from the RV volume on RV volumes and function is profound in patients with RV pressure overload. In all patient populations with RV pressure overload, exclusion of trabeculae from the RV blood pool volume results in substantial differences in RV volumes and function. Moreover, this effect is much greater in patients compared to controls – thus rendering patients much closer to normal values. The difference in RV ejection fraction (RVEF) between both methods was highest in subaortic RVs, yielding a mean absolute difference in ejection fraction of 10%. This is similar to the results published by Winter et al, however using manual tracing this study showed very poor reproducibility.[15] Using semi-automatic pixel-intensity based software, exclusion of trabeculae is no longer hampered by poor reproducibility. As the mean changes in RVEF pressure-loaded patients are up to 10% and in RVEDV up to 29 ml/m^2, exclusion of trabeculae from blood volume may profoundly influence therapeutic and follow-up strategy in patients with CHD. Examples of this are valve repair in severe systemic atrio-ventricular valve regurgitance provided RVEF is >45%, pulmonary valve intervention in patients with tetralogy of Fallot or considering patients for CRT-D if systemic ventricular function is poor.[9,16,17] As there is no gold standard, it is difficult to state the most accurate technique. However - at least theoretically - exclusion of trabeculae is more accurate. Considering the major effects of excluding trabeculae on RV volumes and EF – we believe it should be the

preferred method for follow-up.
Tricuspid regurgitation (TR) frequently complicates PH and right-sided CHD and is associated with increased mortality and morbidity.[18-20] Echocardiography currently is the preferred technique for grading TR. Unfortunately, the accuracy of echocardiographic TR grading is uncertain[10, 21] and reproducibility is suboptimal.[22] In *chapter 5* we show that 4D-flow MRI derived tricuspid flow measurements are accurate compared to stroke volume across the pulmonary valve, with acceptable reproducibility. Furthermore, we show that echocardiographic and 4D flow based TR grading differ substantially. However, a no or a trace TR on echocardiography excluded clinically relevant (moderate or severe) tricuspid regurgitation with 4D flow MRI in all patients. Therefore, echocardiography is still an excellent screening tool. As accurate determination of the degree of TR can help physicians better understand a patients' physiology and ensure timely referral of patients for surgery or transplant,[20,23] more detailed examination of TR grade using 4D-flow MRI should be considered in patients with more than a trace TR on echocardiography.

Limitations and future perspectives
Currently, the post-processing time of new imaging techniques often limits their transition into daily clinical practice. However, the additional time required for semi-automated pixel-based exclusion of trabeculae was very limited with a mean of 67 sec and would not limit its use in daily practice.[24] Furthermore, cardiac magnetic resonance imaging is more expensive and less readily available than echocardiography. Further studies are needed to establish clinically relevant cut-off points for tricuspid regurgitate fraction and RV volumes and function excluding trabeculae. Furthermore, it is important to correlate these measurements to clinical end points such as mortality, hospitalization or outcome after surgery.
Detoriation of RVEF is associated with increased mortality rates in PH and CHD and has therapeutic implications.[25-27] However, echocardiography is readily available, cheaper and more patient-friendly than CMR and, in clinical practice, used for routine follow-up. Therefore, it is important to have reproducible echocardiographic markers that are correlated to clinical end-points and/or can identify deterioration in RV function (to assure timely referral for additional – CMR or invasive – investigations). As mentioned above, TAPSE has proven not to be reliable in CHD. We show that both right atrial area and fractional area change show moderate to good correlation to RVEF in our patients with pressure loaded RVs. An even better correlation to RVEF is obtained by global RV longitudinal strain and measures of transverse motion (*Chapter 7*). Importantly, in this study transverse function was studied using CMR. This measurement would need validation using echocardiography. Additional studies are needed to assess whether echocardiographic strain and/or transverse function indeed correspond to clinical endpoints such as deterioration in clinical status or RVEF.

Differences in RV adaptation between pressure loaded conditions
The second part of this thesis focuses on RV adaptation to pressure load among different clinical entities. In patient groups with outflow tract obstruction (i.e. after arterial switch procedure in *Chapter 6* or pulmonic valve stenosis in *Chapter 7*) the RV maintains its triangular geometry in the presence of normal (or even decreased) RV volumes and normal to hyperdynamic function. In contrast, patient groups with an RV facing high vascular resistance (i.e. PH and subaortic RVs) were found to have RV dilation combined with decrease in global function. These observations underscore that distinctly different forms of increased afterload – which is the load the ventricle

must overcome to eject blood – present with distinctly different characteristics of RV remodeling. In accordance with Laplace's law, higher systolic ventricular pressures need to be met by proportional RV hypertrophy in order to reduce afterload and/or increase contractile strength. If this process is adequate, stroke volume can be maintained. However, if the change in afterload is incompletely compensated by hypertrophy, RV dilation will ensue to maintain stroke volume through the Frank-Starling mechanism, a phenomenon known as pre-load recruitable stroke work. If the combination of both mechanisms is insufficient to compensate for the increased afterload, the ventricular myocytes will remain stretched throughout systole, decreasing velocity of fiber shortening and increasing duration of contraction.[28]
Following these pathophysiological mechanisms, we hypothesize three types of RV adaptation to increased afterload: 1) compensated afterload by hypertrophy without utilizing preload recruitable stroke work; 2) compensated afterload by hypertrophy and utilization of pre-work recruitable stroke work, and 3) insufficiently compensated afterload despite hypertrophy and dilation or ventriculo-arterial uncoupling (i.e. increase in arterial elastance insufficiently compensated by increase of endsystolic elastance; more detailed explanation below). In the latter, myocytes remain stretched throughout systole, prolonging the duration of contraction. With regard to the patient categories described in *Chapters 6-8* we conclude that patients with RV outflow tract obstruction seem to compensate for their increased afterload by adequate RV hypertrophy without RV dilation. In contrast, both patient groups with an RV facing high vascular resistance were found to have dilated ventricles (i.e. using pre-load recruitable stroke work) in addition to RV hypertrophy. Although estimated wall stress (*chapter 7*) was not significantly different between patients with PH and subaortic RVs, only PH patients were found to have poor global function *as well as* prolonged RV free wall shortening. Both of which are likely signs of stretch on the myocytes from incompletely compensated afterload.[29,30]

Ventricular interaction

In *chapter 9* we describe the interventricular interaction in patients with increased RV pressures. We found PH patients to exhibit early and late systolic septal movement, mediated by altered timing of RV free wall motion, leading to RV-LV dyssynchrony and post systolic RV shortening. Following the rationale outlined in the previous paragraph (decreased velocity of fiber shortening and increased duration of contraction), we can better understand the prolonged RV free wall thickening.[29,30] Conceivably, this reflects the insufficient reduction of afterload and/or insufficient increase of contractile function in PH patients.[30] Previous studies have found prolonged RV free wall shortening and concomitant dyssynchrony as well as septal displacement to be associated with RV dysfunction [31,32], which underscores that its occurrence should be considered as a sign of failing adaptation.[29,30] Interestingly, the time to RV free wall peak strain (*Chapter* 7) and peak thickening (*Chapter 9*) were also slightly prolonged in PS patients compared to healthy controls. However, in PS this did not lead to interventricular dyssynchrony or rapid leftward septal movement, as the LV thickening was equally prolonged.

Why are patient groups different?

The ultimate goal of RV adaptation is for the ventricle to stay coupled to its afterload.[33] This coupling can be estimated using the ratio between end-systolic ventricular elastance (a load-independent measure of ventricular contractility) and arterial elastance (a ventricular-independent measure of arterial function), requiring a series of pressure volume loops.[33] In the individual

patient this will be determined by ventricular load, adequacy of RV remodeling and ability to increase myocardial contractile force (i.e. by intrinsic myocardial properties). Differences in function and remodeling can originate from differences in these characteristics.

Ventricular load

The load cardiomyocytes encounter can not be measured directly and is often assessed by (imperfect) estimates of end-systolic wall stress [29,34,35], although there is debate if the highest wall stress is reached at end-systole.[36] These estimates only take into account the static load on the ventricle (i.e. due to increased resistance), while total ventricular load is also determined by the oscillatory load (i.e. vascular stiffness, compliance and reflected waves).[37,38]

Firstly, it is unclear whether a load resulting from resistance at the valvular level poses the same load as that posed by high vascular resistance. Borow et al. showed for different LV pressure load conditions that end-systolic pressures - and consequently end-systolic wall stress - differed significantly at similar peak systolic pressures.[34] Whether this is true for different RV load conditions has never been studied. Furthermore, in our results peak systolic pressures and likely resistance were much higher in subaortic RVs compared with PH or PS patients – increasing static load.

Second, oscillatory load is likely very different between the conditions (although invasive data are lacking). The RV in patients with outflow tract obstruction has access to a normal pulmonary vascular bed, with presumably normal arterial stiffness and a high capacitance. In contrast, in PH capacitance is decreased and arterial stiffness as well as reflected pressure waves are increased – increasing oscillatory load.[37,38] The subaortic RV has access to a much larger vascular bed than PH patients, with likely normal systemic vascular properties. Along these lines of reasoning, we conclude that the oscillatory load is likely much higher in PH patients than in PS and subaortic RV patients, although the static load caused by the resistance (dynes*sec/cm^5) *per se* is likely highest in patients with subaortic RVs. What this implicates for total hydraulic load is as yet unclear.

RV remodeling

Both end-systolic wall stress and end-systolic elastance are co-determined by end-systolic volume or diameter. Therefore, the RV in patients with RV outflow tract obstruction clearly maintains a much preferable shape and size compared with the RV in PH and subaortic RVs. In accordance with previous studies, both congenital heart disease groups show superior mass-volume ratios compared to PH, indicating a higher degree of hypertrophy (*chapter 7*).[39,40] This may be explained by different time of onset of disease, as the RV exposed to high pressures from fetal life onwards may maintain its "fetal" fenotype – with a thick RV myocardium.[41-43] Conversely, in PH patients the RV has likely adapted to normal pulmonary vascular resistance after birth and has to generate higher pressures later in life – over a shorter period of time.

RV myocardial properties

Lastly, myocardial properties might differ between different patient groups. Most research on metabolic and ischemic pathways (negatively) influencing RV myocardial performance have been conducted in PH patients but little is known about this in CHD.[44] In an animal model of RV outflow tract obstruction and PH, Bogaard et al. showed similar differences in RV remodeling as seen in our study. They associate relative RV ischemia, oxidative stress and fibrosis to negative RV remodeling and decreased myocardial contractile function in the PH model.[45,46] It remains unclear whether these same metabolic changes are also responsible for RV failure in CHD.[47] However,

Plymen et al. did show a higher degree of diffuse myocardial fibrosis of in the septal region of patients with subaortic RVs.[48]
A fundamental question that remains is whether all clinical entities with increased RV pressure follow one similar pathway to RV failure – and just represent different stages of the same pathway – or that some clinical entities represent distinctly different pathways to RV failure. Based on the results presented in this thesis, we conclude that patients with RV outflow tract obstruction represent exhibit an entirely different pathway to RV failure. This is supported by the contrasting correlation of RVSP and strain in pediatric PS and PH in *Chapter 8* of this thesis. This different pathway is likely explained by a combination of a very different total load, at similar RVSP, and an intrinsically different myocardial response compared to PH patients. For subaortic RVs and the RV in PH patients this question is more difficult to answer. It is clear the subaortic RV is much better able to maintain RV function over a long period of time, as is also true for patients with Eisenmenger's syndrome, likely a combination of better remodeling (i.e. mass-volume ratio) and preferable myocardial properties (i.e. fetal organization of the RV myocardium that persists throughout postnatal life or less myocardial damage).[42,43]

Future prespectives
Although we provide a detailed comparison of the differences between the patient populations, some questions remain to be answered. Firstly, invasive studies are instrumental for reliable measurements of pressures in all cavities and vascular systems. It is likely that these would lead to more accurate estimates of afterload (i.e. arterial elastance) and ventricular contractility (i.e. end-systolic elastance), which would help in the understanding of (causes of) differences in RV remodeling.
To clarify if all pressure-loaded patient groups follow a common pathway towards RV failure, differences in RV mechanics could be assessed in patients with equal degrees of RV dysfunction. This could be studied, for example, by matching patients for RVEF and/or stroke volume. Optimal treatment of RV failure remains a challenge in all patient groups. Understanding the pathway to RV failure and mechanisms causing dysfunction will help us treat and early-identify patients better. Comparing patient groups at tissue level will provide better information on RV myocardial properties. Identifying pathways involved in adequate RV remodeling and possible genetic changes involved, can help design specific therapies for RV dysfunction.

Reference list

1. Engelings CC, Helm PC, Abdul-Khaliq H, et al. Cause of death in adults with congenital heart disease - An analysis of the German National Register for Congenital Heart Defects. Int J Cardiol 2016;211:31-36.
2. D'Alonzo GE, Barst RJ, Ayres SM, et al. Survival in patients with primary pulmonary hypertension. Results from a national prospective registry. Ann Intern Med 1991;115:343-349.
3. Verheugt CL, Uiterwaal CS, van der Velde ET, et al. Mortality in adult congenital heart disease. Eur Heart J 2010;31:1220-1229.
4. Motoji Y, Tanaka H, Fukuda Y, et al. Association of Apical Longitudinal Rotation with Right Ventricular Performance in Patients with Pulmonary Hypertension: Insights into Overestimation of Tricuspid Annular Plane Systolic Excursion. Echocardiography 2016;33:207-215.
5. van Kessel M, Seaton D, Chan J, et al. Prognostic value of right ventricular free wall strain in pulmonary hypertension patients with pseudo-normalized tricuspid annular plane systolic excursion values. Int J Cardiovasc Imaging 2016;32:905-912.
6. De Caro E, Bondanza S, Calevo MG, et al. Tricuspid annular plane systolic excursion for the assessment of ventricular function in adults operated on with mustard procedure for complete transposition of the great arteries. Congenit Heart Dis 2014;9:252-258.
7. Mercer-Rosa L, Parnell A, Forfia PR, Yang W, Goldmuntz E, Kawut SM. Tricuspid annular plane systolic excursion in the assessment of right ventricular function in children and adolescents after repair of tetralogy of Fallot. J Am Soc Echocardiogr 2013;26:1322-1329.
8. Galie N, Humbert M, Vachiery JL, et al. 2015 ESC/ERS Guidelines for the diagnosis and treatment of pulmonary hypertension: The Joint Task Force for the Diagnosis and Treatment of Pulmonary Hypertension of the European Society of Cardiology (ESC) and the European Respiratory Society (ERS): Endorsed by: Association for European Paediatric and Congenital Cardiology (AEPC), International Society for Heart and Lung Transplantation (ISHLT). Eur Heart J 2016;37:67-119.
9. Baumgartner H, Bonhoeffer P, De Groot NM, et al. ESC Guidelines for the management of grown-up congenital heart disease (new version 2010). Eur Heart J 2010;31:2915-2957.
10. Valente AM, Cook S, Festa P, et al. Multimodality imaging guidelines for patients with repaired tetralogy of fallot: a report from the AmericanSsociety of Echocardiography: developed in collaboration with the Society for Cardiovascular Magnetic Resonance and the Society for Pediatric Radiology. J Am Soc Echocardiogr 2014;27:111-141.
11. Fratz S, Chung T, Greil GF, et al. Guidelines and protocols for cardiovascular magnetic resonance in children and adults with congenital heart disease: SCMR expert consensus group on congenital heart disease. J Cardiovasc Magn Reson 2013;15:51-429X-15-51.
12. Therrien J, Provost Y, Merchant N, Williams W, Colman J, Webb G. Optimal timing for pulmonary valve replacement in adults after tetralogy of Fallot repair. Am J Cardiol 2005;95:779-782.
13. van Wolferen SA, Marcus JT, Boonstra A, et al. Prognostic value of right ventricular mass, volume, and function in idiopathic pulmonary arterial hypertension. Eur Heart J 2007;28:1250-1257.
14. Oosterhof T, van Straten A, Vliegen HW, et al. Preoperative thresholds for pulmonary valve replacement in patients with corrected tetralogy of Fallot using cardiovascular magnetic resonance. Circulation 2007;116:545-551.
15. Winter MM, Bernink FJ, Groenink M, et al. Evaluating the systemic right ventricle by CMR: the importance of consistent and reproducible delineation of the cavity. J Cardiovasc Magn Reson 2008;10:40.
16. Vehmeijer JT, Brouwer TF, Limpens J, et al. Implantable cardioverter-defibrillators in adults with congenital heart disease: a systematic review and meta-analysis. Eur Heart J 2016;37:1439-1448.
17. Priori SG, Blomstrom-Lundqvist C, Mazzanti A, et al. 2015 ESC Guidelines for the management of patients with ventricular arrhythmias and the prevention of sudden cardiac death: The Task Force for the Management of Patients with Ventricular Arrhythmias and the Prevention of Sudden Cardiac Death of the European Society of Cardiology (ESC)Endorsed by: Association for European Paediatric and Congenital Cardiology (AEPC). Europace 2015;17:1601-1687.
18. Nath J, Foster E, Heidenreich PA. Impact of tricuspid regurgitation on long-term survival. J Am Coll Cardiol 2004;43:405-409.
19. Bokma JP, Winter MM, Oosterhof T, et al. Severe tricuspid regurgitation is predictive for adverse events in tetralogy of Fallot. Heart 2015;101:794-799.
20. Dandel M, Knosalla C, Kemper D, Stein J, Hetzer R. Assessment of right ventricular adaptability to loading conditions can improve the timing of listing to transplantation in patients with pulmonary arterial hypertension. J Heart Lung Transplant 2015;34:319-328.
21. Grossmann G, Stein M, Kochs M, et al. Comparison of the proximal flow convergence method and the jet area method for the assessment of the severity of tricuspid regurgitation. Eur Heart J 1998;19:652-659.
22. Grant AD, Thavendiranathan P, Rodriguez LL, Kwon D, Marwick TH. Development of a consensus algorithm to improve interobserver agreement and accuracy in the determination of tricuspid regurgitation severity. J Am Soc Echocardiogr 2014;27:277-284.
23. Baumgartner H, Bonhoeffer P, De Groot NM, et al. ESC Guidelines for the management of grown-up congenital heart disease (new version 2010). Eur Heart J 2010;31:2915-2957.
24. Freling HG, van Wijk K, Jaspers K, et al. Impact of right ventricular endocardial trabeculae on volumes and function assessed by CMR in patients with tetralogy of Fallot. Int J Cardiovasc Imaging 2012.
25. van Wolferen SA, Marcus JT, Boonstra A, et al.

Prognostic value of right ventricular mass, volume, and function in idiopathic pulmonary arterial hypertension. Eur Heart J 2007;28:1250-1257.
26. van de Veerdonk MC, Kind T, Marcus JT, et al. Progressive right ventricular dysfunction in patients with pulmonary arterial hypertension responding to therapy. J Am Coll Cardiol 2011;58:2511-2519.
27. Koyak Z, de Groot JR, Bouma BJ, et al. Sudden cardiac death in adult congenital heart disease: can the unpredictable be foreseen? Europace 2017;19:401-406.
28. ter Keurs HE, Rijnsburger WH, van Heuningen R, Nagelsmit MJ. Tension development and sarcomere length in rat cardiac trabeculae. Evidence of length-dependent activation. Circ Res 1980;46:703-714.
29. Marcus JT, Gan CT, Zwanenburg JJ, et al. Interventricular mechanical asynchrony in pulmonary arterial hypertension: left-to-right delay in peak shortening is related to right ventricular overload and left ventricular underfilling. J Am Coll Cardiol 2008;51:750-757.
30. Palau-Caballero G, Walmsley J, van Empel VP, Lumens J, Delhaas T. Why Septal Motion is a Marker of Right Ventricular Failure in Pulmonary Arterial Hypertension: Mechanistic Analysis Using a Computer Model. Am J Physiol Heart Circ Physiol 2016:ajpheart.00596.2016.
31. Lopez-Candales A, Bazaz R, Edelman K, Gulyasy B. Apical systolic eccentricity index: a better marker of right ventricular compromise in pulmonary hypertension. Echocardiography 2010;27:534-538.
32. Tsugu T, Murata M, Kawakami T, et al. Changes in Right Ventricular Dysfunction After Balloon Pulmonary Angioplasty in Patients With Chronic Thromboembolic Pulmonary Hypertension. Am J Cardiol 2016;118:1081-1087.
33. Vonk Noordegraaf A, Westerhof BE, Westerhof N. The Relationship Between the Right Ventricle and its Load in Pulmonary Hypertension. J Am Coll Cardiol 2017;69:236-243.
34. Borow KM, Colan SD, Neumann A. Altered left ventricular mechanics in patients with valvular aortic stenosis and coarction of the aorta: effects on systolic performance and late outcome. Circulation 1985;72:515-522.
35. Mauritz GJ, Vonk-Noordegraaf A, Kind T, et al. Pulmonary endarterectomy normalizes interventricular dyssynchrony and right ventricular systolic wall stress. J Cardiovasc Magn Reson 2012;14:5.
36. Chirinos JA, Segers P, Gupta AK, et al. Time-varying myocardial stress and systolic pressure-stress relationship: role in myocardial-arterial coupling in hypertension. Circulation 2009;119:2798-2807.
37. Wang Z, Chesler NC. Pulmonary vascular wall stiffness: An important contributor to the increased right ventricular afterload with pulmonary hypertension. Pulm Circ 2011;1:212-223.
38. Lankhaar JW, Westerhof N, Faes TJ, et al. Quantification of right ventricular afterload in patients with and without pulmonary hypertension. Am J Physiol Heart Circ Physiol 2006;291:H1731-7.
39. Jurcut R, Giusca S, Ticulescu R, et al. Different patterns of adaptation of the right ventricle to pressure overload: a comparison between pulmonary hypertension and pulmonary stenosis. J Am Soc Echocardiogr 2011;24:1109-1117.
40. Giusca S, Popa E, Amzulescu MS, et al. Is Right Ventricular Remodeling in Pulmonary Hypertension Dependent on Etiology? An Echocardiographic Study. Echocardiography 2016;33:546-554.
41. Zhang L, Allen J, Hu L, Caruthers SD, Wickline SA, Chen J. Cardiomyocyte architectural plasticity in fetal, neonatal, and adult pig hearts delineated with diffusion tensor MRI. Am J Physiol Heart Circ Physiol 2013;304:H246-52.
42. Hopkins WE. The remarkable right ventricle of patients with Eisenmenger syndrome. Coron Artery Dis 2005;16:19-25.
43. Hopkins WE, Waggoner AD. Severe pulmonary hypertension without right ventricular failure: the unique hearts of patients with Eisenmenger syndrome. Am J Cardiol 2002;89:34-38.
44. Ryan JJ, Archer SL. The right ventricle in pulmonary arterial hypertension: disorders of metabolism, angiogenesis and adrenergic signaling in right ventricular failure. Circ Res 2014;115:176-188.
45. Bogaard HJ, Natarajan R, Henderson SC, et al. Chronic pulmonary artery pressure elevation is insufficient to explain right heart failure. Circulation 2009;120:1951-1960.
46. Voelkel NF, Quaife RA, Leinwand LA, et al. Right ventricular function and failure: report of a National Heart, Lung, and Blood Institute working group on cellular and molecular mechanisms of right heart failure. Circulation 2006;114:1883-1891.
47. Iacobazzi D, Suleiman MS, Ghorbel M, George SJ, Caputo M, Tulloh RM. Cellular and molecular basis of RV hypertrophy in congenital heart disease. Heart 2016;102:12-17.
48. Plymen CM, Sado DM, Taylor AM, et al. Diffuse myocardial fibrosis in the systemic right ventricle of patients late after Mustard or Senning surgery: an equilibrium contrast cardiovascular magnetic resonance study. Eur Heart J Cardiovasc Imaging 2013;14:963-968.

CHAPTER 11 - APPENDIX

Summary
Nederlandse Samenvatting
List of affiliations
List of publications
Dankwoord

Summary

Heart failure is a clinical syndrome characterized by typical symptoms, such as ankle swelling, breathlessness and fatigue. Currently, its prevalence is estimated at 1-2% of the adult population. 1 Because the majority of patients suffer from diastolic or systolic left ventricular (LV) heart failure, most research has focused on the LV. [1] Right ventricular (RV) failure has a different genesis than LV failure and is generally caused by increased volume- or pressure load imposed on the ventricle.[2] Primary right-sided heart failure is the biggest driver of morbidity and mortality in patients with congenital heart disease (CHD) and pulmonary hypertension (PH).[3-5] Survival in PH and CHD has improved over the past decades.[5, 6] Consequently, the group of patients suffering from RV dysfunction is increasing, necessitating sensitive markers for follow-up and a more complete understanding of the mechanism involved in RV dysfunction. The aim of this thesis was to evaluate imaging markers of RV function in PH and CHD patients. The second aim of this thesis is to provide a better understanding of RV adaptation to high RV systolic pressures by comparing different patient entities with RV pressure-load.

Imaging the right ventricle

In *Chapter 2* we review the prognostic value of echocardiographic measurements, for clinical deterioration, in patients with PH. Using meta-analysis and sensitivity analysis, presence of pericardial effusion pooled HR 1.70; 95% CI 1.44–1.99), right atrial area (pooled HR 1.71; 95% CI 1.38–2.13) and tricuspid annular plane systolic excursion (TAPSE; pooled HR 1.72; 95% CI 1.34–2.20) were the most robust predictors of clinical deterioration. These findings are in agreement with the 2015 guidelines for pulmonary hypertension.[7] In CHD, follow-up relies more heavily on cardiac magnetic resonance imaging (CMR). *Chapter 3* provides an overview of state-of-the-art CMR acquisition and post-processing techniques, relevant to imaging in CHD. We show that CMR is able to generate anatomical information, functional assessment and tissue characterization in a single comprehensive CMR study.

As patients with CHD and PH often suffer from RV dilation and have distorted RV geometry, validation of new imaging or post-processing techniques is important before implementation in clinical practice. Although RV volume and function are included in almost every CMR evaluation, there is no consensus on whether trabeculae should be in- or excluded from the RV blood volume.[8] In *Chapter 4* we investigate the impact and reproducibility of excluding vs. including trabeculae using semi-automatic pixel-based software, on RV volume and function in patients with pressure-loaded RVs (who often have coarse RV trabeculae). While the impact is small in healthy controls (difference RV end-diastolic volume -5.7 ± 1.7 ml/m^2, RV ejection fraction 3.4 ± 0.8%) the impact is significantly more profound in all pressure-loaded groups (all $p<0.001$) with differences in RV end-diastolic volume and ejection fraction as high as 29.6 ± 6.6 ml/m^2 and 10.1 ± 2.3% in patients with subaortic RVs. Reproducibility was equal for in- and exclusion of trabeculae. In *Chapter 5* we assess the accuracy and reproducibility 4-dimensional (4-D) flow across the tricuspid valve in patients with pressure-loaded RVs and varying degrees of tricuspid regurgitation. We investigate this new method because the currently used method: echocardiography – is not well validated and has only moderate reproducibility. Four-dimensional effective flow across the tricuspid valve showed good agreement to 2D effective flow across the pulmonary valve (ICC=0.899 and mean difference 1.79 ml [-20.39 to 16.81]) and good reproducibility. Using 4-D

flow across the tricuspid valve, TR grade was classified different from echocardiography in 25/65 (38.5%) of patients.

The pressure-loaded right ventricle

The second part of this thesis continues with *Chapter 6,* studying the impact of RV sequelae after arterial switch operation for transposition of the great arteries. Main, right and left pulmonary artery areas were decreased in patients compared to healthy controls (190 vs 269 mm^2/m^2, 59 vs 157 mm^2/m^2, 98 vs 139 mm^2/m^2, respectively, all $p<0.001$). Patients also had smaller RV end-diastolic ($p=0.014$) and end-systolic ($p=0.002$) volumes and higher RV ejection fraction (55±5% vs 53±4%, $p=0.048$). In multivariate analysis, main pulmonary artery area – i.e. measure of RV outflow tract obstruction – was the only significant predictor ($\beta=0.102$, $p=0.032$) of exercise capacity in patients post-arterial switch.

Outcomes can vary widely between patient entities suffering from chronic increase of RV pressure, very good in patients with RV outflow tract obstruction and very poor in PH. We hypothesize this is debit to differences in RV remodeling and mechanics. *Chapter 7* provides a detailed comparison of RV remodeling and function in patients with pulmonary valve stenosis (PS), subaortic RV and PH, using both CMR and echocardiography. The most important findings were: decreased RV volumes ($p <0.01$) and increased RV ejection fraction (61.1 ± 9.6% vs 53.2 ± 4.5%, $p <0.05$) in PS patients compared with controls, contrasting to RV dilation and decreased RV ejection fractions in patients with subaortic RVs (46.3 ± 10.1%; $p <0.001$) or PH (36.9 ± 9.6%; $p < 0.001$). Global function in PH was decreased compared to subaortic RVs, this was mediated by prolonged RV free wall shortening – causing post-systolic shortening and intra-ventricular dyssynchrony. We hypothesize this is due to insufficiently compensated afterload in PH patients. *Chapter 8* compares pediatric PS and PH patients using echocardiography. In agreement with the results in adult patients, RV geometry and cavity size were preserved in PS and distorted in PH. Mechanisms of RV dysfunction in PH include: decreased global RV free wall and global strain PH vs. PS patients (respectively -14.2±4.4 vs. -28.2±1.8 and -12.1±4.4 vs. -22.7±2.1%; all $p<0.001$), more frequent post-systolic shortening and decreased RV transverse shortening (−1.62%±11.11% in PH vs 31.75%±10.35% in PS; $p <0.001$). In *Chapters 7 and 8* prolonged RV free wall shortening seemed to be one of the key mechanisms of RV dysfunction in PH. *Chapter 9* studies this further by comparing interventricular interaction in PH to PS and controls. We show that prolonged RV free wall contraction in PH, but not PS, is associated with early and late-systolic (i.e. early LV diastolic) septal displacements and adverse ventricular-ventricular interaction. This results in reduced RV contractile efficiency and decreased early diastolic LV filling.

Reference list

1. Ponikowski P, Voors AA, Anker SD, et al. 2016 ESC Guidelines for the diagnosis and treatment of acute and chronic heart failure: The Task Force for the diagnosis and treatment of acute and chronic heart failure of the European Society of Cardiology (ESC)Developed with the special contribution of the Heart Failure Association (HFA) of the ESC. Eur Heart J 2016;37:2129-2200.
2. Haddad F, Doyle R, Murphy DJ, Hunt SA. Right ventricular function in cardiovascular disease, part II: pathophysiology, clinical importance, and management of right ventricular failure. Circulation 2008;117:1717-1731.
3. Verheugt CL, Uiterwaal CS, van der Velde ET, et al. Mortality in adult congenital heart disease. Eur Heart J 2010;31:1220-1229.
4. Zomer AC, Vaartjes I, van der Velde ET, et al. Heart failure admissions in adults with congenital heart disease; risk factors and prognosis. Int J Cardiol 2013.
5. Humbert M, Sitbon O, Chaouat A, et al. Survival in patients with idiopathic, familial, and anorexigen-associated pulmonary arterial hypertension in the modern management era. Circulation 2010;122:156-163.
6. van der Bom T, Zomer AC, Zwinderman AH, Meijboom FJ, Bouma BJ, Mulder BJ. The changing epidemiology of congenital heart disease. Nat Rev Cardiol 2011;8:50-60.
7. Galie N, Humbert M, Vachiery JL, et al. 2015 ESC/ERS Guidelines for the diagnosis and treatment of pulmonary hypertension: The Joint Task Force for the Diagnosis and Treatment of Pulmonary Hypertension of the European Society of Cardiology (ESC) and the European Respiratory Society (ERS): Endorsed by: Association for European Paediatric and Congenital Cardiology (AEPC), International Society for Heart and Lung Transplantation (ISHLT). Eur Heart J 2016;37:67-119.
8. Fratz S, Chung T, Greil GF, et al. Guidelines and protocols for cardiovascular magnetic resonance in children and adults with congenital heart disease: SCMR expert consensus group on congenital heart disease. J Cardiovasc Magn Reson 2013;15:51-429X-15-51.

Nederlanse samenvatting

Hartfalen is een klinische aandoening die gekarakteriseerd wordt door symptomen als: enkeloedeem, kortademigheid en overmatige vermoeidheid. Bij hartfalen is het hart onvoldoende in staat om het bloed rond te pompen. De prevalentie is gestaag toegenomen in de afgelopen 20 jaar en ligt in de volwassen bevolking rond de 1-2%.[1] De overgrote meerderheid van deze patiënten lijdt aan falen van de linkerhartkamer (oftewel linkerventrikel). Daardoor zijn ook behandelrichtlijnen en onderzoek ook lange tijd vooral gericht geweest op linkerkamer falen. Primair falen van de rechterhartkamer heeft een andere oorzaak en een ander beloop dan linkerkamer falen en wordt meestal veroorzaakt door volume- of drukbelasting van de rechterkamer.2 In dit proefschrift onderzoeken we de laatste groep met drukbelasting. Normaal gesproken is de druk die de rechterhartkamer moet opbouwen gedurende systole (= knijpfase van het hart) heel laag, omdat de weerstand in de bloedsomloop van de longen (in tegenstelling tot die van het lichaam) laag is. Bij drukbelasting moet de rechterhartkamer een hogere druk opbouwen. Oorzaken hiervan kunnen zijn een vernauwde klep/longslagader, een hogere weerstand in de bloedsomloop van de longen (pulmonale hypertensie) of omdat de rechterhartkamer de lichaamsbloedsomloop verzorgt (dit wordt ook wel een subaortale rechterhartkamer genoemd).
Rechterkamer falen is de belangrijkste veroorzaker van symptomen, ziekenhuis-opnames en overlijden in patiënten met aangeboren hartafwijkingen en pulmonale hypertensie.[3-5] De overleving van deze groepen patiënten is de afgelopen jaren sterk verbeterd, door vooruitgang in hartchirurgie en medicamenteuze therapie, waardoor de groep van patiënten met verminderde functie van de rechterkamer navenant gegroeid is.[5,6] Het is daarom van groot belang om goede meetmethoden te vinden die een verminderde functie van de rechterkamer vroeg op kunnen sporen en om het ontstaan van rechterkamer falen goed te begrijpen. Derhalve is het eerste doel van dit proefschrift, om een overzicht te geven van metingen die gebruikt kunnen worden bij patiënten met pulmonale hypertensie en aangeboren hartafwijkingen. Het tweede doel van het proefschrift is om een beter begrip te krijgen van de aanpassingsmogelijkheden van de rechterkamer, door verschillende patiëntengroepen met drukbelasting van de rechterhartkamer te vergelijken.

Beeldvorming van de rechterhartkamer
In *hoofdstuk 2* van dit proefschrift onderzoeken we de voorspellende waarde van verschillende echocardiografische (=echo van het hart) metingen voor achteruitgang (bijv. ziekenhuisopname, hartfalen, overlijden) in patiënten met pulmonale hypertensie. Met behulp van een meta-analyse hebben wij aangetoond dat de aanwezigheid van pericardeffusie (pooled HR 1.70; 95% CI 1.44–1.99), rechterboezem oppervlakte (pooled HR 1.71; 95% CI 1.38–2.13) en systolische verplaatsing van de tricuspidalisklep annulus (TAPSE; pooled HR 1.72; 95% CI 1.34–2.20) de meest sterkste voorspellers zijn van klinische achteruitgang. Dit komt overeen met de metingen die aanbevolen worden bij routine controle van patiënten met pulmonale hypertensie.[7]
In patiënten met aangeboren hartafwijkingen zijn deze metingen veel minder betrouwbaar, daarom ondergaan deze patiënten ook vaak een MRI onderzoek. In *Hoofdstuk 3* geven we daarom een overzicht van de nieuwste MRI opname technieken en meetmethodes, die relevant zijn voor evaluatie van patiënten met aangeboren hartafwijkingen. We concluderen dat in het huidige tijdperk één MRI onderzoek een volledig beeld kan geven van anatomie, functioneren van beide hartkamers, lekkage van hartkleppen én weefselsamenstelling van de hartspier.

In *Hoofdstuk 4 en Hoofdstuk 5* gaan we verder door de nauwkeurigheid en betrouwbaarheid van nieuwe meetmethodes te onderzoeken in patiënten met aangeboren hartafwijkingen en pulmonale hypertensie. Gezien de veranderde vorm en grootte van de rechterhartkamer is het immers niet zeker dat de betrouwbaarheid en nauwkeurigheid van deze meetmethodes even goed zijn in patiënten als in de gezonde bevolking. *In hoofdstuk 4* beginnen we door te onderzoeken wat het effect is van verschillende meetmethodes op rechterkamer volume en systolische (=knijpkracht) functie – maten die veelal bepalend zijn voor de behandeling van deze patiënten. De rechterhartkamer bevat veel trabekels en het is in de literatuur niet eenduidig of deze moeten worden geïncludeerd of geëxcludeerd bij het meten van rechterkamer grootte. Wij laten zien dat het effect van exclusie van trabekels op rechterkamer volume en ejectie fractie (maat voor knijpkracht) gering is bij gezonde controles (verschil in eind-diastolisch volume -5.7 ± 1.7 ml/m^2, ejectie fractie 3.4 ± 0.8%) maar hoog kan oplopen in patiënten met drukbelaste rechterhartkamers (tot een verschil in eind-diastolisch volume van 29.6 ± 6.6 ml/m^2 en een verschil in ejectie fractie van 10.1 ± 2.3% in patiënten met subaortale rechterkamer). De betrouwbaarheid van de meting met in- en exclusie van trabekels is niet verschillend. Met andere woorden: als trabekels niet worden meegerekend in het bloedvolume dan heeft dat een groot effect op rechterkamer volume en ejectie fractie meting, waardoor deze bij patiënten met drukbelaste rechterhartkamers veel dichter bij normaalwaardes komen te liggen.
In *hoofdstuk 5* onderzoeken we tenslotte een nieuwe MRI techniek (4D flow MRI) en een nieuwe meetmethode om lekkage van de tricuspidalisklep te kwantificeren, omdat de huidige meetmethode – echocardiografie – slechts matig betrouwbaar is. Het slagvolume over de tricuspidalisklep gemeten met 4-D flow komt goed overeen met het slagvolume over de pulmonalisklep (techniek die normaal gebruikt wordt om slagvolume te meten) gemeten met 2-D flow (intraclass correlatie coëfficiënt=0.899 en gemiddeld verschil 1.79 ml [-20.39 tot 16.81]), met een goede reproduceerbaarheid. Daarnaast laten we zien dat we met behulp van de MRI de ernst van tricuspidalisklep insufficiëntie anders graderen in 25/65 (38.5%) patiënten ten opzichte van echocardiografie.

De drukbelaste rechterhartkamer
In *hoofdstuk 6* onderzoeken we de gevolgen van vernauwing van het rechterkamer uitstroomtraject (oftewel longslagader) op rechterkamer functie en inspanningsvermogen, in patiënten met transpositie van de grote vaten na arteriële switch operatie. De oppervlakte van de hoofdstam, linker- en rechterzijtak van de longslagader zijn een stuk kleiner in patiënten na arteriële switch operatie vergeleken met gezonde controles (respectievelijk 190 vs 269 mm^2/m^2, 59 vs 157 mm^2/m^2, 98 vs 139 mm^2/m^2, allemaal $p<0.001$). Patiënten hebben kleinere rechterkamer volumes en een hogere ejectie fractie in vergeleken met gezonde controles (55±5% vs 53±4%, p=0.048). In een multivariabele analyse is de oppervlakte van de stam van de longslagader de enige factor geassocieerd met inspanningsvermogen (β=0.102, p=0.032) in deze patiëntengroep.
De overleving en het klachtenpatroon (bijv. wel of niet hartfalen) is erg verschillend tussen verschillende patiëntgroepen met rechterkamer drukbelasting. We denken dat dit verschil samenhangt met verschillen in hoe de rechterhartkamer zich aanpast aan de drukbelasting. Om dit beter te begrijpen, vergelijken we in *Hoofdstuk 7* de vorm en systolische functie (knijpkracht) van de rechterhartkamer in verschillende patiëntgroepen met drukbelasting van de rechterkamer: vernauwing van longslagaderklep, subaortale rechterhartkamer en pulmonale hypertensie. Een van de belangrijkste bevindingen is dat patiënten met een vernauwde longslagaderklep, net als

de patiënten in *Hoofdstuk 6*, een kleinere volume (inhoud) van de rechterkamer en een hogere ejectie fractie (61.1±9.6% vs 53.2±4.5%, p<0.05) hebben vergeleken met gezonde controles. Dit in tegenstelling tot patiënten met een subaortale rechterhartkamer en pulmonale hypertensie, die juist een vergrootte rechterhartkamer (hoger volume) en een lagere ejectie fractie (slechtere knijpkracht; respectievelijk 46.3±10.1% en 36.9±9.6%; p<0.001) hebben vergeleken met controles. De globale systolische functie van de rechterhartkamer is echter veel slechter in pulmonale hypertensie dan in patiënten met een subaortale rechterkamer, dit lijkt deels te komen doordat de vrije wand van de rechterkamer veel langer samenknijpt dan normaal, waardoor de effectiviteit minder wordt.
In *Hoofdstuk 8* vergelijken we pulmonale hypertensie en vernauwing van de longslagader klep in kinderen. Globaal zien we ook hier dat in pulmonale hypertensie de kamer verwijd raakt, een ronde vorm krijgt en globaal een verminderde systolische functie heeft, terwijl dit bij een vernauwde longslagaderklep niet gebeurd. De verslechtering van rechterkamer systolische functie uit zich in: een verslechtering van de longitudinale (lange as) functie, met verminderde verkorting van de vrije wand en het kamer tussenschot in pulmonale hypertensie vs. patiënten met een vernauwde longslagaderklep (respectievelijk -14.2±4.4 vs. -28.2±1.8 en -10.0±4.3 vs. -17.5±2.5%; allemaal p<0.001). Daarnaast zien we dat ook de knijpkracht in transversale (korte as) richting verminderd is (−1.62%±11.11% in pulmonale hypertensie vs 31.75%±10.35% in longslagaderklep vernauwing; p <0.001).
In zowel *Hoofdstuk 7* als *Hoofdstuk 8* is toegenomen duur van de samentrekking van de rechterkamer vrije wand in pulmonale hypertensie een opvallend verschijnsel. In *Hoofdstuk 9* kijken we tenslotte wat het effect hiervan is op de samenwerking tussen linker en rechterhartkamer. De toegenomen duur van rechterkamer vrije wand samentrekking in patiënten met pulmonale hypertensie, maar niet in patiënten met een vernauwde longslagaderklep, zorgt voor verplaatsing van het kamertussenschot aan het begin en aan het einde van rechterkamer systole (samentrekkings-/knijpfase van het hart). Dit zorgt ervoor dat de samentrekking van rechterkamer vrije wand, linkerkamer vrije wand en kamertussenschot niet meer synchroon lopen, waardoor een deel van de samentrekking van de rechterkamer vrije wand verspeeld wordt aan het verplaatsen van het kamertussenschot in plaats van het uitpompen van bloed. Daarnaast zorgt die verplaatsing van het kamertussenschot richting de linkerkamer ervoor dat deze zich niet goed kan vullen.

Referenties

1. Ponikowski P, Voors AA, Anker SD, et al. 2016 ESC Guidelines for the diagnosis and treatment of acute and chronic heart failure: The Task Force for the diagnosis and treatment of acute and chronic heart failure of the European Society of Cardiology (ESC)Developed with the special contribution of the Heart Failure Association (HFA) of the ESC. Eur Heart J 2016;37:2129-2200.
2. Haddad F, Doyle R, Murphy DJ, Hunt SA. Right ventricular function in cardiovascular disease, part II: pathophysiology, clinical importance, and management of right ventricular failure. Circulation 2008;117:1717-1731.
3. Verheugt CL, Uiterwaal CS, van der Velde ET, et al. Mortality in adult congenital heart disease. Eur Heart J 2010;31:1220-1229.
4. Zomer AC, Vaartjes I, van der Velde ET, et al. Heart failure admissions in adults with congenital heart disease; risk factors and prognosis. Int J Cardiol 2013;168:2487-2493.
5. Humbert M, Sitbon O, Chaouat A, et al. Survival in patients with idiopathic, familial, and anorexigen-associated pulmonary arterial hypertension in the modern management era. Circulation 2010;122:156-163.
6. van der Bom T, Mulder BJ, Meijboom FJ, et al. Contemporary survival of adults with congenital heart disease. Heart 2015;101:1989-1995.
7. Galie N, Humbert M, Vachiery JL, et al. 2015 ESC/ERS Guidelines for the diagnosis and treatment of pulmonary hypertension: The Joint Task Force for the Diagnosis and Treatment of Pulmonary Hypertension of the European Society of Cardiology (ESC) and the European Respiratory Society (ERS): Endorsed by: Association for European Paediatric and Congenital Cardiology (AEPC), International Society for Heart and Lung Transplantation (ISHLT). Eur Heart J 2016;37:67-119.

Author affiliations

Drs. Vivan J.M. Baggen	Department of Cardiology, University Medical Center Utrecht, Utrecht, the Netherlands Department of Cardiology, Erasmus Medical Center, Rotterdam, the Netherlands
Prof. dr. Bart H. Bijnens	Institució Catalana de Recerca I Estudis Avançats (ICREA), University Pompeu Fabra, Barcelona, Spain KU Leuven, Leuven, Belgium
Dr. Annemien E. van den Bosch	Department of Cardiology, Erasmus Medical Center, Rotterdam, the Netherlands
Dr. Johannes M.P.J. Breur	Department Pediatric Cardiology, University Medical Center Utrecht, Wilhelmina Children's Hospital, Utrecht, the Netherlands
Dr. Ricardo P.J. Budde	Department of Radiology, University Medical Center Utrecht, Utrecht, the Netherlands
Dr. Arie P.J. van Dijk	Department of Cardiology, Radboud University Medical Center, Nijmegen, the Netherlands
Prof. dr. Pieter A. Doevendans	Department of Cardiology, University Medical Center Utrecht, Utrecht, the Netherlands
Dr. Andreea Dragulescu	Department of Pediatric Cardiology, Labatt Family Heart Center, Hospital for Sick Children, Toronto, Canada
Drs. Mieke M.P. Driessen	Department of Cardiology and Radiology, University Medical Center Utrecht, Utrecht, the Netherlands ICIN-NHI, Utrecht, the Netherlands Department of Pediatric Cardiology, Labatt Family Heart Center, Hospital for Sick Children, Toronto, Canada Department of Cardiology, Radboud University Medical Center, Nijmegen, the Netherlands (current)
Dr. Hendrik G. Freling	Department of Radiology, University Medical Center Groningen, Groningen, the Netherlands
Dr. Mark K. Friedberg	Department of Pediatric Cardiology, Labatt Family Heart Center, Hospital for Sick Children, Toronto, Canada

Drs. Wei Hui	Department of Pediatric Cardiology, Labatt Family Heart Center, Hospital for Sick Children, Toronto, Canada
Dr. Erik H. Hulzebos	Department of Pediatric Physical Therapy and Exercise Physiology, Child Development and Exercise Center, Wilhelmina Children's Hospital, Utrecht, the Netherlands
Dr. Nicolaas J.G. Jansen	Department of Pediatric Intensive Care, Wilhelmina Children's Hospital, Utrecht, the Netherlands
Dr. Roland J. van Kimmenade	Department of Cardiology, University Medical Center Utrecht, Utrecht, the Netherlands Department of Cardiology, Radboud University Medical Center, Nijmegen, the Netherlands (current)
Prof. dr. Tim Leiner	Department of Radiology, University Medical Center Utrecht, Utrecht, the Netherlands
Dr. Folkert J. Meijboom	Department of Cardiology, University Medical Center Utrecht, Utrecht, the Netherlands
Prof. dr. Luc Mertens	Department of Pediatric Cardiology, Labatt Family Heart Center, Hospital for Sick Children, Toronto, Canada
Dr. Joep W.M. van Oorschot	Department of Radiology, University Medical Center Utrecht, Utrecht, the Netherlands
Dr. Petronella G. Pieper	Department of Cardiology, University Medical Center Groningen, Groningen, the Netherlands
Dr. Marco C. Post	Department of Cardiology, St. Antonius Medical Center, Nieuwegein, the Netherlands
Prof. dr. Jolien W. Roos-Hesselink	Department of Cardiology, Erasmus Medical Center, Rotterdam, the Netherlands
Drs. Marjolijn A. Schings	Department of Cardiology and Radiology, University Medical Center Utrecht, the Netherlands
Dr. Paul H. Schoof	Department of Pediatric Cardiothoracic Surgery, Wilhelmina Childrens' Hospital, Utrecht, the Netherlands
Dr. Gertjan Tj. Sieswerda	Department of Cardiology, University Medical Center Utrecht, Utrecht, the Netherlands

Dr. Repke J. Snijder	Department of Pulmonology, St. Antonius Hospital, Nieuwegein, the Netherlands
Dr. Tim Takken	Department of Pediatric Physical Therapy and Exercise Physiology, Child Development and Exercise Center, Wilhelmina Children's Hospital, Utrecht, the Netherlands
Prof. dr. Hanneke J.M. Takkenberg	Department of Cardio-thoracic surgery, Erasmus Medical Center, Rotterdam, the Netherlands
Dr. Jos J.M. Westenberg	Department of Radiology, Leiden University Medical Center, Leiden, the Netherlands
Drs. Sebastiaan W.H. van Wijk	Department of Cardiology, University Medical Center Utrecht, Utrecht, the Netherlands Department Pediatric Cardiology, Wilhelmina Childrens' Hospital, Utrecht, the Netherlands
Dr. Tineke P. Willems	Department of Radiology, University Medical Center Groningen, Groningen, the Netherlands

A

List of publications

Regional right ventricular remodeling and function in Children with Idiopathic Pulmonary Arterial Hypertension versus those with Pulmonary Valve Stenosis: Insights into mechanics of right ventricular dysfunction
Driessen MMP, Meijboom FJ, Hui W, Dragulescu A, Mertens L, Friedberg MK (Echocardiography. 2017 34:888-897)

Adverse ventricular–ventricular interactions in right ventricular pressure load: Insights from pediatric pulmonary hypertension versus pulmonary stenosis
Driessen MMP, Hui W, Bijnens BH, Dragulescu A, Mertens L, Meijboom FJ, Friedberg MK (Phys reports. 2016 4:1-10)

Echocardiographic findings associated with mortality or transplant in patients with pulmonary arterial hypertension: A systematic review and meta-analysis
Baggen VJ, **Driessen MM**, Post MC, van Dijk AP, Roos-Hesselink JW, van den Bosch AE, Takkenberg JJ, Sieswerda GTj
(Neth Heart J. 2016 24:374-389)

Main Pulmonary Artery Area Limits Exercise Capacity in Patients Long-term After Arterial Switch Operation.
Driessen MMP*, Baggen VJM*, Meijboom FJ, Leiner T, Haas F, Jansen NJG, van Wijk WHS, Strengers J, Doevendans PA, Sieswerda GT, Takken T, Breur JMPJ
(J Thorac Cardiovasc Surg. 2015 150:918-25) *both authors contributed equally

Advances in cardiac magnetic resonance imaging of congenital heart disease.
Driessen MMP, Breur JMPJ, Sieswerda G Tj, Meijboom FJ, Budde, RJ, Leiner T
(Pediatr Radiol. 2015 45:5-19)

Pressure overloaded right ventricles: a multicenter study on the importance of trabeculae in RV function measured by CMR.
Driessen MMP*, Baggen VJM*, Freling HG, Pieper PG, van Dijk AP, Doevendans PA, Snijder RJ, Post MC, Meijboom FJ, Sieswerda GjT, Leiner T, Willems TP (Int J CV Imaging. 2014 30:599-608) *both authors contributed equally

Bed-side prediction rule of infections after pediatric cardiac surgery.
Driessen MMP*, Algra SO*, Schadenberg AWL, Haas F, Bollen CW, Houben ML, Jansen NJG
(Intensive Care Med. 2012 38:474-81.) *both authors contributed equally

Assessment of LV ejection fraction in daily practice using real-time 3D echocardiography; direct comparison of the volumetric and speckle tracking methodologies to CMR.
Driessen MMP, Kort E, Cramer MJM, Doevendans PA, Angevaare MJ, Leiner T, Meijboom FJ, Chamuleau SAJ, Sieswerda GTj (Neth Heart J. 2014 22:383-90)

Knowledge based 3D reconstruction of the right ventricle: comparison with cardiac magnetic resonance in adults with congenital heart disease
Trzebiatowska-Krzyska A, **Driessen MMP**, Sieswerda GT, Wallby L, Swahn E, Meijboom FJ (Echo Res Prac. 2015 2:109-116)

Dankwoord

Een dag voordat het proefschrift naar de drukker moet, kan ik eindelijk het allerlaatste stukje van mijn proefschrift schrijven, het dankwoord! Naast alle hulp en steun die ik van iedereen gekregen heb, had ik ook nooit durven dromen dat ik zoveel leuke dingen zou meemaken.

Om te beginnen het promotieteam, ik denk met veel plezier terug aan alle besprekingen. Vanaf Nijmegen werd het wat moeilijker, maar jullie kwamen mij tegemoet door “halverwege” af te spreken bij Broers (onder het genot van een biertje en bitterballen).

Professor Leiner, beste **Tim**, toen ik begon, was jij net overgekomen uit Maastricht en enthousiast om nieuw onderzoek naar aangeboren hartafwijkingen op te zetten. Ik wist nog helemaal niks van de MRI, maar met jouw hulp zat ik binnen 1.5 jaar zelf achter de scanner! Bij elke bespreking stond de Nespresso klaar. Bedankt voor alles wat ik van je heb geleerd, je enthousiasme en je snelle revisies en antwoorden wanneer nodig.

Professor Doevendans, beste **Pieter,** ten eerste bedankt voor de mogelijkheid om twee projecten binnen de aangeboren hartafwijkingen op te starten. Helaas ging dat niet zonder slag of stoot en heeft mijn promotie lang geduurd… Maar nooit hoorde ik tijdens de bespreking een twijfel of het wel ging lukken, dank voor uw vertrouwen dat het goed zou komen en alle support door de jaren heen!

Beste **Gertjan, dr. Sieswerda,** als co-promotor heb je me altijd 100% gesteund en in me geloofd! Ik kon jou altijd storen als ik ergens niet uitkwam of even de frustratie kwijt moest. Jij zorgde dat ik niet zou vergeten te genieten van mijn promotietijd, door elke keer een ‘potje’ te vinden voor congres of cursus. Heel erg bedankt voor de goede samenwerking en alle echokennis die ik opgedaan heb.

Beste **Folkert, dr. Meijboom,** hoewel je geen officiële plek hebt in mijn promotieteam, heb ik mijn plek in dit promotietraject aan jou te danken. Het leven ging als promovendus niet altijd over rozen, maar ik heb ontzettend veel mooie dingen meegemaakt. Bedankt voor de vele revisies, snelle reacties en altijd leuke discussies (“je sais que je ne sais pas” Jean Gabin)! Zelfs toen je enkele maanden niet kon werken, heb je mij geholpen waar mogelijk. Bovenal was het erg gezellig, van congres in Wenen tot meeting via Skype (mits het aanmelden gelukt was) vanuit Canada, er was altijd tijd even bij te kletsen.

Dank aan alle patienten die deelgenomen hebben aan het onderzoek en aan alle collega’s die geholpen hebben dit onderzoek tot een succes te maken: **dr. Marco Post en dr. Repke Snijder** in het Antonius Ziekenhuis, **dr. Arie van Dijk** in het Radboud UMC.

Aan de **leescommissie** veel dank voor beoordeling van mijn proefschrift. **Professor Birgitta Velthuis** bedankt dat je het voorzitterschap op je wilde nemen. Gedurende mijn promotie heb ik veel van je mogen leren en was het een plezier met je samen te werken! **Professor Steven Chamuleau**, met bewondering heb ik gekeken naar alle projecten die jij de afgelopen jaren leidde en je benoeming tot hoogleraar. Op echogebied heb ik veel van je kunnen leren, maar je danspasjes hebben een echt onuitwisbare indruk gemaakt (ook op Roos en Frebus)! **Professor Barbara Mulder,** heel erg bedankt voor de tijd die u gestoken heeft in het lezen van mijn proefschrift. Uw rol binnen onderzoek naar aangeboren hartafwijkingen wereldwijd is inspirerend. **Professor Marc**

Vos, dank voor uw deelname in de leescommissie. Toen ik mijn proefschrift kwam brengen zei u tegen de aanwezige promovendi: “When this is you, it will be the happiest day of your live”. Op dat moment stond ik er pas bijstil dat het af was, ben direct daarna champagne gaan drinken! **Dr. Tineke Willems**, heel erg bedankt dat je zo secuur mijn proefschrift hebt doorgenomen en de kleine typefoutjes eruit gehaald hebt. Bedankt voor de samenwerking aan Chapter 4 en voor het applaus bij WCPPC in Barcalona!
Uiteraard wil ik ook graag **dr. Arie van Dijk en professor de Jong** bedanken voor het plaatsnemen in de oppositie!

I was very fortunate to visit Sick Kids Hospital in Toronto for 9 months. First of all, thanks to **dr. Mark Friedberg**, who supervised my research fellowship in Toronto and helped me understand my data. Our research meetings were always fun and motivating! Thanks for all the invites to brunch and dinners, making sure I was having fun in Toronto (although you were amazed by my busy social calendar). Secondly, thanks to **professor Luc Mertens**, who helped improve the Utrecht projects. Thanks for the beers and “borrels” in Toronto and helping me decide on my future career path! Thanks to **dr. Andreea Dragulescu, Wei Hui** and all staff of Sick Kids Cardiology deparment for welcoming me (and all fellows) to their department.
A special thanks to my roommates at Sick Kids, starting with **Barbara Cifra**. Although you kept your distance in the beginning – I’m so happy we became the friends we are today! Love seeing you every time we have a chance to meet up and I’m so proud of all you are accomplishing! Thanks to **Micheal Grattan, Bridget Zoeller, Amanda Hauck, Carmen, Deane Yim and Annika** Öhman for all the fun in our echo fellowsroom, hope to see you all at future conferences! Special thanks to Heynric Grotenhuis and Martijn Slieker, who gave the room a Dutch feel.

Ik heb gedurende mijn tijd als arts-onderzoeker met veel mensen mogen samenwerken en veel leuke dingen mogen doen. Hoogtepunt was toch wel de Utopia run, dank voor die topervaring **Tycho, Margot, Linda, Joris, Jeroen, Annemieke, Susan, Margot, Geert, Marieke, Irene, Vincent, Stefan en Manon.** Door stromende regen en een pikzwarte nacht rennen was echt onvergetelijk! **Geert, Marieke en Margot** – aan de start van mijn onderzoek hebben jullie me wegwijs gemaakt! **Manon, Willemien en Martine** daarna heb ik met jullie talloze theetjes gedronken en dropjes gegeten! **Jetske, Roos, Judith, Freek, Mariam en Irene** – dank voor de gezelligheid in het Q gebouw. Hoop jullie allemaal nog tegen te komen in de toekomst! Mannen van de bunker (die heel snel niet meer groot genoeg was); **Tycho, Stefan, Frebus, René, Ing Han en later Remco** – bedankt voor alle gezelligheid in het UMCU en op congres! R&D team **Han, Jeanette, Yvonne, Ellie en Astrid** – dank voor alle gezelligheid tijdens lunch, feestjes en BBQs. Daarnaast heel veel dank aan **Merian, Tamara, Sylvia en Jantine** voor alle ondersteuning!
De echodames: **Elly (x2), Ineke, Jeanette en Annemarie** heel erg bedankt voor jullie ondersteuning en hulp bij maken van echo’s. Bedankt aan de echocardiologen: **Maarten-Jan**, bedankt voor je aanstekelijke enthousiasme en altijd positieve instelling! **Roland,** jij bedankt voor alle sparringsessies, gezelligheid en kennis. Gelukkig mag ik nu weer met je samenwerken in het Radboud UMC!

Bedankt aan **Erik Hulzebos** en **Tim Takken** voor het uitvoeren van alle inspanningstesten en de fijne samenwerking! Bedankt aan alle studenten die een bijdrage hebben geleverd aan dit onderzoek, in bijzonder; **Vivan Baggen** en **Sebastiaan van Wijk**.

Alle Radiologie medewerkers, Anneke bedankt voor de flexibele planning. Niels, Guus, Jorgen, Daniel en alle andere MRI laboranten - dank voor jullie uitleg en geduld (als ik de planning toch net anders wilde)!

Ik ben ontzettend blij dat ik mijn opleiding tot cardioloog mag doen in het Radboud UMC Nijmegen. Aan alle cardiologen in het Radboud ontzettend bedankt voor de prettige plek om te werken! **Dr. Arie van Dijk en dr. Peter Kievit** dank dat jullie mij hebben aangenomen voor de opleiding. **Arie,** daarnaast ontzettend bedankt voor jouw hulp bij het onderzoek de afgelopen jaren. We hadden geen makkelijk onderwerp gekozen voor dit proefschrift, dank voor de kritische input bij het schrijven van de manuscripten en voor je (herhaalde) uitleg!
Zowel in het **Radboud,** als nu in het **Meander MC,** ben ik in een superleuke groep met arts-assistenten terecht gekomen! **Collega's uit het Radboud**; er gaat niks boven de Nijmeegse gezelligheid. Van pizza's bakken tot een nachtelijk jeu de boules toernooi – ik heb zin om over 2 jaar weer terug te zijn in het Radboud! **Collega's in het Meander MC**; top assistentenweekend, borrels op vrijdag en als kers op de taart aankomende februari de Ski-reis – ik heb er zin in!
Alle internisten, longartsen en MDL-artsen in het Meander MC bedankt voor jullie enthousiasme, ik heb het dankzij jullie ontzettend naar mijn zin tijdens de vooropleiding Interne Geneeskunde. **Renate en Rob**, jullie zijn echt ontzettend leuke opleiders!
Alle **cardiologen in het Rijnstate ziekenhuis** – jullie hebben mij de eerste kneepjes van het vak geleerd. Ik heb zin om over 8 maanden weer bij jullie aan de slag te gaan!

Alle vrienden en vriendinnen die altijd ontzettend lief geluisterd hebben naar mijn frustraties of begrip hebben getoond als ik iets af moest krijgen: bedankt! Ook voor alle tijden dat jullie van mij niet naar de promotie mochten vragen (en dat ook niet deden): bedankt!
Fim-la-fim – **Franca, Imke, Marlies, Lieke, Anne, Fleur en Irene;** we zijn inmiddels al meer dan de helft van mijn leven vriendinnen! Ik ben ontzettend blij dat we elkaar de laatste jaren steeds vaker zien, want vrienden die je al 17 jaar kent is toch wel erg speciaal. Bedankt voor jullie gezelligheid, luisterend oor en de knuffels!
Kader – wie had gedacht dat we 10 jaar na dato nog steeds vrienden zouden zijn. **Iwan, Thijs, Alwin en Marijne** elke keer als we afspreken is het een gegarandeerde topavond! **Marijne** van feestjes tot samen op de spoedeisende hulp; ik hoop dat het nog vele jaren zo blijft (zonder SEH bezoeken dan). **Heleen**, ondanks dat we op andere continenten wonen is het ons gelukt om vriendinnen te blijven!
Carolien, door de jaren heen al vele pieken en dalen meegemaakt… Je gaat altijd vol voor je doel, heel veel succes met je nieuwe opleiding! **Jolien**, onze roeicarrière speelde zich met name af buiten het water. Toen biertjes drinkend aan de bar en nu lekker eten en kletsen op de bank. **Mirjam** ik hoop nog vele wijntjes samen in jouw tuin te mogen drinken (zodra het weer kan)! **Eva, Marly, Patty en Marieke,** bedankt voor alle gezelligheid, in de roeiboot en vooral daarbuiten.
Meikevers – Charlotte, Laura, Fleur, Floortje, Sjon, Vic en Esmée, eigenlijk begonnen op festivals met de voetjes van de vloer, maar nu een heerlijke borrelgroep! **Geneeskundevriendinnen: Hanneke, Nicolette, Margot K, Margot M en Marleen** – van de eerste werkgroep tot allemaal op onze eigen plek!
And of course my friends across the pond – who have made my PhD time unforgettable. I came to Toronto when it was -20 Celsius, not really the best season to meet people. But within weeks I had an entire group of friends (it was either my sparkly personality or baking pancakes that won you over)! Thank you **Yousaf, Ali, Danielle, Ryan, Wendy, Alison, Merin, Aaron, Ella, Nico and Rebecca –** for an awesome time in Toronto! Miss you guys a lot!

Ik wil ook graag mijn lieve familie bedanken voor hun interesse en steun. **Oma Driessen**, dank voor de vele jaren dat wij mochten komen logeren, ik weet zeker dat **Opa** trots naar beneden kijkt! Bedankt - **Oma Roefs** waar ik ziek op de bank lag tijdens mijn cito toets en **Opa Beurskens** die altijd voor ons klaar stond. **Aafke** bedankt voor het mooie boekje dat je voor me gemaakt hebt!

Roel en **Peter** – jullie zijn inmiddels al lange tijd onderdeel van ons gezin. Bedankt dat de deur altijd voor mij open staat!
Nout en Jolien, jullie zijn veel te klein om dit te lezen, maar jullie tante zijn geeft mij echt zoveel plezier! Ik vind het heerlijk om met jullie verstoppertje te spelen of trampoline te springen, houd ontzettend veel van jullie!

Pap en Riny ontzettend knap hoe jullie altijd overal je schouders onder gezet hebben. Een voorbeeld voor mij als ik even geen zin meer had in de promotie. Bedankt voor alle gezellige avonden en voor opbeurende woorden door de jaren heen, ook aan **Nick** en **Amanda**.

Lotte, mijn paranimf! Wij hebben veel dieptepunten en hoogtepunten samen meegemaakt en van sommige momenten weet ik niet zeker ik ze onder de hoogte- of dieptepunten moet plaatsen (strand op de Perhentian islands)! Je hebt me op mijn best gezien (duikend in de turquoise zee op Zanzibar) en op mijn slechtst (van top tot teen onder de urticaria in Itete). Bedankt dat je van dat laatste moment geen foto's hebt gemaakt! Fijn om je 28 september naast me te hebben.

Loes, zusje en nu mijn paranimf – ik zou kantjes kunnen volschrijven, maar dat doe ik niet. Ik ben blij dat de dagen van knijpen en haren trekken ver achter ons liggen en we nu altijd bij elkaar terecht kunnen. Ik ben trots op je en kan me geen betere grote zus wensen!

Mam, ik kan je niet genoeg bedanken! Jij hebt Loes en mij altijd gemotiveerd om door te leren en onafhankelijk te zijn – en volgens mij is dat gelukt! Hoewel je liever had dat ik dit binnen de landgrenzen deed, was je ook blij voor me toen ik naar Toronto kon gaan. Dank voor de talloze keren dat je voor me klaarstond!

Curriculum vitae

Mieke Driessen was born on the 19th of November 1984 in Venlo, the Netherlands. She graduated from secondary school at the Valuas College Venlo in 2003. This same year she started medical school at the University of Utrecht and graduated in February 2010. During the final year of her study, she participated in research on congenital heart disease at the Pediatric Intensive Care Unit. After graduation she continued research on congenital heart disease at the Cardiology department of the University Medical Center Utrecht, under supervision of prof. dr. P. Doevendans, prof. dr. T. Leiner, dr. G. Sieswerda and dr. F. Meijboom. After working on the arterial switch project, she went on to research the pressure-loaded right ventricle, the results of which are presented in this thesis. In 2014 an ICIN-NHI fellowship grant was awarded to her. This grant was used to study right ventricular remodeling in children at Sick Kids Hospital Toronto, under supervision of Dr. M. Friedberg. In October 2014 she started clinical work at the Cardiology deparment of Rijnstate Ziekenhuis and thereafter Radboud University Medical Center. In July 2016 she started her residency as Cardiologist-in-training at the Radboud University Medical Center Nijmegen under supervision of dr. A.P.J. van Dijk and Dr. P. Kievit. She is currently doing her Internal Medicine rotation at Meander Medical Center Amersfoort under supervision of dr. R. Bosma and dr. R. Fijnheer.